

FUNCTIONAL DIVERSIFICATION OF THE UNFOLDED PROTEIN RESPONSE IN
ARABIDOPSIS

By

Evan Russell Angelos

A DISSERTATION

Submitted to
Michigan State University
in partial fulfillment of the requirements
for the degree of

Biochemistry and Molecular Biology- Doctor of Philosophy

2021

ABSTRACT

FUNCTIONAL DIVERSIFICATION OF THE UNFOLDED PROTEIN RESPONSE IN ARABIDOPSIS

By

Evan Russell Angelos

Much like a factory, the endoplasmic reticulum (ER) assembles simple cellular building blocks into complex molecular machines known as proteins. In order to protect the delicate protein folding process and ensure the proper cellular delivery of protein products under environmental stresses, eukaryotes have evolved a set of signaling mechanisms known as the unfolded protein response (UPR) to increase the folding capacity and resiliency of the ER. While the UPR is a conserved aspect of nearly all eukaryotic cells, this process is particularly important in plants, because their sessile nature commands adaptation for survival rather than escape from stress. As such, plants make special use of the UPR, and evidence indicates that the master regulators and downstream effectors of the UPR have distinct roles in mediating cellular processes that affect plant growth, development and stress responses. In my research I sought to contribute to the general knowledge of how the plant UPR is integrated with, and connected to other critical signal transduction mechanisms in stress and development. My work has helped to connect plant UPR activities with reactive oxygen species (ROS) signaling under canonical ER stress situations, by demonstrating that this ROS is required for ER stress survival. In collaboration with the National Aeronautics and Space Administration (NASA) I was able to explore the relevance of the UPR to spaceflight associated stress, and uncovered novel connections between the UPR and plant-specific abiotic stress responses. Finally, I establish a role for the UPR in the regulation of widely conserved metabolic signaling pathways, which are critical to maintain plant organ growth.

To Sandy and Tim, to Lauren, and to Ben.
None of this would have been possible without your unwavering love and support.

ACKNOWLEDGEMENTS

I will be forever grateful to Dr. Binney Girdler, who recognized my potential, and put up with me while I explored the scientific process for the first time. Those early experiments may have made a mess, and stunk up the biology labs, but they set me on the path I walk today. I am also grateful to Dr. Jonathan Walton, who gave me a chance as an undergraduate, and then offered support and mentorship long afterward. Without Dr. Walton and Binney's advice in those formative years, I do not know where I would be.

I would like to thank Dr. Federica Brandizzi, my Ph.D supervisor. Over the years she has guided me and help me turn raw enthusiasm for science and an unending curiosity into a productive research career. She has supported me through the good times and the bad, in any way that she could, and I will always be grateful for that. To the past and current members of the Brandizzi lab, I would not have gotten through this time without you. In particular, Melissa, Starla, Anne, Gianni, Luciana, Sang-Jin, Cristina, you all offered friendship, support, and took the time to answer my thousands of questions with patience and respect. To Noelia, you kept me going when things were at their worst, I can't thank you enough.

I would also like to thank the members of my Ph.D Committee and Comprehensive Exam committee: Dr. Sharkey, Dr. Hamberger, Dr. Hu, Dr. Hsu, and Dr. Kuhn. Their feedback, guidance, discussions, and validation have been invaluable to my progress, which would not have been possible without their support. In addition, I would like to thank Dr. David Arnosti, the BMB graduate programs director, who has been a sympathetic and understanding advisor throughout my time here and provided many opportunities for growth and development as a researcher and as a member of the BMB community. I would also like to thank Dr. Robert Last,

and the other members of the Plant Biotechnology for Health and Sustainability program who provided financial support and invaluable leadership experience during my time at MSU. I have been walking among giants here at the PRL for the last ten years, I couldn't have imagined a better place to launch my career.

TABLE OF CONTENTS

LIST OF FIGURES	ix
KEY TO ABBREVIATIONS.....	xi
CHAPTER I INTRODUCTION.....	1
THE UNFOLDED PROTEIN RESPONSE MONITORS ENDOPLASMIC RETICULUM HOMEOSTASIS.....	2
<i>Entrance to the Secretory Pathway.....</i>	2
<i>A Varied Toolbox: The Primary Regulators of the Unfolded Protein Response</i>	4
FUNCTIONAL DIVERSIFICATION OF THE UPR IN ADAPTATION TO ENVIRONMENTAL STRESS	10
<i>From Humans to Arabidopsis: A Myriad of Cell Stresses Elicit UPR Activation</i>	10
<i>Functional Diversification of IRE1 Activation and Effects</i>	16
<i>Functional Diversification of UPR Transcription Factors.....</i>	21
FUNCTIONAL DIVERSIFICATION OF THE UPR IN DEVELOPMENT	26
<i>The UPR is Essential to Multicellular Metazoan Development</i>	26
<i>Physiological Roles of the Plant UPR in Development</i>	29
RATIONAL FOR STUDY	35
REFERENCES	37
CHAPTER II NADPH OXIDASE ACTIVITY IS REQUIRED FOR ER STRESS SURVIVAL IN PLANTS	52
ABSTRACT.....	53
INTRODUCTION	53
MATERIALS AND METHODS.....	58
<i>Plant Materials and Growth Conditions</i>	58
<i>Superoxide Histochemical Staining and Quantification.....</i>	58
<i>Extraction and Quantification of H₂O₂ in Seedling Tissues Using Amplex Ultra Red.....</i>	59
<i>RNA Extraction and Quantitative RT-PCR Analyses</i>	62
<i>Recovery from ER Stress and Chronic ER Stress Phenotypic Analyses</i>	63
<i>Electrolyte Leakage Measurements</i>	64
RESULTS	65
<i>ER Stress Induces Accumulation of Superoxide by NADPH Oxidases.....</i>	65
<i>ER Stress Induces Accumulation of Hydrogen Peroxide Dependent upon RBOHD and RBOHF Activity and Intact UPR Signaling.....</i>	67
<i>UPR Regulators Influence RBOHD and RBOHF Expression During Adaptive UPR ..</i>	70
<i>RBOHD and RBOHF are Necessary for Recovery from Short-Term and Chronic ER Stress</i>	74
<i>RBOHD and RBOHF Contribute to Preventing ER Stress Induced Cell Death</i>	75
DISCUSSION.....	80
<i>NADPH Oxidases Contribute to ROS Production in Conditions of ER Stress</i>	80

<i>Unlike in Metazoans, NADPH Oxidase-Produced ROS are Beneficial to Overcome ER Stress in Plants</i>	82
<i>Homeostasis of NADPH oxidase activity is required to maintain an effective UPR</i>	83
<i>In ER Stress Conditions, the Production of ROS is Antagonized by IRE1 and the bZIP60/bZIP28 Transcription Factors</i>	84
ACKNOWLEDGEMENTS	87
REFERENCES	88

CHAPTER III RELEVANCE OF THE UNFOLDED PROTEIN RESPONSE TO SPACEFLIGHT INDUCED TRANSCRIPTIONAL REPROGRAMMING IN ARABIDOPSIS	95
ABSTRACT.....	96
INTRODUCTION	97
MATERIALS AND METHODS.....	100
<i>Launch Hardware and Experimental Timeline</i>	100
<i>Germplasm and Culture Conditions</i>	101
<i>Sample Processing and Experimental Material Assessment</i>	102
<i>Library Preparation, Sequencing, and Bioinformatics Analysis</i>	102
RESULTS	104
<i>Spaceflight Alters the Growth of Seedlings Independent of an Intact UPR Signaling</i>	104
<i>Spaceflight Results in an Increase of Total RNA</i>	104
<i>Global Transcriptomic Analyses Indicate that Gene Expression Reprogramming in Response to Spaceflight Depends Partially on Intact UPR Signaling</i>	108
<i>Biological Pathways Connected to DEGs Between Flight and Ground</i>	110
<i>The UPR Regulators Exert a Minor but Significant Role on Gene Expression in Spaceflight</i>	113
DISCUSSION	118
DATA AVAILABILITY	125
ACKNOWLEDGEMENTS	125
AUTHOR CONTRIBUTIONS.....	126
APPENDIX.....	127
REFERENCES	130

CHAPTER IV THE UPR REGULATOR IRE1 PROMOTES BALANCED ORGAN DEVELOPMENT BY RESTRICTING TOR DEPENDANT CONTROL OF CELLULAR DIFFERENTIATION IN ARABIDOPSIS.....	136
ABSTRACT.....	137
INTRODUCTION	138
MATERIALS AND METHODS.....	142
<i>Plant Material and High-Quality Seed Production</i>	142
<i>Plant Phenotyping</i>	143
<i>mPS-PI Staining and Meristem Cellular Organization Analysis</i>	144
<i>TOR Activity Assays</i>	145
<i>EdU Pulse-Chase Experiments</i>	147
<i>Data Reporting and Statistical Analysis</i>	148
RESULTS	150

<i>IRE1 Promotes Root Growth in an Age-Dependent Manner</i>	150
<i>IRE1 is Required for Proper Cell Elongation in the Root Meristem</i>	154
<i>The Emergence of the ire1a ire1b Root Growth Phenotype Depends on High Rates of Root Growth</i>	157
<i>TOR Inhibition Rescues the ire1a ire1b Primary Root Growth Phenotypes</i>	161
<i>TOR is Hyperactive at the Growing Primary Root Tips of the ire1a ire1b Mutant</i>	165
<i>TOR Inhibition Rescues the ire1a ire1b Cellular Elongation Phenotypes at the Root Meristem</i>	167
<i>TOR Hyper-activity in the ire1a ire1b Mutant Promotes Differentiation Rather than Cellular Proliferation</i>	170
DISCUSSION	175
<i>IRE1 can Regulate TOR Activity in a Multicellular Eukaryote</i>	176
<i>IRE1 is Necessary to Control TOR Activity at Tissue- and Development-Specific Levels</i>	176
<i>IRE1-Dependent Repression of TOR is Independent from the Unconventional Splicing of bZIP60</i>	178
<i>TOR Activity Regulates Cellular Differentiation and Cell Elongation in Actively Growing Arabidopsis Root Tips</i>	179
ACKNOWLEDGEMENTS	182
APPENDIX.....	183
REFERENCES	193
CHAPTER V FUTURE PERSPECTIVES.....	200
<i>Chapter 2: Integrating ER Stress Response with NADPH Oxidase Signaling</i>	202
<i>Chapter 3: UPR Transcriptome in Spaceflight Experiment Reveals Possible Novel Roles for UPR TFs</i>	204
<i>Chapter 4: Old Friends with a New Relationship, IRE1 and TOR</i>	206
REFERENCES	208

LIST OF FIGURES

Figure 1.1. The IRE1 and ATF6 dependent arms of the UPR are conserved in Arabidopsis	8
Figure 1.2. Simplified models comparing RNase activation mechanism of mammalian and <i>S. cerevisiae</i> IRE1s.....	18
Figure 1.3. The UPR TFs interact with a variety of conserved and plant specific partners to regulate transcription.	24
Figure 2.1. NADPH oxidase-dependent O_2^- is generated during ER stress partially through RBOHD and RBOHF.	66
Figure 2.2. ER Stress-induced H_2O_2 is controlled by RBOHD and RBOHF as well as intact UPR signaling.....	69
Figure 2.3. Intact UPR signaling is required to maintain homeostasis of RBOH transcript levels and ROS signaling, while RBOH activity affects UPR homeostasis.	72
Figure 2.4. RBOHD and RBOHF are required in the recovery from temporary ER stress.....	76
Figure 2.5. RBOHD and RBOHF are required for adaptation to chronic ER stress.	77
Figure 2.6. RBOHD and RBOHF act to prevent ER stress-induced cell death.....	79
Figure 3.1. Growth of etiolated hypocotyls was altered by spaceflight.....	105
Figure 3.2. RNA quality assessment of flight and ground control samples.	107
Figure 3.3. Overall quality assessment of RNA-sequencing dataset.	109
Figure 3.4. Summary of differential gene expression analysis.	110
Figure 3.5. Representative biological processes gene ontologies over- or under-represented by upregulated or downregulated DEGs in the WT background.....	112
Figure 3.6. K-means clustering analysis of all 3465 DEGs in at least 1 background.....	114
Figure 3.7. Simplified model of regulatory framework controlling stress responsive DEGs.....	122
Figure 3.S1. Representative Bioanalyzer traces of ground and flight samples	128
Figure 3.S2. Number of total mapped reads and mapping rate per sample	128

Figure 3.S3. Number of DEGs which had WT FPKM values which were significantly different from WT in at least one mutant genotype.....	129
Figure 3.S4. Percentage of DEGs with statistically different ground FPKM values in the indicated UPR mutant genotype compared to the WT ground FPKM values.....	129
Figure 4.1. The <i>ire1a ire1b</i> double mutant shows age dependent primary root growth defects .	151
Figure 4.2. Meristem organization defects in <i>ire1a ire1b</i> are first manifested in cell elongation in the elongation zone	155
Figure 4.3. The emergence of the <i>ire1a ire1b</i> root phenotype depends on a high rate of root growth	159
Figure 4.4. TOR inhibition rescues the <i>ire1a ire1b</i> root growth phenotype.....	163
Figure 4.5. TOR is hyperactive in the <i>ire1a ire1b</i> mutant root tips but not in the mature root...	166
Figure 4.6. Meristem organization defects in <i>ire1a ire1b</i> are rescued by TOR inhibition.....	168
Figure 4.7. TOR hyperactivity in the <i>ire1a ire1b</i> mutant promotes differentiation rather than cellular proliferation.....	172
Figure 4.S1. Rate of shoot fresh weight accumulation and primary root growth for data displayed in Figure 4.1	184
Figure 4.S2. At D5 there are no significant defects in the <i>ire1a ire1b</i> meristem organization ...	185
Figure 4.S3. Average root tip cellular organization metrics displayed over time in WT and <i>ire1a ire1b</i>	186
Figure 4.S4. TOR inhibitor AZD-8055 concentration response analysis.....	187
Figure 4.S5. TOR inhibitor TORIN2 rescues the <i>ire1a ire1b</i> root growth phenotypes	188
Figure 4.S6. Other chemical inhibitors of root growth do not rescue the <i>ire1a ire1b</i> root length phenotype.....	189
Figure 4.S7. Auxin inhibition of root growth and TOR inhibition of root growth are additive effects in WT and <i>ire1a ire1b</i> plants	190
Figure 4.S8. Full blot images from Figure 4.5 and images of blots after Ponceau's stain to demonstrate equal protein loading	191
Figure 4.S9. Simplified model showing that TOR activity must be carefully balanced to maintain optimal cell elongation.....	192
Figure 5.1. Summary Graphic of Dissertation Investigations.....	201

KEY TO ABBREVIATIONS

$^1\text{O}_2$ - singlet oxygen

ADP- adenosine diphosphate

AGB1- Arabidopsis G β subunit 1

ANOVA- analysis of variance

ATF6- Activating Transcription Factor 6

AUR- Amplex Ultra Red

BAK1- BRI1-associated receptor kinase 1

BAX- Bcl-2 associated X

BI1- BAX inhibitor 1

BiPs- luminal binding proteins

BR- brassinosteroid

BRI1- brassinosteroid insensitive 1 receptor

BRIC- Biological Research In a Canister

BSA- bovine serum albumin

bZIP- basic leucine zipper

chl- chlorophyll A oxygenase mutant

CL- continuous light

clv- CLAVATA mutant

COPII- coat protein complex II

CoV- coefficients of variation

CPR5- constitutive expressor of pathogenesis-related genes-5

ddH₂O- double distilled water

DEGs- differentially expressed genes

DMSO-dimethyl sulfoxide

DPI-diphenyleneiodonium chloride

EB- extraction buffer

EdU- ethynyl-2'-deoxyuridine

EF-Tu- elongation factor Tu receptor
eIF- eukaryotic translation initiation factors
ER- endoplasmic reticulum
ERAD- ER-associated protein degradation
ERdj3- ER resident J domain 3
ERO1- ER oxidoreductin 1
ERQC endoplasmic reticulum quality control
ERSE- ER Stress Response Elements
EZ- elongation zone
FPKM- fragments per kilobase exon model per million mapped reads
FRET- Förster resonance energy transfer
GLS- Golgi localization sequence
GO- Gene Ontology
H₂O₂- hydrogen peroxide
HRP- horseradish peroxidase
HSP- heat shock protein
HY5- Elongated Hypocotyl 5
IP3R- inositol triphosphate receptor
IRE1- Inositol Requiring Enzyme 1
ISS- International Space Station
ISSES- ISS Environmental Simulator
JA- jasmonic acid
KSC- Kennedy Space Center
LS- Linsmaier and Skoog
LSD1- Lesion Stimulating Disease 1
MEcPP- 2-C-methyl-D-erythritol-2,4-cyclopyrophosphate
MEP- methylerythritol phosphate
mPS-PI- modified pseudo-Schiff propidium iodide
MS- Murashige and Skoog
mTORC1- mammalian TOR complex 1

MTTFs- membrane tethered bZIP transcription factors
MZ- meristematic zone
NAA-1-naphthaleneacetic acid
NBT- Nitro Tetrazolium Blue
NF-Y- Nuclear Y Factor
NOX- NADPH Oxidases
NPR1- Nonexpressor of Pathogenesis Related 1
NTCA- neutralized trichloroacetic acid
 O_2^- - superoxide
OST- oligosaccharyltransferase
PA- periodic acid
PAMP- pathogen-associated molecular pattern
PBS- phosphate buffered saline
PCA- principal component analysis
PCD- programmed cell death
PDFU- Petri Dish Fixation Unit
PDI- protein disulfide isomerase
PERK- Protein kinase R-like Endoplasmic Reticulum Kinase
PM- plasma membrane
R/FR- red/ far red light
RBOH- respiratory burst oxidase homolog
RHI- root hair initial
RIDD- Regulated IRE1 Dependent Decay
RIN- RNA Integrity Number
RIP- regulated intramembrane proteolysis
RNAi- RNA interference
RNase- endoribonuclease
RNA-seq- RNA-sequencing
ROS- reactive oxygen species
rRNA- ribosomal RNA

RT-PCR- reverse transcriptase PCR
S1P- Site-1 Proteases
S2P- Site-2 Proteases
S6K- Serine Kinase 6
SA- salicylic acid
SAR- systemic acquired resistance
SAS- shade avoidance syndrome
SD- standard deviation
SE- standard error
SERCA- sarcoplasmic/endoplasmic reticulum calcium ATPase
SERK4- somatic embryo receptor kinase 4
SFW- shoot fresh weight
shd- heat shock protein 90.7 mutant
SOD- superoxide dismutase
STT3a- staurosporin and temperature sensitive 3
TBST- tris buffered saline plus Tween20
TCA- trichloroacetic acid
TF- transcription factor
Tm- tunicamycin
tms1- Thermosensitive Male Sterile 1
TOR- Target of Rapamycin kinase
TRAF2- TNFR-associated factor 2
TZ- transition zone
UGGT- UDP-glucose glycoprotein-glucosyltransferase
UPR- Unfolded Protein Response
UPRE- Unfolded Protein Response Element
wANOVA- weighted least squares analysis of variance
WT- wild type
XBP1- X-box binding protein 1

CHAPTER I

INTRODUCTION

Parts of the work presented in this chapter has been published in *The Plant Journal* and *Trends in Biochemical Sciences*:

Angelos E., Ruberti C., Kim S.J., and Brandizzi F. (2017) Maintaining the factory: the roles of the unfolded protein response in cellular homeostasis in plants. *Plant Journal*. 90(4):671-682.

Pastor-Cantizano N., Ko D.K., Angelos E., Pu Y., and Brandizzi F. (2020) Functional Diversification of ER Stress Responses in Arabidopsis. *Trends in Biochemical Sciences*. 45(2):123-136.

THE UNFOLDED PROTEIN RESPONSE MONITORS ENDOPLASMIC RETICULUM HOMEOSTASIS

Entrance to the Secretory Pathway

If the plant cell was reimagined as a city, it would be easy to see how the endoplasmic reticulum (ER) could be described as the town's central factory. At the ER, shipments of raw materials in the form of amino acids and carbohydrates are reshaped and assembled into fully-functional molecular machines in the form of proteins. Properly folded proteins are then shipped out and utilized for a variety of different purposes in different places throughout or outside the cell. In order to prevent the production of faulty goods, the ER has specific machinery, collectively called ER quality control (ERQC), to survey the protein folding status, facilitate folding and ensure quality of the produced protein (Ron and Walter 2007). The production of most secretory proteins begins with the co-translational introduction of the protein into the ER. In this process, specific peptide sequences target nascent polypeptide chains to the ER and are translocated across the membrane as they are synthesized via the Sec translocon (Denecke *et al.* 1993, Akopian *et al.* 2013, Schweiger and Schwenkert 2013).

Then, a dedicated battery of ER-resident proteins work to prevent misfolding of nascent polypeptide chains and facilitate the proper folding of the client proteins via post-translational modification (Dobson 2003, Gupta and Tuteja 2011). As the polypeptide enters the ER lumen, molecular chaperones such as the luminal binding proteins (BiPs), bind to the chain of the nascent polypeptides and prevent premature folding (Foresti *et al.* 2003, Carvalho *et al.* 2014). The oligosaccharyltransferase (OST) complex (Lerouxel *et al.* 2005) recognizes specific amino acid sequences and transfers *N*-linked glycans to the peptides. In some cases, this post translational modification adds to the intrinsic stability or solubility of a protein, and importantly, it functions

as a recognition beacon for major ER luminal foldase complexes (Sinclair and Elliott 2005). Nascent polypeptides undergo iterative folding cycles where they are passed between the calnexin/calreticulin complex, and UDP-glucose glycoprotein-glucosyltransferase (UGGT), which monitor protein folding and retains unfolded proteins in the ER (Totani *et al.* 2009) as a part of the ERQC. Other proteins participate in folding cycles under the purview of these central ER foldase complexes, such as thioredoxins (i.e. protein disulfide isomerases; PDIs), which catalyze the reduction and reformation of disulfide bonds (Bottomley *et al.* 2001, Wilkinson and Gilbert 2004). Properly folded proteins are then transported to the Golgi apparatus, while the unfolded or irretrievably misfolded proteins are picked up by proteins like OS9 of the ER-associated protein degradation (ERAD) system, dislocated out of the ER, ubiquitinated, and finally degraded by the 26S proteasome (Hüttner *et al.* 2012).

Due to intrinsic nature of the ER as the entry point to secretory pathway (Vitale and Denecke 1999), a site of phospholipid synthesis (Ohlrogge and Browse 1995), a hub for critical stress and growth signaling molecules (Ron and Walter 2007, Shore *et al.* 2011, Light *et al.* 2016), a calcium storage site (Kaufman and Malhotra 2014), and an assembly plant for a third of a cell's total proteome (Wallin and Heijne 1998), interruptions in ER function can have vast consequences in cellular health. For example, the ERQC mediates the proper folding of critical client plasma membrane receptor proteins in plants, including the Arabidopsis elongation factor Tu (EF-Tu) receptor which mediates pathogen associated molecular pattern-based immunity (Li *et al.* 2009) and brassinosteroid insensitive 1 (BRI1) receptor (Li and Chory 1997). Beyond enabling proper function of cellular signaling pathways with receptors at the plasma membrane (like EF-Tu and BRI1), the specificity of N-linked glycosylation-bearing proteins has recently been shown to play important roles in regulating cell death. The Arabidopsis BAK1 (BRI1-associated receptor kinase

1) and SERK4 (somatic embryo receptor kinase 4) both interact with immune receptors and BRI1 and negatively regulate hypersensitive response-like programmed cell death (PCD) through yet-unknown mechanisms (Li *et al.* 2002, Nam and Li 2002, Roux *et al.* 2011, Gou *et al.* 2012). Intriguingly, loss of STT3a (staurosporin and temperature sensitive 3), one of the two catalytic subunits of the OST complex involved in N-glycosylation of ER proteins, is linked to the cell death phenotype observed in BAK1/SERK4 silenced plants (de Oliveira *et al.* 2016). Together these examples underscore the importance of maintaining the ER as a fully-functional protein folding factory.

A Varied Toolbox: The Primary Regulators of the Unfolded Protein Response

In eukaryotic organisms, exogenous environmental stresses and increased demands for protein folding can perturb the delicate folding machinery inside the ER leading, to the accumulation of unfolded or misfolded proteins (Hetz and Papa 2018, Mitra and Ryoo 2019). This accumulation leads to a potentially lethal condition known as ER stress (Dobson 2003, Hartl and Hayer-Hartl 2009, Buchberger *et al.* 2010). Indeed, under prolonged or severe levels of stress, the accumulation and aggregation of unfolded proteins can become cytotoxic and lead to death of eukaryotic cells (Ron and Walter 2007). The unfolded protein response (UPR) is a set of signaling mechanisms which are meant to prevent accumulation of misfolded proteins in the ER (Walter and Ron 2011). Specialized ER-localized membrane proteins are able to detect the buildup of unfolded proteins and activate intracellular signaling cascades in response (Ron and Walter 2007). The activated UPR sensors upregulate the synthesis of ER protein chaperones, expand the size of the ER by increasing the rate of membrane synthesis, while also limiting the overall rate of protein translation in the cell (Ron and Walter 2007, Ruberti and Brandizzi 2014, Han and Kaufman 2017).

In metazoans there are three “arms” to the UPR, each controlled by one of the three primary ER-localized stress sensors. These sensors are the Inositol Requiring Enzyme 1 (IRE1), Activating Transcription Factor 6 (ATF6) and Protein kinase R-like Endoplasmic Reticulum Kinase (PERK) (Wang *et al.* 1998, Harding *et al.* 1999, Shen *et al.* 2002). In unicellular organisms such as yeast and algae (i.e. *S. cerevisiae* and *Chlamydomonas reinhardtii*) only IRE1 homologs have been identified (Nikawa and Yamashita 1992, Yamaoka *et al.* 2018). In multicellular plants, homologs of the of the IRE1 and ATF6 sensors have been identified (Ruberti and Brandizzi 2014). To date, no direct homolog or functional analog of the metazoan PERK enzyme has been identified in either yeast or plants (Ruberti and Brandizzi 2014). However, accumulating evidence suggests that there are remarkable similarities between the core complement of UPR sensors in mammals and Arabidopsis.

In mammals, two IRE1 paralogs are encoded in the genome, identified as IRE α and IRE1 β . Both of these sensors contain an ER luminal domain (which mediates protein-protein interactions) connected by a type I transmembrane domain to cytosolic serine/threonine kinase and endoribonuclease (RNase) subdomains (Cox *et al.* 1993, Morl *et al.* 1993). Of these two isoforms, IRE α is the predominate protein and is widely expressed in most tissue types, whereas IRE1 β expression is limited primarily to the gut epithelium and mucosal airways (Riaz *et al.* 2020). Of the IRE1 paralogs in the Arabidopsis genome, two of them (IRE1a and IRE1b) closely resemble the IRE1 found in metazoans and yeast (Figure 1.1A; Koizumi *et al.* 2001). IRE1b is the predominate form in Arabidopsis and is expressed in nearly all tissue types (Pu *et al.* 2019). IRE1a is primarily expressed in root tissues, but is also expressed in seed and embryos (Koizumi *et al.* 2001, Noh *et al.* 2002, Pu *et al.* 2019). Arabidopsis and other Brassicaceae also have a third IRE1 isoform named IRE1c which lacks an ER luminal domain and has considerable sequence

divergence compared to other IRE1s (Mishiba *et al.* 2019, Pu *et al.* 2019). However, the relevance of the IRE1c to ER stress responses is yet unknown (Mishiba *et al.* 2019, Pu *et al.* 2019).

The accumulation of unfolded and irretrievably misfolded proteins leads to the activation of IRE1 (Riaz *et al.* 2020). Although the activation mechanism of IRE1 has yet to be established in plants, there is a large body of work describing these mechanisms in both yeast and metazoan models (Korennykh *et al.* 2009, Ali *et al.* 2011). Under non-stressed conditions BiP protein chaperones bind the IRE1 luminal domain, which forces the IRE1 proteins to retain a monomeric organization (Figure 1.1A; Zhou *et al.* 2006). However, during ER stress conditions BiP chaperones preferentially bind to increased numbers of unfolded proteins, thereby freeing the ER luminal domains of IRE1 (Pincus *et al.* 2010). These newly freed luminal domains lead to homo-oligomerization of IRE1, and subsequently to trans-autophosphorylation of the IRE1 kinase subdomains (Shamu and Walter 1996, Welihinda and Kaufman 1996, Korennykh *et al.* 2009, Ali *et al.* 2011). Sensor residues near the IRE1 transmembrane domain can also detect aberrant ER membrane composition, leading to IRE1 oligomerization and autophosphorylation even in the absence of proteotoxic stress (Volmer *et al.* 2013, Halbleib *et al.* 2017). In both methods of IRE1 activation, autophosphorylation of the kinase subdomain causes secondary structural changes which greatly increases the activity of the RNase domain (Zhou *et al.* 2006). Previous research has shown that the Arabidopsis IRE1a and IRE1b genes can dimerize and auto-phosphorylate (Koizumi *et al.* 2001, Noh *et al.* 2002, Zhang *et al.* 2015) suggesting similar overall functions in Arabidopsis, however more study is needed to uncover the structural mechanisms by which IRE1 is activated in plants.

The overall effects of metazoan and plant IRE1s on downstream UPR gene regulation is also relatively similar. In each kingdom the activated IRE1 RNase subdomain catalyzes the

unconventional splicing of a mRNA encoding a conserved basic leucine zipper (bZIP) type transcription factor (TF; Figure 1.1A (Pathway 1) ; Ruberti *et al.* 2015). This splicing of the mammalian *XBPI* and the plant *bZIP60* leads to a translational frameshift of the mRNA eliminating an ER transmembrane anchor domain. (Cox and Walter 1996, Mori *et al.* 1996, Yoshida *et al.* 2001, Deng *et al.* 2011, Nagashima *et al.* 2011). This process is initiated when the IRE1 RNase domains binds to and cleaves two consensus hairpin motifs in these mRNAs (Ron and Walter 2011, Ruberti *et al.* 2015). Then a specific tRNA ligase ligates the 5` and 3` ends of the transcript without the excised section (Sawaya *et al.* 2003, Steiger *et al.* 2005, Jurkin *et al.* 2014, Nagashima *et al.* 2016). The spliced *XBPI* and *bZIP60* transcripts are then translated without their ER anchors, allowing for translocation of the active TF to the nucleus where they modulate downstream target genes (Zhang *et al.* 2016). Intriguingly, the RNase activity of IRE1 is not limited to unconventional splicing of these transcription factors. In metazoans, plants, and some yeasts Regulated IRE1 Dependent Decay (RIDD) affects the abundance of many cytosolic and ER associated mRNAs other than *XBPI/bZIP60* in the response to ER stress (Figure 1.1A; Pathway 2; Hollien *et al.* 2009, Tam *et al.* 2014). IRE1 is also known to perform a number of RNase-independent functions (Riaz *et al.* 2020). In metazoans, the active IRE1 is known to act as a protein scaffold, which enables interactions between the UPR and other cellular signaling pathways (Urano *et al.* 2000, Adams *et al.* 2019). For example, binding of the active IRE1 by TNFR-associated factor 2 (TRAF2) leads to activation of a MAP kinase signal cascade known as the JNK pathway, which regulates cell death in mammalian cells under ER stress conditions (Figure 1.1A; Pathway 3; Urano *et al.* 2000). Whether or not a pathway analogous to the IRE1-TRAF2-JNK signaling axis is conserved in plants remains an exciting topic for future study.

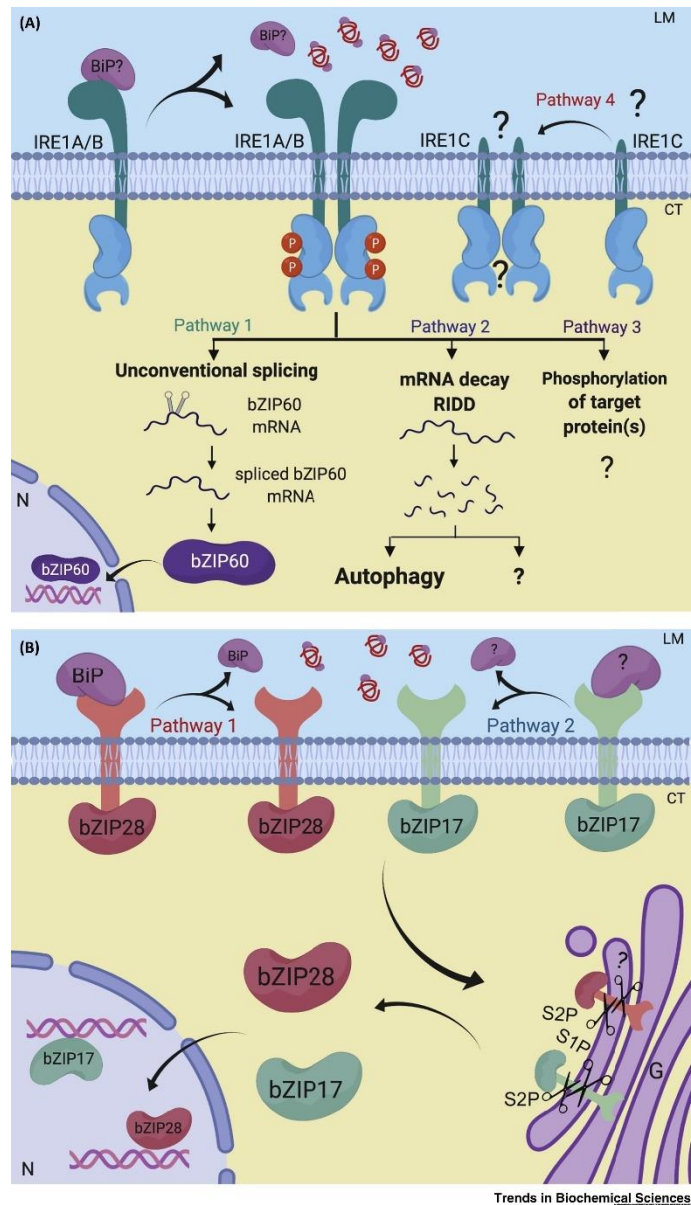


Figure 1.1. The IRE1 and ATF6 dependent arms of the UPR are conserved in Arabidopsis.

A) Monomeric IRE1a/b are kept inactive by binding of BiP proteins to the IRE1 luminal domain. Buildup of unfolded proteins allows dimerization and trans-autophosphorylation of IRE1 monomers leading to their activation. B) Release of BiP proteins allows for trafficking of the Arabidopsis ATF6 homolog, bZIP28, to the Golgi. Subsequent regulated intramembrane proteolysis (RIP) releases the active transcription factor for nuclear translocation. This figure was previously published in Pastor-Cantizano *et al.* (2020).

There are also strong similarities between the mammalian and plant ATF6-dependent arms of the UPR. In mammals there are two ATF6 paralogs (ATF6a and ATF6b; Figure 1.1B; Haze *et al.* 1999). Both of these sensors consist of an ER luminal domain which mediates protein-protein interactions and ER retention, a type II transmembrane domain, and a cytosolic bZIP TF domain (Haze *et al.* 1999). In Arabidopsis two ATF6 homologs exist, bZIP17 and bZIP28 (Liu *et al.* 2007, Liu *et al.* 2007, Kim *et al.* 2018). Under normal conditions BiP proteins bind to and cover the Golgi localization signals (GLSs) found in the ER luminal domain of ATF6a and ATF6b trapping them in an inactive state in the ER (Ye *et al.* 2000). Under ER stress conditions, the BiP chaperones dissociate from ATF6, and translocate to the Golgi where they undergo regulated intramembrane proteolysis (RIP) by the Site-1 and Site-2 Proteases (S1P; S2P) (Ye *et al.* 2000). The freed TFs are then translocated to the nucleus to regulate UPR gene expression similar to XBP1/bZIP60 (Ye *et al.* 2000). In Arabidopsis, bZIP28 has been shown to undergo similar regulation and processing (Liu *et al.* 2007), however an interaction between bZIP17 and BiP has yet to be verified. The mammalian ATF6a, and the Arabidopsis bZIP28 TFs are the primary contributors to the ER stress response from this arm of the UPR (Thürauf *et al.* 2004, Thürauf *et al.* 2007, Kim *et al.* 2018). Together, this information supports the supposition that the core elements of the plant UPR, namely IRE1 and bZIP17/28, have retained remarkable similarities to the mammalian UPR despite millions of years of evolutionary divergence. In the following section I will discuss how these conserved elements are applied in organism specific contexts, and discuss the ways in which plants have co-opted this machinery to adapt to their unique environmental circumstances.

FUNCTIONAL DIVERSIFICATION OF THE UPR IN ADAPTATION TO ENVIRONMENTAL STRESS

From Humans to Arabidopsis: A Myriad of Cell Stresses Elicit UPR Activation

The study of the UPR in human and animal models is largely focused on how altered ER proteostasis and aberrant UPR signaling is related to the development of a number of human diseases, including metabolic diseases, chronic inflammation, neurodegeneration, and cancer (Hetz *et al.* 2020). Some of these studies examine how genetic defects allow the buildup of misfolded proteins, and seek to mitigate the cytotoxic effects of the resulting aggregates (Stefani and Dobson 2003, Rao and Bredesen 2004). However, most studies look to utilize the selective manipulation of UPR components in disease intervention by targeting the UPR signaling network with small molecule and gene therapy approaches (Hetz *et al.* 2020).

The mammalian UPR is a key modulator of the body's response to overnutrition stress. High fat diets or diets high in saturated fatty acids promote lipid accumulation in the liver, which is sensed by IRE1 as ER membrane disequilibrium in those tissues (Halbleib *et al.* 2017, Hetz *et al.* 2020). Subsequent activation of IRE1 controls the expression of a number of downstream effectors boosting lipolysis, fatty acid oxidation, and promoting anti-inflammatory responses in the affected cells (Zhang *et al.* 2011, Wang *et al.* 2018). However, sustained IRE1 activation in the liver was found to be linked with hepatic insulin resistance and the development of type 2 diabetes through inhibition of insulin receptor signaling (Özcan *et al.* 2004). The IRE1 dependent arm of the UPR also plays a critical role in the development of diabetes by controlling the survival of insulin producing pancreatic β -cells (Hetz *et al.* 2020). Previous reports have demonstrated that IRE1 activity needs to be carefully balanced in these cells as both hyperactivation of IRE1 and

loss-of-function mutations in IRE1 lead to low β -cell survival (Lipson *et al.* 2006, Hassler *et al.* 2015).

The role of the UPR in the progression of cancer and tumor growth is also an increasingly studied topic. Cancer cells rapidly proliferate and metabolize large quantities of glucose (Urta *et al.* 2016). In addition, tumor masses can be poorly vascularized which may lead to a number of cellular stresses such as nutrient and oxygen deprivation conditions which are known to stimulate UPR activation in mammalian models (Urta *et al.* 2016). Furthermore, the overexpression of oncogenes in tumors also leads to higher rates of protein synthesis and increased overall demands on the secretory pathway (Urta *et al.* 2016). As such, all arms of the UPR are known to promote oncogenic transformation by contributing to tumor growth, angiogenesis, and immune system evasion (Urta *et al.* 2016). High expression of the spliced XBP1 isoform in lymphoma, multiple myeloma, brain cancer and breast cancer biopsies correlates with low patient survival rates (Urta *et al.* 2016). Together, these examples of UPR involvement in overnutrition stress and cancer growth demonstrate a large potential to treat prevalent human diseases by targeting UPR activities. However, these therapies must be carefully designed, as misregulation of the UPR in off target tissues could be more detrimental than the primary disease.

In contrast with mammals and humans, which can alter their environment, or move to avoid environmental stressors, the sessile nature of plants demands physiological adaptation to environmental change. As such, study of the plant UPR has largely focused on improving plant growth and crop yield under adverse environmental conditions. There is a large potential for biotechnological applications for UPR-related mechanisms in ensuring plant productivity. However, considerable work must be done to understand how the conserved elements of the UPR are integrated into intra- and inter-cellular signaling mechanisms that are plant specific. Even

though there is considerable evidence to suggest that the UPR components are required for many different aspects of plant physiology (Chen and Brandizzi 2012, Chen and Brandizzi 2012, Barba-Espín *et al.* 2014, Ruberti and Brandizzi 2014, Verchot and Pajerowska-Mukhtar 2021), we are only beginning to connect the molecular activities of IRE1 and bZIP17/bZIP28 to the modulation of plant-specific stress resistance.

Enhancing the UPR appears potentially critical to efforts to maintain crop productivity by priming plants to survive under a diverse array of adverse environmental conditions (Tateda *et al.* 2008, Carvalho *et al.* 2014, Xiang *et al.* 2016, Verchot and Pajerowska-Mukhtar 2021). In particular, a number of studies have demonstrated a significant contribution of the UPR to plant responses to pathogen attack. Of these, viral pathogens predictably activate UPR signaling (Verchot and Pajerowska-Mukhtar 2021). The translation of ER-targeted viral proteins has been demonstrated to activate the UPR (Verchot and Pajerowska-Mukhtar 2021). However, the overall effects of UPR activation are dependent upon the specific viral pathogen (Bao and Howell 2017). During infection by most viral pathogens, the UPR actively prevents infection spread to surrounding and systemic tissues (Caplan *et al.* 2009). However, some viruses have been shown hijack the UPR to promote viral pathogenesis, as ablation of UPR components in these contexts prevents viral replication and disease progression (Bao and Howell 2017). Although these are promising first steps, further research is required to better understand the mechanisms by which the UPR affects these outcomes in order to utilize UPR to promote viral resistance.

Pathogen attack by fungi or bacteria can also elicit a UPR response, however the mechanisms behind the activation of the UPR sensors in these contexts is less clear. During bacterial infection by pathogens such as *Pseudomonas syringae*, it has been hypothesized that increased transcription and translation of secretory pathway components required for the cell's

immune system response leads to activation of UPR (Verchot and Pajerowska-Mukhtar 2021). However, treatment of Arabidopsis plants with the biotic stress-hormone salicylic acid (SA) was also shown to activate both arms of the UPR controlled by IRE1 and bZIP28 (Moreno *et al.* 2012, Nagashima *et al.* 2014). Although, the mechanism by which the UPR is activated by SA and microbial pathogens is not well understood, further findings have demonstrated that IRE1a and IRE1b are required to fully establish systemic acquired resistance (SAR) to these microbial pathogens (Nagashima *et al.* 2014). Recent research has also demonstrated that the IRE1-bZIP60 dependent arm of the UPR positively affects infection outcomes of the necrotic fungal pathogen, *Alternaria alternata* in the *Nicotiana attenuata* model (Xu *et al.* 2019). That work demonstrates that the *N. attenuata* homologs of IRE1 and bZIP60 are activated by the defense hormone jasmonic acid (JA) and upregulate UPR chaperones during fungal infection (Xu *et al.* 2019). Whether or not JA upregulation of the UPR is a broadly conserved trait in different plant species has yet to be determined. Overall, the UPR has a clearly demonstrated role in mediating plant-pathogen interactions. However further work is needed to understand what the effects of UPR activation are at the molecular level before this information can be utilized in biotechnological applications.

In addition to the verified activation of the UPR in biotic stress contexts, the UPR is also known to be activated by a wide range of abiotic stresses which can affect plant health. One of the most thoroughly described environmental UPR inducer is heat stress (Duke and Doehlert 1996, Gao *et al.* 2008, Yang *et al.* 2009, Deng *et al.* 2011, Schmollinger *et al.* 2013) which affects the rate at which proteins fold, and negatively affects the productivity of ER protein folding machinery (Dobson 2003). UPR activation in these contexts promotes cell and plant survival (Gao *et al.* 2008, Yang *et al.* 2009, Zhang *et al.* 2017). Extreme osmotic stress, salt stress, and exposure to heavy

metals such as selenium have also been shown to induce some of the downstream effects of the UPR such as increased transcription of the BiP chaperone (Liu *et al.* 2007, Van Hoewyk 2016). Among these heavy metals, cadmium stress was shown to activate both arms of the UPR (Xi *et al.* 2016). In these contexts, growth inhibition of *Arabidopsis* seedlings by cadmium treatment was shown to be a UPR dependent process, as this growth inhibition was rescued in a *bzip60 bzip28* double mutant (Xi *et al.* 2016). Furthermore, cadmium toxicity in *Arabidopsis* was also alleviated by co-treatment with small molecule chemical chaperones which are known to reduce ER stress and prevent protein misfolding (Xi *et al.* 2016). How heavy metal, salt, and osmotic stresses can cause ER stress has yet to be determined, however, these examples suggest that manipulation of the UPR could help to improve plant growth under abiotic stress.

A possible route to activation of the UPR by these biotic and abiotic stresses may lie in novel associations between ER and plastid stress signaling cascades. A forward genetics screen for genes involved in retrograde signaling from chloroplast to nucleus identified the *ceh1* mutation in the 4-hydroxy-3methylbut-2-enyl diphosphate synthase enzyme (Xiao *et al.* 2012). This enzyme is a part of the plastidial methylerythritol phosphate (MEP) pathway, and further study of this mutant demonstrated that the isoprenoid precursor 2-C-methyl-D-erythritol-2,4-cyclopyrophosphate (MEcPP) acts as a retrograde signal during diverse stress responses, including wounding and high light responses (Xiao *et al.* 2012). In these conditions, cellular accumulation of MEcPP activates transcription of JA and SA biosynthesis enzymes in the nucleus (Xiao *et al.* 2012). In later studies, it was demonstrated that the UPR is strongly activated in the *ceh1* mutant in both SA-dependent and SA-independent manners (Benn *et al.* 2016).

This chloroplast-stress related UPR activation was also given further context by the interesting effect of plastid sourced reactive oxygen species (ROS) on the induction of the UPR

(Ozgur *et al.* 2015). It was demonstrated that plastid-originated ROS production induced UPR activation, further suggesting that plastidial stress may be intimately linked with UPR signaling mechanisms (Ozgur *et al.* 2015). Indeed, recent reports have also demonstrated the plant UPR plays a critical role in the response to high light induced singlet oxygen ($^1\text{O}_2$ -), a particularly damaging ROS generated as a by-product of photosynthesis in the chloroplast (Triantaphylidès *et al.* 2008, Xu *et al.* 2017, Beaugelin *et al.* 2020). In a study of the downstream effectors of $^1\text{O}_2$ -, Beaugelin *et al.* (2020) utilized the *chl* Arabidopsis mutant, which carries a mutation in the Chlorophyll A Oxygenase gene and leads to $^1\text{O}_2$ - production in plants treated with high levels of light. Acute treatment of this mutant with high light leads to induction of $^1\text{O}_2$ - dependent cell death (Beaugelin *et al.* 2020). The authors found that when this mutant is treated with acute high light the UPR is activated, as denoted by strong induction of transcriptional markers of both the IRE1 and bZIP28 dependent arms of the UPR, in an SA-dependent manner (Beaugelin *et al.* 2020). Additionally, they found that the *bzip60 bzip28* double mutant was resistant to high light induced cell death suggesting the plant UPR promotes programmed cell death in this context. Accordingly, pretreatment of plants with chemical chaperones known to alleviate ER stress and reduce UPR responses also lead to lower level of damage in high light treated Arabidopsis leaves (Beaugelin *et al.* 2020). However, the authors of this study also noted that mild ER stress and UPR activation had a protective effect in high light conditions. The cell death phenotype of the *chl* mutant can be avoided by gradual acclimation (hereafter referred to as light acclimation) of the *chl* mutant to these conditions prior to acute high light treatment. They found that light acclimation followed by high light treatment led to the selective induction of BiP3 transcription and a lower level of transcription in all other UPR markers compared to the high light treatment alone. Accordingly, they also found that genetic ablation of BiP3 in the *bip3* mutant led to an increase in high light

induced cell death (Beaugelin *et al.* 2020). As increased BiP chaperone levels are an inherent negative regulator of UPR sensor activation, the authors hypothesized that the UPR fulfills a dual role in high light stress, wherein a mild UPR activation is part of the acclimatory response to $^1\text{O}_2$, and intense UPR activation leads to cell death. This example suggests that, similar to UPR targeting in human disease therapy, UPR based biotechnology meant to improve plant growth and stress responses must be carefully designed to limit off target effects.

While researching the UPR in the context of these biotic and abiotic stresses is important to fully understand the endogenous functions of the UPR in plant life, the highly variable nature of secondary stress responses complicates the study of the direct effects of UPR sensors. Therefore, in the lab, chemical UPR inducers such as tunicamycin, which inhibits N-linked glycosylation in the ER lumen, are often used to investigate the UPR by mimicking the conditions associated with environmental stresses that cause the buildup of unfolded proteins in the ER (Welihinda and Kaufman 1996). Furthermore, the biochemical effect of these chemical ER stress inducers is conserved in most eukaryotic model organisms, which allows for comparison of *in vivo* UPR mechanisms between kingdoms.

Functional Diversification of IRE1 Activation and Effects

Although IRE1 is the only UPR sensor found in metazoans, plants, and fungi, in-depth investigations of IRE1 structure have revealed remarkable differences between kingdoms. This is particularly true in the study of biochemical and structural modifications required to activate IRE1 RNase activity. Although very little is known about the plant IRE1 activation mechanism, the mammalian and yeast IRE1s exhibit striking differences in their activation prerequisites and signaling outputs (Figure 1.2; Bashir *et al.* 2021). After being released from BiP chaperones,

mammalian and yeast IRE1 luminal domains interact, bringing the IRE1 cytosolic domains into close proximity (Figure 1.2A, B Step 1; Kimata *et al.* 2007, Amin-Wetzel *et al.* 2017). The cytosolic domains of the mammalian IRE1 then interact and form what is known as a face-to-face dimer. In this formation, the kinase active sites are sufficiently close to the target phosphorylation site on the opposing IRE1 monomer to catalyze the reaction (Figure 1.2A, Step 2; Zhou *et al.* 2006, Oikawa *et al.* 2009). In the next step, trans-autophosphorylation of the mammalian IRE1 leads to a structural conformation shift that forces monomer reorientation into an RNase active back-to-back formation (Figure 1.2A, Step 3; Bashir *et al.* 2021). In contrast, the *S. cerevisiae* IRE1 monomers initially form back-to-back dimers with protein-protein contacts on the RNase subdomains, which do not allow for trans-autophosphorylation. Then these dimers further aggregate into inactive higher-order IRE1 oligomers (Figure 1.2B, Step 2; Kimata *et al.* 2007, Gardner and Walter 2011). Finally, the inactive *S. cerevisiae* IRE1 oligomers require binding of unfolded proteins to their luminal domains, which induces a structural conformation shift allowing for trans-autophosphorylation of nearby IRE1 monomers within the oligomer, leading to RNase activation (Figure 1.2B, Step 3; Kimata *et al.* 2007, Gardner and Walter 2011). In mammalian models activated IRE1 can also aggregate into higher-order oligomers depending upon the severity and duration of ER stress. This oligomerization has also been attributed to unfolded protein binding to the IRE1 luminal domains (Karagöz *et al.* 2017). While the endpoint effect (i.e. RNase activation) is similar between these two models, there are dramatic differences in the RNase signaling outputs between mammalian and *S. cerevisiae* IRE1 (Bashir *et al.* 2021). This is exemplified by the differences between the *in vitro* RNase activity of mammalian and *S. cerevisiae* IRE1. When the cytosolic domain of each IRE1 is heterologously expressed in *E.coli* and incubated with a Förster resonance energy transfer (FRET) RNA substrate, only the mammalian

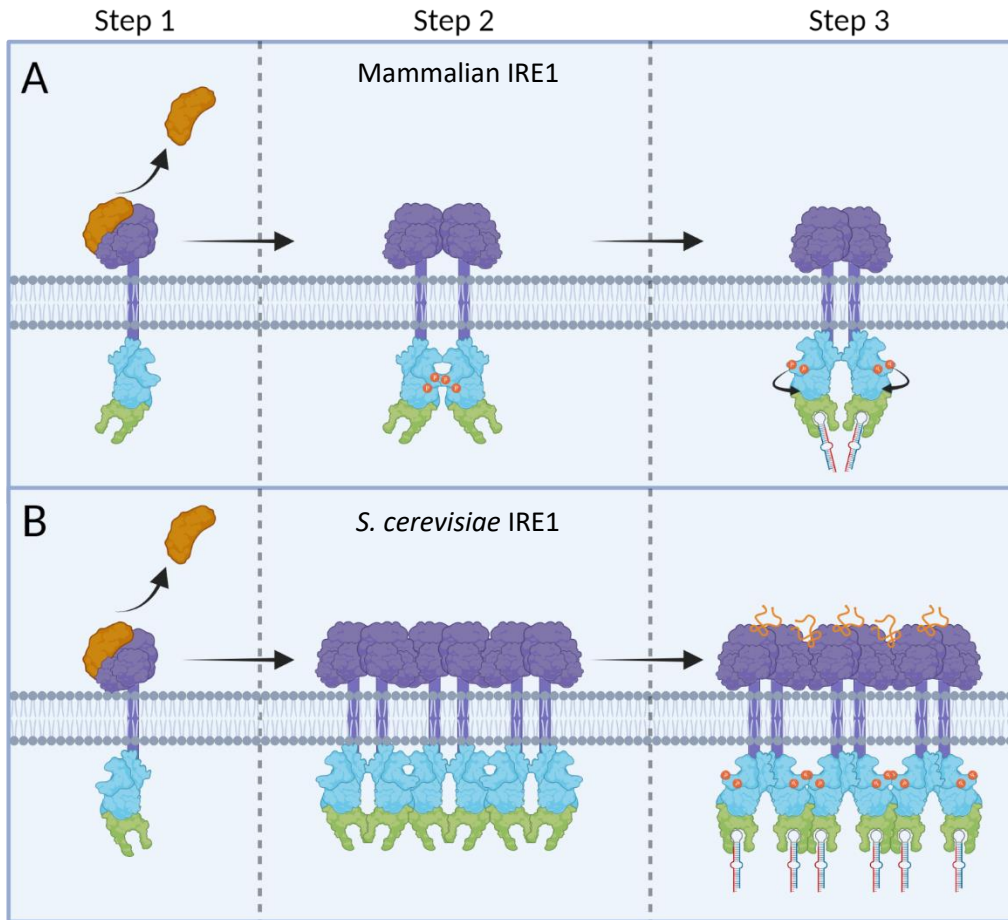


Figure 1.2. Simplified models comparing RNase activation mechanism of mammalian and *S. cerevisiae* IRE1s.

A) After being released from BiP (orange) in Step 1, mammalian IRE1 form a face-to-face dimer allowing trans-autophosphorylation of the kinase domain (cyan) in Step 2. Phosphorylation causes a shift in secondary structure leading to monomer rotation and forming the RNase-active back-to-back dimer in Step 3. **B)** After being released from BiP (orange) in Step 1, *S. cerevisiae* forms back-to-back dimers that cannot autophosphorylate, which then aggregate into higher order oligomers in Step 2. Unfolded proteins then bind the luminal domain, leading to a shift in secondary structure that allows autophosphorylation and subsequent RNase activation.

IRE1 displays constitutive RNase activity at low nanomolar concentrations of enzyme (Cross *et al.* 2012). The *S. cerevisiae* IRE1 requires micromolar concentrations of enzyme and millimolar concentrations of ADP (adenosine diphosphate) and salt to elicit appreciable *in vitro* RNase activity (Wiseman *et al.* 2010). *In vivo* experiments have provided further context to these

observations, by demonstrating that mutations in the *S. cerevisiae* IRE1 that promote a lower activation threshold lead to inhibition of yeast growth under physiological conditions (Bashir *et al.* 2021). This suggest that IRE1 activity may only be required under severe stress in *S. cerevisiae*. Additionally, whereas mammalian IRE1 exhibits XBP1 splicing activity and RIDD activity *in vivo*, the only known function of *S. cerevisiae* IRE1 is splicing of the XBP1 homolog HAC1, as no other mRNA targets have been identified (Bashir *et al.* 2021). However, these differences may be attributable to functional diversification of IRE1 activity within yeasts, as a close relative of *S. cerevisiae*, *S. pombe*, does not have a HAC1 homolog in its genome and exclusively performs RIDD activities under ER stress (Kimmig *et al.* 2012, Maurel *et al.* 2014, Guydosh *et al.* 2017). Whether Arabidopsis and other plant IRE1s exhibit activity closer to mammalian or *S. cerevisiae* IRE1 has yet to be established. Previous results have demonstrated the Arabidopsis IRE1a and IRE1b have RIDD activity similar to the mammalian IRE1, however fluorescent protein labeled IRE1b formed aggregate foci under ER stress when expressed in *S. cerevisiae* similar to the native protein (Mishiba *et al.* 2013, Zhang *et al.* 2016). Characterization of IRE1a and IRE1b *in vitro* activity may help to clarify this point. In Arabidopsis and other Brassicaceae even further work is required to elucidate the function of the divergent IRE1c gene. Although it lacks an ER luminal domain and has several mutations in residues conserved between mammals, yeasts, and plants, this isoform was still found to have essential and overlapping functions with IRE1A and IRE1B (discussed in a later section; Mishiba *et al.* 2019, Pu *et al.* 2019). On the whole, this establishes Arabidopsis as a new frontier in the study of IRE1 functional diversification.

This is further illustrated by a number of studies on the regulatory factors which are upstream of IRE1 activation. In addition to the presence of unfolded client proteins inside the ER, accumulating evidence suggests that other ER resident proteins and chaperones can affect IRE1

activity (Hetz *et al.* 2020). One of those regulators that has been well studied in mammalian models is the ER transmembrane protein Bcl-2 associated X (BAX) inhibitor 1 (BI1), which has a well conserved homolog in Arabidopsis (Kawai-Yamada *et al.* 2001, Chae *et al.* 2003, Kawai-Yamada *et al.* 2004). In mammals, BI1 was found to physically interact with the mammalian IRE1, inhibiting its RNase activity and the pro-survival role of IRE1 under ER stress (Lisbona *et al.* 2009). However, under chronic ER stress the mammalian BI1 also inhibits its namesake factor, the pro-apoptotic BAX, leading to a dual role of BI1 in stress situations. Initial studies of BI1 in Arabidopsis treated with osmotic stress suggested that this role may have been conserved in plants (Kawai-Yamada *et al.* 2001, Chae *et al.* 2003). Upon closer inspection, it was demonstrated that this was not the case, as a loss-of-function mutation in BI1 had no effect on IRE1 mediated splicing of bZIP60 under ER stress conditions (Ruberti *et al.* 2018). In surprising contrast, BI1 was actually found to be a negative regulator of the Arabidopsis ATF6 homolog, bZIP28, as genetic ablation of BI1 in the *bzip28* mutant background partially rescued the ER stress sensitivity of the *bzip28* mutant (Ruberti *et al.* 2018). This suggests that plants have acquired new ways to regulate and fine tune the responses of UPR sensors under ER stress.

Evidence of IRE1 functional diversification is also demonstrated by the different effects of IRE1 RIDD activity in mammals and Arabidopsis. Overall, RIDD is suggested to be a pro-survival process which functions by reducing the abundance of ER client mRNAs under ER stress (Walter and Ron 2011, Maurel *et al.* 2014). However, in mammals RIDD activity has a dual role which can promote cell survival under mild ER stress, but transitions to pro-apoptotic functions in prolonged or severe ER stress situations. In these conditions, mammalian RIDD activity targets a series of micro-RNA (miRNA) transcripts which ordinarily prevent the translation of the pro-apoptotic caspase 2 protease (CASP2; Han *et al.* 2009, Maurel *et al.* 2014). In plants, neither the

miRNAs nor CASP2 are directly conserved. Thus far, what we know about the Arabidopsis IRE1s suggests that their RIDD functionality has strong pro-survival roles (Ruberti *et al.* 2015). This is particularly evident when comparing the differences between the stress responsive phenotypes of the IRE1 and bZIP60 loss-of-function mutants. Germination of the *ire1a ire1b* double mutant seeds on media containing a mere 25 ng/ml of tunicamycin is seedling lethal, while wild type (WT) seedlings are relatively unaffected (Chen and Brandizzi 2012). In these conditions, commonly referred to as chronic ER stress treatment, the *bzip60* mutant has a WT-like phenotype (Chen and Brandizzi 2012). Furthermore, complementation of the *ire1a ire1b* mutant with an RNase dead IRE1b variant did not complement the *ire1a ire1b* ER stress lethality (Deng *et al.* 2013). This therefore suggests that RNase activity other than *bZIP60* splicing is critical to the pro-survival ER stress response in Arabidopsis. Recent investigations have found that a number of Arabidopsis RIDD targets are suppressors of autophagy, leading to the hypothesis that Arabidopsis RIDD activities coordinate upregulation of autophagy during ER stress (Bao *et al.* 2018). On the whole, this demonstrates that the bZIP60-independent functions of IRE1 have a substantial pro-survival impact in Arabidopsis during ER stress situations, and contrasts with mammalian models where XBP1-independent effects have mixed outcomes (Maurel *et al.* 2014), or the *S. cerevisiae* model where IRE1 has no HAC1-independent effects (Bashir *et al.* 2021).

Functional Diversification of UPR Transcription Factors

Similar to IRE1, the core functionality of the ATF6 homologs in mammals and plants is conserved (Liu *et al.* 2007, Ruberti and Brandizzi 2014). However, there are a number of important distinctions between the activation mechanisms of the mammalian ATF6, and Arabidopsis bZIP28 (Pastor-Cantizano *et al.* 2020). In mammals, the accumulation of unfolded proteins leads to the

release of ATF6 by the BiP chaperones, subsequently revealing two Golgi Localization Signals (GLSs) in the ER luminal domain (Shen *et al.* 2002, Schindler and Schekman 2009). A yet unknown cargo receptor then links these signals with the cytosolic coat protein complex II (COPII) forming an association which leads to translocation of ATF6 from the ER to the Golgi via COPII vesicular transport (Nadanaka *et al.* 2004, Schindler and Schekman 2009, Srivastava *et al.* 2012). In contrast, bZIP28 does not have luminal GLS sequences (Srivastava *et al.* 2012). Instead, two dibasic motifs on the cytosolic face of the protein near the transmembrane domain are required for translocation to the Golgi via COPII vesicles (Srivastava *et al.* 2012). Once translocated to the Golgi it was widely assumed that bZIP28 was processed by S1P and S2P proteases, similar to ATF6, due to the conserved S1P and S2P consensus sites (Srivastava *et al.* 2014). However, it was recently demonstrated that the S1P protease does not participate in bZIP28 processing, instead a yet unknown protease was found to remove the ER/Golgi luminal domain from the bZIP28 transmembrane domain (Iwata *et al.* 2017). Due to the conservation of the dibasic trafficking motifs between bZIP28 and bZIP17, it is assumed that the trafficking and proteolytic processing is the same for these two regulators. However, further study is needed to confirm this hypothesis, as recent findings have shown that bZIP17 and bZIP28 do not respond identically to different forms of ER stress (Liu *et al.* 2007, Kim *et al.* 2018). Whereas bZIP28 primarily mediates tunicamycin induced ER chaperone transcription, bZIP17 is the primary contributor to ER chaperone transcription under salt stress conditions (Liu *et al.* 2007, Kim *et al.* 2018). Interestingly, differences in the response to varied cell stresses by these UPR TFs is not regulated exclusively by the factors controlling their release at the ER.

In addition to the primary activation of bZIP17, bZIP28 and bZIP60 at the Golgi and ER, the downstream effects of these UPR TFs are also controlled by their interactions with other

proteins in the nucleus (Figure 1.3). After being translocated, bZIP28 and bZIP60 bind promoter sequences known as the ER Stress Response Elements (ERSE-I 5'-CCAAT-N10-CACG-3') and the Unfolded Protein Response Element-1 (UPRE-I 5'-TGACGTGR-3' ; Liu and Howell 2010). In the nucleus the UPR TFs are assisted by the CCAAT-box-binding TF complex which is conserved between mammals and plants (Liu and Howell 2010). This complex consists of three Nuclear Y Factor (NF-Y) subunits, NF-YA, NF-YB, and NF-YC. In Arabidopsis there are 36 genes encoding NF-Y subfactors, four of which were demonstrated to interact with bZIP28 at the ERSE-I promoter motif (Liu and Howell 2010). Although there is a large potential for differential regulation of bZIP28 target binding based on the number of possible interactions with NF-Y subunits, the overall effect of this interaction in ER stress resistance is yet unknown (Liu and Howell 2010). In order to facilitate the formation of the transcription preinitiation complex at their target binding sites, bZIP28 and bZIP60 must also interact with Ash2 and WDR5 proteins, which are the core components of the COMPASS-like complex (Song *et al.* 2015). This interaction with the COMPASS-like complex directs H3K4me3 deposition onto the promoters of UPR target genes, a crucial step in gene specific transcription (Song *et al.* 2015). While a number of downstream target genes are specific to either bZIP28 or bZIP60, they can also interact with each other in a mechanism conserved between mammals and plants that coordinates UPR transcription for a subset of downstream targets (Liu and Howell 2010, Ruberti and Brandizzi 2014).

Recent research has also revealed a number of interactions between bZIP28 and bZIP60 with plant-specific TFs. These interactions allow for the integration of UPR transcriptional responses with other stress related pathways. Prior to the discovery of UPR involvement with high-light induced PCD (Beaugelin *et al.* 2020), it was found that Arabidopsis seedlings grown under high-light conditions exhibited a marked increase in ER stress sensitivity (Nawkar *et al.*

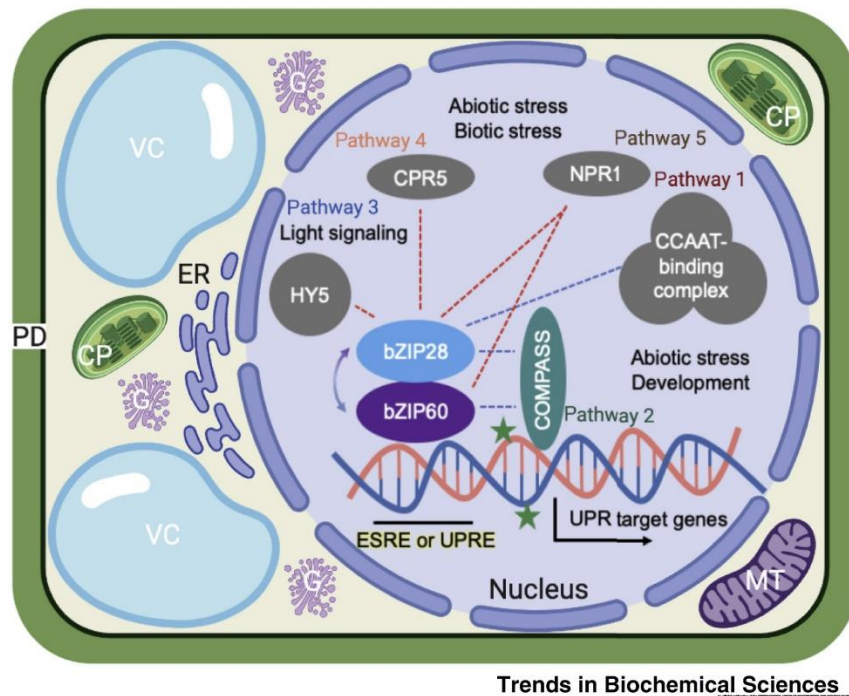


Figure 1.3. The UPR TFs interact with a variety of conserved and plant specific partners to regulate transcription.

This figure was previously published in Pastor-Cantizano *et al.* (2020).

2017). This investigation determined that the causative mechanism was competitive interaction between the UPR and a photoreceptor signaling cascade (Nawkar *et al.* 2017). Another bZIP TF downstream of these photoreceptors, Elongated Hypocotyl 5 (HY5; Osterlund *et al.* 2000), was found to compete with bZIP28 in the binding of ERSE-I promoter motifs, which have overlapping sequence with HY5's target G-box element (CACGTG; Nawkar *et al.* 2017). The physiological relevance of this interaction was demonstrated by a HY5 loss-of-function mutant which exhibited higher expression of UPR marker genes and increased ER stress resistance compared to wild-type *Arabidopsis* plants (Nawkar *et al.* 2017).

Interactions between UPR TFs and nuclear SA signaling have also been described (Nagashima *et al.* 2014). In addition to the previously discussed role of SA in the situational

activation of the UPR response, a number of SA signaling components have also been shown to interact with UPR TFs to fine tune their activities (Nagashima *et al.* 2014, Meng *et al.* 2016, Lai *et al.* 2018). Among these is the constitutive expressor of pathogenesis-related genes-5 (CPR5) a nuclear envelope localized protein which represses SA accumulation under non-stressed conditions to promote growth (Bowling *et al.* 1997). The *cpr5* mutant had constitutively higher UPR transcription, which surprisingly was found to be SA independent (Meng *et al.* 2016). It was found that CPR5 physically interacted with bZIP60 and bZIP28 and repressed their transcriptional activities (Meng *et al.* 2016). As such, the *cpr5* mutant was found to be strongly resistant to chronic ER stress. In addition, bZIP60 and bZIP28 were found to interact with the Nonexpressor of Pathogenesis Related 1 (NPR1) protein (Lai *et al.* 2018). NPR1 is an SA receptor that forms homo-oligomers in the cytosol through interprotein disulfide bonds in an inactive state (Mou *et al.* 2003). Upon SA accumulation or SA treatment, cells first undergo a cytosolic reduction, reducing the NPR1 disulfide bonds and freeing the monomers which are then translocated to the nucleus (Mou *et al.* 2003). Upon SA binding, conformational changes in NPR1 activate the protein, which forms a transcriptional enhancer complex with the TGA2 clade of bZIP transcription factors (Mou *et al.* 2003, Wu *et al.* 2012). ER stress conditions also lead to cytosolic reduction and nuclear translocation of NPR1 in a SA-independent manner (Lai *et al.* 2018). In contrast with its SA receptor function, NPR1 under ER stress interacted with bZIP60 and bZIP28 in the nucleus repressing their activities (Lai *et al.* 2018). As such, the *npr1* loss of function mutant was also strongly resistant to ER stress treatment and exhibited increased transcription of UPR chaperones (Lai *et al.* 2018). On the whole, these collective results demonstrate that the UPR TFs have a strong role in mediating growth and defense trade-offs by integrating UPR functionality with other plant cell signaling mechanisms activated by a diverse set of cell stressors.

FUNCTIONAL DIVERSIFICATION OF THE UPR IN DEVELOPMENT

The UPR is Essential to Multicellular Metazoan Development

In addition to the clear roles of the UPR in adaptation to environmental stress, accumulating evidence suggests that the UPR also makes significant contributions to the normal growth and development of multicellular eukaryotes. Basic models of UPR activation often suggest that UPR regulators are completely inactive under physiological conditions (i.e., in the absence of exogenously applied stress). However, the evidence that complete loss-of-function mutations of UPR sensors in multicellular eukaryotes are lethal under physiological conditions suggests that this may be inaccurate (Mitra and Ryoo 2019). In heterotrophic and autotrophic unicellular model organisms (i.e., *S. cerevisiae* and *Chlamydomonas reinhardtii*) complete loss-of-function mutations in their sole UPR regulator, IRE1, are viable (Nikawa and Yamashita 1992, Yamaoka *et al.* 2018). Given standard culture conditions, both organisms proliferate at WT levels. Only when challenged with nutrient starvation or induced ER stress do these mutants display appreciable growth phenotypes.

In marked contrast, complete loss-of-function mutations of mammalian, *Xenopus* (frog), *Drosophila* (fruit fly), and *Oryzias* (medaka fish) IRE1s are all embryo lethal (Mitra and Ryoo 2019). In each of the models, IRE1 activities were found to be critical to developmental programming of certain tissue types (Mitra and Ryoo 2019). In each case, the tissue specificity and IRE1 mechanism (i.e., XBP1 splicing or RIDD) required for proper development are highly dependent on the organism in question. In mammalian models, IRE1 is required for B cell differentiation (Reimold *et al.* 2000, Reimold *et al.* 2001). In response to antigen detection, pre-B

cells differentiate into antibody secreting plasma cells, which involves secretion of a large quantity of immunoglobulins and a dramatic expansion of ER size (Iwakoshi *et al.* 2003, Van Anken *et al.* 2003). IRE1 dependent activation of XBP1 is necessary to actuate these changes (Iwakoshi *et al.* 2003, Van Anken *et al.* 2003). However, the embryo lethality of both IRE1 and XBP1 knockout mice was commonly traced to liver dysfunction during embryogenesis (Lee *et al.* 2005). Furthermore, liver specific expression of XBP1 in XBP1 knockout lines, also demonstrated a requirement for XBP1 in the development of the pancreatic and salivary glands (Lee *et al.* 2005). While the majority of tissue specific defects in an IRE1 knockout are shared by XBP1 knockouts in mammals, there are also XBP1-independent requirements for IRE1. For example, defects in extraembryonic tissue development (i.e., the placenta) could not be rescued by complementation with a spliced XBP1 isoform (Iwawaki *et al.* 2009). In medaka fish and frogs IRE1 and XBP1 were required for notochord and hatching glad development (Bennett *et al.* 2007, Tanegashima *et al.* 2009). In contrast with mammalian models, which have XBP1-independent roles for IRE1 in development, developmental defects of the IRE1 knockout in medaka fish are entirely rescued by transgene expression of the spliced XBP1 isoform, indicating that in that organism there are no XBP1-independent rolls for IRE1 in development (Ishikawa *et al.* 2017). In *Drosophila* there are both XBP1-dependent and XBP1-independent roles of IRE1 in development, although there has been a particular emphasis on the study of RIDD function in photoreceptor cells of pupal eyes (Coelho *et al.* 2013, Huang *et al.* 2017). In this tissue XBP1 expression is not detectable, instead loss of IRE1 leads to RIDD target accumulation, promoting fatty acid transport and impairment of Rhodopsin-1 trafficking during photoreceptor cell differentiation (Coelho *et al.* 2013). On the whole, these examples demonstrate a strict requirement for at least one facet of IRE1 activity in most metazoan model organisms.

Similar to IRE1, complete loss-of-function mutations in the ATF6 arm of the UPR also exhibit considerable differences in their effect on development of metazoan models. In invertebrate species, there is a single copy of the ATF6 gene which is largely dispensable for UPR gene transcription (Mitra and Ryoo 2019). Although ATF6 in these organisms has not been studied extensively, ATF6 knockouts in *Caenorhabditis elegans*, and *Drosophila* are viable (Mitra and Ryoo 2019). In vertebrates (i.e., mice and medaka fish), single knockouts of either ATF6 α or ATF6 β are viable and fertile, however the double knockout has an early embryo lethal phenotype which is noted for being more severe than other UPR knockouts such as IRE1 or XBP1 (Yamamoto *et al.* 2007, Ishikawa *et al.* 2011, Ishikawa *et al.* 2013). It has been suggested that this is due to the vertebrate ATF6 having an outsized role in the upregulation of ER chaperones and UPR signaling mediators under physiological conditions (Yoshida *et al.* 2001, Yamamoto *et al.* 2008, Ishikawa *et al.* 2013). Overall, this supports the hypothesis that conserved UPR components have been adapted in novel ways by different organisms to perform critical cell functions.

In most of these examples, the cell and tissue types affected by genetic ablation of UPR regulators correspond to tissues with high secretory requirements (Mitra and Ryoo 2019). Experiments in *Drosophila* have provided evidence that endogenous developmental processes were negatively impacting ER proteostasis by increasing levels of unfolded proteins in the ER (Mitra and Ryoo 2019). In these studies, it was shown that an IRE1 which lack unfolded protein sensing abilities was unable to complement the development defects of an IRE1 knockout line suggesting that increased secretory demand was a causative factor. Together, this information demonstrates the essential nature of UPR function to multicellular development, and further suggests that while core UPR mechanisms have been conserved, the relevance of these mechanisms is strongly dependent on the individual organism and tissue contexts.

Physiological Roles of the Plant UPR in Development

Similar to multicellular metazoans, mutations in UPR components also have severe impacts on the growth, development and reproduction of plants. In rice (*Oryza sativa*), there is a single IRE1 homolog, OsIRE1 (Wakasa *et al.* 2012). To understand OsIRE1's role in development, a recent study introduced specific missense mutations in conserved residues in the native OsIRE1 by homologous recombination-based gene targeting (Wakasa *et al.* 2012). This was done in order to overcome the potential lethality of complete loss-of-function mutations. In the first set of transformations, they mutated a conserved lysine residue in the OsIRE1 kinase active site, and in a second set of transformations they mutated a lysine in the RNase active site. From multiple independent transformants, the authors were unable to obtain transformants which were homozygous for the kinase domain mutation, however they were able to obtain transformants for the RNase domain transformation. Furthermore, the RNase domain mutation did not produce any discernable effects on transformant development, despite the verified inability of the mutant OsIRE1 to splice the bZIP60 homolog *OsZIP50* (Wakasa *et al.* 2012). Further investigations have shown that an RNAi knockdown of *OsIRE1* leads to defective shoot, root and reproductive organ growth, while RNAi knockdown of *OsZIP50* had no effect on development (Hayashi *et al.* 2012). Together this suggests that the kinase, and not the RNase activity of OsIRE1 is critical to rice development and reproduction. Although the metazoan IRE1 has downstream mechanisms which are independent of the RNase activity, i.e., the IRE1-TRAF2-JNK signaling axis, whether or not these activities affect metazoan development has yet to be elucidated. As such, determining the RNase-independent role of OsIRE1 in development may help to inform the study of IRE1 in other organisms.

In Arabidopsis there are three copies of the IRE1 gene: IRE1a, IRE1b, and IRE1c which perform partially redundant functions (Mishiba *et al.* 2019, Pu *et al.* 2019). Single mutant phenotypes of each IRE1 gene are identical to WT plants under normal Arabidopsis culture conditions, however high-order mutations cause increasingly severe developmental defects. The *ire1b ire1c* double mutant has a gamete lethal phenotype (Pu *et al.* 2019). Defects in male and female gamete viability were observed (Mishiba *et al.* 2019, Pu *et al.* 2019). The *ire1a ire1b* double mutant reproduces normally, but has a short root phenotype (Chen and Brandizzi 2012). The differences between the double mutant phenotypes are likely to be caused by selective tissue expression of the IRE1 homologs rather than divergent functions of the IRE1 proteins. IRE1c is expressed heavily in reproductive tissues during gametogenesis, whereas IRE1a is more heavily expressed in root tissues; the IRE1b homolog is expressed at a similar level in nearly all tissue types (Koizumi *et al.* 2001, Noh *et al.* 2002, Mishiba *et al.* 2019, Pu *et al.* 2019). Like the *ire1b ire1c* double mutant the *ire1a ire1b ire1c* triple mutant is also gamete lethal (Mishiba *et al.* 2019). However, plants which are heterozygous for *ire1c* and homozygous for *ire1a* and *ire1b* have severe developmental defects in all tissue types (Mishiba *et al.* 2019). How the Arabidopsis IRE1 genes affect growth and development is still unknown. Although functional complementation of the *ire1a ire1b* mutant with kinase-dead and RNase dead mutations have been performed, the growth phenotypes of these complemented lines in the absence of stress has yet to be published (Deng *et al.* 2013). However, loss of function mutations in the Arabidopsis XBP1 homolog bZIP60 do not have any growth or reproductive phenotypes under standard Arabidopsis growth conditions (Nagashima *et al.* 2011, Chen and Brandizzi 2012, Moreno *et al.* 2012). This would indicate that like OsIRE1, the Arabidopsis IRE1s promotes plant growth through an alternative mechanism which is independent of bZIP60. On the whole, these phenotypes suggest that IRE1 performs

critical functions which promote the growth and development of monocot and dicot model plants, although more research is needed to understand whether IRE1 promotes plant growth through alternative RNase activities or kinase dependent activities. Furthermore, how these effects of IRE1 are integrated with other growth and development regulating pathways is also not well understood. It will be interesting to understand how this IRE1- dependent mechanism might be connected with other conserved pathways that regulate eukaryotic growth and development, such as the Target of Rapamycin kinase (Shi *et al.* 2018).

Loss-of-function mutations in the UPR TFs bZIP17 and bZIP28 also have severe effects on Arabidopsis growth and development. The *bzip17 bzip28* double mutant was originally thought to be an unobtainable, lethal mutation. However, after screening thousands of seedlings Kim *et al.* (2018) was able to isolate a viable mutant with extreme growth defects. This *bzip17 bzip28* double mutant was found to have rosettes a third of the size of WT rosettes (Kim *et al.* 2018). When grown in standard sterile culture conditions for 12 days *bzip17 bzip28* roots were a mere 0.5 cm long, compared to almost 7 cm long in the WT background. Although transcriptome analysis of this mutant under normal conditions demonstrated significant dysregulation of genes involved with root growth, it is still unknown which genes are relevant to the growth promoting effects of bZIP17 and bZIP28 (Kim *et al.* 2018). However, in a previous study of the growth defects induced by mutation of the S2P protease which activates these UPR TFs, it was demonstrated that bZIP17 and bZIP28 promote brassinosteroid (BR) hormone signaling (Che *et al.* 2010). The authors found that the *bzip17*, *bzip28*, and the *S2P* single mutants were less sensitive to exogenous BR. Furthermore, the authors demonstrated that expression of a constitutively active bZIP17 and bZIP28 can partially rescue the growth of a BR insensitive 1 (BRI1) mutant allele (Che *et al.* 2010). BRI1 is a plasma membrane (PM) BR receptor (Li and Chory 1997). The specific mutant used in the Che

et al. (2010) study, *bri1-5*, has full BR binding and signaling capabilities, however it is not effectively trafficked to the PM and accumulates in the ER (Hong *et al.* 2008). In contrast with the rescue of *bri1-5* by expression of activated bZIP17/28, expression of a constitutively active bZIP17 and bZIP28 had no effect on the growth of the *bri1-6* allele. In this mutant BRI1 is effectively trafficked to the PM but is defective in BR signaling (Li and Jin 2007). Therefore, Che *et al.* (2010) suggest that the increased level of ER chaperones induced by BZIP17, bZIP28 and S2P, promotes the proper delivery of BRI1 to the PM to affect BR signaling. Whether or not defective BR signaling underlies the severe defects of the *bzip17 bzip28* double mutant remains an exciting topic for future study.

Genetic interactions between the IRE1 and bZIP17/BZIP28 dependent arms of the UPR have also been studied in Arabidopsis by crossing viable UPR mutants (Deng *et al.* 2013, Kim *et al.* 2018, Bao *et al.* 2019). When the *bzip17 bzip28* mutant was crossed with the *bzip60* single mutant, no triple mutants could be obtained (Kim *et al.* 2018). However, plants which were homozygous for *bzip17* and *bzip28*, and heterozygous for *bzip60* had more severe developmental defects than the *bzip17 bzip28* double mutant and were completely sterile (Kim *et al.* 2018). This suggests that the downstream transcriptional regulation performed by bZIP60 and bZIP17/28 have overlapping or compensatory functions in developmental contexts (Kim *et al.* 2018). This is supported by qRT-PCR data which showed a 3-fold increase in the basal levels of *bZIP60* splicing in the *bzip17 bzip28* double mutant in unstressed conditions (Kim *et al.* 2018). bZIP17 and bZIP28 mutants have also been crossed into IRE1 mutant lines. The *ire1a ire1b bzip28* triple mutant was not obtainable in previous studies (Deng *et al.* 2013), however, more recent work has obtained an *ire1a ire1b bzip17* triple mutant, which was found to have a more severe root growth defect than the *ire1a ire1b* double mutant (Bao *et al.* 2019). Although it was not determined if bZIP17 or

bZIP28 were activated as a compensatory mechanism in the *ire1a ire1b* mutant, these studies demonstrate that there may be considerable interactions between the two arms of the UPR in Arabidopsis (Bao *et al.* 2019). Further research is needed to understand whether these interactions are due to convergent regulation of the same genes through alternative mechanisms, or whether separate defects in gene regulation downstream of these UPR sensors has synergistic, negative effects on plant growth.

In addition to the important roles of the core UPR sensors have in promoting plant growth, accumulating evidence suggests that the downstream genes targeted by the UPR also have significant roles in development. One of these targets Arabidopsis Heat Shock Protein 90.7 (HSP90.7), which is highly upregulated under ER stress conditions, was also found to have specific functions in proliferating tissues (Ishiguro *et al.* 2002, Klein *et al.* 2006). The *shd* (*hsp90.7*) knockout mutant is phenotypically identical to *clv*, a mutant defective in CLAVATA signaling (a critical negative modulator of shoot apical meristem activity) indicating that HSP90.7 may be required for plant-specific production of the CLAVATA peptide (Miwa *et al.* 2009, Aichinger *et al.* 2012). Further examples of UPR effectors with plant-specific roles in growth and development can also be found with respect to ERdj3 (ER resident J domain 3) protein function during gametophyte development (Yamamoto *et al.* 2008). J domain proteins (Hsp40) found in the ER lumen bind BiP proteins and stabilize their interactions with unfolded client proteins (Misselwitz *et al.* 1998, Yamamoto *et al.* 2008). ERdj3A, which is induced under ER stress, contains a C-terminal protein disulfide isomerase domain that has reductive capabilities on substrates in vitro (Yang *et al.* 2009), in addition to the canonical HSP40 ATPase activity that these proteins usually possess (Ma *et al.* 2015). This suggests that ERdj3A may act on a plant-specific subset of client proteins and may also have novel protein folding properties. Further *in vivo* analyses of ERdj3A

and its homologs ERdj3B and P58IPK support this possibility by demonstrating their importance in development (Maruyama *et al.* 2014). Indeed, genetic analysis of the mutant Thermosensitive Male Sterile 1 (*tms1*) revealed a nonfunctional allele of ERdj3A, that under elevated temperatures was defective in pollen tube growth (Yang *et al.* 2009). Under normal conditions, in conjunction with P58IPK and ERdj3b, ERdj3A was also shown to mediate polar haploid nuclei fusion in female gametophytes (Maruyama *et al.* 2014) prior to double fertilization. During this nuclear fusion process, the perinuclear ER fuses with the outer nuclear envelope and creates a continuous outer membrane around the two haploid nuclei, which is followed by a second fusion of the inner nuclear membranes (Jensen 1964). Recently it was demonstrated that ERdj3A and P58IPK are required for the fusion of the ER membrane with the outer nuclear membranes. A double knockout (*erdj3a p58ipk*) resulted in seed abortion after fertilization due to aberrant endosperm proliferation, similar to that found in *bip1 bip2* double mutants (Maruyama *et al.* 2010, Maruyama *et al.* 2014). The inner membrane fusion requires the ERdj3B/P58IPK pair, and although the *erdj3b p58ipk* double mutants had unfused haploid nuclei in close proximity, unlike *erdj3a p58ipk*, no aborted seeds were found (Maruyama *et al.* 2014). The developmental defects found in plants with mutant alleles of UPR induced ER-resident proteins (e.g., ERdj, BiP, SHD) are consistent with the evidence that high-order mutations in Arabidopsis IRE1 lead to both male and female gametophyte lethality (Mishiba *et al.* 2019, Pu *et al.* 2019) and with the evidence that the *bzip17 bzip28 bzip60* is sterile (Kim *et al.* 2018). This underscores the need to fully understand the detailed functional mechanisms of downstream UPR components in addition to the core UPR sensors. Although studies exploring the similarities between yeast, mammalian and plant UPR have led to significant advances in plant ER stress research, in order to fully understand the mechanisms connecting the UPR to plant specific physiology it will also be important to look at the contrasting characteristics.

RATIONAL FOR STUDY

The molecular products assembled inside the ER have an ever-expanding relevance to plants under environmental stress and in developmental contexts. Although many open questions still plague the study of the UPR in plants, including the identity of the molecular mechanisms for the activation and de-activation of the master regulator IRE1, the general relevance of the UPR in maintaining ER homeostasis is clear. The ERQC and UPR maintain the folding properties of the ER, and in doing so, enable a wide range of downstream processes from proper heat stress adaptation and defense against pathogens, to root growth. Specifically, the downstream effectors of the UPR have been implicated in transcriptional and post transcriptional regulation of both ER homeostatic genes, and developmental processes. However, new oddities arising in research focusing upstream and downstream of the UPR offer ever expanding possibilities where the UPR may play a defining role in plant physiology. UPR activation in response to plastid metabolic dysfunction and oxidative stress implicates the potential for the UPR to respond in many different signal transduction cascades that utilize ROS as a secondary messenger. Further inquiry exploring the canonical UPR, in non-canonical and tissue-specific contexts, may help elucidate hidden functions and better integrate our understanding of UPR functionality in plant life.

As such, in my dissertation research I examined the roles of the UPR in both stress and developmental contexts. In these studies, I investigate the nature of the relationship between the conserved core UPR sensors and signaling pathways which are specific to plants, or are conserved in eukaryotes but have taken on new functions in Arabidopsis. First, I elucidated the cellular and physiological consequences of ROS generation by conserved NADPH oxidases under ER stress conditions in Chapter II. Second, I explored the functional significance of the UPR in regulation of transcription during spaceflight associated stresses in Chapter III. Third, I demonstrate an

important functional connection between IRE1 and Target of Rapamycin (TOR) signaling in the context of seedling growth and development in Chapter IV. On the whole, these works provide important new information on how the plant UPR is integrated into broader plant signaling pathways and deepen our understanding of how the conserved UPR mechanisms have been adapted by plants to meet the requirements of their unique ecological niche.

REFERENCES

REFERENCES

- Adams C.J., Kopp M.C., Larburu N., Nowak P.R. and Ali M.M.U. (2019). Structure and Molecular Mechanism of ER Stress Signaling by the Unfolded Protein Response Signal Activator IRE1. *Frontiers in Molecular Biosciences* 6(11).
- Aichinger E., Kornet N., Friedrich T. and Laux T. (2012). Plant stem cell niches. *Annual Review of Plant Biology* 63: 615-636.
- Akopian D., Shen K., Zhang X. and Shan S.-o. (2013). Signal recognition particle: an essential protein-targeting machine. *Annual review of biochemistry* 82: 693-721.
- Ali M.M., Bagratuni T., Davenport E.L., Nowak P.R., Silva-Santisteban M.C., Hardcastle A., McAndrews C., Rowlands M.G., Morgan G.J. and Aherne W. (2011). Structure of the Ire1 autophosphorylation complex and implications for the unfolded protein response. *The EMBO journal* 30(5): 894-905.
- Ali M.M.U., Bagratuni T., Davenport E.L., Nowak P.R., Silva-Santisteban M.C., Hardcastle A., McAndrews C., Rowlands M.G., Morgan G.J., Aherne W., Collins I., Davies F.E. and Pearl L.H. (2011). Structure of the Ire1 autophosphorylation complex and implications for the unfolded protein response. *The EMBO journal* 30(5): 894-905.
- Amin-Wetzel N., Saunders R.A., Kamphuis M.J., Rato C., Preissler S., Harding H.P. and Ron D. (2017). A J-protein co-chaperone recruits BiP to monomerize IRE1 and repress the unfolded protein response. *Cell* 171(7): 1625-1637. e1613.
- Bao Y., Bassham D.C. and Howell S.H. (2019). A Functional Unfolded Protein Response Is Required for Normal Vegetative Development. *Plant Physiology* 179(4): 1834-1843.
- Bao Y. and Howell S.H. (2017). The Unfolded Protein Response Supports Plant Development and Defense as well as Responses to Abiotic Stress. *Frontiers in Plant Science* 8(344).
- Bao Y., Pu Y., Yu X., Gregory B.D., Srivastava R., Howell S.H. and Bassham D.C. (2018). IRE1B degrades RNAs encoding proteins that interfere with the induction of autophagy by ER stress in *Arabidopsis thaliana*. *Autophagy* 14(9): 1562-1573.
- Barba-Espín G., Dedvisitsakul P., Hägglund P., Svensson B. and Finnie C. (2014). Gibberellic acid-induced aleurone layers responding to heat shock or tunicamycin provide insight into the N-glycoproteome, protein secretion, and endoplasmic reticulum stress. *Plant Physiology* 164(2): 951-965.
- Bashir S., Banday M., Qadri O., Bashir A., Hilal N., Nida i F., Rader S. and Fazili K.M. (2021). The molecular mechanism and functional diversity of UPR signaling sensor IRE1. *Life Sciences* 265: 118740.

- Beaugelin I., Chevalier A., D'Alessandro S., Ksas B. and Havaux M. (2020). Endoplasmic reticulum-mediated unfolded protein response is an integral part of singlet oxygen signalling in plants. *The Plant Journal* 102(6): 1266-1280.
- Benn G., Bjornson M., Ke H., De Souza A., Balmond E.I., Shaw J.T. and Dehesh K. (2016). Plastidial metabolite MEcPP induces a transcriptionally centered stress-response hub via the transcription factor CAMTA3. *Proc Natl Acad Sci U S A* 113(31): 8855-8860.
- Bennett J.T., Joubin K., Cheng S., Aanstad P., Herwig R., Clark M., Lehrach H. and Schier A.F. (2007). Nodal signaling activates differentiation genes during zebrafish gastrulation. *Developmental biology* 304(2): 525-540.
- Bottomley M.J., Batten M.R., Lumb R.A. and Bulleid N.J. (2001). Quality control in the endoplasmic reticulum: PDI mediates the ER retention of unassembled procollagen C-propeptides. *Current Biology* 11(14): 1114-1118.
- Bowling S.A., Clarke J.D., Liu Y., Klessig D.F. and Dong X. (1997). The *cpr5* mutant of *Arabidopsis* expresses both NPR1-dependent and NPR1-independent resistance. *Plant Cell* 9(9): 1573-1584.
- Buchberger A., Bukau B. and Sommer T. (2010). Protein quality control in the cytosol and the endoplasmic reticulum: brothers in arms. *Molecular cell* 40(2): 238-252.
- Caplan J.L., Zhu X., Mamillapalli P., Marathe R., Anandalakshmi R. and Dinesh-Kumar S.P. (2009). Induced ER chaperones regulate a receptor-like kinase to mediate antiviral innate immune response in plants. *Cell host & microbe* 6(5): 457-469.
- Carvalho H.H., Silva P.A., Mendes G.C., Brustolini O.J., Pimenta M.R., Gouveia B.C., Valente M.A., Ramos H.J., Soares-Ramos J.R. and Fontes E.P. (2014). The endoplasmic reticulum binding protein BiP displays dual function in modulating cell death events. *Plant Physiol* 164(2): 654-670.
- Chae H.-J., Ke N., Kim H.-R., Chen S., Godzik A., Dickman M. and Reed J.C. (2003). Evolutionarily conserved cytoprotection provided by Bax Inhibitor-1 homologs from animals, plants, and yeast. *Gene* 323: 101-113.
- Che P., Bussell J.D., Zhou W., Estavillo G.M., Pogson B.J. and Smith S.M. (2010). Signaling from the Endoplasmic Reticulum Activates Brassinosteroid Signaling and Promotes Acclimation to Stress in *Arabidopsis*. *Science Signaling* 3(141): ra69-ra69.
- Chen Y. and Brandizzi F. (2012). AtIRE1A/AtIRE1B and AGB1 independently control two essential unfolded protein response pathways in *Arabidopsis*. *The Plant Journal* 69(2): 266-277.
- Coelho D.S., Cairrão F., Zeng X., Pires E., Coelho A.V., Ron D., Ryoo H.D. and Domingos P.M. (2013). Xbp1-independent Ire1 signaling is required for photoreceptor differentiation and rhabdomere morphogenesis in *Drosophila*. *Cell reports* 5(3): 791-801.
- Cox J.S., Shamu C.E. and Walter P. (1993). Transcriptional induction of genes encoding endoplasmic reticulum resident proteins requires a transmembrane protein kinase. *Cell* 73(6): 1197-1206.

- Cox J.S. and Walter P. (1996). A Novel Mechanism for Regulating Activity of a Transcription Factor That Controls the Unfolded Protein Response. *Cell* 87(3): 391-404.
- Cross B.C.S., Bond P.J., Sadowski P.G., Jha B.K., Zak J., Goodman J.M., Silverman R.H., Neubert T.A., Baxendale I.R., Ron D. and Harding H.P. (2012). The molecular basis for selective inhibition of unconventional mRNA splicing by an IRE1-binding small molecule. *Proceedings of the National Academy of Sciences* 109(15): E869-E878.
- DENECKE J., EK B., CASPERS M., SINJORGO K.M. and PALVA E.T. (1993). Analysis of sorting signals responsible for the accumulation of soluble reticuloplasmins in the plant endoplasmic reticulum. *Journal of experimental botany*: 213-221.
- Deng Y., Humbert S., Liu J.-X., Srivastava R., Rothstein S.J. and Howell S.H. (2011). Heat induces the splicing by IRE1 of a mRNA encoding a transcription factor involved in the unfolded protein response in *Arabidopsis*. *Proceedings of the National Academy of Sciences* 108(17): 7247-7252.
- Deng Y., Humbert S., Liu J.X., Srivastava R., Rothstein S.J. and Howell S.H. (2011). Heat induces the splicing by IRE1 of a mRNA encoding a transcription factor involved in the unfolded protein response in *Arabidopsis*. *Proc Natl Acad Sci U S A* 108(17): 7247-7252.
- Deng Y., Srivastava R. and Howell S.H. (2013). Protein kinase and ribonuclease domains of IRE1 confer stress tolerance, vegetative growth, and reproductive development in *Arabidopsis*. *Proceedings of the National Academy of Sciences* 110(48): 19633-19638.
- Deng Y., Srivastava R., Quilichini T.D., Dong H., Bao Y., Horner H.T. and Howell S.H. (2016). IRE1, a component of the unfolded protein response signaling pathway, protects pollen development in *Arabidopsis* from heat stress. *The Plant Journal*.
- Dobson C.M. (2003). Protein folding and misfolding. *Nature* 426(6968): 884-890.
- Duke E.R. and Doehlert D.C. (1996). Effects of heat stress on enzyme activities and transcript levels in developing maize kernels grown in culture. *Environmental and experimental botany* 36(2): 199-208.
- Foresti O., Frigerio L., Holkeri H., de Virgilio M., Vavassori S. and Vitale A. (2003). A phaseolin domain involved directly in trimer assembly is a determinant for binding by the chaperone BiP. *Plant Cell* 15(10): 2464-2475.
- Fragkostefanakis S., Mesihovic A., Hu Y. and Schleiff E. (2016). Unfolded protein response in pollen development and heat stress tolerance. *Plant Reprod* 29(1-2): 81-91.
- Gao H., Brandizzi F., Benning C. and Larkin R.M. (2008). A membrane-tethered transcription factor defines a branch of the heat stress response in *Arabidopsis thaliana*. *Proceedings of the National Academy of Sciences* 105(42): 16398-16403.
- Gardner B.M. and Walter P. (2011). Unfolded proteins are Ire1-activating ligands that directly induce the unfolded protein response. *Science* 333(6051): 1891-1894.

- Gou X., Yin H., He K., Du J., Yi J., Xu S., Lin H., Clouse S.D. and Li J. (2012). Genetic evidence for an indispensable role of somatic embryogenesis receptor kinases in brassinosteroid signaling. *PLoS Genet* 8(1): e1002452.
- Gupta D. and Tuteja N. (2011). Chaperones and foldases in endoplasmic reticulum stress signaling in plants. *Plant Signal Behav* 6(2): 232-236.
- Guydosh N.R., Kimmig P., Walter P. and Green R. (2017). Regulated Ire1-dependent mRNA decay requires no-go mRNA degradation to maintain endoplasmic reticulum homeostasis in *S. pombe*. *eLife* 6.
- Halbleib K., Pesek K., Covino R., Hofbauer H.F., Wunnicke D., Hanelt I., Hummer G. and Ernst R. (2017). Activation of the Unfolded Protein Response by Lipid Bilayer Stress. *Mol Cell* 67(4): 673-684 e678.
- Han D., Lerner A.G., Vande Walle L., Upton J.P., Xu W., Hagen A., Backes B.J., Oakes S.A. and Papa F.R. (2009). IRE1 α kinase activation modes control alternate endoribonuclease outputs to determine divergent cell fates. *Cell* 138(3): 562-575.
- Han J. and Kaufman R.J. (2017). Physiological/pathological ramifications of transcription factors in the unfolded protein response. *Genes & Development* 31(14): 1417-1438.
- Harding H.P., Zhang Y. and Ron D. (1999). Protein translation and folding are coupled by an endoplasmic-reticulum-resident kinase. *Nature* 397(6716): 271-274.
- Hartl F.U. and Hayer-Hartl M. (2009). Converging concepts of protein folding in vitro and in vivo. *Nature structural & molecular biology* 16(6): 574.
- Hassler J.R., Scheuner D.L., Wang S., Han J., Kodali V.K., Li P., Nguyen J., George J.S., Davis C. and Wu S.P. (2015). The IRE1 α /XBP1s pathway is essential for the glucose response and protection of β cells. *PLoS Biol* 13(10): e1002277.
- Hayashi S., Wakasa Y., Takahashi H., Kawakatsu T. and Takaiwa F. (2012). Signal transduction by IRE1-mediated splicing of bZIP50 and other stress sensors in the endoplasmic reticulum stress response of rice. *The Plant Journal* 69(6): 946-956.
- Haze K., Yoshida H., Yanagi H., Yura T. and Mori K. (1999). Mammalian Transcription Factor ATF6 Is Synthesized as a Transmembrane Protein and Activated by Proteolysis in Response to Endoplasmic Reticulum Stress. *Molecular biology of the cell* 10(11): 3787-3799.
- Hetz C. and Papa F.R. (2018). The Unfolded Protein Response and Cell Fate Control. *Molecular cell* 69(2): 169-181.
- Hetz C., Zhang K. and Kaufman R.J. (2020). Mechanisms, regulation and functions of the unfolded protein response. *Nature reviews Molecular cell biology* 21(8): 421-438.
- Hollien J., Lin J.H., Li H., Stevens N., Walter P. and Weissman J.S. (2009). Regulated Ire1-dependent decay of messenger RNAs in mammalian cells. *J Cell Biol* 186(3): 323-331.

- Hong Z., Jin H., Tzfira T. and Li J. (2008). Multiple Mechanism-Mediated Retention of a Defective Brassinosteroid Receptor in the Endoplasmic Reticulum of Arabidopsis. *The Plant Cell* 20(12): 3418-3429.
- Huang H.-W., Zeng X., Rhim T., Ron D. and Ryoo H.D. (2017). The requirement of IRE1 and XBP1 in resolving physiological stress during *Drosophila* development. *Journal of Cell Science* 130(18): 3040-3049.
- Hüttner S., Veit C., Schoberer J., Grass J. and Strasser R. (2012). Unraveling the function of *Arabidopsis thaliana* OS9 in the endoplasmic reticulum-associated degradation of glycoproteins. *Plant Molecular Biology* 79(1-2): 21-33.
- Ishiguro S., Watanabe Y., Ito N., Nonaka H., Takeda N., Sakai T., Kanaya H. and Okada K. (2002). SHEPHERD is the Arabidopsis GRP94 responsible for the formation of functional CLAVATA proteins. *The EMBO journal* 21(5): 898-908.
- Ishikawa T., Kashima M., Nagano A.J., Ishikawa-Fujiwara T., Kamei Y., Todo T. and Mori K. (2017). Unfolded protein response transducer IRE1-mediated signaling independent of XBP1 mRNA splicing is not required for growth and development of medaka fish. *eLife* 6: e26845.
- Ishikawa T., Okada T., Ishikawa-Fujiwara T., Todo T., Kamei Y., Shigenobu S., Tanaka M., Saito T.L., Yoshimura J., Morishita S., Toyoda A., Sakaki Y., Taniguchi Y., Takeda S. and Mori K. (2013). ATF6 α/β -mediated adjustment of ER chaperone levels is essential for development of the notochord in medaka fish. *Molecular biology of the cell* 24(9): 1387-1395.
- Ishikawa T., Taniguchi Y., Okada T., Takeda S. and Mori K. (2011). Vertebrate Unfolded Protein Response: Mammalian Signaling Pathways Are Conserved in Medaka Fish. *Cell Structure and Function* 36(2): 247-259.
- Iwakoshi N.N., Lee A.-H., Vallabhajosyula P., Otipoby K.L., Rajewsky K. and Glimcher L.H. (2003). Plasma cell differentiation and the unfolded protein response intersect at the transcription factor XBP-1. *Nature immunology* 4(4): 321-329.
- Iwata Y., Ashida M., Hasegawa C., Tabara K., Mishiba K.-i. and Koizumi N. (2017). Activation of the Arabidopsis membrane-bound transcription factor bZIP28 is mediated by site-2 protease, but not site-1 protease. *The Plant Journal* 91(3): 408-415.
- Iwawaki T., Akai R., Yamanaka S. and Kohno K. (2009). Function of IRE1 alpha in the placenta is essential for placental development and embryonic viability. *Proceedings of the National Academy of Sciences* 106(39): 16657-16662.
- Jensen W.A. (1964). Observations on the fusion of nuclei in plants. *The Journal of cell biology* 23(3): 669-672.
- Jurkin J., Henkel T., Nielsen A.F., Minnich M., Popow J., Kaufmann T., Heindl K., Hoffmann T., Busslinger M. and Martinez J. (2014). The mammalian tRNA ligase complex mediates splicing of XBP1 mRNA and controls antibody secretion in plasma cells. *The EMBO journal* 33(24): 2922-2936.

- Karagöz G.E., Acosta-Alvear D., Nguyen H.T., Lee C.P., Chu F. and Walter P. (2017). An unfolded protein-induced conformational switch activates mammalian IRE1. *eLife* 6: e30700.
- Kaufman R.J. and Malhotra J.D. (2014). Calcium trafficking integrates endoplasmic reticulum function with mitochondrial bioenergetics. *Biochimica et Biophysica Acta (BBA)-Molecular Cell Research* 1843(10): 2233-2239.
- Kawai-Yamada M., Jin L., Yoshinaga K., Hirata A. and Uchimiya H. (2001). Mammalian Bax-induced plant cell death can be down-regulated by overexpression of Arabidopsis Bax Inhibitor-1 (AtBI-1). *Proceedings of the National Academy of Sciences* 98(21): 12295-12300.
- Kawai-Yamada M., Ohori Y. and Uchimiya H. (2004). Dissection of Arabidopsis Bax inhibitor-1 suppressing Bax-, hydrogen peroxide-, and salicylic acid-induced cell death. *Plant Cell* 16(1): 21-32.
- Kim J.-S., Yamaguchi-Shinozaki K. and Shinozaki K. (2018). ER-Anchored Transcription Factors bZIP17 and bZIP28 Regulate Root Elongation. *Plant Physiology* 176(3): 2221-2230.
- Kimata Y., Ishiwata-Kimata Y., Ito T., Hirata A., Suzuki T., Oikawa D., Takeuchi M. and Kohno K. (2007). Two regulatory steps of ER-stress sensor Ire1 involving its cluster formation and interaction with unfolded proteins. *Journal of Cell Biology* 179(1): 75-86.
- Kimmig P., Diaz M., Zheng J., Williams C.C., Lang A., Aragón T., Li H. and Walter P. (2012). The unfolded protein response in fission yeast modulates stability of select mRNAs to maintain protein homeostasis. *eLife* 1: e00048.
- Klein E.M., Mascheroni L., Pompa A., Ragni L., Weimar T., Lilley K.S., Dupree P. and Vitale A. (2006). Plant endoplasmic reticulum supports the protein secretory pathway and has a role in proliferating tissues. *Plant J* 48(5): 657-673.
- Koizumi N., Martinez I.M., Kimata Y., Kohno K., Sano H. and Chrispeels M.J. (2001). Molecular characterization of two Arabidopsis Ire1 homologs, endoplasmic reticulum-located transmembrane protein kinases. *Plant Physiol* 127(3): 949-962.
- Korennykh A.V., Egea P.F., Korostelev A.A., Finer-Moore J., Zhang C., Shokat K.M., Stroud R.M. and Walter P. (2009). The unfolded protein response signals through high-order assembly of Ire1. *Nature* 457(7230): 687-693.
- Lai Y.-S., Renna L., Yarema J., Ruberti C., He S.Y. and Brandizzi F. (2018). Salicylic acid-independent role of NPR1 is required for protection from proteotoxic stress in the plant endoplasmic reticulum. *Proceedings of the National Academy of Sciences*.
- Lee A.H., Chu G.C., Iwakoshi N.N. and Glimcher L.H. (2005). XBP-1 is required for biogenesis of cellular secretory machinery of exocrine glands. *The EMBO journal* 24(24): 4368-4380.
- Lerouxel O., Mouille G., Andème-Onzighi C., Bruyant M.P., Séveno M., Loutelier-Bourhis C., Driouich A., Höfte H. and Lerouge P. (2005). Mutants in DEFECTIVE GLYCOSYLATION, an Arabidopsis homolog of an oligosaccharyltransferase complex subunit, show protein underglycosylation and defects in cell differentiation and growth. *The Plant Journal* 42(4): 455-468.

- Li J. and Chory J. (1997). A putative leucine-rich repeat receptor kinase involved in brassinosteroid signal transduction. *Cell* 90(5): 929-938.
- Li J. and Jin H. (2007). Regulation of brassinosteroid signaling. *Trends Plant Sci* 12(1): 37-41.
- Li J., Wen J., Lease K.A., Doke J.T., Tax F.E. and Walker J.C. (2002). BAK1, an Arabidopsis LRR receptor-like protein kinase, interacts with BRI1 and modulates brassinosteroid signaling. *Cell* 110(2): 213-222.
- Li J., Zhao-Hui C., Batoux M., Nekrasov V., Roux M., Chinchilla D., Zipfel C. and Jones J.D. (2009). Specific ER quality control components required for biogenesis of the plant innate immune receptor EFR. *Proc Natl Acad Sci U S A* 106(37): 15973-15978.
- Light K.M., Wisniewski J.A., Vinyard W.A. and Kieber-Emmons M.T. (2016). Perception of the plant hormone ethylene: known-knowns and known-unknowns. *JBIC Journal of Biological Inorganic Chemistry* 21(5-6): 715-728.
- Lipson K.L., Fonseca S.G., Ishigaki S., Nguyen L.X., Foss E., Bortell R., Rossini A.A. and Urano F. (2006). Regulation of insulin biosynthesis in pancreatic beta cells by an endoplasmic reticulum-resident protein kinase IRE1. *Cell Metabolism* 4(3): 245-254.
- Lisbona F., Rojas-Rivera D., Thielen P., Zamorano S., Todd D., Martinon F., Glavic A., Kress C., Lin J.H., Walter P., Reed J.C., Glimcher L.H. and Hetz C. (2009). BAX Inhibitor-1 Is a Negative Regulator of the ER Stress Sensor IRE1 α . *Molecular cell* 33(6): 679-691.
- Liu J.-X. and Howell S.H. (2010). bZIP28 and NF-Y Transcription Factors Are Activated by ER Stress and Assemble into a Transcriptional Complex to Regulate Stress Response Genes in Arabidopsis. *The Plant Cell* 22(3): 782-796.
- Liu J.-X., Srivastava R., Che P. and Howell S.H. (2007). An Endoplasmic Reticulum Stress Response in Arabidopsis Is Mediated by Proteolytic Processing and Nuclear Relocation of a Membrane-Associated Transcription Factor, bZIP28. *The Plant Cell* 19(12): 4111-4119.
- Liu J.X., Srivastava R., Che P. and Howell S.H. (2007). Salt stress responses in Arabidopsis utilize a signal transduction pathway related to endoplasmic reticulum stress signaling. *The Plant Journal* 51(5): 897-909.
- Ma Z.-X., Leng Y.-J., Chen G.-X., Zhou P.-M., Ye D. and Chen L.-Q. (2015). The THERMOSENSITIVE MALE STERILE 1 Interacts with the BiPs via DnaJ Domain and Stimulates Their ATPase Enzyme Activities in Arabidopsis. *PLoS One* 10(7): e0132500.
- Maruyama D., Endo T. and Nishikawa S.-i. (2010). BiP-mediated polar nuclei fusion is essential for the regulation of endosperm nuclei proliferation in *Arabidopsis thaliana*. *Proceedings of the National Academy of Sciences* 107(4): 1684-1689.
- Maruyama D., Yamamoto M., Endo T. and Nishikawa S.-i. (2014). Different Sets of ER-Resident J-Proteins Regulate Distinct Polar Nuclear-Membrane Fusion Events in *Arabidopsis thaliana*. *Plant and Cell Physiology* 55(11): 1937-1944.

- Maurel M., Chevet E., Tavernier J. and Gerlo S. (2014). Getting RIDD of RNA: IRE1 in cell fate regulation. *Trends in biochemical sciences* 39(5): 245-254.
- Meng Z., Ruberti C., Gong Z. and Brandizzi F. (2016). CPR5 modulates salicylic acid and unfolded protein response to manage tradeoffs between plant growth and stress responses. *The Plant Journal*.
- Mishiba K.-i., Iwata Y., Mochizuki T., Matsumura A., Nishioka N., Hirata R. and Koizumi N. (2019). Unfolded protein-independent IRE1 activation contributes to multifaceted developmental processes in Arabidopsis. *Life science alliance* 2(5).
- Mishiba K.-i., Nagashima Y., Suzuki E., Hayashi N., Ogata Y., Shimada Y. and Koizumi N. (2013). Defects in IRE1 enhance cell death and fail to degrade mRNAs encoding secretory pathway proteins in the Arabidopsis unfolded protein response. *Proceedings of the National Academy of Sciences* 110(14): 5713-5718.
- Misselwitz B., Staack O. and Rapoport T.A. (1998). J proteins catalytically activate Hsp70 molecules to trap a wide range of peptide sequences. *Molecular cell* 2(5): 593-603.
- Mitra S. and Ryoo H.D. (2019). The unfolded protein response in metazoan development. *Journal of Cell Science* 132(5): jcs217216.
- Miwa H., Kinoshita A., Fukuda H. and Sawa S. (2009). Plant meristems: CLAVATA3/ESR-related signaling in the shoot apical meristem and the root apical meristem. *Journal of Plant Research* 122(1): 31-39.
- Moreno A.A., Mukhtar M.S., Blanco F., Boatwright J.L., Moreno I., Jordan M.R., Chen Y., Brandizzi F., Dong X. and Orellana A. (2012). IRE1/bZIP60-mediated unfolded protein response plays distinct roles in plant immunity and abiotic stress responses. *PLoS One* 7(2).
- Mori K., Kawahara T., Yoshida H., Yanagi H. and Yura T. (1996). Signalling from endoplasmic reticulum to nucleus: transcription factor with a basic-leucine zipper motif is required for the unfolded protein-response pathway. *Genes to Cells* 1(9): 803-817.
- Morl K., Ma W., Gething M.-J. and Sambrook J. (1993). A transmembrane protein with a cdc2+ CDC28-related kinase activity is required for signaling from the ER to the nucleus. *Cell* 74(4): 743-756.
- Mou Z., Fan W. and Dong X. (2003). Inducers of Plant Systemic Acquired Resistance Regulate NPR1 Function through Redox Changes. *Cell* 113(7): 935-944.
- Nadanaka S., Yoshida H., Kano F., Murata M. and Mori K. (2004). Activation of mammalian unfolded protein response is compatible with the quality control system operating in the endoplasmic reticulum. *Mol Biol Cell* 15(6): 2537-2548.
- Nagashima Y., Iwata Y., Ashida M., Mishiba K.-i. and Koizumi N. (2014). Exogenous salicylic acid activates two signaling arms of the unfolded protein response in Arabidopsis. *Plant and Cell Physiology* 55(10): 1772-1778.

- Nagashima Y., Iwata Y., Mishiba K.-i. and Koizumi N. (2016). Arabidopsis tRNA ligase completes the cytoplasmic splicing of bZIP60 mRNA in the unfolded protein response. *Biochemical and Biophysical Research Communications* 470(4): 941-946.
- Nagashima Y., Mishiba K.-i., Suzuki E., Shimada Y., Iwata Y. and Koizumi N. (2011). Arabidopsis IRE1 catalyses unconventional splicing of bZIP60 mRNA to produce the active transcription factor. *Scientific reports* 1: 29.
- Nam K.H. and Li J. (2002). BRI1/BAK1, a receptor kinase pair mediating brassinosteroid signaling. *Cell* 110(2): 203-212.
- Nawkar G.M., Kang C.H., Maibam P., Park J.H., Jung Y.J., Chae H.B., Chi Y.H., Jung I.J., Kim W.Y., Yun D.-J. and Lee S.Y. (2017). HY5, a positive regulator of light signaling, negatively controls the unfolded protein response in Arabidopsis. *Proceedings of the National Academy of Sciences* 114(8): 2084-2089.
- Nikawa J.I. and Yamashita S. (1992). IRE1 encodes a putative protein kinase containing a membrane-spanning domain and is required for inositol phototrophy in *Saccharomyces cerevisiae*. *Molecular microbiology* 6(11): 1441-1446.
- Noh S.-J., Kwon C.S. and Chung W.-I. (2002). Characterization of two homologs of Ire1p, a kinase/endoribonuclease in yeast, in *Arabidopsis thaliana*. *Biochimica et Biophysica Acta (BBA) Gene Structure and Expression* 1575(1): 130-134.
- Ohlrogge J. and Browse J. (1995). Lipid biosynthesis. *The Plant Cell* 7(7): 957-970.
- Oikawa D., Kimata Y., Kohno K. and Iwawaki T. (2009). Activation of mammalian IRE1 α upon ER stress depends on dissociation of BiP rather than on direct interaction with unfolded proteins. *Experimental cell research* 315(15): 2496-2504.
- Osterlund M.T., Hardtke C.S., Wei N. and Deng X.W. (2000). Targeted destabilization of HY5 during light-regulated development of Arabidopsis. *Nature* 405(6785): 462-466.
- Özcan U., Cao Q., Yilmaz E., Lee A.-H., Iwakoshi N.N., Özdelen E., Tuncman G., Görgün C., Glimcher L.H. and Hotamisligil G.S. (2004). Endoplasmic reticulum stress links obesity, insulin action, and type 2 diabetes. *Science* 306(5695): 457-461.
- Ozgur R., Uzilday B., Sekmen A.H. and Turkan I. (2015). The effects of induced production of reactive oxygen species in organelles on endoplasmic reticulum stress and on the unfolded protein response in arabidopsis. *Ann Bot* 116(4): 541-553.
- Pastor-Cantizano N., Ko D.K., Angelos E., Pu Y. and Brandizzi F. (2020). Functional Diversification of ER Stress Responses in Arabidopsis. *Trends in biochemical sciences* 45(2): 123-136.
- Pincus D., Chevalier M.W., Aragón T., Van Anken E., Vidal S.E., El-Samad H. and Walter P. (2010). BiP binding to the ER-stress sensor Ire1 tunes the homeostatic behavior of the unfolded protein response. *PLoS Biol* 8(7): e1000415.

- Pu Y., Ruberti C., Angelos E.R. and Brandizzi F. (2019). AtIRE1C, an unconventional isoform of the UPR master regulator AtIRE1, is functionally associated with AtIRE1B in Arabidopsis gametogenesis. *Plant Direct* 3(11): e00187.
- Rao R.V. and Bredesen D.E. (2004). Misfolded proteins, endoplasmic reticulum stress and neurodegeneration. *Current opinion in cell biology* 16(6): 653-662.
- Reimold A.M., Etkin A., Clauss I., Perkins A., Friend D.S., Zhang J., Horton H.F., Scott A., Orkin S.H. and Byrne M.C. (2000). An essential role in liver development for transcription factor XBP-1. *Genes & Development* 14(2): 152-157.
- Reimold A.M., Iwakoshi N.N., Manis J., Vallabhajosyula P., Szomolanyi-Tsuda E., Gravalles E.M., Friend D., Grusby M.J., Alt F. and Glimcher L.H. (2001). Plasma cell differentiation requires the transcription factor XBP-1. *Nature* 412(6844): 300-307.
- Riaz T.A., Junjappa R.P., Handigund M., Ferdous J., Kim H.-R. and Chae H.-J. (2020). Role of Endoplasmic Reticulum Stress Sensor IRE1 α in Cellular Physiology, Calcium, ROS Signaling, and Metaflammation. *Cells* 9(5): 1160.
- Ron D. and Walter P. (2007). Signal integration in the endoplasmic reticulum unfolded protein response. *Nature reviews Molecular cell biology* 8(7): 519-529.
- Roux M., Schwessinger B., Albrecht C., Chinchilla D., Jones A., Holton N., Malinovskiy F.G., Tör M., de Vries S. and Zipfel C. (2011). The Arabidopsis leucine-rich repeat receptor-like kinases BAK1/SERK3 and BKK1/SERK4 are required for innate immunity to hemibiotrophic and biotrophic pathogens. *The Plant Cell* 23(6): 2440-2455.
- Ruberti C. and Brandizzi F. (2014). Conserved and plant-unique strategies for overcoming endoplasmic reticulum stress. *Front Plant Sci* 5: 69.
- Ruberti C., Kim S.-J., Stefano G. and Brandizzi F. (2015). Unfolded protein response in plants: One master, many questions. *Current opinion in plant biology* 27: 59-66.
- Ruberti C., Lai Y.S. and Brandizzi F. (2018). Recovery from temporary endoplasmic reticulum stress in plants relies on the tissue-specific and largely independent roles of bZIP28 and bZIP60, as well as an antagonizing function of BAX-Inhibitor1 upon the pro-adaptive signaling mediated by bZIP28. *Plant Journal* 93(1): 155-165.
- Sawaya R., Schwer B. and Shuman S. (2003). Genetic and biochemical analysis of the functional domains of yeast tRNA ligase. *Journal of Biological Chemistry* 278(45): 43928-43938.
- Schindler A.J. and Schekman R. (2009). In vitro reconstitution of ER-stress induced ATF6 transport in COPII vesicles. *Proceedings of the National Academy of Sciences* 106(42): 17775-17780.
- Schmollinger S., Schulz-Raffelt M., Strenkert D., Veyel D., Vallon O. and Schroda M. (2013). Dissecting the heat stress response in *Chlamydomonas* by pharmaceutical and RNAi approaches reveals conserved and novel aspects. *Mol Plant* 6(6): 1795-1813.

- Schweiger R. and Schwenkert S. (2013). AtTPR7 as part of the Arabidopsis Sec post-translocon. *Plant signaling & behavior* 8(8): e25286.
- Shamu C.E. and Walter P. (1996). Oligomerization and phosphorylation of the Ire1p kinase during intracellular signaling from the endoplasmic reticulum to the nucleus. *The EMBO journal* 15(12): 3028-3039.
- Shen J., Chen X., Hendershot L. and Prywes R. (2002). ER Stress Regulation of ATF6 Localization by Dissociation of BiP/GRP78 Binding and Unmasking of Golgi Localization Signals. *Developmental cell* 3(1): 99-111.
- Shi L., Wu Y. and Sheen J. (2018). "TOR signaling in plants: conservation and innovation." *Development* 145(13): dev160887.
- Shore G.C., Papa F.R. and Oakes S.A. (2011). Signaling cell death from the endoplasmic reticulum stress response. *Current opinion in cell biology* 23(2): 143-149.
- Sinclair A.M. and Elliott S. (2005). Glycoengineering: the effect of glycosylation on the properties of therapeutic proteins. *Journal of pharmaceutical sciences* 94(8): 1626-1635.
- Song Z.-T., Sun L., Lu S.-J., Tian Y., Ding Y. and Liu J.-X. (2015). Transcription factor interaction with COMPASS-like complex regulates histone H3K4 trimethylation for specific gene expression in plants. *Proceedings of the National Academy of Sciences* 112(9): 2900-2905.
- Song Z.-T., Sun L., Lu S.-J., Tian Y., Ding Y. and Liu J.-X. (2015). Transcription factor interaction with COMPASS-like complex regulates histone H3K4 trimethylation for specific gene expression in plants. *Proceedings of the National Academy of Sciences* 112(9): 2900.
- Srivastava R., Chen Y., Deng Y., Brandizzi F. and Howell S.H. (2012). Elements proximal to and within the transmembrane domain mediate the organelle-to-organelle movement of bZIP28 under ER stress conditions. *The Plant Journal* 70(6): 1033-1042.
- Srivastava R., Deng Y. and Howell S. (2014). Stress sensing in plants by an ER stress sensor/transducer, bZIP28. *Frontiers in Plant Science* 5(59).
- Stefani M. and Dobson C.M. (2003). Protein aggregation and aggregate toxicity: new insights into protein folding, misfolding diseases and biological evolution. *Journal of molecular medicine* 81(11): 678-699.
- Steiger M.A., Jackman J.E. and Phizicky E.M. (2005). Analysis of 2'-phosphotransferase (Tpt1p) from *Saccharomyces cerevisiae*: Evidence for a conserved two-step reaction mechanism. *RNA* 11(1): 99-106.
- Tam A.B., Koong A.C. and Niwa M. (2014). Ire1 has distinct catalytic mechanisms for XBP1/HAC1 splicing and RIDD. *Cell reports* 9(3): 850-858.
- Tanegashima K., Zhao H., Rebbert M.L. and Dawid I.B. (2009). Coordinated activation of the secretory pathway during notochord formation in the *Xenopus* embryo. *Development* 136(21): 3543-3548.

- Tateda C., Ozaki R., Onodera Y., Takahashi Y., Yamaguchi K., Berberich T., Koizumi N. and Kusano T. (2008). NtbZIP60, an endoplasmic reticulum-localized transcription factor, plays a role in the defense response against bacterial pathogens in *Nicotiana tabacum*. *Journal of Plant Research* 121(6): 603-611.
- Thuerauf D.J., Marcinko M., Belmont P.J. and Glembotski C.C. (2007). Effects of the Isoform-specific Characteristics of ATF6 α and ATF6 β on Endoplasmic Reticulum Stress Response Gene Expression and Cell Viability*. *Journal of Biological Chemistry* 282(31): 22865-22878.
- Thuerauf D.J., Morrison L. and Glembotski C.C. (2004). Opposing Roles for ATF6 α and ATF6 β in Endoplasmic Reticulum Stress Response Gene Induction*. *Journal of Biological Chemistry* 279(20): 21078-21084.
- Totani K., Ihara Y., Tsujimoto T., Matsuo I. and Ito Y. (2009). The recognition motif of the glycoprotein-folding sensor enzyme UDP-Glc: glycoprotein glucosyltransferase. *Biochemistry* 48(13): 2933-2940.
- Triantaphylidès C., Krischke M., Hoerberichts F.A., Ksas B., Gresser G., Havaux M., Van Breusegem F. and Mueller M.J. (2008). Singlet Oxygen Is the Major Reactive Oxygen Species Involved in Photooxidative Damage to Plants. *Plant Physiology* 148(2): 960-968.
- Urano F., Wang X., Bertolotti A., Zhang Y., Chung P., Harding H.P. and Ron D. (2000). Coupling of stress in the ER to activation of JNK protein kinases by transmembrane protein kinase IRE1. *Science* 287(5453): 664-666.
- Urta H., Dufey E., Avril T., Chevet E. and Hetz C. (2016). Endoplasmic reticulum stress and the hallmarks of cancer. *Trends in cancer* 2(5): 252-262.
- Van Anken E., Romijn E.P., Maggioni C., Mezghrani A., Sitia R., Braakman I. and Heck A.J. (2003). Sequential waves of functionally related proteins are expressed when B cells prepare for antibody secretion. *Immunity* 18(2): 243-253.
- Van Hoewyk D. (2016). Defects in endoplasmic reticulum-associated degradation (ERAD) increase selenate sensitivity in *Arabidopsis*. *Plant Signal Behav*: 0.
- Verchot J. and Pajerowska-Mukhtar K.M. (2021). UPR signaling at the nexus of plant viral, bacterial, and fungal defenses. *Current Opinion in Virology* 47: 9-17.
- Vitale A. and Denecke J. (1999). The endoplasmic reticulum—Gateway of the secretory pathway. *The Plant Cell* 11(4): 615-628.
- Volmer R., van der Ploeg K. and Ron D. (2013). Membrane lipid saturation activates endoplasmic reticulum unfolded protein response transducers through their transmembrane domains. *Proceedings of the National Academy of Sciences* 110(12): 4628-4633.
- Wakasa Y., Hayashi S., Ozawa K. and Takaiwa F. (2012). Multiple roles of the ER stress sensor IRE1 demonstrated by gene targeting in rice. *Scientific reports* 2(1): 944.
- Wallin E. and Heijne G.V. (1998). Genome-wide analysis of integral membrane proteins from eubacterial, archaean, and eukaryotic organisms. *Protein Science* 7(4): 1029-1038.

- Walter P. and Ron D. (2011). The Unfolded Protein Response: From Stress Pathway to Homeostatic Regulation. *Science* 334(6059): 1081.
- Wang J.-M., Qiu Y., Yang Z., Kim H., Qian Q., Sun Q., Zhang C., Yin L., Fang D. and Back S.H. (2018). IRE1 α prevents hepatic steatosis by processing and promoting the degradation of select microRNAs. *Science Signaling* 11(530).
- Wang X.Z., Harding H.P., Zhang Y., Jolicoeur E.M., Kuroda M. and Ron D. (1998). Cloning of mammalian Ire1 reveals diversity in the ER stress responses. *The EMBO journal* 17(19): 5708-5717.
- Welihinda A.A. and Kaufman R.J. (1996). The unfolded protein response pathway in *Saccharomyces cerevisiae*: oligomerization and trans-phosphorylation of Ire1p (Ern1p) are required for kinase activation. *Journal of Biological Chemistry* 271(30): 18181-18187.
- Wilkinson B. and Gilbert H.F. (2004). Protein disulfide isomerase. *Biochimica et Biophysica Acta (BBA)-Proteins and Proteomics* 1699(1-2): 35-44.
- Wiseman R.L., Zhang Y., Lee K.P., Harding H.P., Haynes C.M., Price J., Sicheri F. and Ron D. (2010). Flavonol activation defines an unanticipated ligand-binding site in the kinase-RNase domain of IRE1. *Mol Cell* 38(2): 291-304.
- Wu Y., Zhang D., Chu Jee Y., Boyle P., Wang Y., Brindle Ian D., De Luca V. and Després C. (2012). The Arabidopsis NPR1 Protein Is a Receptor for the Plant Defense Hormone Salicylic Acid. *Cell reports* 1(6): 639-647.
- Xi H., Xu H., Xu W., He Z., Xu W. and Ma M. (2016). A SAL1 Loss-of-Function Arabidopsis Mutant Exhibits Enhanced Cadmium Tolerance in Association with Alleviation of Endoplasmic Reticulum Stress. *Plant and Cell Physiology* 57(6): 1210-1219.
- Xiang Y., Sun X., Gao S., Qin F. and Dai M. (2016). Deletion of an endoplasmic reticulum stress response element in a ZmPP2C-A gene facilitates drought tolerance of maize seedlings. *Molecular Plant*.
- Xiao Y., Savchenko T., Baidoo Edward E.K., Chehab Wassim E., Hayden Daniel M., Tolstikov V., Corwin Jason A., Kliebenstein Daniel J., Keasling Jay D. and Dehesh K. (2012). Retrograde Signaling by the Plastidial Metabolite MEcPP Regulates Expression of Nuclear Stress-Response Genes. *Cell* 149(7): 1525-1535.
- Xu J., Tran T., Padilla Marcia C.S., Braun D.M. and Goggin F.L. (2017). Superoxide-responsive gene expression in *Arabidopsis thaliana* and *Zea mays*. *Plant Physiology and Biochemistry* 117: 51-60.
- Xu Z., Song N., Ma L. and Wu J. (2019). IRE1-bZIP60 Pathway Is Required for *Nicotiana attenuata* Resistance to Fungal Pathogen *Alternaria alternata*. *Frontiers in Plant Science* 10(263).
- Yamamoto K., Sato T., Matsui T., Sato M., Okada T., Yoshida H., Harada A. and Mori K. (2007). Transcriptional Induction of Mammalian ER Quality Control Proteins Is Mediated by Single or Combined Action of ATF6 and XBP1. *Developmental cell* 13(3): 365-376.

- Yamamoto M., Maruyama D., Endo T. and Nishikawa S.-i. (2008). *Arabidopsis thaliana* has a set of J proteins in the endoplasmic reticulum that are conserved from yeast to animals and plants. *Plant and Cell Physiology* 49(10): 1547-1562.
- Yamaoka Y., Choi B.Y., Kim H., Shin S., Kim Y., Jang S., Song W.-Y., Cho C.H., Yoon H.S., Kohno K. and Lee Y. (2018). Identification and functional study of the ER stress sensor IRE1 in *Chlamydomonas reinhardtii*. *The Plant Journal*: n/a-n/a.
- Yamaoka Y., Choi B.Y., Kim H., Shin S., Kim Y., Jang S., Song W.Y., Cho C.H., Yoon H.S. and Kohno K. (2018). Identification and functional study of the endoplasmic reticulum stress sensor IRE 1 in *Chlamydomonas reinhardtii*. *The Plant Journal* 94(1): 91-104.
- Yang K.Z., Xia C., Liu X.L., Dou X.Y., Wang W., Chen L.Q., Zhang X.Q., Xie L.F., He L., Ma X. and Ye D. (2009). A mutation in Thermosensitive Male Sterile 1, encoding a heat shock protein with DnaJ and PDI domains, leads to thermosensitive gametophytic male sterility in *Arabidopsis*. *Plant J* 57(5): 870-882.
- Ye J., Rawson R.B., Komuro R., Chen X., Davé U.P., Prywes R., Brown M.S. and Goldstein J.L. (2000). ER Stress Induces Cleavage of Membrane-Bound ATF6 by the Same Proteases that Process SREBPs. *Molecular cell* 6(6): 1355-1364.
- Yoshida H., Matsui T., Yamamoto A., Okada T. and Mori K. (2001). XBP1 mRNA Is Induced by ATF6 and Spliced by IRE1 in Response to ER Stress to Produce a Highly Active Transcription Factor. *Cell* 107(7): 881-891.
- Zhang K., Wang S., Malhotra J., Hassler J.R., Back S.H., Wang G., Chang L., Xu W., Miao H. and Leonardi R. (2011). The unfolded protein response transducer IRE1 α prevents ER stress-induced hepatic steatosis. *The EMBO journal* 30(7): 1357-1375.
- Zhang L., Chen H., Brandizzi F., Verchot J. and Wang A. (2015). The UPR branch IRE1-bZIP60 in plants plays an essential role in viral infection and is complementary to the only UPR pathway in yeast. *PLoS genetics* 11(4).
- Zhang L., Zhang C. and Wang A. (2016). Divergence and Conservation of the Major UPR Branch IRE1-bZIP Signaling Pathway across Eukaryotes. *Scientific reports* 6(1): 27362.
- Zhang S.-S., Yang H., Ding L., Song Z.-T., Ma H., Chang F. and Liu J.-X. (2017). Tissue-specific transcriptomics reveals an important role of the unfolded protein response in maintaining fertility upon heat stress in *Arabidopsis*. *The Plant Cell* 29(5): 1007-1023.
- Zhou J., Liu C.Y., Back S.H., Clark R.L., Peisach D., Xu Z. and Kaufman R.J. (2006). The crystal structure of human IRE1 luminal domain reveals a conserved dimerization interface required for activation of the unfolded protein response. *Proc Natl Acad Sci U S A* 103(39): 14343-14348.

CHAPTER II
NADPH OXIDASE ACTIVITY IS REQUIRED FOR ER STRESS
SURVIVAL IN PLANTS

The work presented in this chapter has been published in *The Plant Journal*:

Angelos E, Brandizzi F. (2018) NADPH oxidase activity is required for ER stress survival in plants. *Plant Journal*. 96(6):1106-1120.

ABSTRACT

In all eukaryotes, the unfolded protein response (UPR) relieves endoplasmic reticulum (ER) stress, which is a potentially lethal condition caused by the accumulation of misfolded proteins in the ER. In mammalian and yeast cells, reactive oxygen species (ROS) generated during ER stress attenuate the UPR, negatively impacting cell survival. In plants, the relationship between the UPR and ROS is less clear. Although ROS develop during ER stress, the sources of ROS linked to ER stress responses and the physiological impact of ROS generation on the survival from proteotoxic stress are yet unknown. Here we show that in *Arabidopsis thaliana* the respiratory burst oxidase homologs, RBOHD and RBOHF, contribute to the production of ROS during ER stress. We also demonstrate that during ER stress RBOHD and RBOHF are necessary to properly mount the adaptive UPR and overcome temporary and chronic ER stress situations. These results ascribe a cytoprotective role to RBOH-generated ROS in the defense from proteotoxic stress in an essential organelle, and support a plant-specific feature of the UPR management among eukaryotes.

INTRODUCTION

Physiological and stress situations causing insufficiency of the endoplasmic reticulum (ER) to meet cellular demands for secretory protein folding lead to a potentially lethal condition, known as ER stress (Gething *et al.* 1992). To overcome ER stress and restore homeostasis, protective signaling cascades, collectively called the unfolded protein response (UPR), originate at the ER and lead to the synthesis of ER chaperones and foldases to attenuate ER stress. If this adaptive UPR fails, such as in conditions of unresolved or chronic ER stress, cells commit to programmed cell death (Ron *et al.* 2007, Ruberti *et al.* 2015, Angelos *et al.* 2017). In all eukaryotes, the adaptive phase of the UPR is initiated with the activation of IRE1, an ER-associated membrane kinase and ribonuclease, which catalyzes the unconventional splicing of transcripts of bZIP-transcription factors: yeast Hac1, mammalian Xbp1, or plant bZIP60. This step is necessary for the production of an active transcription factor that controls the expression of UPR target genes (Deng *et al.* 2011, Nagashima *et al.* 2011, Moreno *et al.* 2012). In multicellular eukaryotes, the UPR has expanded to include additional UPR effectors, such as membrane tethered bZIP transcription factors (MTTFs), namely mammalian ATF6 and plant bZIP28. Upon sensing ER stress, these MTTFs translocate to the Golgi, where the cytosol-exposed transcription factor domain is proteolytically removed from the transmembrane anchor and translocated to the nucleus for the transcriptional regulation of UPR target genes (Liu *et al.* 2007b, Gao *et al.* 2008, Srivastava *et al.* 2013, Sun *et al.* 2013).

In metazoan cells, a third arm of the UPR is activated by the ER associated PKR-like ER kinase (PERK) protein, which oligomerizes and autophosphorylates in conditions of ER stress. PERK activity results in the phosphorylation and inactivation of the eukaryotic translation initiation

factors eIF2A thereby promoting a global repression of the rate of the protein translation (Harding *et al.* 1999, Shen *et al.* 2002). The transcription factors ATF4 and Nrf2 downstream of PERK are able to escape this translational repression and upregulate an oxidative stress response through the production of antioxidant proteins (Harding *et al.* 2000, Cullinan *et al.* 2003). Indeed, mutations in PERK signaling markedly increase the generation of reactive oxygen species (ROS), which negatively affect UPR efficiency and the ability of cells to survive ER stress (Marciniak *et al.* 2004, Back *et al.* 2009, Han *et al.* 2013, Maity *et al.* 2016). In yeast, which similarly to plants lack PERK, a dysregulated production of H₂O₂ under ER stress results in a translational attenuation of ER stress genes (Maity *et al.* 2016). Therefore, in metazoans and yeast, ROS cause attenuation of the cytoprotective functions of the UPR and acceleration of responses leading to cell death. In humans, this process potentiates the development of multiple diseases including diabetes, neurodegenerative diseases, and atherosclerosis (Malhotra *et al.* 2007).

In plants, a functional connection between ROS and the UPR management has not yet been clearly defined. During growth and in conditions of stress, several organelles including the mitochondria, chloroplasts, and peroxisomes generate ROS (Tripathy *et al.* 2012). ROS are also produced in the apoplast mainly by the activity of the membrane-bound NADPH Oxidase (NOX) enzymes, known in plants as respiratory burst oxidase homologues (RBOH) (Torres *et al.* 2002). The NOX/RBOH enzymes generate O₂⁻ through electron transfer from NADPH to oxygen (Gapper *et al.* 2006). O₂⁻ is highly reactive and is dismutated to H₂O₂ either via the superoxide dismutase (SOD) enzymes or spontaneously (Mori *et al.* 2004). H₂O₂ is more stable than O₂⁻ and moves through membranes via aquaporins (Bienert *et al.* 2007), and it is therefore considered as a potent signaling ROS in plants (Sadhukhan *et al.* 2017). Thus far in plants, an increase of soluble H₂O₂ and lipid peroxidation during ER stress have been reported (Ozgur *et al.* 2014, Ozgur *et al.* 2015,

Ozgur *et al.* 2018) but the source of ROS during ER stress and the influence of ER-stress generated ROS on UPR signaling are not yet established. The oxidative function of ERO1 (ER oxidoreductin 1) in the ER lumen is a significant source of ER peroxides both in homeostatic conditions of growth and during ER stress; however, an increase in NADPH Oxidase activity has also been observed via biochemical assays during the early UPR (Tu *et al.* 2004, Sevier *et al.* 2008, Zito 2015, Ozgur *et al.* 2018). Under similar conditions, small inductions in transcript levels of RBOHD and RBOHF, two plasma membrane-localized NADPH Oxidases (Torres *et al.* 2002, Torres *et al.* 2005), were also noted in tissues subjected to ER stress treatment, leading to the suggestion that increases in ROS levels were due to the respiratory burst oxidase homologs D and F (RBOHD and RBOHF) (Ozgur *et al.* 2014). Nonetheless, it is yet to be experimentally tested to what extent RBOH activity contributes to the ROS levels during ER stress, and whether these enzymes are necessary for the actuation of effective ER stress responses. More generally, the downstream effects of increased ROS levels during plant ER stress responses are also largely unmapped. Previous reports have shown a variable regulation of the antioxidant defense systems under conditions of ER stress. For example, in conditions of ER stress the O₂⁻ scavenging activity of superoxide dismutase is induced in roots, but down-regulated in shoots. Conversely, H₂O₂ scavenging activities of catalase and ascorbate peroxidase are upregulated in shoots but have no change in roots (Ozgur *et al.* 2014). However, in both roots and shoots a significantly increased glutathione content and glutathione reductase activity during ER stress lends weight to the conclusion that antioxidant defenses are upregulated to manage the increased ROS production in ER stress (Ozgur *et al.* 2014). Nonetheless, critical questions remain unanswered. For example, it is yet unknown what effects an increase in ROS levels may have on the adaptive UPR, nor is it understood whether ROS may contribute to life or death decisions in temporary and chronic ER

stress. To address these fundamental questions, in this work we explored the functional connection between ROS and the UPR in plants. We demonstrate that O_2^- and H_2O_2 are significantly contributed by RBOHD and RBOHF during ER stress. We also show that RBOHD and RBOHF elicit a transcriptional response to ROS during ER stress in the adaptive UPR. Furthermore, we provide evidence for a stringent requirement of RBOHD and RBOHF to prevent the progression of cell death in recovery from temporary ER stress and under chronic ER stress. Together, these findings support a positive role of superoxide signaling in potentiating the cell's ability to survive temporary and chronic ER stress and ascribe a significant role to two RBOH proteins in this process.

MATERIALS AND METHODS

Plant Materials and Growth Conditions

Arabidopsis thaliana ecotype Columbia (Col-0), *rboh1 rboh2*, (Torres *et al.* 2002) *ire1a ire1b*, and *bzip60 bzip28* (Chen *et al.* 2012, Deng *et al.* 2013) plants were used in this study. For all experiments, surface-sterilized seeds were plated directly onto petri dishes containing half-strength Linsmaier and Skoog ($\frac{1}{2}$ LS) medium, 1.0% w/v sucrose, and 1.0% agar and then cold treated (4°C) in the dark for 2 days to synchronize germination. Plates were then transferred to a Percival growth chamber and incubated for the indicated time at 21°C under continuous light (130 μ E).

Superoxide Histochemical Staining and Quantification

WT or *rboh1 rboh2* seedlings were grown vertically on for 7 days, and then transferred to $\frac{1}{2}$ LS media containing 1.0 μ g/ml Tm, 1.0 μ g/ml TM + 2.5 μ M DPI, or DMSO and allowed to grow for a further 24 or 48 hours (hr) in the growth chamber. Whole seedlings were used for the subsequent Nitro Tetrazolium Blue (NBT) staining which took place at the same time on each day. NBT was dissolved to a concentration of 1 mg/ml in 20 mM HEPES pH 6.1, and protected from light until used. To reduce the inherent variability created by staggered staining of the seedlings for very short incubation periods, all experimental groups were treated with NBT solution at the same time. To do so, six 60 mm Petri dishes containing 2 ml of ddH₂O were prepared. Fifteen individuals from each genotype/treatment were then transferred to separate dishes with forceps. Once all seedlings were transferred, 15 ml of NBT solution was added to each dish and covered

for 15 minutes (min). For each plate, the NBT solution was quickly removed with a seriological pipette and replaced with ~20 ml of ddH₂O to remove excess NBT. Restarting at the first dish, the ddH₂O was then removed, and seedlings were submerged in 95-100% ethanol for 10 min to fix the root tissues. Seedlings were then mounted on slides in a 1:1 ethanol:glycerol solution with a coverslip covering just the roots. Images were obtained using the microscope function of an Olympus Tough F2.0 camera outfitted with ring LED light guide. Over a white surface, slides were placed on a 60 mm Petri dish marked with a reference distance. The slide and 60 mm dish were then placed in the center of a 100 mm square Petri dish and covered with the lid. The camera was placed directly on the square lid for imaging to ensure consistent distance from the subject. Three independent experiments were performed with similar results.

To quantify the stain intensity along the root, unedited images were converted to 32 bit black and white in ImageJ. Beginning at the root apex, pixel intensities were recorded along a traced line segment (1000 individual measurements). The same line traces were then moved immediately left or right of the root and background pixel intensities were recorded. For each root, relative pixel stain intensity was calculated by subtracting the background value from the original trace value. For each experimental group the relative stain intensity from 8 roots was averaged and standard error calculated. Three independent experiments were performed with similar results.

Extraction and Quantification of H₂O₂ in Seedling Tissues using Amplex Ultra Red

Two H₂O₂ extraction methods described previously (Chakraborty *et al.* 2016, Le *et al.* 2016) were tested: 1) phosphate buffer (K₂HPO₄, 20 mM pH 6.5) and 2) neutralized Trichloroacetic Acid (TCA). For phosphate buffer extractions, 200 µl was added to frozen tissue

then briefly vortexed. Samples were then centrifuged at 21000 $\times g$ and 4°C for 20 min to ensure plant debris was pelleted then used immediately for H₂O₂ quantification. NTCA extractions were performed as follows: ten percent trichloroacetic acid (TCA), and 1 M sodium bicarbonate solutions were prepared and kept on ice. Two hundred microliters of 10% TCA was added to still frozen samples on ice and briefly vortexed until mixture was homogenous and centrifuged at 21000 $\times g$ and 4°C for 20 min. In separate microcentrifuge tubes 86.6 μl of sodium bicarbonate solution was aliquoted and 150 μl of the centrifuged 10% TCA supernatant extract was added to bicarbonate containing tubes on ice. Any pink coloration due anthocyanin content in extracts should change to a dark blue hue after neutralization. One hundred microliters of the neutralized supernatants were arranged in 96 well plates on ice, to allow for sample transfer to assay with a multichannel pipette.

A working solution of catalase was prepared by centrifuging 10 μl of ammonium sulfate catalase suspension (Sigma, C3515-10MG). The clear ammonium sulfate supernatant was then removed before catalase pellet was dissolved in 600 μl of ddH₂O. Five microliters of catalase working solution was then added to the remaining neutralized sample extracts in microcentrifuge tubes. These samples were incubated at room temperature for a minimum of 10 min. One hundred microliters of the catalase treated supernatants were then stored in the same 96 well plate on ice.

An H₂O₂ standard curve was prepared by serial dilution of 30% H₂O₂ to concentrations of 100 μM , 50 μM 25 μM 10 μM and 5 μM which were then diluted 10x (from 50 microliter aliquots) by sequential addition of 200 μl of 10% TCA, 122 μl of 1M sodium bicarbonate and 128 μl of ddH₂O to mimic extraction procedure. Final concentrations of H₂O₂ standards therefore ranged from 10 μM to 0.5 μM . NTCA extraction resulted in no net loss of H₂O₂. H₂O₂ standards were prepared fresh daily.

Amplex Ultra Red (AUR) working solution was prepared by dissolving one vial of AUR in 340 μ l of DMSO per manufacturer's instructions to make a 10 mM AUR stock. AUR assay solutions were prepared immediately before use. Fifty microliters of AUR stock was added to 10 ml of ddH₂O containing 5 μ g/ml commercial horseradish peroxidase (AUR-HRP) and to another 10 ml of ddH₂O without HRP (AUR-NoHRP). Solutions were kept on ice and protected from light. All assays were performed in clear 96 well microplates and prepared on a cold block. Twenty five microliters of neutralized samples and catalase treated samples were always pipetted prior to addition of 75 μ l of the appropriate AUR assay solution by multichannel pipette. The plate was then briefly incubated (5 min) at room temperature in the dark. Longer incubation periods did not lead to greater differences between catalase treated samples and untreated samples, only increases in AUR chemical auto-oxidation. The microplates were read using a SpectramaxM2 (Molecular Devices) equipped with fluorescence detection capabilities. The excitation wavelength was set to 544 nm, and emission was recorded at 590 nm.

Experiments were performed to test the effectiveness of extraction procedures, dose response, and catalase treatment (Figure 1.2A,B,C). WT seedlings (~2g) were ground in a mortar with liquid nitrogen, to a fine powder and separated into triplicate 40, 30, 20, or 10 mg aliquots. Extraction procedures were performed as described above and assayed with AUR-HRP or AUR-NoHRP as indicated.

To assay H₂O₂ accumulation under ER stress conditions WT, *rboh*d *rboh*f, *ire1*a *ire1*b, and *bzip*60 *bzip*28 were grown for 7 days and transferred to plates containing 1.0 μ g/ml Tm or DMSO for 6, 24, or 48 hr as indicated, and harvested at the same time on consecutive days. Three biological replicates consisting of approximately 30-60 mg of seedling tissue each were briefly dried on a Kimwipe and exact fresh weight recorded before samples were placed in 1.7 ml

microcentrifuge tubes with two glass beads, and frozen in liquid nitrogen. Samples were ground to a fine powder in a Retch MM301 (Retch; Haan, Germany) by agitation at a frequency of 30/second (sec) for two sets of 30 sec which were separated by refreezing in liquid nitrogen and stored in liquid nitrogen. Samples were extracted with NTCA, and then treated with catalase as indicated. For each biological replicate the neutralized samples and catalase samples were assayed in two technical replicates in the same plate with a standard curve. Each genotype was assayed in a separate plate. The catalase labile signal was calculated by subtracting average fluorescence intensity of catalase treated replicates from the average fluorescence intensity of the neutralized sample replicates. The samples were compared to the individual H₂O₂ standard curves to derive an [H₂O₂] of the samples, and total micromoles of H₂O₂ in the extract. This was normalized to recorded sample fresh weights.

RNA Extraction and Quantitative RT-PCR Analyses

The RNA measurement experiments were performed in parallel with the H₂O₂ quantification experiments. Seedlings germinated under normal growth conditions and grown for 7 days were transferred to plates containing ½ LS media with 1.0% sucrose and 1.0 µg/ml Tm or DMSO for 6, 24, or 48 hr as indicated, and harvested at the same time on 2 consecutive days. Groups of 5-10 seedlings were pooled placed in 1.7 ml microcentrifuge tubes with two glass beads, and frozen in liquid nitrogen. Total RNA was extracted from whole seedlings using a NucleoSpin Plant RNA kit (Machery-Nagel) according to the manufacturer's instructions, including on column DNase Digestion. All samples within the experiment were reverse-transcribed using iScript Reverse Transcriptase. RT-PCR with SYBR Green detection using a $\Delta\Delta^{ct}$ method was performed in technical triplicates using the Applied Biosystem 7500 Fast Real-Time 7500 PCR system, and

data normalized to the expression of UBQ10 (AT4G05320). The values presented are the mean of three independent biological replicates \pm SE.

Recovery from ER Stress, and Chronic ER Stress Phenotypic Analyses

For the recovery from ER stress experiments WT, *rboh*d *rboh*f, and *ire1*a *ire1*b were germinated on ½ LS plates grown vertically for 5 days, transferred to liquid ½ LS media containing 1.0 μ g ml⁻¹ Tm for 6 hr, then replated on ½ LS plates and grown vertically for a further 3 days. The plates were then photographed and the root lengths of at least 30 individuals from 4 separate plates were determined using ImageJ; the mean \pm SE was then calculated. In groups of two shoots were excised, fresh weight recorded, placed in 1.7 ml microcentrifuge tubes with two glass beads, and frozen in liquid nitrogen.

For the chronic ER stress experiments WT, *rboh*d *rboh*f, *ire1*a *ire1*b, and *bzip*60 *bzip*28 were germinated on ½ LS plates containing DMSO, 5 ng/ml, 10 ng/ml, or 25 ng/ml Tm and grown for two weeks then photographed. In groups of five, shoots were excised, fresh weight recorded, placed in 1.7 ml microcentrifuge tubes with two glass beads, and then frozen in liquid nitrogen.

For both ER stress recovery and chronic stress experiments, total chlorophyll content (chlorophyll a+ chlorophyll b) per mg fresh weight was determined as described previously (Tait *et al.* 2003). Samples were ground to a fine powder in a Retch MM301 (Retch; Haan, Germany) by agitation at a frequency of 30/sec for two sets of 30 sec which were separated by refreezing in liquid nitrogen. From the liquid nitrogen 1 ml of DMSO was added to the sample tubes, inverted until mixed then incubated at room temperature for 20 min in the dark. Samples were then centrifuged at 21000xg and 200 μ l aliquots added to a clear 96 well plate for spectrophotometric quantification

of chlorophyll content using a SpectramaxM2 (Molecular Devices). For all experiments at least 10 biological replicates for each experimental group were recorded, presented data represents the mean \pm SE.

Electrolyte Leakage Measurements

WT, *rboh*d *rboh*f, *ire1*a *ire1*b, and *bzip*60 *bzip*28 seedlings were grown for 7 days then transferred to plates containing 1.0 μ g/ml Tm, or DMSO. Seedlings were imaged after six days on treatment plates. After 48 and 144 hr the extent of cell death was determined by quantification of percent electrolyte leakage as described previously with minor modifications (Dong *et al.* 2006, Lee *et al.* 2010). Groups of five seedlings were briefly washed in ddH₂O, and then incubated in 4 ml of ddH₂O for 3 hr in glass culture tubes with gentle agitation. Liquid conductivity was measured (Measurement 1). The tubes were autoclaved with caps and allowed to cool under gentle agitation for 3 hr. Total conductivity was measured (measurement 2) and percentage of the total was calculated as ($\% = \text{measurement1} / \text{measurement2} * 100$).

RESULTS

ER Stress Induces Accumulation of Superoxide by NADPH Oxidases

We first aimed to test whether ER stress activates NADPH oxidases by establishing the levels of O_2^- , the product of NADPH oxidases, in seedlings subjected to induced ER stress conditions. To do so, we followed O_2^- accumulation *in situ* using nitrotriazolium blue (NBT), a chromogenic substrate for oxidases commonly applied to the study of NADPH Oxidase activity *in vivo* (Dunand *et al.* 2007). We analyzed roots of wild type (WT) and a double RBOHD and RBOHF knockout seedlings (herein dubbed *rbohd rboh*f (Torres *et al.* 2002)). RBOHD and RBOHF belong to a ten-member family of proteins and are mainly expressed in the shoot and vascular tissue (Morales *et al.* 2016) After 7 days of growth on solid ½ LS media, the seedlings were transferred to solid ½ LS media containing the well-established ER stress inducer tunicamycin (Tm) for 24 or 48 hr to induce the adaptive UPR in a plate system (Iwata *et al.* 2005, Liu *et al.* 2007a, Chen *et al.* 2013).. We found that at 24 hr, the levels of NBT staining were only slightly increased, mainly at the root tip, both in Tm-treated WT and *rbohd rboh*f compared to the respective DMSO controls (Tm solvent) (Figure 2.1A; root tip indicated with Δ). However, at 48 hr of TM treatment, in WT and in the *rbohd rboh*f line the levels of NBT staining had dissipated at the root tip and increased along the maturation zone and mature root tissues (Figure 2.1A; mature zone and maturation zone indicated with \dagger and \ddagger , respectively). The NBT staining was higher in the mature zone of WT roots compared to *rbohd rboh*f. These observations were validated by measurements of the relative levels of NBT staining along the root length using ImageJ (Figure 2.1B). These verified differences in NBT staining at the tissue level are consistent with the notion that RBOHD and RBOHF are expressed largely in shoot tissues and

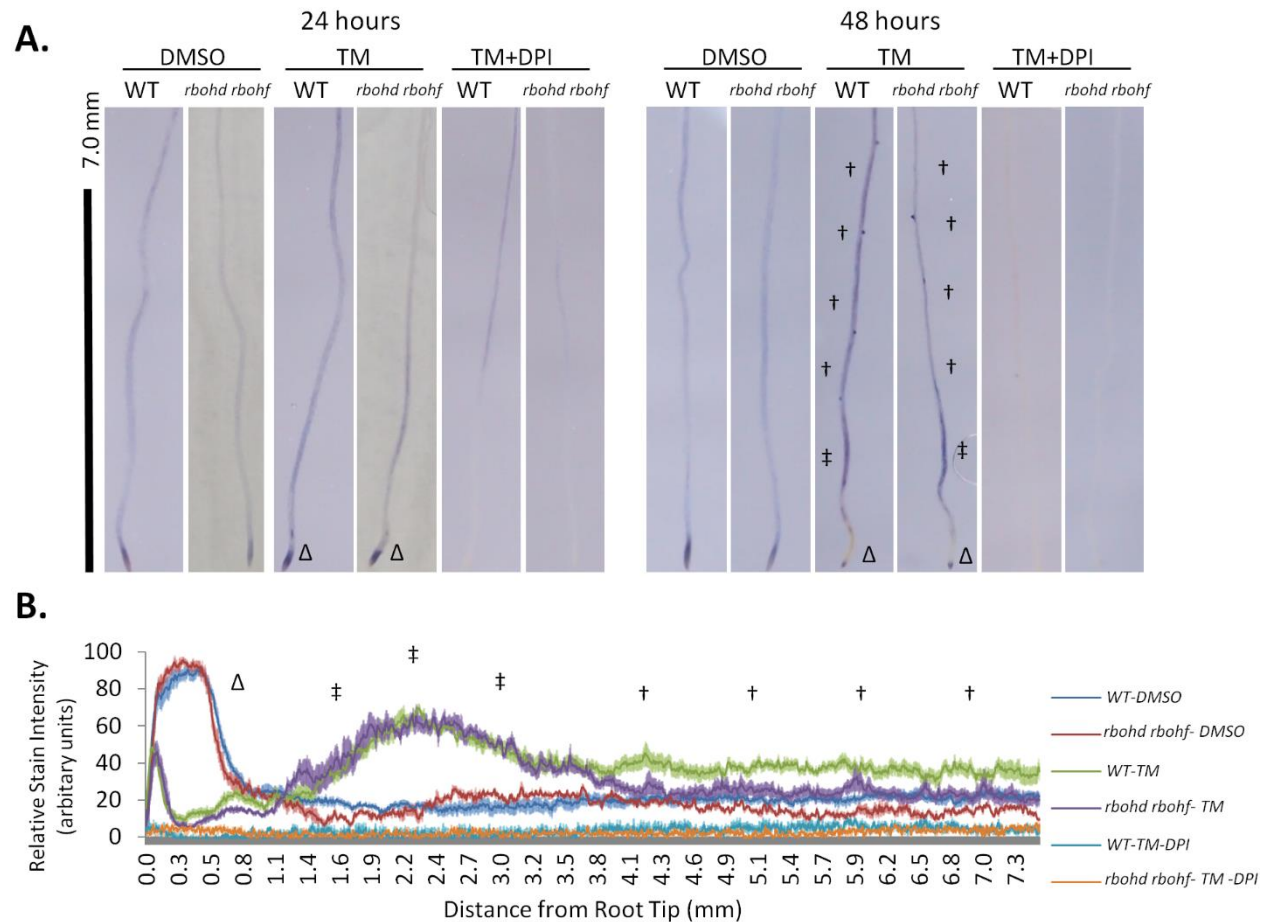


Figure 2.1. NADPH oxidase-dependent O_2^- is generated during ER Stress partially through RBOHD and RBOHF activity.

In situ detection and semi-quantification of superoxide in root tissues by staining with nitro-tetrazolium blue (NBT) **A**) WT or *rbohΔ rbohF* seedlings treated with 1.0 $\mu\text{g/ml}$ Tm, 1.0 $\mu\text{g/ml}$ TM + 2.5 μM DPI, or DMSO were stained with NBT after 24 or 48 hr. †: mature zone; ‡: maturation zone; Δ : root tip. **B**) Tissue-specific differences in superoxide are shown by relative pixel intensities of NBT stain from the root tip \pm SE.

mature root tissues but not at the root tip in *Arabidopsis* (Morales *et al.* 2016). We next tested whether the observed NBT staining in *rboh1 rboh2* could be due to other RBOH activity. Therefore, we supplemented the Tm-treated samples with diphenyleneiodonium (DPI), a broad spectrum flavoprotein inhibitor that is commonly applied in the study of RBOH proteins (Ogasawara *et al.* 2008). We found that DPI-treatment largely ablated the Tm-induced NBT-staining in WT and *rboh1 rboh2* (Figure 2.1A, B). These results indicate that the remaining Tm-induced NBT staining found at the root tips may be sourced from the activity of RBOH other enzymes functioning redundantly to RBOH1 and RBOH2 (Huang *et al.* 2016). Together, these results indicate that RBOH1, RBOH2, and potentially other RBOH enzymes are involved in ER stress-induced O_2^- production, which at least for RBOH1 and RBOH2 is consistent with the previously described expression pattern at the tissue level.

ER Stress Induces Accumulation of Hydrogen Peroxide Dependent upon RBOH1 and RBOH2 Activity and Intact UPR Signaling

Because O_2^- is converted to H_2O_2 , we next aimed to establish the levels of accumulation of H_2O_2 in seedlings undergoing ER stress. To do so, we first set up an assay to measure reliably H_2O_2 levels in untreated tissues. We utilized a sensitive enzymatic fluorimetric assay based on the stoichiometric oxidization of non-fluorescent Amplex Ultra Red (AUR) by H_2O_2 by exogenous horseradish peroxidase (HRP) to brightly fluorescent resorufin (Queval *et al.* 2008, Zhu *et al.* 2010, Chakraborty *et al.* 2016). We expected that this assay would lead to the detection of resorufin fluorescence in the presence of HRP and to reduced levels of resorufin fluorescence in the absence of this enzyme. We first conducted tissue extraction using potassium phosphate buffer (Chakraborty *et al.* 2016, Le *et al.* 2016), and found no significant differences in oxidization of

non-fluorescent AUR by added HRP compared to the control (Figure 2.2A). These results indicate either that the assay was not sensitive enough or that the AUR oxidation was saturated in the absence of HRP. To test this, we implemented a 10% trichloroacetic acid extraction (neutralized: NTCA) to precipitate possibly interfering enzymatic reactions, and then assayed the levels of H_2O_2 . Consistent with our original hypothesis, we found that, in the presence of HRP, the levels of resorufin fluorescence were significantly higher than in the absence of the enzyme compared to the control (Figure 2.2A). As a further control for the validity of our assay, we treated the samples with catalase, which specifically dismutates H_2O_2 in the extract and should therefore further lower the levels of resorufin fluorescence in HRP-treated samples. Conversely, we expected no differences in catalase treatment of samples extracted in potassium phosphate buffer compared the untreated control. In samples extracted with NTCA, we found that the levels of resorufin fluorescence were significantly lower in catalase-treated samples compared untreated samples (Figure 2.2C). As expected also, the addition of catalase did not alter the levels of fluorescence of potassium phosphate buffer-extracted samples compared to untreated samples (Figure 2.2B). These results support that the resorufin fluorescence levels detected in the potassium phosphate buffer-extracted samples are due to H_2O_2 -independent oxidation of AUR. Importantly, these results also indicate that we have established a quantitative approach to track specifically H_2O_2 levels in tissues.

We then used this assay to measure the levels of H_2O_2 in seedlings experiencing ER stress during the adaptive phase of the UPR. Using the same plate system detailed earlier (Figure 2.1), we compared the effects of Tm treatment for 6, 24, and 48 hr against seedlings growing on plates containing DMSO as control. We tested WT, *rbohD rbohF*, a mutant lacking the two IRE1 isoforms (*ire1a ire1b*; (Chen *et al.* 2012)) and a double mutant lacking functional bZIP60 and

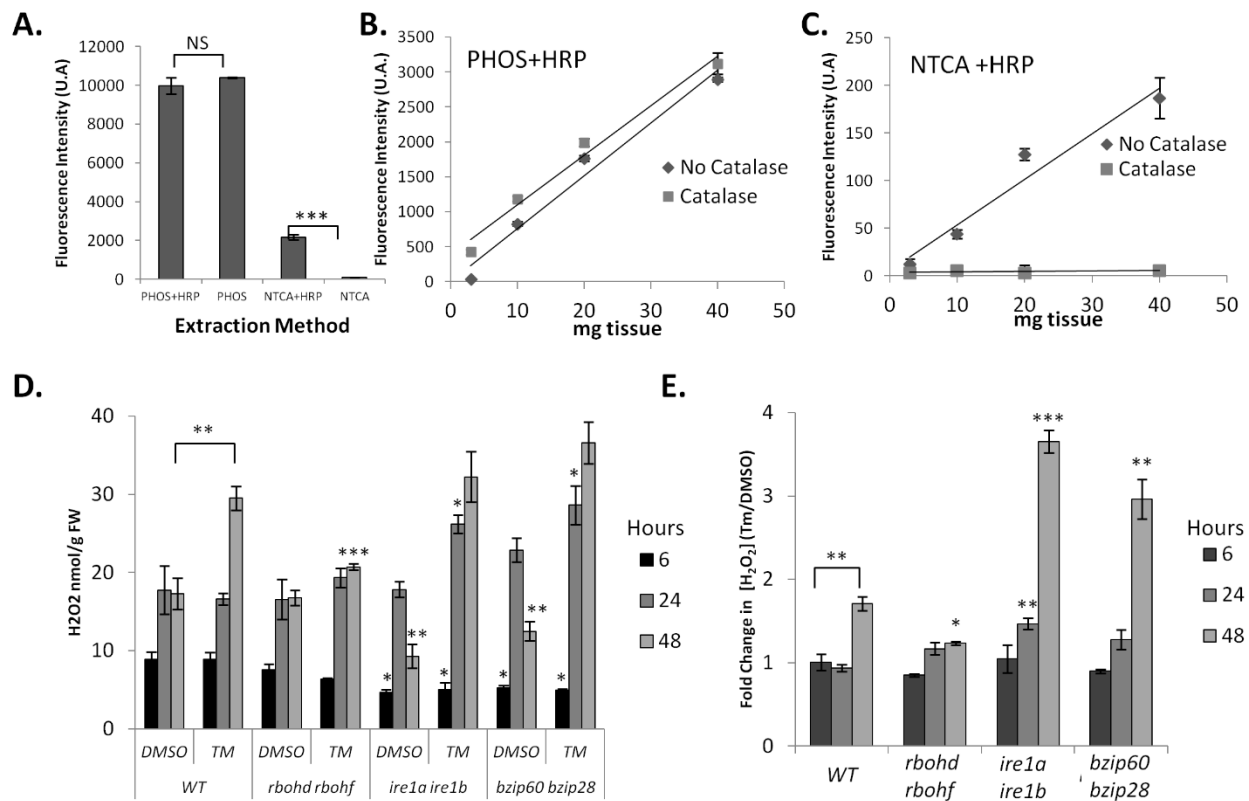


Figure 2.2. ER Stress induced H_2O_2 are controlled by RBOHD and RBOHF as well as intact UPR signalling.

Development and application of an Amplex Ultra Red protocol for H_2O_2 quantification from seedling tissues subjected to ER stress. **A)** Comparison of H_2O_2 extraction methods using potassium phosphate buffer (PHOS) or 10% TCA neutralized with $NaHCO_3$ (NTCA) incubated in the presence or absence of horseradish peroxidase (HRP). **B)** Evaluation of tissue loading during PHOS extraction and catalase treatment. **C)** Evaluation of tissue loading during NTCA extraction and catalase treatment. **D)** WT, *rbohD rbohF*, *ire1A ire1B*, and *bzip60 bzip28* seedlings were treated in a plate system with Tm or DMSO for the indicated time and H_2O_2 quantified; see materials and methods. Data represent the mean concentration \pm SE. **E)** From the values in (D) average fold change \pm SE (Tm/DMSO) was determined from biological replicates in the order that they were measured. Statistical significance compared to equivalent WT value, unless a bracket is used to indicate comparison. Statistical significance determined using Student's unpaired t-test and indicated by: *= $p < 0.05$, **= $p < 0.005$ ***= $p < 0.0005$, NS=not significant.

bZIP28 transcription factors (*bzip60 bzip28*; (Deng *et al.* 2013)). We found differences in H₂O₂ concentrations among the various backgrounds and their controls (Figure 2.2D), in support of a significant bearing of RBOHD and RBOHF activity as well as intact UPR on H₂O₂ production. To better illustrate such differences we estimated the fold change in concentration between Tm/DMSO (Figure 2.2E). Specifically, we found that in all backgrounds at 6-hr of treatment there were no differences in fold change of H₂O₂ concentrations (TM/DMSO; Figure 2.2E). At 24 hr, we established that Tm-treatment led to a small but significant increase in H₂O₂ levels in the *ire1a ire1b* mutant background only. However, at 48 hr, coincident with significant increases in O₂⁻ in mature WT tissues (Figure 2.1B), we found a significant increase in H₂O₂ levels in WT that were not observed in the *rboh1 rboh2* mutant (Figure 2.2E), indicating that RBOHD and RBOHF are required for the accumulation of H₂O₂ under ER stress conditions. Noticeably, the increase of H₂O₂ verified in WT but not *rboh1 rboh2* was significantly greater in *ire1a ire1b* and *bzip60 bzip28* mutants (Figure 2.2E), supporting a requirement of an intact UPR signaling for the management of H₂O₂ levels in conditions of ER stress. Together, these results indicate that H₂O₂ accumulates in response to ER stress in the adaptive phase of the UPR dependent on RBOHD and RBOHF activity and also influenced by the integrity of UPR signaling.

UPR Regulators Influence RBOHD and RBOHF Expression During Adaptive UPR

Having established that RBOHD and RBOHF activity is required for ER stress-induced O₂⁻ and H₂O₂ production (Figures 2.1, 2.2), we next aimed to determine if the canonical UPR arms affected *RBOHD* or *RBOHF* expression at the transcriptional level. Therefore, we tested whether ER stress modulated *RBOHF* or *RBOHD* transcript levels as it occurs for other ER stress responsive genes, such as *bZIP60*, *BiP3*, *ERdj3A* and *ERdj3B* (Chen *et al.* 2012, Ruberti *et al.*

2018). To do so, a subset of seedlings from the H₂O₂ quantification experiments (Figure 2.2) were used to follow the changes in gene transcript levels by quantitative RT-PCR (qRT-PCR) during TM treatment in the plate system (Iwata *et al.* 2005, Liu *et al.* 2007a, Chen *et al.* 2013). We found no changes in the *RBOHF* transcript levels in the WT, *ire1a ire1b*, or *bzip60 bzip28* lines at 6 hr of treatment. However, at 24 and 48 hr of TM treatment, the *bzip60 bzip28* line had slightly lower levels of the *RBOHF* transcripts compared to WT (Figure 2.3A). Conversely, in the WT and *ire1a ire1b*, the *RBOHD* transcripts were transiently induced at 24 hr and then restored to basal levels at 48 hr. We also observed that the *RBOHD* induction was significantly higher in *ire1a ire1b* compared to WT (Figure 2.3B). The *RBOHD* transcript levels in the *bzip60 bzip28* line we found to be slightly repressed at 6 hr of treatment (with a TM/DMSO ratio of ~0.8; Figure 2.3B). Noticeably, however, at 24 hr in the *bzip60 bzip28* line the *RBOHD* transcript levels were significantly lower compared to WT and *ire1a ire1b*. Together these results demonstrate that although the integrity of UPR signaling is required for maintaining homeostatic levels of *RBOH* expression during ER stress, the timing of the observed changes does not directly correlate with *RBOHD* and *RBOHF* dependent O₂⁻ (Figure 2.1) or H₂O₂ production (Figure 2.2) in WT plants. This indicates that other factors, such as post translational modifications, protein-protein interactions, or altered endomembrane trafficking of the protein product may contribute to these outcomes.

To provide further evidence that the observed increases in O₂⁻ (Figure 2.1) are dependent upon *RBOHD* and *RBOHF* activity during ER stress, we quantified the expression of *ZAT12*, an O₂⁻ responsive marker gene (Miller *et al.* 2009, Xu *et al.* 2017). Consistent with transiently increased levels of NBT staining at 24 hr in the root tip, which was largely independent of *RBOHD* and *RBOHF* activity (Figure 1A), we found a 6-fold upregulation in *ZAT12* levels in the

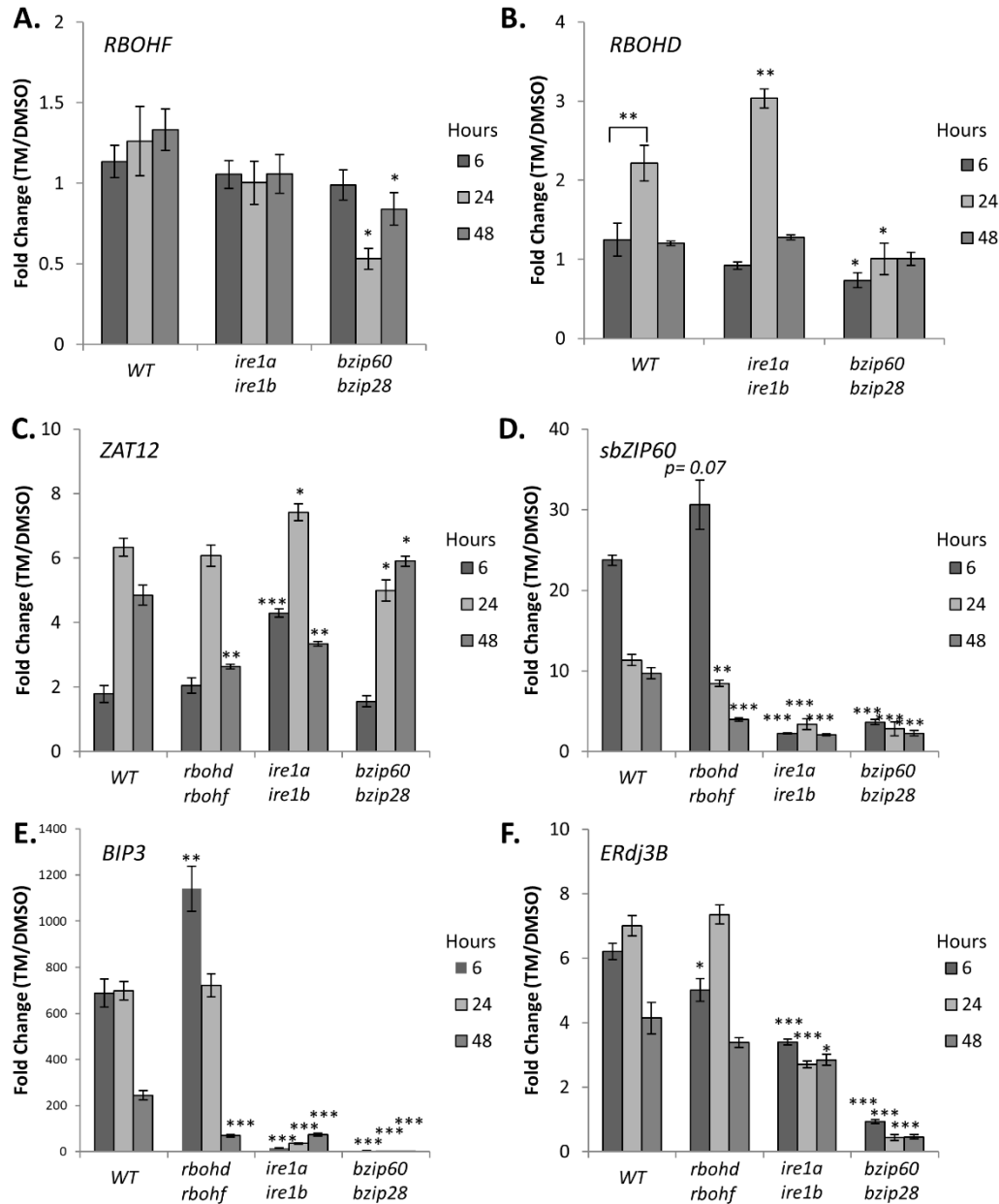


Figure 2.3. Intact UPR signaling is required to maintain homeostasis of RBOH transcript levels and ROS signaling, while RBOH activity affects UPR homeostasis.

Time course gene expression analysis of WT, *rboh* *rboh*, *ire1a ire1b*, and *bzip60 bzip28* seedlings subjected to ER stress. qRT-PCR analyses were performed using primers specific for either A) *RBOHF*, B) *RBOHD*, C) *ZAT12*, D) *spliced bZIP60* (*sbZIP60*), E) *BIP3*, or F) *ERdj3B*. Data represent the mean ratio \pm SE (biological replicates=3); Statistical significance compared to equivalent WT value, unless a bracket is used to indicate comparison. Statistical significance determined using Student's unpaired t-test and indicated by: *= $p < 0.05$, **= $p < 0.005$, ***= $p < 0.005$, NS=not significant.

WT and WT and *rboh* *rboh* lines (Figure 2.3C). Significantly at 48 hr, where we observed an increase in NBT staining of mature root tissues and upregulated H₂O₂ levels in WT but not *rboh* *rboh* seedlings (Figures 2.1, 2.2), we also found that *rboh* *rboh* seedlings had significantly lower levels of *ZAT12* transcript (Figure 2.3C). These results demonstrate that 48 hr of ER stress induces O₂⁻ accumulation via RBOHD and RBOHF (Figure 2.1) to a level that elicits a transcriptional response.

We next aimed to test whether UPR regulation of *RBOHD* and *RBOHF* transcripts or H₂O₂ levels (Figures 2.2, 2.3A, 2.3B) was correlated with changes in superoxide-dependent signaling. We found that at 6 hr of Tm treatment in *ire1a ire1b* the levels of *ZAT12* were significantly higher compared to WT. At 24 hr of treatment, *ZAT12* levels in *bzip60 bzip28* and *ire1a ire1b* mutants were slightly lower and higher than WT levels, respectively. Conversely, at 48 hr of treatment *ZAT12* levels in *bzip60 bzip28* and *ire1a ire1b* mutants were higher and lower than WT levels, respectively (Figure 2.3C). Although the increased *ZAT12* levels in the *ire1a ire1b* mutant are consistent with the verified increase in transcription of *RBOHD* and H₂O₂ accumulation at 24 hr, the regulation of *ZAT12* in both UPR mutant lines does not correlate with the RBOH transcription, or H₂O₂ accumulation at 48 hr. We therefore propose that an impaired UPR response likely has pleiotropic effects in the regulation of superoxide production, superoxide signaling, and H₂O₂ accumulation during adaptation to ER stress.

We next tested whether impaired RBOHD and RBOHF activity affected the canonical UPR at a transcriptional level. We tested the levels of ER stress-responsive genes such as spliced *bZIP60* transcripts (*sbZIP60*) and *BIP3*, whose abundance is primarily regulated by IRE1-bZIP60, as well as *ERDJ3B*, whose expression is primarily regulated by bZIP28 (Ruberti *et al.*, 2018). In WT, we found that the Tm treatment led to increased levels of *sbZIP60* transcripts at 6 hr, which were

attenuated at 24 and 48 hr (Figure 2.3D). Compared to WT, in the *rbohd rboh* line, we observed no significant changes in the induction of *sbZIP60* levels at 6 hr but a significant ~2 fold reduction of *sbZIP60* levels at 48 hr (Figure 2.3D). An altered UPR signaling in *rbohd rboh* was reflected in our analyses of *BIP3* transcript levels, which were ~2-fold higher at 6 hr of treatment and ~4 fold lower at 48 hr in the *rbohd rboh* line compared to WT (Figure 2.3E). Conversely, *ERdj3B* was found to be ~1.2-fold lower at 6 hr in the *rbohd rboh* line compared to WT, but was otherwise insignificantly different. Taken together, these results indicate that RBOHD and RBOHF contribute to maintain UPR signaling homeostasis during ER stress.

RBOHD and RBOHF are Necessary for Recovery from Short-Term and Chronic ER Stress

We next aimed to test whether RBOHD and RBOHF could contribute to ER stress resolution in situations subsequent to the adaptive phase. In this context, progression of the plant UPR has been studied in conditions of relief from ER stress (temporary ER stress; (Ruberti *et al.* 2018)) and in conditions of unresolved ER stress (chronic ER stress; (Chen *et al.* 2013)). Therefore, we first tested the role of RBOHD and RBOHF in recovery from temporary ER stress. In this assay, 7-day old-seedlings are transferred to liquid media containing Tm for 6 hr, and then replated on growth medium without Tm. After 3 further days of growth, shoot fresh weight, root length and chlorophyll content are assayed to assess the ability of the various genetic backgrounds to overcome ER stress upon relief from an ER stress inducer. For the assay, we used WT, *rbohd rboh* and *ire1a ire1b*. Consistent with previous findings (Ruberti *et al.* 2018), at the completion of the recovery phase, we found that the shoots of the *ire1a ire1b* mutant weighed significantly less than DMSO-treated controls and lost most of their chlorophyll; the root also ceased further

growth (Figure 2.4A-D). We also found that although the shoots of the Tm-treated *rbohd rboh* plants weighed similarly to the Tm-treated WT (Figure 2.4B), a significant reduction of chlorophyll content was evident (Figure 2.4C). The roots of Tm-treated *rbohd rboh* also showed an overall reduction in length compared to WT (Figure 2.4D). These results indicate that RBOHD and RBOHF are necessary to successfully overcome temporary ER stress.

We then tested the requirement of RBOHD and RBOHF for overcoming chronic ER stress. To do so, we followed the customary approach to germinate seeds on growth medium containing Tm for comparison with seedlings germinated on control plates (Chen *et al.* 2012). As positive controls, we again used *ire1a ire1b* as well as *bzip60 bzip28*, which are hypersensitive to chronic ER stress (Liu *et al.* 2007a, Chen *et al.* 2012). After 14 days of growth, we examined shoot fresh weight and chlorophyll content (Figure 2.5A-C). Consistent with previous findings (Chen *et al.* 2012, Ruberti *et al.* 2018), the *ire1a ire1b* and *bzip60 bzip28* mutants showed a strong phenotype with marked reduction in shoot fresh weight and loss of chlorophyll content. When we analyzed *rbohd rboh*, we found a significant reduction in the average shoot fresh weight and chlorophyll content compared to WT. These results indicate that, similar to temporary ER stress recovery, RBOHD and RBOHF are required to successfully overcome chronic ER stress.

RBOHD and RBOHF Contribute to Preventing ER Stress Induced Cell Death

Previous reports have detailed the protective role that RBOHD and RBOHF play in preventing the spread of cell death during plant immune system response through yet undetermined mechanisms (Torres *et al.* 2005). Having established that RBOHD and RBOHF are required for successful recovery from temporary ER stress and survival from chronic ER stress, we postulated

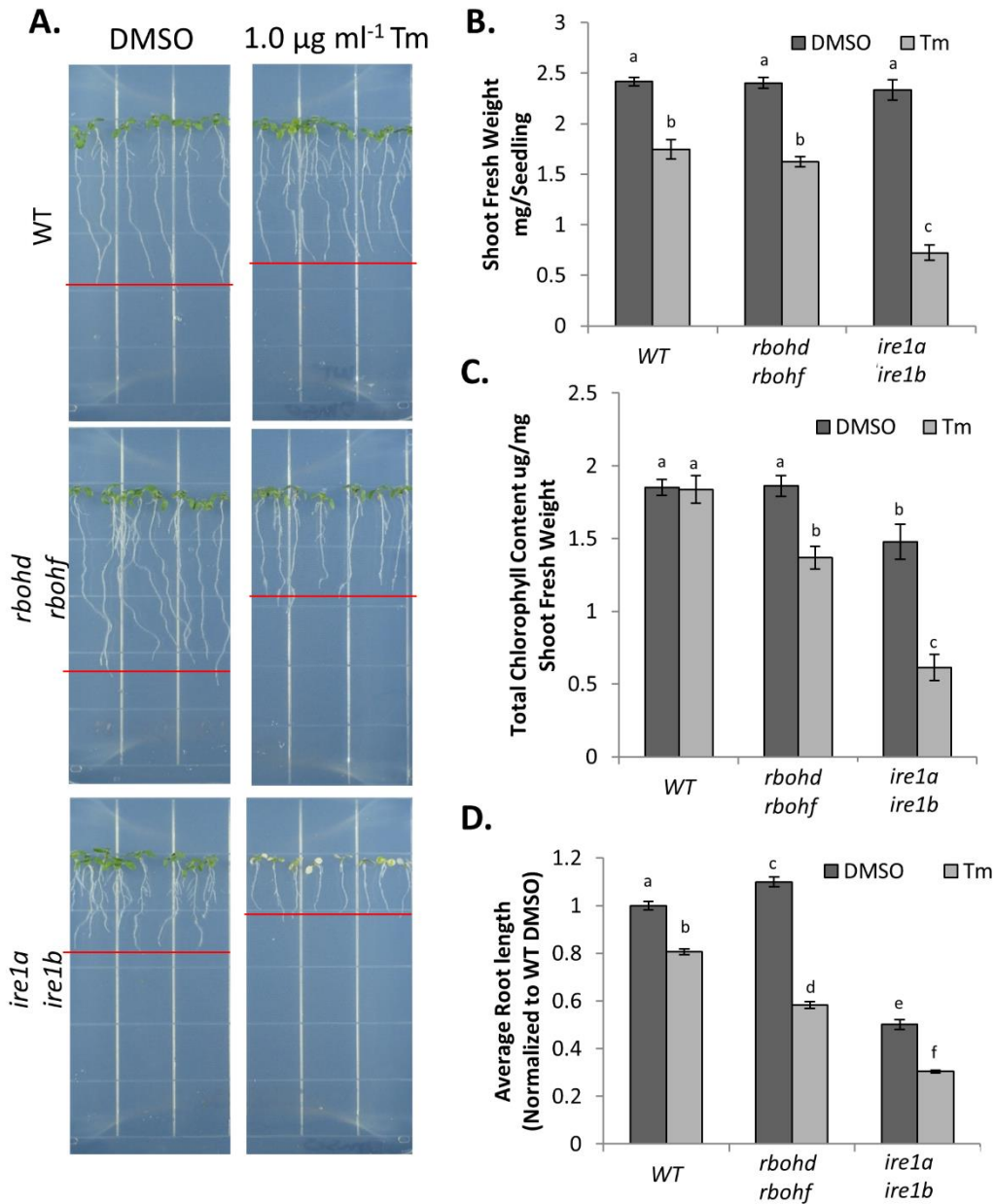


Figure 2.4. RBOHD and RBOHF are required in the recovery from temporary ER stress.

Phenotypic analyses of the various genetic backgrounds subjected to temporary ER stress. **A).** WT, *rboh1d rboh1f*, and *ire1a ire1b* seedlings were subjected to ER stress and were imaged after a 3 day recovery. From the seedlings grown in (A) shoot fresh weight (**B**), average total chlorophyll (**C**), and root length (**D**), were recorded as described in the materials and methods. Data represent the mean \pm SE. (at least 10 biological replicates). Letters above each data point indicate statistically significant groups using Student's unpaired t-test ($p < 0.05$).

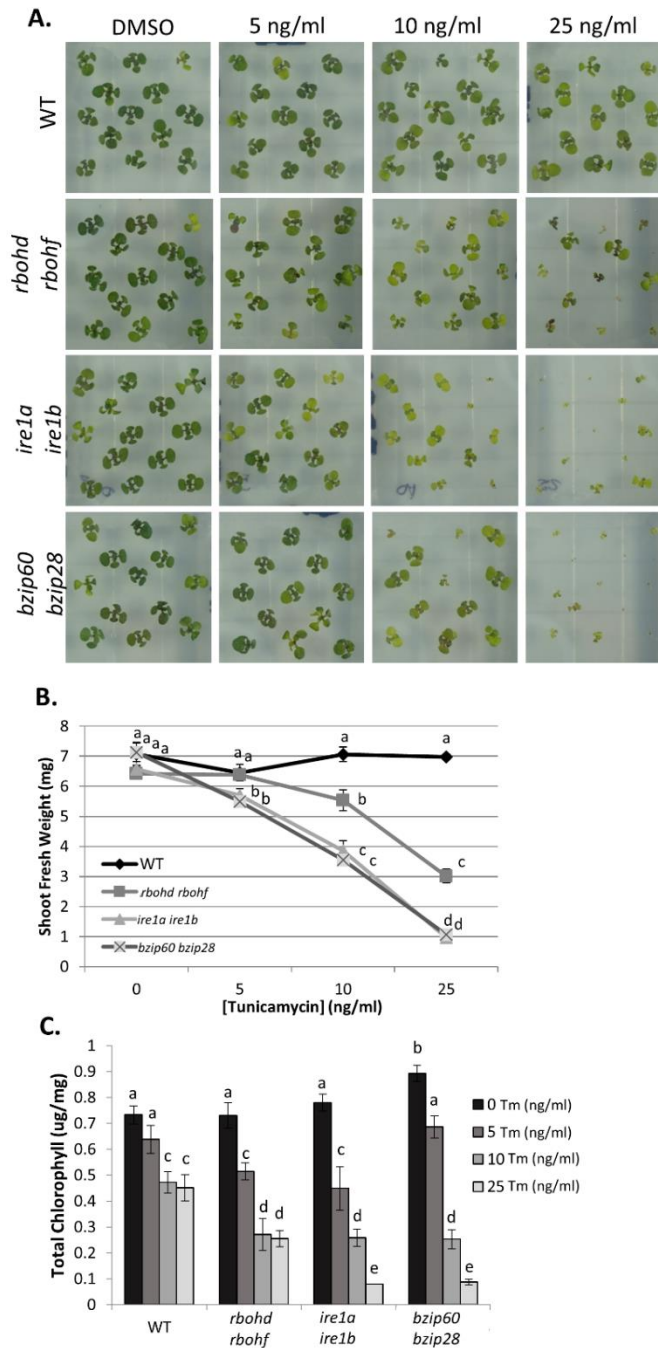


Figure 2.5. RBOHD and RBOHF are required for adaptation to chronic ER stress.

Phenotypic analysis of different seedling genetic backgrounds subjected to chronic ER stress. **A)** WT, *rboh rboh*, *ire1a ire1b*, and *bzip60 bzip28* were germinated on media containing the indicated concentration of Tm or DMSO grown for two weeks. **B)** Shoots fresh weight, and **C)** total chlorophyll content were measured. Data represent the mean \pm SE (at least 10 biological replicates). Letters above each data point indicate statistically significant groups using Student's unpaired t-test ($p < 0.05$).

that these enzymes could be involved in mechanisms preventing cell death caused by ER stress.

To test this hypothesis, we followed cell death by quantification of electrolyte leakage (Lee *et al.* 2010) in WT, *rboh*d *rboh*f, *ire1*a *ire1*b, and *bzip*60 *bzip*28 seedlings exposed to Tm for 2 and 6 days (Figure 2.6A, B). We found that although the shoot and root of Tm-treated WT seedlings grew considerably less compared to DMSO control, no significant differences were detected in electrolyte leakage levels (Figure 2.6B). As expected, the *bzip*60 *bzip*28 and *ire1*a *ire1*b mutants showed considerable chlorophyll loss with electrolyte leakage reaching almost 50% at 6 days of Tm treatment. We found that *rboh*d *rboh*f plants also showed a significant chlorophyll loss and electrolyte leakage by 6 days of Tm-treatment (Figure 2.6B) compared to WT plants. These results indicate that RBOHD and RBOHF contribute in preventing cell death in ER stress conditions.

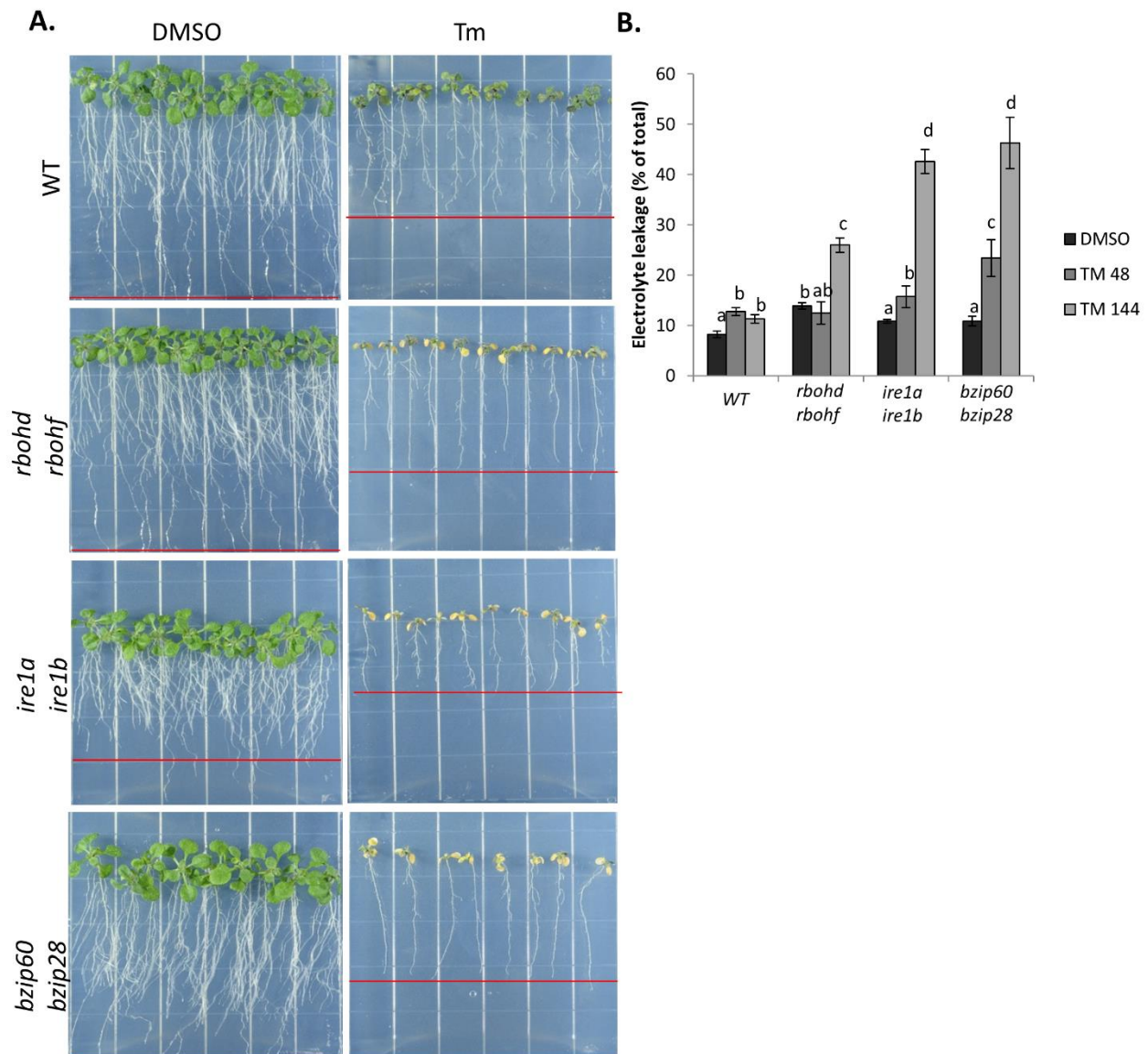


Figure 2.6. RBOHD and RBOHF act to prevent ER stress induced cell death.

Determining the extent of cell death in seedlings of different genetic background subjected to prolonged ER stress. **A)** WT, *rboh*d *rboh*f, *ire1*a *ire1*b, and *bzip*60 *bzip*28 seedlings treated with Tm in a plate system for 48 and 144 hr, and then photographed at 144 hr. **B)** The extent of cell death was determined by quantification of percent electrolyte leakage. Data represent the mean \pm SE (4 biological replicates). Letters above each data point indicate statistically significant groups using Student's unpaired t-test ($p < 0.05$).

DISCUSSION

In plants, the identity of several critical sensors and transducers of ER stress has been unraveled (Angelos *et al.* 2017), and the challenge ahead is to discover additional factors that participate in the UPR management. In this work, we have established that two NADPH oxidases are necessary to overcome specific situations of ER stress, such as recovery from ER stress conditions and unresolved ER stress. These results enrich the general knowledge of the identity of the proteins and signaling pathways that contribute to ER stress survival in plants. The ability of mammalian cells to overcome ER stress is negatively influenced by NADPH Oxidases-produced ROS (Li *et al.* 2010). In plants, the relationship between ROS and the UPR was unknown. In this work, we showed that, in conditions of an intact UPR signaling, NADPH Oxidases-produced ROS exert a positive role on the ability of the plant to overcome ER stress. These findings support the conclusion that, despite the functional conservation of canonical ER stress sensors and transducers such as IRE1 and bZIP-transcription factors, plants have evolved unique strategies for ER stress survival.

NADPH Oxidases Contribute to ROS Production in Conditions of ER Stress

Several metabolic and signaling processes affect cellular concentrations of H₂O₂ in plants, including biotic and abiotic stress responses (Miller *et al.* 2009), nutrient availability (Contento *et al.* 2010), circadian rhythms (Zhong *et al.* 1994), and gravity (Hausmann *et al.* 2014). In Arabidopsis there are also studies indicating that ER stress affects cellular concentrations of H₂O₂, through both direct measurements (Ozgur *et al.* 2014, Ozgur *et al.* 2018) and analyses of redox-related biochemical activities that are intimately linked with cellular H₂O₂ levels (Ozgur *et al.*

2014). However, prior to our work the nature of the enzymes contributing to H₂O₂ levels in conditions of ER stress had yet to be clearly established in plants. In this work, we have set up a sensitive assay to measure H₂O₂ levels (Figure 2.2). Using this assay, superoxide staining and a genetic background lacking RBOHD and RBOHF, we showed that ER stress causes activation of NADPH Oxidase-coupled superoxide production, leading to the accumulation of H₂O₂ (Figures 2.1, 2.2). We further show that a superoxide-responsive signaling pathway (Xu *et al.* 2017) is also activated, as demonstrated by transcriptional induction of the marker gene *ZAT12* (Figure 2.3C). The concomitant reduction of three different ROS reporters in the *rboh* *rboh* line compared to WT under conditions of ER stress (Figures 2.1, 2.2, 2.3; 48 hr) supports that the elevation of H₂O₂ in conditions of stress is contributed partially by RBOHD and RBOHF. Therefore, these findings identify two of the enzymes that operate in ROS management during ER stress potentially sharing redundant functions with other RBOH-enzymes.

Although, the exact molecular mechanisms leading to activation of these enzymes in response to ER stress have yet to be elucidated, a regulation of RBOH enzymes by altered cytosolic calcium levels and association with G-protein signaling components may be postulated as contributing factors. In metazoans cellular calcium ion homeostasis is intimately linked with ER stress, as calcium is required for the proper functioning of ER luminal foldase activities (Krebs *et al.* 2015). Inhibition of sarcoplasmic/endoplasmic reticulum calcium ATPase (SERCA) transporters leads to the induction of ER stress and the UPR (Krebs *et al.* 2015). Upon prolonged UPR activation, a number of factors, including ER lumen hyper-oxidation by ER oxidase 1a (ERO1a), leads to calcium release from the ER through activation of inositol triphosphate receptors (IP3R) and apoptotic events (Sovolyova *et al.* 2014). Although IP3R-like ER calcium channels have yet to be identified in plants, SERCA-like transporters have been identified (Liang

et al. 1997). Therefore it is possible that ER stress/UPR induction could alter ER and cytosolic calcium levels, which can promote RBOHD activation (Ogasawara *et al.* 2008). Furthermore, in plant responses to bacterial pathogen attack, it has also been demonstrated that a null mutation in the Arabidopsis G β subunit (*agb1*) of the heterotrimeric G-protein plasma membrane signaling complex was epistatic to the *rboh*d *rboh*f null mutation (Torres *et al.* 2013). The AGB1 gene acts in concert with receptor-like kinases to mediate oxidative burst response to pathogen-associated molecular pattern (PAMP) triggered immunity (Liu *et al.* 2013, Liu *et al.* 2016b). Although it is yet to be tested whether AGB1 interacts genetically with RBOHD and RBOHF in ER stress, similar to *rboh*d *rboh*f, *agb1* is sensitive to chronic ER stress (Chen *et al.* 2012). It is therefore possible that AGB1 may contribute to RBOH signaling in conditions of ER stress.

Unlike in Metazoans, NADPH Oxidase-Produced ROS are Beneficial to Overcome ER Stress in Plants

Many aspects of the UPR regulators are conserved between plants and metazoans at a functional level even when compared to yeast wherein only IRE1 arm of the UPR is genetically encoded (Ron *et al.* 2007, Ruberti *et al.* 2015, Liu *et al.* 2016a). However, it is increasingly obvious that the different evolutionary contexts between plants and animals have forced the development of different survival strategies in overcoming ER stress. The lack of a plant homolog of the mammalian PERK UPR pathway is evidence to that effect. NADPH Oxidases are largely conserved between mammals and plants (Suzuki *et al.* 2011). However, the activities of mammalian NADPH Oxidase 2 (Nox2) and NADPH Oxidase 4 (Nox4), two homologs of RBOHD and RBOHF, promote apoptosis during ER stress (Pedruzzi *et al.* 2004, Li *et al.* 2010). Specifically, an intravenous tunicamycin challenge in *Nox2*^{-/-} mice resulted in a dramatic

reduction of renal cell apoptosis and increased protection against renal dysfunction when compared to WT mice (Li *et al.* 2010). In this work, we show that *rboh* *rboh* plants display a significant sensitivity to ER stress conditions (Figures 2.4, 2.5, 2.6). Specifically, in the recovery from acute Tm treatment, in *rboh* *rboh*, the resumption of plant growth is markedly delayed, and under chronic stress conditions (Figures 2.5, 2.6), *rboh* *rboh* plants exhibit enhanced progression of cell death (Figure 2.6). Therefore, differently from the mammalian system, during ER stress NADPH Oxidases RBOHD and RBOHF exert a pro-survival role in the ER stress response. As such, the results presented in this study identify RBOHD and RBOHF as important positive contributors to UPR adaptation in plants in a manner that runs differently from the mammalian cell system.

Homeostasis of NADPH Oxidase Activity is Required to Maintain an Effective UPR

Several studies, including studies of RBOH activity during heat stress response in plants, support a non-specific “transcriptional priming” by which fast acting ROS production by RBOHD amplifies initial stress-specific transcriptional responses in local and systemic tissues (Mittler *et al.* 2015). In our analyses, we established that the RBOHD and RBOHF are involved in the adaptive phase of the UPR (Figure 2.3D-F) as well as in recovery from temporary ER stress and in situations of chronic ER stress (Figures 2.4, 2.5). Consistent with a priming role of RBOH activity in stress responses, the verified misregulation of the adaptive phase of the UPR due to a compromised RBOH activity may lead to a defective actuation of proper cytoprotective responses necessary for surviving temporary and chronic ER stress. Interestingly, when compared to *ERdj3B* levels, we verified a stronger impact on the induction levels of *sbZIP60* and *BIP3* in *rboh* *rboh* compared to WT (Figure 2.3D-E). Based on the findings that *BIP3* expression is principally

controlled by the IRE1-bZIP60 arm and that the *ERdj3B* is principally controlled by bZIP28 arm, we propose that the activity of RBOHD and RBOHF positively influences the transcriptional role of bZIP60. This hypothesis does not exclude that other RBOH enzymes may affect the transcriptional role of bZIP60 as well as bZIP28. Indeed, in our work, while we demonstrate that RBOHD and RBOHF activity is required for successfully overcoming these specific conditions of ER stress, the activity of these enzymes is not strictly essential. This is supported by the relative survival of *rbohd rbohlf* compared to *ire1a ire1b* and *bzip60 bzip28* in temporary and chronic ER stress conditions (Figures 2.4, 2.5, 2.6). Given the relatively large size of RBOH family and the residual NADPH Oxidase marker activity observed in the *rbohd rbohlf* line (Figure 2.1), it is possible that RBOHD and RBOHF share redundant activity with other RBOH enzymes in temporary and chronic ER stress conditions.

In ER Stress Conditions, the Production of ROS is Antagonized by IRE1 and the bZIP60/bZIP28 Transcription Factors

The plant IRE1 as well as the availability of bZIP28 and bZIP60 together are strictly necessary to overcome temporary and prolonged stress, as demonstrated by the evidence that death is accelerated in the *ire1a ire1b* and *bzip60 bzip28* mutants compared to WT in situations of recovery from temporary ER stress or in conditions of chronic ER stress ((Nagashima *et al.* 2011, Chen *et al.* 2012, Deng *et al.* 2013, Liu *et al.* 2016a); Figures 2.4, 2.5). An analysis of ER stress response in *Chlamydomonas reinhardtii* reported a significant transcriptional induction of ROS-dependent marker genes in *IRE1* knockouts (Yamaoka *et al.* 2018). These findings led to the hypothesis that an increase in ROS may contribute to the ER stress sensitivity of *ire1* knockout lines in this model system (Yamaoka *et al.* 2018). Our results that in the Arabidopsis *ire1a ire1b*

line, which is hypersensitive to ER stress (Figures 2.4-2.6; Chen *et al.* 2012), the H₂O₂ levels are higher at 24 and 48 hr of Tm treatment compared to WT (Figure 2.2E) corroborate this hypothesis. Our results also provide direct evidence in support of the hypothesis that UPR regulators are required to manage cellular H₂O₂ concentrations under ER stress conditions in plants like they do in metazoans (Hourihan *et al.* 2016). However, the verified increases in H₂O₂ content in the *ire1a ire1b* and *bzip60 bzip28* mutants were not directly correlated with the observed misregulation of *ZAT12/RBOHD* transcript levels in these lines compared to WT, which may indicate that an intact UPR signaling potentially coordinates ROS production/signaling through multiple mechanisms to promote proper ER stress management. Conversely, the verified differences in transcript induction of UPR marker genes (i.e., *sbZIP60*, *BIP3* and *ERdj3B*) in *rboh1 rboh1f* compared to WT (Figure 2.3D-E) indicate that RBOH activity is required to maintain proper UPR signaling. How the observed increase in H₂O₂ levels may affect the UPR is yet undetermined at a mechanistic level. Recent findings have shown that ER stress alters the cytosolic redox potential, which in turn modulates the activity of the transcriptional coregulatory NPR1 (nonexpressor of PR genes), which binds and represses the transcriptional function of bZIP28 and bZIP60 (Lai *et al.* 2018). It is similarly possible that an excessive elevation of H₂O₂ in conditions of ER stress changes the activity of UPR and programmed cell death modulators. The ROS species produced by RBOHD and RBOHF suppress the spread of runaway cell death in a pathway parallel to the Lesion Stimulating Disease 1 (LSD1) zinc-finger protein under normal growth conditions, in response to salicylic acid, extracellular superoxide, and pathogen induced hypersensitive response (Torres *et al.* 2005). The results of our study indicate that RBOHD and RBOHF may also prevent the propagation of cell death in response to chronic ER stress (Figure 2.6). Under this light, the noted misregulation of RBOH activity and accumulation of H₂O₂ in *ire1a ire1b* and *bzip60 bzip28*

mutants during ER stress (Figures 2.2E, 2.3C) may represent convergent signals that initiate processes leading toward programmed cell death, and could at least partially explain the hypersensitivity of these lines to ER stress conditions (Figure 2.4-2.6) (Chen *et al.* 2012, Deng *et al.* 2013). Therefore, together our results support the hypothesis for a dual role of H₂O₂ in ER stress-induced programmed cell death, which is differently manifested in WT and mutants of the UPR signaling pathway. Specifically, in cells with an intact UPR, RBOH activity and H₂O₂ levels are maintained to levels that promote survival; however, a defective UPR likely causes misregulation of RBOH activity and excess H₂O₂ accumulation that may lead to cell death. The latter scenario may be beneficial for plants to favor the survival only of cells with an intact ability to overcome proteotoxic stress.

ACKNOWLEDGEMENTS

We acknowledge support by the Chemical Sciences, Geosciences and Biosciences Division, Office of Basic Energy Sciences, Office of Science, U.S. Department of Energy (award number DE-FG02-91ER20021) for infrastructure, NASA (award NNX12AN71G), NIH R01-GM101038, and a fellowship from Michigan State University under the Training Program in Plant Biotechnology for Health and Sustainability (T32-GM110523).

REFERENCES

REFERENCES

- Angelos E., Ruberti C., Kim S. J. and Brandizzi, F. (2017). Maintaining the factory: the roles of the unfolded protein response in cellular homeostasis in plants. *Plant J* 90(4): 671-682.
- Back S. H., Scheuner D., Han J., Song B., Ribick M., Wang J., Gildersleeve R. D., Pennathur S., and Kaufman, R. J. (2009). Translation Attenuation through eIF2alpha Phosphorylation Prevents Oxidative Stress and Maintains the Differentiated State in Beta Cells. *Cell Metabolism* 10(1): 13-26.
- Bienert G. P., Møller A. L. B., Kristiansen K. A., Schulz A., Møller I. M., Schjoerring J. K., and Jahn T. P. (2007). Specific Aquaporins Facilitate the Diffusion of Hydrogen Peroxide across Membranes. *Journal of Biological Chemistry* 282(2): 1183-1192.
- Chakraborty S., Hill A. L., Shirsekar, G., Afzal A. J., Wang G. L., Mackey D., and Bonello P. (2016). Quantification of hydrogen peroxide in plant tissues using Amplex Red. *Methods* 109: 105-113.
- Chen Y. and Brandizzi, F. (2012). AtIRE1A/AtIRE1B and AGB1 independently control two essential unfolded protein response pathways in Arabidopsis. *Plant J* 69(2): 266-277.
- Chen Y. and Brandizzi, F. (2013). Analysis of Unfolded Protein Response in Arabidopsis. *G Protein-Coupled Receptor Signaling in Plants: Methods and Protocols*. M. P. Running. Totowa, NJ, Humana Press, 10.1007/978-1-62703-532-3_8: 73-80.
- Contento A. L., and Bassham D. C. (2010). Increase in catalase-3 activity as a response to use of alternative catabolic substrates during sucrose starvation. *Plant Physiology and Biochemistry* 48(4): 232-238.
- Cullinan S. B., Zhang D., Hannink M., Arvisais E., Kaufman R. J., and Diehl J. A. (2003). Nrf2 is a direct PERK substrate and effector of PERK-dependent cell survival. *Mol Cell Biol* 23(20): 7198-7209.
- Deng Y., Humbert S., Liu J. X., Srivastava R., Rothstein S. J., and Howell S. H. (2011). Heat induces the splicing by IRE1 of a mRNA encoding a transcription factor involved in the unfolded protein response in Arabidopsis. *Proc Natl Acad Sci* 108(17): 7247-7252.
- Deng Y., Srivastava R., and Howell S. H. (2013). Protein kinase and ribonuclease domains of IRE1 confer stress tolerance, vegetative growth, and reproductive development in Arabidopsis. *Proc Natl Acad Sci* 110(48): 19633-19638.
- Dong C. H., Hu X., Tang W., Zheng X., Kim Y. S., Lee B. H., and Zhu J. K. (2006). A putative Arabidopsis nucleoporin, AtNUP160, is critical for RNA export and required for plant tolerance to cold stress. *Mol Cell Biol* 26(24): 9533-9543.

Dunand C., Crèvecoeur M., and Penel C. (2007). Distribution of superoxide and hydrogen peroxide in *Arabidopsis* root and their influence on root development: possible interaction with peroxidases. *New Phytologist* 174(2): 332-341.

Gao H., Brandizzi F., Benning C., and Larkin R. M. (2008). A membrane-tethered transcription factor defines a branch of the heat stress response in *Arabidopsis thaliana*. *Proc Natl Acad Sci U S A* 105(42): 16398-16403.

Gapper C. and Dolan L. (2006). Control of Plant Development by Reactive Oxygen Species. *Plant Physiology* 141(2): 341-345.

Gething M. J. and Sambrook J. (1992). Protein folding in the cell. *Nature* 355(6355): 33-45.

Han J., Back S. H., Hur J., Lin Y.-H., Gildersleeve R., Shan J., Yuan C. L., Krokowski D., Wang S., Hatzoglou M., Kilberg M. S., Sartor M. A., and Kaufman R. J. (2013). ER-stress-induced transcriptional regulation increases protein synthesis leading to cell death. *Nature Cell Biology* 15: 481.

Harding H. P., Novoa I., Zhang Y., Zeng H., Wek R., Schapira M., and Ron, D. (2000). Regulated translation initiation controls stress-induced gene expression in mammalian cells. *Mol Cell* 6(5): 1099-1108.

Harding H. P., Zhang Y., and Ron D. (1999). Protein translation and folding are coupled by an endoplasmic-reticulum-resident kinase. *Nature* 397(6716): 271-274.

Hausmann N., Fengler S., Hennig A., Franz-Wachtel M., Hampp R., and Neef M. (2014). Cytosolic calcium, hydrogen peroxide and related gene expression and protein modulation in *Arabidopsis thaliana* cell cultures respond immediately to altered gravitation: parabolic flight data. *Plant Biology* 16: 120-128.

Hourihan John M., Moronetti Mazzeo Lorenza E., Fernández-Cárdenas L. P., and Blackwell T. K. (2016). Cysteine Sulfenylation Directs IRE-1 to Activate the SKN-1/Nrf2 Antioxidant Response. *Molecular Cell* 63(4): 553-566.

Huang S., Van Aken O., Schwarzländer M., Belt K., and Millar A. H. (2016). The Roles of Mitochondrial Reactive Oxygen Species in Cellular Signaling and Stress Response in Plants. *Plant Physiology* 171(3): 1551-1559.

Iwata Y. and Koizumi N. (2005). An *Arabidopsis* transcription factor, AtbZIP60, regulates the endoplasmic reticulum stress response in a manner unique to plants. *Proc Natl Acad Sci* 102(14): 5280-5285.

Krebs J., Agellon L. B., and Michalak M. (2015). Ca²⁺ homeostasis and endoplasmic reticulum (ER) stress: An integrated view of calcium signaling. *Biochemical and Biophysical Research Communications* 460(1): 114-121.

Lai Y.-S., Renna L., Yarema J., Ruberti C., He S. Y., and Brandizzi F. (2018). Salicylic acid-independent role of NPR1 is required for protection from proteotoxic stress in the plant endoplasmic reticulum. *Proc Natl Acad Sci*, 10.1073/pnas.1802254115.

Le C. T. T., Brumbarova T., Ivanov R., Stoof C., Weber E., Mohrbacher J., Fink-Straube C., and Bauer P. (2016). ZINC FINGER OF ARABIDOPSIS THALIANA12 (ZAT12) Interacts with FER-LIKE IRON DEFICIENCY- INDUCED TRANSCRIPTION FACTOR (FIT) Linking Iron Deficiency and Oxidative Stress Responses. *Plant Physiology* 170(1): 540-557.

Lee B.-h., and Zhu J.-K. (2010). Phenotypic Analysis of Arabidopsis Mutants: Electrolyte Leakage after Freezing Stress. *Cold Spring Harbor Protocols* 2010(1): pdb.prot4970.

Li G., Scull C., Ozcan L., and Tabas I. (2010). NADPH oxidase links endoplasmic reticulum stress, oxidative stress, and PKR activation to induce apoptosis. *J Cell Biol* 191(6): 1113-1125.

Liang F., Cunningham K. W., Harper J. F., and Sze H. (1997). ECA1 complements yeast mutants defective in Ca²⁺ pumps and encodes an endoplasmic reticulum-type Ca²⁺-ATPase in Arabidopsis thaliana . *Proc Natl Acad Sci*94(16): 8579-8584.

Liu, J.-X., Srivastava, R., Che, P. and Howell S. H. (2007a). An Endoplasmic Reticulum Stress Response in Arabidopsis Is Mediated by Proteolytic Processing and Nuclear Relocation of a Membrane-Associated Transcription Factor, bZIP28. *The Plant Cell* 19(12): 4111-4119.

Liu, J., Ding, P., Sun, T., Nitta, Y., Dong, O., Huang, X., Yang, W., Li, X., Botella, J. R. and Zhang Y. (2013). Heterotrimeric G Proteins Serve as a Converging Point in Plant Defense Signaling Activated by Multiple Receptor-Like Kinases. *Plant Physiology* 161(4): 2146-2158.

Liu, J. X. and Howell S. H. (2016a). Managing the protein folding demands in the endoplasmic reticulum of plants. *New Phytol* 211(2): 418-428.

Liu, J. X., Srivastava, R., Che, P. and Howell S. H. (2007b). Salt stress responses in Arabidopsis utilize a signal transduction pathway related to endoplasmic reticulum stress signaling. *The Plant Journal* 51(5): 897-909.

Liu Y., and He C. (2016b). Regulation of plant reactive oxygen species (ROS) in stress responses: learning from AtRBOHD. *Plant Cell Reports* 35(5): 995-1007.

Maity S., Rajkumar A., Matai L., Bhat A., Ghosh A., Agam G., Kaur S., Bhatt N. R., Mukhopadhyay A., Sengupta S., and Chakraborty K. (2016). Oxidative Homeostasis Regulates the Response to Reductive Endoplasmic Reticulum Stress through Translation Control. *Cell Rep* 16(3): 851-865.

Malhotra J. D., and Kaufman R. J. (2007). Endoplasmic reticulum stress and oxidative stress: a vicious cycle or a double-edged sword? *Antioxid Redox Signal* 9(12): 2277-2293.

Marciniak S. J., Yun C. Y., Oyadomari S., Novoa I., Zhang Y., Jungreis R., Nagata K., Harding, H. P., and Ron D. (2004). CHOP induces death by promoting protein synthesis and oxidation in the stressed endoplasmic reticulum. *Genes & Development* 18(24): 3066-3077.

Miller G., Schlauch K., Tam R., Cortes D., Torres M. A., Shulaev V., Dangl J. L., and Mittler R. (2009). The Plant NADPH Oxidase RBOHD Mediates Rapid Systemic Signaling in Response to Diverse Stimuli. *Science Signaling* 2(84): ra45-ra45.

Mittler R., and Blumwald E. (2015). The Roles of ROS and ABA in Systemic Acquired Acclimation. *The Plant Cell* 27(1): 64-70.

Morales J., Kadota Y., Zipfel C., Molina A., and Torres M.-A. (2016). The Arabidopsis NADPH oxidases RbohD and RbohF display differential expression patterns and contributions during plant immunity. *Journal of Experimental Botany* 67(6): 1663-1676.

Moreno A. A., Mukhtar M. S., Blanco F., Boatwright J. L., Moreno I., Jordan M. R., Chen Y., Brandizzi F., Dong X., and Orellana A. (2012). IRE1/bZIP60-mediated unfolded protein response plays distinct roles in plant immunity and abiotic stress responses. *PLoS One* 7(2): e31944.

Mori I. C. and Schroeder J. I. (2004). Reactive Oxygen Species Activation of Plant Ca²⁺ Channels. A Signaling Mechanism in Polar Growth, Hormone Transduction, Stress Signaling, and Hypothetically Mechanotransduction. *Plant Physiology* 135(2): 702-708.

Nagashima Y., Mishiba K., Suzuki E., Shimada Y., Iwata Y., and Koizumi N. (2011). Arabidopsis IRE1 catalyses unconventional splicing of bZIP60 mRNA to produce the active transcription factor. *Sci Rep* 1: 29.

Ogasawara Y., Kaya H., Hiraoka G., Yumoto F., Kimura S., Kadota Y., Hishinuma H., Senzaki E., Yamagoe S., Nagata K., Nara M., Suzuki K., Tanokura M., and Kuchitsu K. (2008). Synergistic activation of the Arabidopsis NADPH oxidase AtrbohD by Ca²⁺ and phosphorylation. *Journal of Biological Chemistry* 283(14): 8885-8892.

Ozgun R., Turkan I., Uzilday B., and Sekmen A. H. (2014). Endoplasmic reticulum stress triggers ROS signalling, changes the redox state, and regulates the antioxidant defence of *Arabidopsis thaliana*. *J Exp Bot* 65(5): 1377-1390.

Ozgun R., Uzilday B., Iwata Y., Koizumi N., and Turkan, I. (2018). Interplay between unfolded protein response and reactive oxygen species: a dynamic duo. *J Exp Bot*, 10.1093/jxb/ery040.

Ozgun R., Uzilday B., Sekmen A. H., and Turkan I. (2015). The effects of induced production of reactive oxygen species in organelles on endoplasmic reticulum stress and on the unfolded protein response in arabidopsis. *Ann Bot* 116(4): 541-553.

Pedruzzi E., Guichard C., Ollivier V., Driss F., Fay M., Prunet C., Marie J.-C., Pouzet C., Samadi M., Elbim C., O'Dowd Y., Bens M., Vandewalle A., Gougerot-Pocidallo M.-A., Lizard G., and Ogier-Denis E. (2004). NAD(P)H Oxidase Nox-4 Mediates 7-Ketocholesterol-Induced Endoplasmic Reticulum Stress and Apoptosis in Human Aortic Smooth Muscle Cells. *Molecular and Cellular Biology* 24(24): 10703-10717.

Queval G., Hager J., Gakière B., and Noctor G. (2008). Why are literature data for H₂O₂ contents so variable? A discussion of potential difficulties in the quantitative assay of leaf extracts. *Journal of Experimental Botany* 59(2): 135-146.

Ron D. and Walter P. (2007). Signal integration in the endoplasmic reticulum unfolded protein response. *Nature reviews Molecular cell biology* 8(7): 519-529.

Ruberti C., Kim S.-J., Stefano G., and Brandizzi F. (2015). Unfolded protein response in plants: One master, many questions. *Current opinion in plant biology* 27: 59-66.

Ruberti C., Lai Y. S., and Brandizzi F. (2018). Recovery from temporary endoplasmic reticulum stress in plants relies on the tissue-specific and largely independent roles of bZIP28 and bZIP60, as well as an antagonizing function of BAX-Inhibitor1 upon the pro-adaptive signaling mediated by bZIP28. *Plant Journal* 93(1): 155-165.

Sadhukhan A., Kobayashi Y., Nakano Y., Iuchi S., Kobayashi M., Sahoo L., and Koyama H. (2017). Genome-wide Association Study Reveals that the Aquaporin NIP1;1 Contributes to Variation in Hydrogen Peroxide Sensitivity in *Arabidopsis thaliana*. *Molecular Plant* 10(8): 1082-1094.

Sevier C. S., and Kaiser C. A. (2008). Ero1 and redox homeostasis in the endoplasmic reticulum. *Biochim Biophys Acta* 1783(4): 549-556.

Shen J., Chen X., Hendershot L., and Prywes R. (2002). ER stress regulation of ATF6 localization by dissociation of BiP/GRP78 binding and unmasking of Golgi localization signals. *Developmental cell* 3(1): 99-111.

Sovolyova N., Healy S., Samali A., and Logue Susan E. (2014). Stressed to death – mechanisms of ER stress-induced cell death. *Biological Chemistry*. 395: 1.

Srivastava R., Deng Y., Shah S., Rao A. G., and Howell S. H. (2013). BINDING PROTEIN is a master regulator of the endoplasmic reticulum stress sensor/transducer bZIP28 in *Arabidopsis*. *The Plant Cell* 25(4): 1416-1429.

Sun L., Lu S.-J., Zhang S.-S., Zhou S.-F., Sun L., and Liu J.-X. (2013). The lumen-facing domain is important for the biological function and organelle-to-organelle movement of bZIP28 during ER stress in *Arabidopsis*. *Molecular plant* 6(5): 1605-1615.

Suzuki N., Miller G., Morales J., Shulaev V., Torres M. A., and Mittler R. (2011). Respiratory burst oxidases: the engines of ROS signaling. *Current Opinion in Plant Biology* 14(6): 691-699.

Tait M. A. and Hik D. S. (2003). Is dimethylsulfoxide a reliable solvent for extracting chlorophyll under field conditions? *Photosynthesis Research* 78(1): 87-91.

Torres M. A., Dangl J. L., and Jones J. D. (2002). *Arabidopsis* gp91phox homologues AtrbohD and AtrbohF are required for accumulation of reactive oxygen intermediates in the plant defense response. *Proc Natl Acad Sci U S A* 99(1): 517-522.

Torres M. A., Jones J. D., and Dangl J. L. (2005). Pathogen-induced, NADPH oxidase-derived reactive oxygen intermediates suppress spread of cell death in *Arabidopsis thaliana*. *Nat Genet* 37(10): 1130-1134.

- Torres M. A., Morales J., Sánchez-Rodríguez C., Molina A., and Dangl J. L. (2013). Functional Interplay Between Arabidopsis NADPH Oxidases and Heterotrimeric G Protein. *Molecular Plant-Microbe Interactions* 26(6): 686-694.
- Tripathy B. C. and Oelmüller R. (2012). Reactive oxygen species generation and signaling in plants. *Plant Signaling & Behavior* 7(12): 1621-1633.
- Tu B. P. and Weissman J. S. (2004). Oxidative protein folding in eukaryotes: mechanisms and consequences. *J Cell Biol* 164(3): 341-346.
- Xu J., Tran T., Padilla Marcia C. S., Braun D. M., and Goggin F. L. (2017). Superoxide-responsive gene expression in *Arabidopsis thaliana* and *Zea mays*. *Plant Physiology and Biochemistry* 117: 51-60.
- Yamaoka Y., Choi B. Y., Kim H., Shin S., Kim Y., Jang S., Song W.-Y., Cho C. H., Yoon H. S., Kohno K., and Lee Y. (2018). Identification and functional study of the ER stress sensor IRE1 in *Chlamydomonas reinhardtii*. *The Plant Journal*, 10.1111/tpj.13844.
- Zhong H. H., Young J. C., Pease E. A., Hangarter R. P., and McClung C. R. (1994). Interactions between Light and the Circadian Clock in the Regulation of CAT2 Expression in Arabidopsis. *Plant Physiology* 104(3): 889-898.
- Zhu A., Romero R., and Petty H. R. (2010). Amplex UltraRed enhances the sensitivity of fluorimetric pyruvate detection. *Anal Biochem* 403(1-2): 123-125.
- Zito E. (2015). ERO1: A protein disulfide oxidase and H₂O₂ producer. *Free Radic Biol Med* 83: 299-304.

CHAPTER III
**RELEVANCE OF THE UNFOLDED PROTEIN RESPONSE TO SPACEFLIGHT-
INDUCED TRANSCRIPTIONAL REPROGRAMMING IN ARABIDOPSIS**

The work presented in this chapter has been published in *Astrobiology*:

Angelos E., Ko D.K, Zemelis-Durfee S and Brandizzi F. (2021) Relevance of the Unfolded Protein Response to Spaceflight-Induced Transcriptional Reprogramming in *Arabidopsis*. *Astrobiology*. 21(3):367-380.

ABSTRACT

Plants are primary producers of food and oxygen on Earth and will likewise be indispensable to the establishment of large-scale sustainable ecosystems and human survival in space. To contribute to the understanding of how plants respond to spaceflight stress, we examined the significance of the unfolded protein response (UPR), a conserved signaling cascade that responds to a number of unfavorable environmental stresses, in the model plant *Arabidopsis thaliana*. To do so, we performed a large-scale comparative transcriptome profiling in wild type (WT) and various UPR-defective mutants during the SpaceX-CRS12 mission to the International Space Station. We established that orbital culture substantially alters the expression of hundreds of stress-related genes compared to ground control conditions. Although expression of those genes varied in the UPR mutants on the ground, it was largely similar across the genotypes in the spaceflight condition. Our results have yielded new information on how plants respond to growth in orbit and support the hypothesis that spaceflight induces the activation of signaling pathways that compensate for the loss of UPR regulators in the control of downstream transcriptional regulatory networks.

INTRODUCTION

Extraterrestrial habitation and prolonged space travel require successful plant growth to recreate livable environments for humans (Ferl *et al.* 2002; Massa *et al.* 2016; Zhou *et al.* 2019). Studies over the past 70 years have sought to develop a better understanding of how plants are affected by and adapt to the significant stresses imposed by spaceflight (e.g., microgravity, radiation, vibration, limited exchange of gases), which can affect plant development and yield (Paul *et al.* 2013). Recent iterations of the sophisticated chamber hardware for plant growth housed on the International Space Station (ISS) have allowed for multigenerational plant growth in space and analyses of plant responses to this environment (Massa *et al.* 2016). However, these facilities are insufficient for large-scale plant growth on extraterrestrial environments due to their size and resource cost. Therefore, generation of germplasm adapted to stresses experienced during growth in extraterrestrial environments is a critical contribution to the realization of sustainable plant cultivation in space.

The UPR is a signaling cascade that responds to a number of unfavorable environmental and cellular stresses. The UPR is generally activated by a buildup of unfolded proteins in the endoplasmic reticulum (ER), a condition known as ER stress (Ron and Walter 2007). The ER stress sensors conserved across metazoans and plants include the ER-associated protein kinase and ribonuclease inositol requiring enzyme 1 (IRE1) and ER membrane-tethered transcription factors (TFs) (metazoan Activating Transcription Factor 6 (ATF6) and plant basic Leucine Zipper 17 (bZIP17) and bZIP28). Activation of IRE1 leads to unconventional splicing of an intron from the mRNA of an IRE1-downstream bZIP-TF (metazoan X-box binding protein 1 (XBP1) and plant bZIP60). The UPR TFs are translocated to the nucleus to control expression of UPR target genes

and restore ER homeostasis (Chen and Brandizzi 2012; Halbleib *et al.* 2017; Kim *et al.* 2018; Koizumi *et al.* 2001; Mishiba *et al.* 2019; Pastor-Cantizano *et al.* 2019; Pu *et al.* 2019; Ruberti *et al.* 2018; Tam *et al.* 2018). Insufficient UPR leads to the actuation of cell death (Ron and Walter 2007; Walter and Ron 2011).

In terrestrially grown plants, the UPR is a key mediator of responses to a variety of stresses including heat, pathogen, and high light / singlet oxygen (Beaugelin *et al.* 2020; Deng *et al.* 2011; Guillemette *et al.* 2014; Moreno *et al.* 2012; Pastor-Cantizano *et al.* 2019; Zhang *et al.* 2015; Zhang *et al.* 2017). Additionally, analyses of higher order UPR mutants have demonstrated that the UPR regulators are necessary for post embryonic growth and reproductive development in *Arabidopsis* under unstressed conditions as well (Chen and Brandizzi 2012; Kim *et al.* 2018; Mishiba *et al.* 2019; Pu *et al.* 2019). Therefore, a better understanding of the UPR can enable efforts to potentiate plant stress responses and improve plant yield.

Given the broad responsiveness of the UPR to environmental stresses, we hypothesized that the UPR effectors could coordinate gene expression reprogramming in spaceflight stress conditions. To test this hypothesis, we analyzed global gene expression changes in WT *Arabidopsis* as well as loss-of-function mutants of *IRE1* (*ire1a ire1b*, herein dubbed *ire1*), *bZIP28* and *bZIP60* (single and double mutants: *bzip28*, *bzip60*, *bzip28 bzip60*), cultivated in orbit during the SpaceX-CRS12 mission to the ISS. We used these genetic backgrounds to identify genes controlled jointly or specifically by the UPR sensors and UPR TFs and define the extent to which the known signaling pathways of the UPR functionally interact in a whole organism under microgravity-associated conditions. We established that, in space and on ground, gene expression undergoes a substantial reprogramming on a genome-scale. Growth in orbit substantially altered the expression of thousands of genes associated with significant biological traits compared to

ground controls. However, while many of these spaceflight-responsive genes were regulated uniquely in certain UPR mutants compared to WT in the ground control, such a genotype-specific regulation was not observed in the spaceflight condition. These observations not only provide new insight into how plants respond to spaceflight, they also establish that spaceflight induced-transcriptional responses mitigate the need for the gene-regulatory networks controlled by the UPR sensors.

MATERIALS AND METHODS

Launch Hardware and Experimental Timeline

This flight experiment utilized 4 Biological Research In a Canister (BRIC) containing a total of 22 Petri Dish Fixation Unit (PDFU) hardware (Wells *et al.* 2001) to cultivate sterile dark grown seedlings germinated aboard the International Space Station (ISS) for a 14 day period. PDFU actuation chambers were loaded with a tissue fixative (RNAlater; Invitrogen) to preserve samples at the conclusion of the flight experiment. An identical set of samples was prepared and grown on earth with a two-day offset at Kennedy Space Center (KSC) ISS Environmental Simulator (ISSES) to allow for data transmission and reproduction of incubation conditions experienced by flight samples in orbit. HOBO data loggers equipped with temperature sensors were integrated into two of the four BRICs to record temperatures experienced by samples during the experiment for *post-hoc* analysis. Launch samples (i.e., Arabidopsis seeds) were integrated into BRIC flight hardware in a sterile hood approximately 48 hr before the August 14th, 2017 launch of SpaceX-CRS12 spacecraft. Integrated science/hardware was kept at 4 °C to maintain seed dormancy prior to packing in cold storage bags while being loaded onto Dragon capsule and during launch. After docking, samples were removed from cold storage bags by ISS astronauts, warmed to ambient ISS temperature, allowing seed germination and experiment initiation in the BRIC. After 14 days, ISS astronauts actuated PDFUs, which were then incubated at room temperature for a further 3 hr before being transferred to the ISS -80 MELFI freezer. Samples were kept at approximately -80 °C until BRICs were conditioned to -32 °C in double cold bag storage (Hutchison and Campana 2009), and stowed in the Dragon capsule before undocking and

atmospheric reentry on September 16th. After returning to KSC, samples were stored at -80 °C until de-integration of the flight and ground samples. De-integration occurred on November 1st, 2017.

Germplasm and Culture Conditions

Arabidopsis thaliana seeds of the following genotypes were used for flight and ground controls: WT (Col-0 ecotype), *atire1* (Chen and Brandizzi 2012; Nagashima *et al.* 2011), *bzip60* (Moreno *et al.* 2012), *bzip28* (Gao *et al.* 2008), and *bzip28 bzip60* (Deng *et al.* 2013). Petri dishes (60 mm) were prepared with 6.7 ml of sterile ½ Murashige and Skoog (MS) media supplemented with Gamborg's B5 Vitamins (PhytoTechnology Laboratories), 0.5% sucrose (Sigma-Aldrich), 0.4% Phytigel (Sigma-Aldrich), pH adjusted to 5.7. In a sterile hood, seeds of WT and UPR mutant genotypes were surface sterilized with one wash of 70% ethanol, one wash of 50% bleach containing 0.5% Tween 20, and then nine additional washes with sterile H₂O distilled twice. After the final wash was removed, seeds were resuspended in 1.5 ml sterile water for wet plating using a 1 mL pipette equipped with sterile filter-tip. For each experimental unit (flight and ground control), five plate replicates of WT and *bzip28/bzip60* genotypes and four plate replicates of *atire1*, *bzip28*, *bzip60* genotypes were prepared. Each plate replicate contained 70-80 seeds evenly spaced in a grid pattern on the plate surface. The Petri dishes were sealed with Parafilm (Heathrow Scientific) and individual plates were then wrapped twice with sterile aluminum foil. Individually wrapped plates were grouped by BRIC configuration and wrapped together with two more layers of sterile aluminum foil prior to sample removal from the sterile hood. Plates were placed at 4 °C until the integration of samples into science hardware the following morning.

Sample Processing and Experimental Material Assessment

Flight and ground control experiments samples were preserved in RNAlater *in situ*, and kept at -80 °C (see results section for experimental timeline). The Petri dishes were removed from packaging and thawed in groups of three to prevent excess exposure to room temperature during sample collection. After removing most of the RNAlater from the plates, sterile forceps were used to transfer seedlings from the plates to microcentrifuge tubes containing two glass beads. Seedlings were then frozen in liquid nitrogen. This procedure was done quickly to maximize RNA recovery. Accordingly, only some pictures were taken of plates before extraction for example purposes. Most pictures were taken after the bulk of the sample was removed, with the remaining seedlings also imaged for *post-hoc* inspection. All plates were free from any visible evidence of bacterial or fungal contamination. Frozen samples were ground to a powder using a Retch Mixer Mill (Retch; Haan, Germany). RNA was extracted from tissues using a NucleoSpin RNA Plant Kit (Machery-Nagel) according to the manufacturer's instructions including DNase Digestion. The overall quality and RNA Integrity Number (RIN) of RNA samples were assessed using Agilent Bioanalyzer 2100 (Agilent, Santa Clara, CA USA).

Library Preparation, Sequencing and Bioinformatics Analysis

RNA-seq libraries were constructed using the Illumina TruSeq Stranded mRNA Library (Illumina, San Diego, CA, USA) and sequenced in single-end mode on the Illumina HiSeq 4000 platform (50-nt) at Research Technology Support Facility Genomics Core at Michigan State University (RTSF-MSU). For each library, read quality was assessed using the FastQC (version 0.11.3) software (<https://www.bioinformatics.babraham.ac.uk/projects/fastqc/>). Reads were

cleaned for quality and adapter sequences with Cutadapt (version 1.8.1) using a minimum base quality 20 retaining reads with a minimum length of 30 nucleotides after trimming (Martin 2011). Quality-filtered reads were aligned to the Col-0 reference genome (TAIR10) using Bowtie (version 2.3.1) and TopHat (version 2.1.1) with a 10 bp minimum intron length and 15,000 bp maximum intron length (Kim *et al.* 2013; Langmead and Salzberg 2012). Fragments per kilobase exon model per million mapped reads (FPKM) were measured using TAIR10 gene model annotation with Cufflinks (version 1.3.0) (Trapnell *et al.* 2010). The log₂ transformed and normalized gene expression levels [FPKM + 1] were used for correlation analysis (Spearman's rank correlation coefficient) between biological replicates and principal component analysis (PCA). Per-gene read counts were identified using HTSeq (version 0.6.1p1) in the union mode with a minimum mapping quality of 20 with stranded reverse counting (Anders *et al.* 2015). Differential gene expression analysis was performed in four biological replicates (for WT and *bzip28 bzip60*, selected based on the correlation with other biological replicates) using DESeq2 (version 1.16.1) within R (version 3.4.0) based on a comparison of spaceflight to ground with adjusted P-value < 0.01 and absolute log₂-transformed fold change > 1.5 (Love *et al.* 2014). Genes of which the total count across all samples is < 100 were not included in the analysis. Gene Ontology (GO) Overrepresentation was performed using PANTHER (Fisher's Exact type with False Discovery Rate correction) (<http://www.pantherdb.org>) (Mi *et al.* 2019a; Mi *et al.* 2019b). K-means clustering analysis on average FPKM values from biological replicates was performed using the Morpheus tool (Morpheus, <https://software.broadinstitute.org/morpheus>). The optimal number of K-means clusters was determined using factoextra package in R.

RESULTS

Spaceflight Alters the Growth of Seedlings Independently from an Intact UPR Signaling

When we inspected the WT and UPR mutant seedlings (*atire1*, *bzip60*, *bzip28* and *bzip28 bzip60*) of the ground control and flight samples at the completion of the mission, we found that in the ground control samples, etiolated hypocotyls (i.e., pale and elongated due to the lack of light) were above the surface of the solidified media while roots had penetrated the growth medium perpendicular to the surface (Figure 3.1A). However, in flight samples, we found that etiolated hypocotyls as well as roots had generally penetrated the growth medium regardless of genotype tested (Figure 3.1A). Interestingly, we also observed that cotyledon petioles of flight sample seedlings were elongated (Figure 3.1B) compared to ground control seedlings (Figure 3.1A). Overall, these observations are consistent with plant growth in the darkness and space, conditions leading to elongated hypocotyls and petioles, and a lack of directional growth, respectively (Paul *et al.* 2017). These observations also suggest that the UPR unlikely exerts a noticeable role in growth direction in response to altered gravity levels.

Spaceflight Results in an Increase of Total RNA

RNA degradation has previously been observed in independent Arabidopsis spaceflight experiments performed in BRIC-PDFUs (Johnson *et al.* 2017; Paul *et al.* 2012). To test the RNA quality of our samples, we measured RNA integrity number (RIN) as an indicator of overall RNA quality (RIN, 1 = low quality; 10 = high quality) of each sample and compared size peaks of 25S and 18S ribosomal RNA (rRNA) among samples (Mueller *et al.* 2004). Note that these

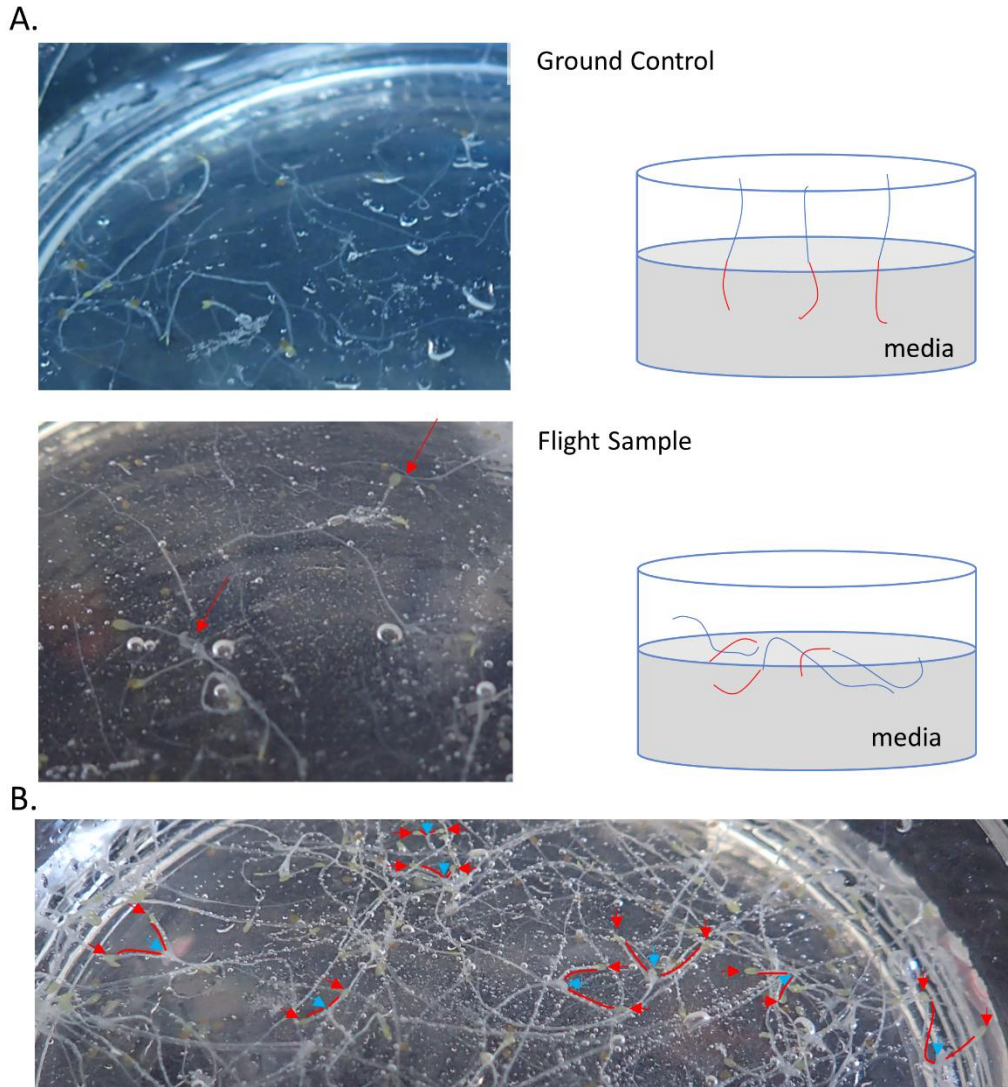


Figure 3.1. Growth of etiolated hypocotyls was altered by spaceflight.

A) Representative ground and flight sample plates (left) were imaged after the bulk of etiolated hypocotyls and RNAlater was removed to ensure maximal RNA integrity. Remaining seedlings were used for post-hoc analysis of morphological/growth differences. **B)** Example plate of a WT flight sample which was imaged after thawing, but prior to seedling removal. Individual seedlings which could be distinguished from the bulk were marked with a blue arrow to mark the shoot meristem. The cotyledons of elongated petioles were marked with a red arrow and a red line used to connect the cotyledon to the meristem of the same seedling. Petioles were elongated compared to ground sample petioles (representative morphology of ground control presented in FIG 1A, right side).

measurements include smaller plastid rRNA peaks, which lower the maximum RIN value to around 8, independent of RNA quality (Babu and Gassmann 2016). We found that all flight samples had RIN values between 7.5 and 8.0, indicating that RNA was of high quality. For ground samples, RIN values were found to be between 4.0 and 7.7, which would ordinarily indicate mild degradation of some samples. However, closer analyses revealed that, in nearly all ground samples (77%), the RIN algorithm failed to identify the correct peaks. In these samples, the algorithm identified the 18S rRNA peak as the 25S rRNA peak, and a putative organelle rRNA peak (Babu and Gassmann 2016) as the 18S rRNA (Figure 3.S1; Supplemental figures found in Chapter Appendix). Therefore, to compare RNA quality between treatments and genotypes from the Bioanalyzer data outputs, we used the ratio of 25S/18S peak heights as a substitute measure. Because the 25S peak height is reduced more quickly than the 18S peak in RNA degrading conditions (e.g., elevated temperature, exogenous RNases, endogenous apoptotic RNase activity) (Babu and Gassmann 2016; Mueller *et al.* 2004), a decreased 25S/18S ratio would indicate RNA degradation. We observed no significant differences of the 25S/18S ratio across all genotypes (Figure 3.2A), therefore, both flight and ground samples had no significant RNA degradation. Interestingly, by comparing the 25S peak height to one of the two other peaks near the 18S peak (i.e., a putative organellar rRNA peak, designated 18S (-3); Figure 3.S1) in each sample, it was clear that the relative ratio of 25S to 18S (-3) was significantly lower in the ground samples compared to flight samples (Figure 3.2B, Figure 3.S1). This low ratio indicates that the ground samples were depleted of nuclear-encoded rRNAs (i.e. 25S and 18S rRNAs) compared to other RNA species. This observation is also consistent with our findings that our ground samples contained significantly less total RNA (of which rRNA is a significant fraction (Lodish 2000)) than flight samples (Figure 3.2C). Because we extracted RNA from a similar number of seedlings

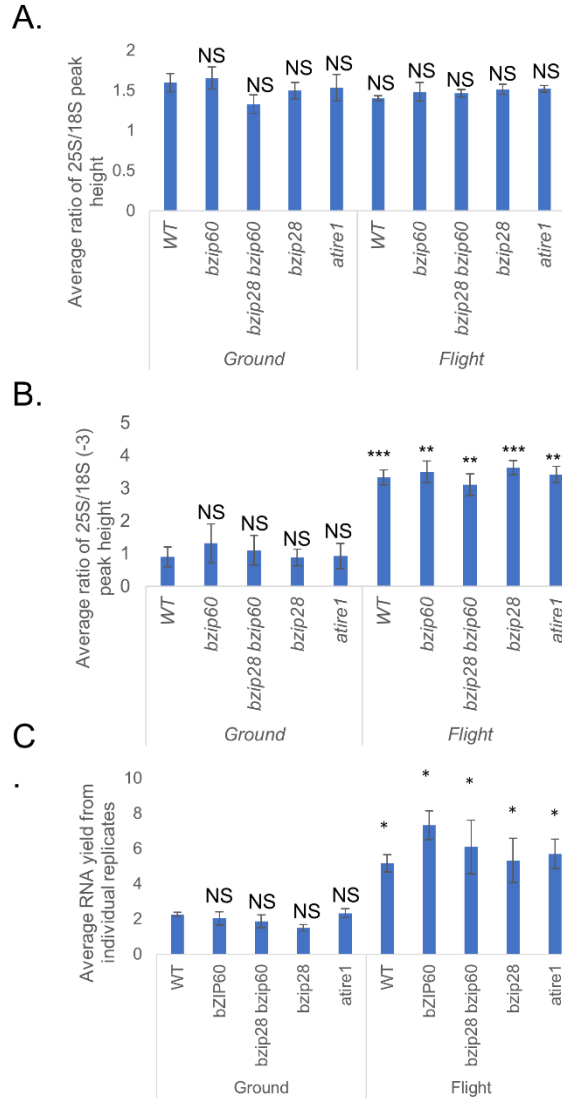


Figure 3.2. RNA quality assessment of flight and ground control samples.

A) Average ratio of 25S/18S peak heights as determined from Bioanalyzer traces from each sample was used as a secondary measure of RNA quality due to the RIN algorithms incorrect identification of the appropriate peaks. **B)** The relative content of rRNA found in each genotype in both conditions was determined by comparing the height of the 25S peak to an organellar rRNA peak (18S (-3)) which was found in each sample. **C)** Average RNA yields from each genotype from flight and ground samples. Statistical significance determined by Welch's T-test, p value represent by NS= >0.05; *= <0.05; **=<0.005; ***=<0.0005.

from flight samples and ground samples, our results indicate that flight samples contained larger amount of total RNA compared to ground samples, which is likely to be caused by elevated levels of nuclear encoded rRNA in flight samples, and unlikely to be due to RNA degradation of the ground samples.

Global Transcriptomics Analyses Indicate that Gene Expression Reprogramming in Response to Spaceflight Depends partially on Intact UPR Signaling

Having established that the total RNA from ground and flight samples was of acceptable quality, we next proceeded to RNA-sequencing (RNA-seq) to investigate the impact of spaceflight on global gene expression changes in the UPR mutants. In RNA-seq library preparation, mRNA was enriched by purification to efficiently remove rRNA (Zhao *et al.* 2018) and mitigate potential sequencing bias due to higher rRNA levels in flight samples. We obtained an average of approximately 32 million reads per sample, of which 95-99% were successfully mapped to the Arabidopsis reference genome (Figure 3.S2). Spearman's rank correlation coefficients calculated between biological replicates showed a high reproducibility of our RNA-seq dataset (Figure 3.3A). Furthermore, principal component analysis (PCA) exhibited a strong separation of ground samples from flight samples (Figure 3.3B) and indicated that ground samples located more closely to each other than the flight samples. Overall, these analyses further supported a statistical robustness of the RNA-Seq and justified further investigation.

To investigate gene expression changes in response to spaceflight, we identified differentially expressed genes (DEGs) in each genotype by comparing gene expression values in ground and flight samples (Supplemental Data File 1.1). A total of 3,465 genes were classified as

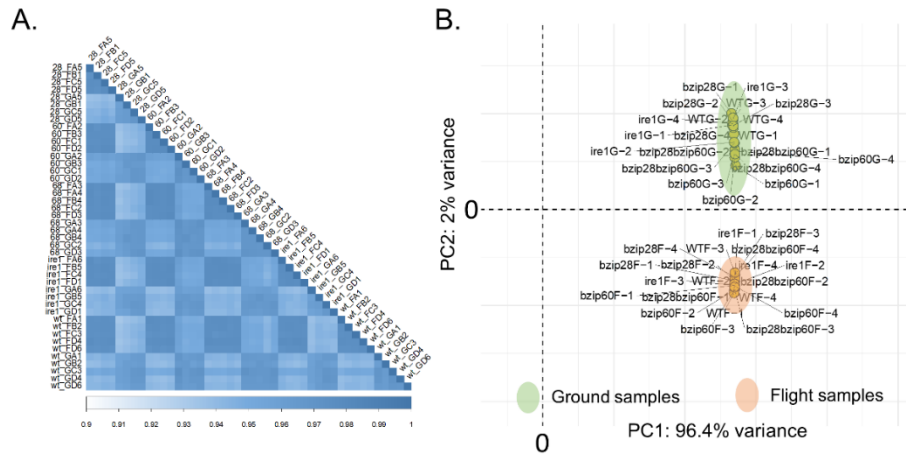


Figure 3.3. Overall quality assessment of RNA-sequencing dataset

A) Spearman's correlation coefficients demonstrate a close relationship between biological replicates. **B)** Principal component analysis demonstrates a clear separation between flight and ground samples.

DEGs in at least one genotypes. WT had the largest number of DEGs (upregulated DEGs in flight compared to ground, $n = 1675$; downregulated DEGs, $n = 831$) among the genotypes tested. The *bzip28 bzip60* mutant had the smallest number of DEGs (upregulated DEGs, $n = 1293$; downregulated DEGs, $n = 562$) (Figure 3.4A, B). In all genotypes, the number of upregulated DEGs were higher than that of downregulated DEGs (WT, 2.02-fold; *atire1*, 1.98-fold; *bzip28*, 2.28-fold; *bzip60*, 1.80-fold; *bzip28 bzip60*, 2.30-fold), indicating a higher impact of space flight on inducing gene expression rather than suppressing it. While the identity of 34.8% (783/2249) of upregulated DEGs and 27.5% (335/1217) of downregulated DEGs overlapped across all genotypes, relatively smaller numbers of DEGs were found to be genotype-specific, ranging from 30 (downregulated exclusively in *bzip28 bzip60*) to 207 (upregulated in WT).

In summary, based on the verified number of upregulated and downregulated DEGs in flight samples compared to ground samples across genotypes, the UPR mutants had consistently

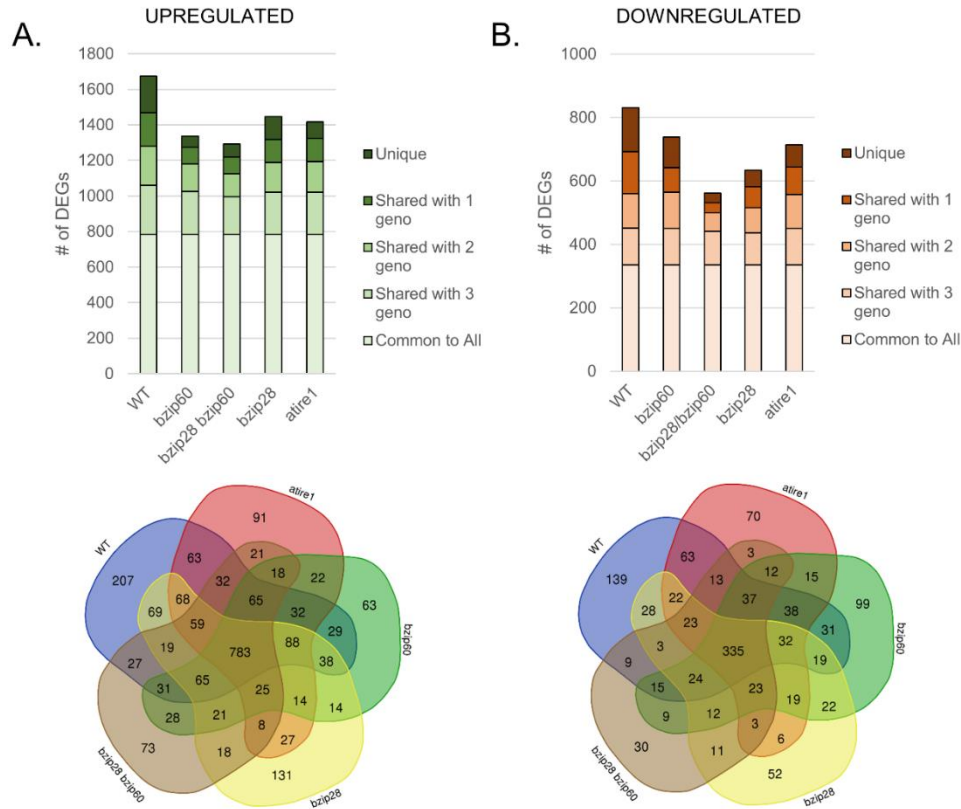


Figure 3.4. Summary of differential gene expression analyses.

Differential expression analysis using the 4 biological replicates with the highest correlation was performed via HTseq v0.6.1pl and DESeq v2. For each genotype and for genes differentially expressed genes in flight samples relative to ground samples were determined using a strict criterion: adjusted P value <0.01 ; $|\log_2FC| > 1.5$. Total number of upregulated **A**) and downregulated **B**) DEGs in each background were analyzed to determine what proportion were shared between the different genotypes.

fewer overall DEGs than WT, indicating that the UPR could play at least a partial a role in regulating the transcriptional reprogramming in space compared to ground control.

Biological Pathways Connected to the DEGs between Flight and Ground

To gain insights in the biological pathways altered in spaceflight in our experimental set up, we performed separate Gene Ontology (GO) analyses on upregulated and downregulated

DEGs in WT (Supplemental Data File 1.2), generating a list of parental-GO terms (more general, represented by a larger number of genes in the reference gene set), and cognate child-GO terms (more specific, smaller numbers of genes in the reference gene set) (Figure 3.5). Intriguingly, we found that stress responsive-genes (e.g., “response to abscisic acid”, “response to hypoxia”, “response to water deprivation” and “response to oxidative stress”) as well as genes involved in physiological responses often associated with stress response adaptation were enriched in downregulated DEGs in WT. This result is consistent with previous studies that reported downregulation of water-stress related genes using Arabidopsis BRIC-PDFU microarray transcriptomes (Johnson *et al.* 2017) and that found abscisic acid response and water stress response overrepresentation in misregulated DEGs in Col-0 WT using RNA-seq (Choi *et al.* 2019). In addition, we observed that metabolic processes associated with stress adaptation (Batista-Silva *et al.* 2019; Hildebrandt *et al.* 2015), including amino acid catabolism and sucrose starvation response, were overrepresented in flight- downregulated DEGs. Ribosome biogenesis, translation and gene expression processes were highly underrepresented in this category, i.e. they were more likely to be upregulated by flight, or remain unchanged. By further analyzing the normalized gene expression values (FPKM), we also found that ribosome biogenesis and rRNA processing GO terms appeared significantly overrepresented in genes upregulated by > 2 fold changes (flight/ground). These, however, were not considered as DEGs based upon the strict statistical criteria applied in our analyses (see methods). The lower FPKMs of ribosome biogenesis-related genes in ground control samples are consistent with our observations that the ground control samples were partially depleted of 25S and 18S rRNA compared to flight samples (Figure 3.2C).

We also found that GO terms enriched in upregulated DEGs included biological processes that have been noted in previous Arabidopsis spaceflight transcriptome analyses, such as

WT-UPREGULATED

DNA replication, DNA repair	# in Ref.	# in DEGs	Expected	Fold Enrichment	FDR
mitotic DNA replication initiation	4	4	0.24	16.81	3.08E-02
cell cycle	486	76	28.91	2.63	4.06E-09
double-strand break repair via break-induced replication	12	8	0.71	11.21	7.31E-04
double-strand break repair via homologous recombination	81	14	4.82	2.91	4.05E-02
DNA replication	124	31	7.38	4.2	5.54E-07
Far Red/Red Light Response	# in Ref.	# in DEGs	Expected	Fold Enrichment	FDR
response to far red light	51	15	3.03	4.94	3.99E-04
response to red or far red light	197	26	11.72	2.22	2.17E-02
response to light stimulus	680	74	40.45	1.83	5.04E-04
response to radiation	705	75	41.94	1.79	6.65E-04
Photosynthesis	# in Ref.	# in DEGs	Expected	Fold Enrichment	FDR
photosynthetic electron transport in photosystem I	17	8	1.01	7.91	3.76E-03
photosynthesis, light reaction	122	31	7.26	4.27	5.93E-07
generation of precursor metabolites and energy	338	42	20.11	2.09	3.54E-03
photosynthesis, light harvesting in photosystem I	23	9	1.37	6.58	3.86E-03
photosynthesis, light harvesting	44	15	2.62	5.73	1.54E-04
Secondary Metabolite Biosynthesis	# in Ref.	# in DEGs	Expected	Fold Enrichment	FDR
glucosinolate metabolic process	112	22	6.66	3.3	6.59E-04
glucosinolate biosynthetic process	39	16	2.32	6.9	1.42E-05
secondary metabolite biosynthetic process	147	22	8.75	2.52	1.65E-02

WT-DOWNREGULATED

Abscisic Acid, Response to Stress	# in Ref.	# in DEGs	Expected	Fold Enrichment	FDR
response to abscisic acid	524	61	15.16	4.02	5.26E-16
response to water deprivation	340	48	9.83	4.88	2.58E-15
cellular response to hypoxia	234	46	6.77	6.8	2.91E-19
response to oxidative stress	392	41	11.34	3.62	3.04E-09
response to stress	3079	200	89.06	2.25	4.75E-24
Amino Acid Catabolism, Sucrose Starvation	# in Ref.	# in DEGs	Expected	Fold Enrichment	FDR
tyrosine catabolic process	5	3	0.14	20.74	4.01E-02
alpha-amino acid catabolic process	65	11	1.88	5.85	7.03E-04
leucine catabolic process	7	4	0.2	19.76	9.01E-03
branched-chain amino acid catabolic process	18	7	0.52	13.44	3.87E-04
cellular amino acid catabolic process	73	15	2.11	7.1	3.02E-06
isoprenoid catabolic process	23	5	0.67	7.52	3.71E-02
lipid catabolic process	108	11	3.12	3.52	2.33E-02
cellular response to sucrose starvation	4	4	0.12	34.57	2.55E-03
Absence of Light	# in Ref.	# in DEGs	Expected	Fold Enrichment	FDR
response to absence of light	44	13	1.27	10.21	7.39E-07
response to light intensity	142	19	4.11	4.63	1.86E-05
response to abiotic stimulus	2062	158	59.64	2.65	9.37E-25
Ribosome Biogenesis, Translation	# in Ref.	# in DEGs	Expected	Fold Enrichment	FDR
ncRNA metabolic process	407	1	11.77	0.08	1.08E-02
ribosome biogenesis	351	1	10.15	0.1	3.57E-02
ribonucleoprotein complex biogenesis	422	2	12.21	0.16	3.57E-02
translation	431	1	12.47	0.08	5.79E-03
RNA metabolic process	1227	6	35.49	0.17	2.94E-07
gene expression	1403	6	40.58	0.15	4.86E-09
cellular protein metabolic process	2699	43	78.07	0.55	8.55E-04

Figure 3.5. Representative biological processes gene ontologies over- or under- represented by upregulated or downregulated DEGs in the WT background.

secondary metabolite biosynthesis associated with defense responses (Choi *et al.* 2019; Johnson *et al.* 2017). Furthermore, we verified the dichotomous occurrence of the “absence of light”, “response to red or far red light (R/FR) response” GO terms in the down- and upregulated gene sets, respectively. The overrepresentation of photosynthetic components in upregulated DEGs is partially consistent with the results of a previous BRIC-PDFU experiment showing light/high light response and some photosynthesis-related genes to be differentially regulated in a subset of the tested genotypes (Choi *et al.* 2019). In addition to the findings consistent with previous spaceflight reports, we also observed a significant enrichment of DNA repair, DNA replication, and cell cycle pathways in the upregulated DEGs, which could be possibly associated with exposure of flight samples, but not ground samples, to ionizing radiation during spaceflight.

Together these results indicate that in our experimental conditions, spaceflight globally affects gene expression changes associated with a broad array of significant biological processes, largely identified also in previous spaceflight transcriptome studies (Choi *et al.* 2019; Johnson *et al.* 2017).

The UPR Regulators Exert a Minor but Significant Role on Gene Expression in Spaceflight

Next, we aimed to gain insights into the transcriptome changes caused by the absence of intact UPR signaling in both ground and spaceflight conditions. To address it, we performed K-means clustering analysis on FPKM values for all DEGs (n = 3,465) obtained in at least one genotype (Figure 3.6; Data File 1.3) and then performed GO analysis to correlate the expression signature of each cluster to biological functions (Data File 1.4). Our clustering analysis suggested that variations in the identified DEGs between different genotypes (Figure 3.4) were primarily the

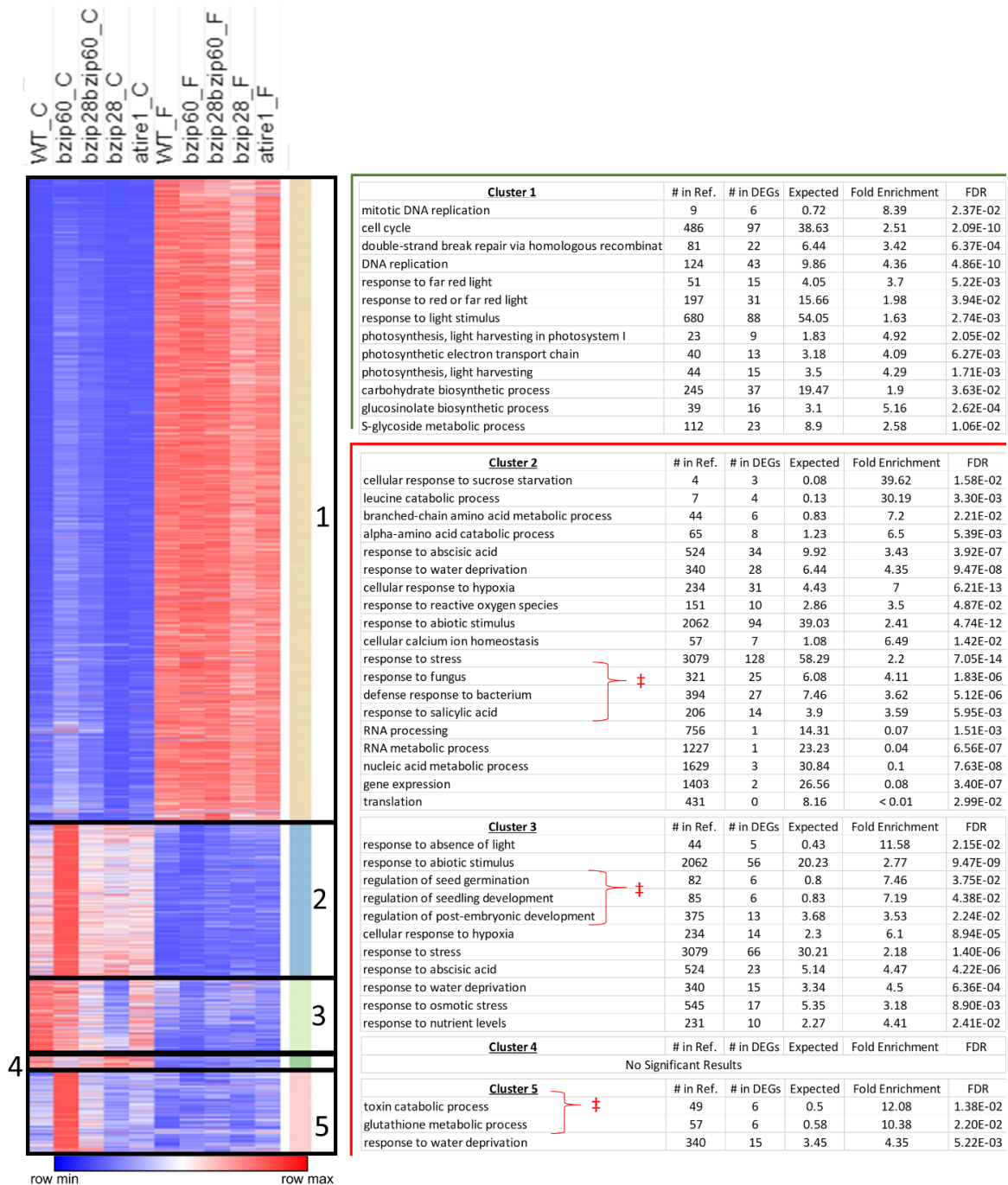


Figure 3.6. K-means clustering analysis of all 3,465 DEGs in at least 1 background.

Each row represents FPKM values of an individual gene averaged between biological replicates. For each row blue represents the minimum relative expression value and red the maximum expression value, white is the middle value. For each cluster GO biological process analysis of DEGs demonstrates a role for UPR regulation of ground control stress responses, which are largely repressed by flight.

result of variable FPKM values in the ground control samples (Figure 3.6). In flight, the FPKM values were roughly equalized to insignificantly different levels of expression across all genotypes. Of the 3,465 DEGs, in the ground samples 517 DEGs had FPKM values that were significantly different ($p\text{-value} \leq 0.01$) in at least one UPR mutant compared to WT; however, in flight samples only 144 genes had FPKM values that were significantly different in at least one UPR mutant genotype compared to WT (Figure 3.6; Figure 3.S3).

The largest cluster (Cluster 1 DEGs; $n = 2299$) consisted of DEGs upregulated to varying degrees in most of the genotypes tested. As such, a nearly identical set of GO terms that were enriched in upregulated DEGs in WT (Figure 3.5) were also enriched in Cluster 1. We then compared the FPKM values of DEGs in ground samples across genotypes, and found that 39.1% and 19.8% of DEGs in Cluster 1 were significantly different in the *bzip60* and *bzip28 bzip60*, respectively, compared to WT, while only 4.6% and 2.9% of DEGs were significantly different in *bzip28* and *atire1* compared to WT (Figure 3.S4). Overall, these results indicate that bZIP60 has functions that are independent of IRE1 and bZIP28, which in turn are required to downregulate Cluster 1 DEGs in ground control conditions. These observations are in accordance with the findings in ground conditions that bZIP28 and bZIP60 control some UPR target genes in an independent manner (Ruberti *et al.* 2018). In Cluster 2 (DEGs; $n = 546$), expression of DEGs was induced exclusively in ground *bzip60* compared to other ground genotypes while highly suppressed to similar levels of expression in flight samples of all genotypes. As such, the proportion of DEGs in *bzip60*, whose expression was significantly different from WT, was much higher (17%) than other genotypes (*bzip28 bzip60*, 0.9%; *bzip28*, 1.0%; *atire1*, 1.2%) (Figure 3.S4). We reasoned that bZIP28 and bZIP60 could have a negative feedback relationship in which the absence of bZIP28 suppressed the effect of *bzip60* mutation exclusively in the ground

condition. The overrepresented GO terms in Cluster 2 were largely similar to the GO terms enriched in the downregulated DEGs genes in the WT genotype: “response to abscisic acid”, “response to water deprivation”, and “response to hypoxia” (Figure 3.5). In addition, Cluster 2 DEGs showed significant enrichment of GO terms associated with biotic stress responses that were not found in analyses of the WT genotype (Figure 3.5) or found to be strongly enriched in the any of the other clusters (Figure 3.6; Data File 1.4). These results indicate that bZIP60 may have repressive roles in regulating genes involved in both abiotic and biotic stress responses.

The gene expression pattern of Cluster 3 (DEGs; n = 274) was also characterized largely by genes with lower expression values in spaceflight compared to ground control across genotypes, except for *bzip28*. However, contrasting with Cluster 2, the FPKM values in the *bzip60* genotype was not different from WT FPKM values; only 3.2% of DEGs showed significantly different FPKM compared to WT (Figure 3.S4). Instead, the absence of bZIP28 (i.e., in the *bzip28* mutant) had a higher impact on gene expression in the ground condition compared to other mutants (Figure 3.S4). Interestingly, these Cluster 3 DEGs had intermediate FPKM values in the *bzip28 bzip60* genotype in ground control compared to the extremes of the *bzip60* and *bzip28* single mutants, indicating an antagonistic regulation of bZIP28 and bZIP60 on these genes in the ground condition, which was largely compensated for in the *bzip28 bzip60* genotype.

Similar to Clusters 2 and 3, Cluster 4 (DEGs; n =55) contained genes, whose expression exhibited overall lower FPKMs in spaceflight compared to ground across genotypes. However, Cluster 4 showed a unique pattern: the expression of the DEGs in this cluster was significantly lower in *bzip60* compared to WT and the other genotypes in the ground condition (Figure 3.S4) and showed no prominent differences across genotypes in the spaceflight condition. Although Cluster 4 was not significantly represented by any biological process GO terms, a closer analysis

revealed that 22% of all DEGs in this cluster were encoded on the mitochondrial genome; mitochondria-encoded genes comprise only 0.5% of all protein-coding genes in the Arabidopsis genome annotation (<https://www.arabidopsis.org>) and 0.3% of DEGs called in this study.

Cluster 5 (DEGs; n= 291) showed a gene expression pattern similar to Cluster 2 with significantly higher levels in the *bzip60* genotype compared to the other genotypes in the ground control samples. (Figure 3.S4). In this Cluster, the DEGs were more affected by the absence of bZIP28 (*bzip28 bzip60* and *bzip28*) in the ground condition compared to Cluster 2. The GO term “response to water deprivation”, which was found to be enriched in Cluster 2, was significantly enriched in Cluster 5. In addition, relatively narrow child GO terms “toxin catabolic process” and “glutathione metabolic process”, which were not enriched in other clusters, were enriched in Cluster 5.

Overall, by comparing the *bzip60* and *bzip28* single mutants with the *bzip28 bzip60* double mutant, our transcriptomic profiling provides evidence for a highly complex, unconventional, regulatory relationship between bZIP60 and bZIP28 under the conditions experienced by ground control seedlings. Furthermore, a small number of significant differences between WT and the UPR mutants in spaceflight were found, supporting a small but significant role of the UPR in gene expression in spaceflight.

DISCUSSION

In this study, we examined the transcriptional responses of WT and seedlings with a compromised UPR to spaceflight to set the foundations to manipulate a critical growth and stress signaling pathway for improving plant adaptation to extraterrestrial environments. We utilized the BRIC-PDFU sterile plant culture hardware during the SpaceX-CRS12 mission to compare the transcriptional responses to the spaceflight between *Arabidopsis thaliana* WT and mutants defective in one or more components of the UPR, namely the TFs bZIP60, bZIP28, and the ER resident kinase/ribonuclease IRE1.

The BRIC-PDFU hardware has been employed in a number of dark-grown *Arabidopsis* transcriptome experiments towards different aims (Choi *et al.* 2019; Johnson *et al.* 2017; Kwon *et al.* 2015; Paul *et al.* 2012). Variability in technical experimental details and limited overlap between spaceflight/ground DEGs have been verified even between the same WT control genotype in simultaneous experiments (Johnson *et al.* 2017). However, some broad biological pathways have been found to be induced or repressed in response to spaceflight, including cell wall modification, response to light / high light, and oxidative stress, osmotic stress response, heat shock, and biotic defense / secondary metabolite synthesis (Choi *et al.* 2019; Johnson *et al.* 2017; Paul *et al.* 2012). Many of these responses were also noted in our study, including the downregulation of water stress response in space, which has been identified in four separate experiments (Choi *et al.* 2019; Johnson *et al.* 2017). However, we also observed correlative differences in seedling growth and an overall gene expression landscape not noted in previous studies. Our ground control seedlings had grown in a predictable manner, consistent with the

expected morphology of terrestrially grown *Arabidopsis* etiolated hypocotyls (Figure 3.1). Flight sample growth was also largely in line with expectations for seedlings grown in microgravity, including the observed petiole elongation which was shared in all flight samples. Indeed a petiole elongation of flight samples was also present in the images published of dark grown *Arabidopsis* experiments in the Col-0 background in previous experiments (Johnson *et al.* 2015; Paul *et al.* 2017). This growth phenotype is consistent with low R/FR ratio and shade avoidance syndrome (SAS) mediated by phytochrome signaling (Franklin 2008). The correlative responses observed in the transcriptome analysis (Figure 3.4) support that differentially regulated growth phenotypes and the large transcriptional rearrangements in flight during our experiment might have been mediated by phytochrome-related signaling, which is also known to constitutively repress abscisic acid signaling (Yang *et al.* 2016), and were found to be repressed in our flight samples. However, these differences in the response to light and the increased expression of photosynthetic components between ground and flight samples are anomalous when considering the spaceflight culture methods used in this study. BRIC-PDFUs are autoclavable, black polymer containers, which are sealed with metal lids during science integration, and allow injection of the chemical preservative without opening the unit. After being sealed on August 12th, the seeds and seedlings germinated from these seeds in the BRICs were not exposed to light during the launch and the 14-day growth period on the ISS. Therefore, the dichotomous occurrence of the “absence of light” overrepresentation in downregulated and of “response to red or far red light response” in upregulated DEGs is unlikely to be the result of actual differential exposure to light. One likely explanation is related to the hypocotyl-tissue media contact that occurred in our flight samples, which lacked a clear growth vector in microgravity, but had not occurred in our ground samples where roots grew perpendicular into the media. In previous experiments by Johnson *et al.* (2015)

and Paul *et al.* (2017), the dark grown ground control plates were oriented vertically and both sample sets displayed petiole elongation, although the precise differences in length or extent of petiole elongation between flight and ground were not quantified. How media contact could induce Red / Far Red (R/FR) light signaling in the dark is not immediately obvious; however, earlier studies showed that media containing sucrose modulated the R/FR signaling mediated by phytochrome A, promoting a red light response (Dijkwel *et al.* 1997). Coincidentally, the higher rRNA and total RNA content observed in flight samples compared to ground control samples in our study (Figure 3.2) is also consistent with an increased exposure of cells to sucrose or glucose, which is known to induce RNA accumulation, rRNA transcription, and ribosome biogenesis in plants (Ishida *et al.* 2016; Kojima *et al.* 2007), yeast (Kunkel *et al.* 2019), and mammals (Hannan *et al.* 2003). Nonetheless, we cannot rule out the remote possibility that our observations may be influenced by possible interactions between ionizing radiation and phytochrome R/FR signaling. For example, low dose gamma (γ) irradiation of lettuce seeds was found to mimic the effects of FR deactivation of red light activated phytochromes (Hsiao and Vidaver 1974). Additionally, a structural study of the bacterial phytochrome from the radiation resistant bacterial *Deinococcus radiodurans* established that X-ray radiation induced deprotonation of chromophore in the inactive phytochrome, a biochemical step thought to be involved in light induced activation of this protein (Li *et al.* 2015). Although the dose required to deprotonate 50% of the phytochrome (Li *et al.* 2015) was orders of magnitude larger than that expected to be experienced during our experimental period on the ISS, differences between prokaryotic and eukaryotic phytochromes could affect relevant properties of a hypothetical phytochrome-radiation interaction.

Interpreting a role for the UPR in the transcriptional response to spaceflight is complicated. We observed clear differences in the number of spaceflight DEGs in the UPR mutant backgrounds

compared to WT (Figure 3.4); and only 1,118 of the 3,465 DEGs were common to all genotypes. This would normally suggest that the transcriptional readjustments that occurred in response to spaceflight were at least partially the result of UPR-dependent processes. However, upon closer analysis of the underlying FPKM values it became clear that the differences in fold change values (flight/ground) across genotypes were more heavily influenced by the differential regulation of expression in the ground samples by the UPR regulators (Figure 3.6). The number of DEGs with FPKM values significantly different from WT FPKM values in at least one UPR mutant genotype was four times greater in the ground samples compared to flight samples (Figure 3.S3). The heat map visualization of these values (Figure 3.6) further suggests that the variations in ground samples expression levels were largely muted by spaceflight, as the endpoint transcript levels in flight samples were nearly uniform in the different genotypes. Overall, this would suggest that the UPR does not have a broad involvement in the response to spaceflight. One explanation for this observation may be related to the concerted downregulation of many stress-responsive processes in the flight samples compared to the ground samples (Figure 3.6). In spaceflight conditions, it seems likely that alternative signaling pathways are actuated, which repress the observed stress responses regulated by the UPR. Given the prevalence of starvation responses in ground samples, it is possible that microgravity induced-changes in growth habit provide better nutrient availability (Figure 3.7). As such, plants in flight may be able to better handle the stresses imposed by culture conditions, without requiring UPR regulator involvement.

Nonetheless, the observations related to an interaction between the UPR regulators bZIP60 and bZIP28 and the stresses imposed on ground control seedlings have yielded important information, which should be explored in the future. In the canonical ER stress response induced chemically or via environmental stress, bZIP60 and bZIP28 transcription factors interact in the

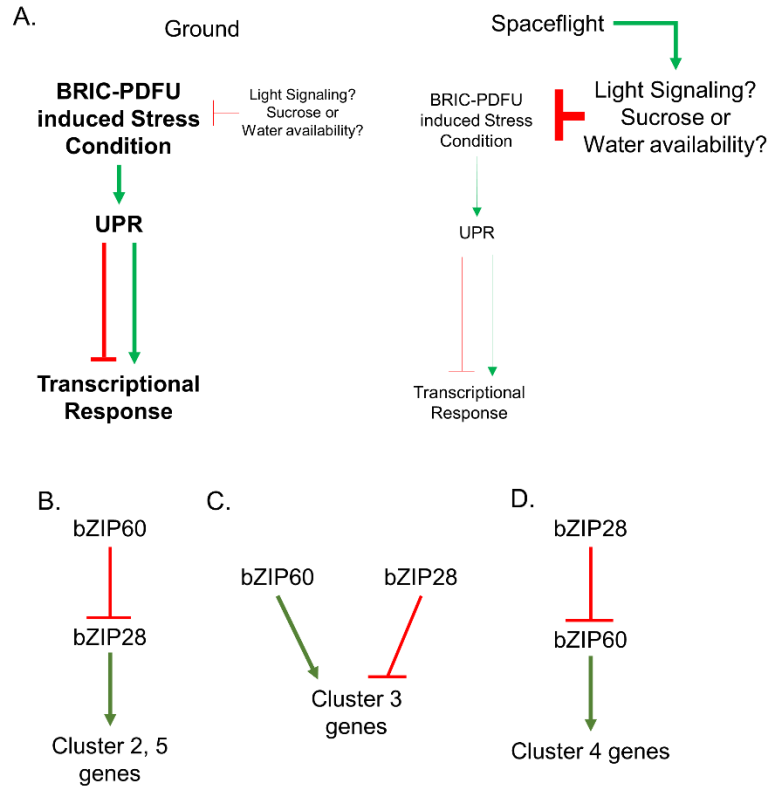


Figure 3.7. Simplified model of regulatory framework controlling stress responsive DEGs.

(A) Hypothesized regulatory framework for stress responsive DEGs found to be regulated by the UPR on the ground but not in flight conditions. Possible interactions between bZIP60 and bZIP28 in the regulation of DEGs found in (B) clusters 2 and 5 (C) cluster 3, and (D) cluster 4.

nucleus and direct the actions of the COMPASS DNA methylation complex to increase transcription of target genes (Song *et al.* 2015). Furthermore, these transcription factors can also bind independently to gene promoters to activate downstream UPR genes, as evidenced by the weaker activation of ER chaperones in the *bzip28 bzip60* double mutant compared to either of the *bzip28* or *bzip60* single mutants (Ruberti *et al.* 2018; this work). Although it has been suggested that bZIP60 and bZIP28 may also have unique target genes (Pastor-Cantizano *et al.* 2019), in our ground control samples the transcriptomic data suggest that bZIP60 and bZIP28 may have a more complex antagonistic relationship in the control of genes related to the response to abscisic acid, hypoxia, water deprivation, and to oxidative stress (Figures 3.6). In Clusters 2 and 5, and Cluster

4, we observed that the expression levels of the DEGs were higher or lower than WT in the *bzip60* genotype, respectively (Figure 3.6, Figure 3.S3). However, these differences were not observed in the *bzip28 bzip60* double mutant as would be expected. Conversely, in Cluster 3 we observed in ground samples that the expression levels of the DEGs were sharply lower in the *bzip28* genotype compared to WT. In the *bzip28 bzip60* genotype, the genes in Cluster 3 had expression levels that were higher than the *bzip28* genotype but were also lower than those of these genes in the WT or *bzip60* genotypes. In response to chemically induced UPR conditions, bZIP60 and bZIP28 cooperatively upregulate several UPR genes (Ruberti *et al.* 2018; Song *et al.* 2015). In our ground controls, the stress responsive genes, largely represented by “response to abscisic acid”, “response to water deprivation”, and “response to hypoxia” abiotic stress responses were regulated by bZIP28 and bZIP60 in a way that suggests that these TFs have antagonistic regulatory effects on these processes (Figure 3.7B-D).

The exact nature of the stress experienced by the ground control seedlings would need to be elucidated to better understand the impact of this information on agronomic and/or spaceflight-applications. Studies on the effect of plant growth in BRIC-PDFUs have already established that significant stress may be imposed on the seedlings grown in these conditions (Basu *et al.* 2017; Johnson *et al.* 2015). Consistent with our results, other BRIC-PDFU transcriptomes have found a downregulation of genes related to water stress responses (Johnson *et al.* 2017). However, as evaporative water loss from the BRIC-PDFUs is unlikely because they are sealed containers, the strongly represented GO terms related to “response to water deprivation” and “response to abscisic acid” are unlikely to be a direct response to actual water loss from the plates. Instead, it may be possible that the ground seedlings with etiolated hypocotyls that are not in contact with the media or have less overall contact with the media are water stressed compared to flight seedlings that are

in direct contact or have penetrated the media. Independently from the underlying stimulus for the observed differences, the possibility that bZIP60 and bZIP28 may have antagonistic interactions related to control of abscisic acid signaling or water deprivation responses should be investigated at the molecular level in the future to improve plant growth and stress responses in space and on the ground.

DATA AVAILABILITY

Raw sequencing data has been deposited at the NCBI Gene Expression Omnibus under the accession number GSE148914. Raw sequencing data has also been deposited at the NASA GeneLab data repository (Ray *et al.* 2018) for spaceflight experiments under the accession number GLDS-321.

ACKNOWLEDGEMENTS

We would like to thank the NASA, KSC, and NASA contractor support staff whose diligent work made these experiments possible. This work was supported primarily by NASA NNX12AN71G with contributing support from Training Program in Plant Biotechnology for Health and Sustainability (T32-GM110523), the DOE Great Lakes Bioenergy Research Center (DOE BER Office of Science DE-FC02-07ER64494 and DE-SC0018409), the Chemical Sciences, Geosciences and Biosciences Division, Office of Basic Energy Sciences, Office of Science, US Department of Energy (award number DE-FG02-91ER20021), National Institutes of Health (GM101038) and AgBioResearch (MICL02598) to FB.

AUTHOR CONTRIBUTIONS

F.B. designed the experiments. S.Z.-D. and E.A. performed preliminary launch preparations. E.A. executed the experiments. D.K.K. performed bioinformatics analysis. E.A., D.K.K., S.Z.-D, and F.B. analyzed data and wrote the article.

APPENDIX

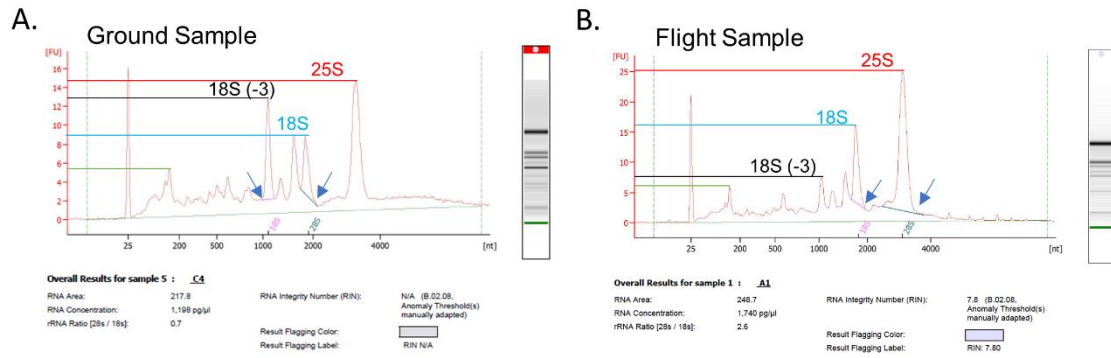


Figure 3.S1. Representative Bioanalyzer traces of ground and flight samples.

Representative Bioanalyzer traces of **A)** ground, and **B)** flight samples illustrating misidentification of peaks by the RIN algorithm in the ground sample, and identification of the correct 25S and 18S peaks in the flight samples. The peak labeled 18S(-3) is an likely organellular rRNA peak which had similar sizes in flight and ground samples which was used to quantify the relative content of 25S rRNA in Figure 3.2.

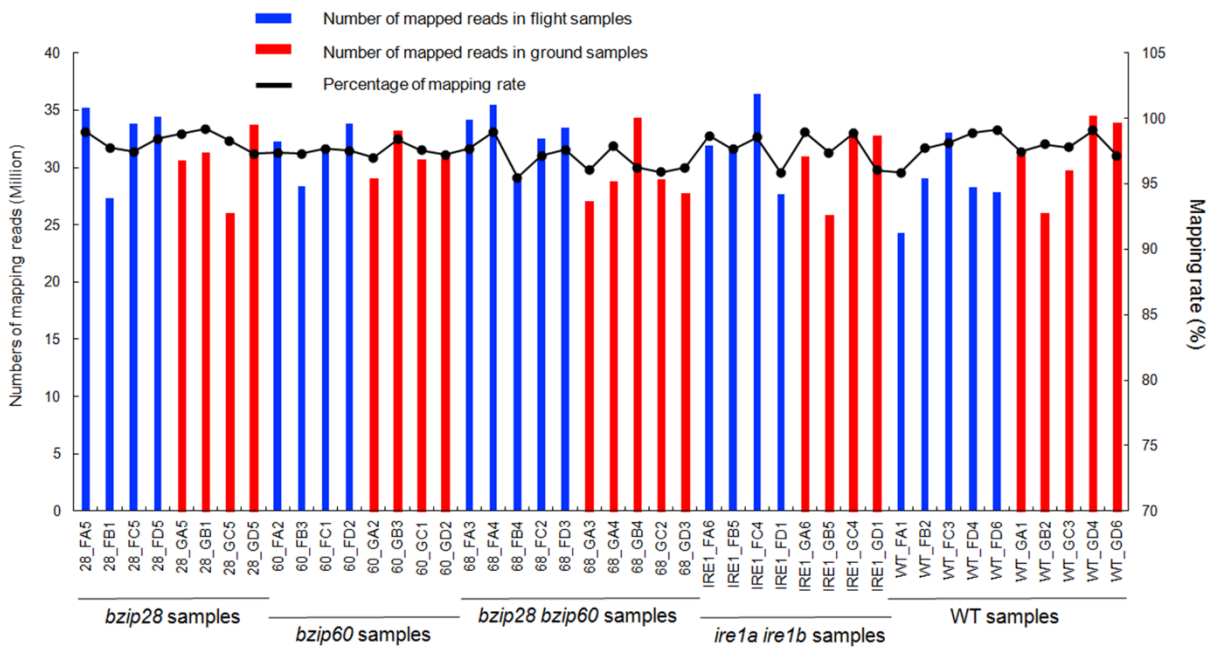


Figure 3.S2. Number of total mapped reads and mapping rate per sample.

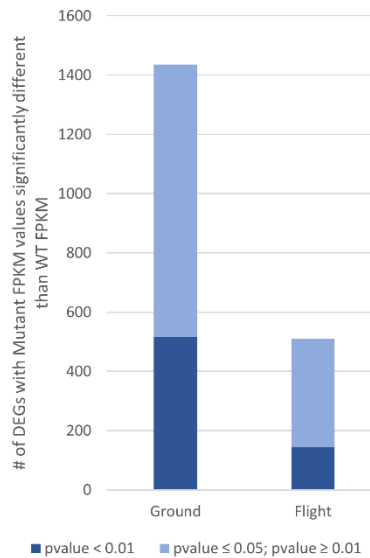


Figure 3.S3. Number of DEGs which had WT FPKM values which were significantly different from WT in at least one mutant genotype.

For all 3,465 DEGs identified, significant differences in FPKMs were identified between WT and each individual mutant genotype using a Welch’s t-test. The number of genes which had p-values between 0.05 and 0.01 and p-values less than 0.01 are indicated by the different colors.

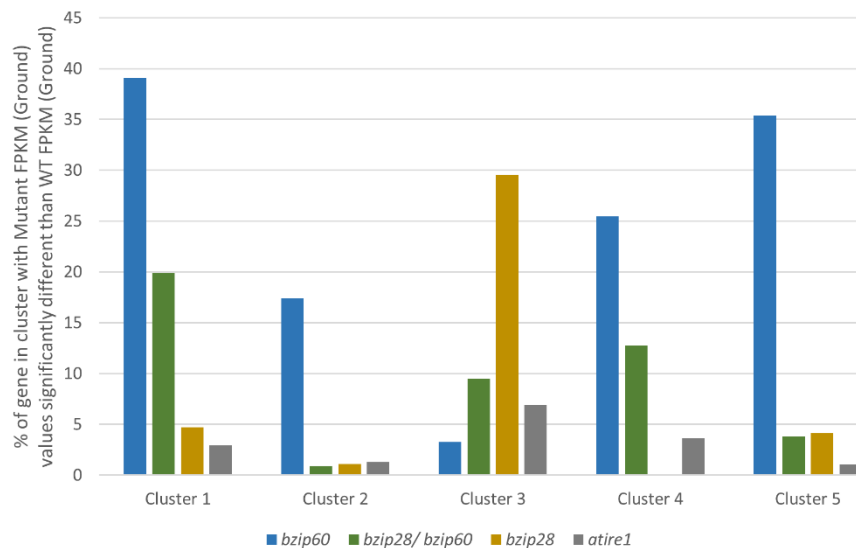


Figure 3.S4. Percentage of DEGs with statistically different ground FPKM values in the indicated UPR mutant genotype compared to WT ground FPKM values.

For each cluster in Figure 3.6, significant differences in FPKMs were identified between WT and each individual mutant genotype using a Welch’s t-test. The number of genes in that cluster which had p-values < 0.05 in the indicated genotype were counted and displayed as a percentage of the total number of genes in that cluster.

REFERENCES

REFERENCES

- Anders S., Pyl P. T., and Huber W. (2015) HTSeq—a Python framework to work with high-throughput sequencing data. *Bioinformatics*, 31: 166-169.
- Babu C. V. S., and Gassmann M. (2016) Assessing integrity of plant RNA with the Agilent 2100 Bioanalyzer System. *Agil Appl Note*, Waldbronn: 5990-8850E.
- Basu P., Kruse C. P. S., Luesse D. R., and Wyatt S. E. (2017) Growth in spaceflight hardware results in alterations to the transcriptome and proteome. *Life Sciences in Space Research*, 15: 88-96.
- Batista-Silva W., Heinemann B., Rugen N., Nunes-Nesi A., Araújo W. L., Braun H.-P., and Hildebrandt T. M. (2019) The role of amino acid metabolism during abiotic stress release. *Plant, Cell & Environment*, 42: 1630-1644.
- Beaugelin I., Chevalier A., d'Alessandro S., Ksas B., and Havaux M. (2020) Endoplasmic reticulum-mediated unfolded protein response is an integral part of singlet oxygen signalling in plants. *The Plant Journal*.
- Chen Y., and Brandizzi F. (2012) AtIRE1A/AtIRE1B and AGB1 independently control two essential unfolded protein response pathways in *Arabidopsis*. *The Plant Journal*, 69: 266-277.
- Choi W. G., Barker R. J., Kim S. H., Swanson S. J., and Gilroy S. (2019) Variation in the transcriptome of different ecotypes of *Arabidopsis thaliana* reveals signatures of oxidative stress in plant responses to spaceflight. *American journal of botany*, 106: 123-136.
- Deng Y., Humbert S., Liu J.-X., Srivastava R., Rothstein S. J., and Howell S. H. (2011) Heat induces the splicing by IRE1 of a mRNA encoding a transcription factor involved in the unfolded protein response in *Arabidopsis*. *Proceedings of the National Academy of Sciences*, 108: 7247-7252.
- Deng Y., Srivastava R., and Howell S. H. (2013) Protein kinase and ribonuclease domains of IRE1 confer stress tolerance, vegetative growth, and reproductive development in *Arabidopsis*. *Proceedings of the National Academy of Sciences*, 110: 19633-19638.
- Dijkwel P. P., Huijser C., Weisbeek P. J., Chua N. H., and Smeekeens S. C. (1997) Sucrose control of phytochrome A signaling in *Arabidopsis*. *The Plant cell*, 9: 583-595.
- Ferl R., Wheeler R., Levine H. G., and Paul A.-L. (2002) Plants in space. *Current opinion in plant biology*, 5: 258-263.
- Franklin K. A. (2008) Shade avoidance. *New Phytologist*, 179: 930-944.

Gao H., Brandizzi F., Benning C., and Larkin R. M. (2008) A membrane-tethered transcription factor defines a branch of the heat stress response in *Arabidopsis thaliana*. *Proceedings of the National Academy of Sciences*, 105: 16398-16403.

Guillemette T., Calmes B., and Simoneau P. (2014) Impact of the UPR on the virulence of the plant fungal pathogen *A. brassicicola*. *Virulence*, 5: 357-364.

Halbleib K., Pesek K., Covino R., Hofbauer H. F., Wunnicke D., Hänelt I., Hummer G., and Ernst R. (2017) Activation of the unfolded protein response by lipid bilayer stress. *Molecular cell*, 67: 673-684.

Hannan K. M., Brandenburger Y., Jenkins A., Sharkey K., Cavanaugh A., Rothblum L., Moss T., Poortinga G., McArthur G. A., Pearson R. B. and others. (2003) mTOR-Dependent Regulation of Ribosomal Gene Transcription Requires S6K1 and Is Mediated by Phosphorylation of the Carboxy-Terminal Activation Domain of the Nucleolar Transcription Factor UBF \dagger . *Molecular and Cellular Biology*, 23: 8862.

Hildebrandt Tatjana M., Nunes Nesi A., Araújo Wagner L., and Braun H.-P. (2015) Amino Acid Catabolism in Plants. *Molecular Plant*, 8: 1563-1579.

Hsiao A. I., and Vidaver W. (1974) Phytochrome-mediated Germination Responses in γ -Irradiated Lettuce Seeds. *Plant Physiology*, 54: 72-75.

Hutchison S., and Campana S. (2009) ISS Payloads Office Cold Stowage Overview.

Ishida T., Maekawa S., and Yanagisawa S. (2016) The Pre-rRNA Processing Complex in *Arabidopsis* Includes Two WD40-Domain-Containing Proteins Encoded by Glucose-Inducible Genes and Plant-Specific Proteins. *Molecular Plant*, 9: 312-315.

Johnson C. M., Subramanian A., Edelmann R. E., and Kiss J. Z. (2015) Morphometric analyses of petioles of seedlings grown in a spaceflight experiment. *Journal of Plant Research*, 128: 1007-1016.

Johnson C. M., Subramanian A., Pattathil S., Correll M. J., and Kiss J. Z. (2017) Comparative transcriptomics indicate changes in cell wall organization and stress response in seedlings during spaceflight. *American journal of botany*, 104: 1219-1231.

Kim D., Pertea G., Trapnell C., Pimentel H., Kelley R., and Salzberg S. L. (2013) TopHat2: accurate alignment of transcriptomes in the presence of insertions, deletions and gene fusions. *Genome biology*, 14: R36.

Kim J.-S., Yamaguchi-Shinozaki K., and Shinozaki K. (2018) ER-anchored transcription factors bZIP17 and bZIP28 regulate root elongation. *Plant physiology*, 176: 2221-2230.

Koizumi N., Martinez I. M., Kimata Y., Kohno K., Sano H., and Chrispeels M. J. (2001) Molecular characterization of two *Arabidopsis* Ire1 homologs, endoplasmic reticulum-located transmembrane protein kinases. *Plant Physiology*, 127: 949-962.

- Kojima H., Suzuki T., Kato T., Enomoto K.-i., Sato S., Kato T., Tabata S., Sáez-Vasquez J., Echeverría M., Nakagawa T. and others. (2007) Sugar-inducible expression of the nucleolin-1 gene of *Arabidopsis thaliana* and its role in ribosome synthesis, growth and development. *The Plant Journal*, 49: 1053-1063.
- Kunkel J., Luo X., and Capaldi A. P. (2019) Integrated TORC1 and PKA signaling control the temporal activation of glucose-induced gene expression in yeast. *Nature Communications*, 10: 3558.
- Kwon T., Sparks J. A., Nakashima J., Allen S. N., Tang Y., and Blancaflor E. B. (2015) Transcriptional response of *Arabidopsis* seedlings during spaceflight reveals peroxidase and cell wall remodeling genes associated with root hair development. *American Journal of Botany*, 102: 21-35.
- Langmead B., and Salzberg S. L. (2012) Fast gapped-read alignment with Bowtie 2. *Nature methods*, 9: 357.
- Li F., Burgie E. S., Yu T., Héroux A., Schatz G. C., Vierstra R. D., and Orville A. M. (2015) X-ray Radiation Induces Deprotonation of the Bilin Chromophore in Crystalline D. radiodurans Phytochrome. *Journal of the American Chemical Society*, 137: 2792-2795.
- Lodish H. F. (2000) *Molecular cell biology*. W.H. Freeman, New York.
- Love M. I., Huber W., and Anders S. (2014) Moderated estimation of fold change and dispersion for RNA-seq data with DESeq2. *Genome biology*, 15: 550.
- Martin M. (2011) Cutadapt removes adapter sequences from high-throughput sequencing reads. *EMBnet. journal*, 17: 10-12.
- Massa G. D., Wheeler R. M., Morrow R. C., and Levine H. G. (2016) Growth chambers on the International Space Station for large plants.
- Mi H., Muruganujan A., Ebert D., Huang X., and Thomas P. D. (2019a) PANTHER version 14: more genomes, a new PANTHER GO-slim and improvements in enrichment analysis tools. *Nucleic acids research*, 47: D419-D426.
- Mi H., Muruganujan A., Huang X., Ebert D., Mills C., Guo X., and Thomas P. D. (2019b) Protocol Update for large-scale genome and gene function analysis with the PANTHER classification system (v. 14.0). *Nature protocols*, 14: 703-721.
- Mishiba K.-i., Iwata Y., Mochizuki T., Matsumura A., Nishioka N., Hirata R., and Koizumi N. (2019) Unfolded protein-independent IRE1 activation contributes to multifaceted developmental processes in *Arabidopsis*. *Life science alliance*, 2.
- Moreno A. A., Mukhtar M. S., Blanco F., Boatwright J. L., Moreno I., Jordan M. R., Chen Y., Brandizzi F., Dong X., and Orellana A. (2012) IRE1/bZIP60-mediated unfolded protein response plays distinct roles in plant immunity and abiotic stress responses. *PLoS One*, 7.

- Mueller O., Lightfoot S., and Schroeder A. (2004) RNA integrity number (RIN)–standardization of RNA quality control. Agilent application note, publication, 1: 1-8.
- Nagashima Y., Mishiba K.-i., Suzuki E., Shimada Y., Iwata Y., and Koizumi N. (2011) Arabidopsis IRE1 catalyses unconventional splicing of bZIP60 mRNA to produce the active transcription factor. *Scientific reports*, 1: 29.
- Pastor-Cantizano N., Ko D. K., Angelos E., Pu Y., and Brandizzi F. (2019) Functional Diversification of ER Stress Responses in Arabidopsis. *Trends in biochemical sciences*.
- Paul A.-L., Sng N. J., Zupanska A. K., Krishnamurthy A., Schultz E. R., and Ferl R. J. (2017) Genetic dissection of the Arabidopsis spaceflight transcriptome: Are some responses dispensable for the physiological adaptation of plants to spaceflight? *PloS one*, 12.
- Paul A.-L., Wheeler R. M., Levine H. G., and Ferl R. J. (2013) Fundamental Plant Biology Enabled by The Space Shuttle. *American Journal of Botany*, 100: 226-234.
- Paul A.-L., Zupanska A. K., Ostrow D. T., Zhang Y., Sun Y., Li J.-L., Shanker S., Farmerie W. G., Amalfitano C. E., and Ferl R. J. (2012) Spaceflight Transcriptomes: Unique Responses to a Novel Environment. *Astrobiology*, 12: 40-56.
- Pu Y., Ruberti C., Angelos E. R., and Brandizzi F. (2019) AtIRE1C, an unconventional isoform of the UPR master regulator AtIRE1, is functionally associated with AtIRE1B in Arabidopsis gametogenesis. *Plant Direct*, 3: e00187.
- Ray, Shayoni, Samrawit Gebre, Homer Fogle, Daniel C Berrios, Peter B Tran, Jonathan M Galazka, and Sylvain V Costes. 2018. 'GeneLab: Omics database for spaceflight experiments', *Bioinformatics*, 35: 1753-59.
- Ron D., and Walter P. (2007) Signal integration in the endoplasmic reticulum unfolded protein response. *Nature reviews Molecular cell biology*, 8: 519-529.
- Ruberti C., Lai Y., and Brandizzi F. (2018) Recovery from temporary endoplasmic reticulum stress in plants relies on the tissue-specific and largely independent roles of bZIP 28 and bZIP 60, as well as an antagonizing function of BAX-Inhibitor 1 upon the pro-adaptive signaling mediated by bZIP 28. *The Plant Journal*, 93: 155-165.
- Song Z.-T., Sun L., Lu S.-J., Tian Y., Ding Y., and Liu J.-X. (2015) Transcription factor interaction with COMPASS-like complex regulates histone H3K4 trimethylation for specific gene expression in plants. *Proceedings of the National Academy of Sciences*, 112: 2900.
- Tam A. B., Roberts L. S., Chandra V., Rivera I. G., Nomura D. K., Forbes D. J., and Niwa M. (2018) The UPR activator ATF6 responds to proteotoxic and lipotoxic stress by distinct mechanisms. *Developmental cell*, 46: 327-343.
- Trapnell C., Williams B. A., Pertea G., Mortazavi A., Kwan G., Van Baren M. J., Salzberg S. L., Wold B. J., and Pachter L. (2010) Transcript assembly and quantification by RNA-Seq reveals

unannotated transcripts and isoform switching during cell differentiation. *Nature biotechnology*, 28: 511.

Walter, Peter, and David Ron. 2011. 'The Unfolded Protein Response: From Stress Pathway to Homeostatic Regulation', *Science*, 334: 1081.

Wells B., McCray R. H., Best M. D., and Levine H. G. (2001) A flight-rated Petri dish apparatus providing two stage fluid injection for aseptic biological investigations in space. SAE Technical Paper.

Yang D., Seaton D. D., Krahmer J., and Halliday K. J. (2016) Photoreceptor effects on plant biomass, resource allocation, and metabolic state. *Proceedings of the National Academy of Sciences*, 113: 7667.

Zhang L., Chen H., Brandizzi F., Verchot J., and Wang A. (2015) The UPR branch IRE1-bZIP60 in plants plays an essential role in viral infection and is complementary to the only UPR pathway in yeast. *PLoS genetics*, 11.

Zhang S.-S., Yang H., Ding L., Song Z.-T., Ma H., Chang F., and Liu J.-X. (2017) Tissue-specific transcriptomics reveals an important role of the unfolded protein response in maintaining fertility upon heat stress in *Arabidopsis*. *The Plant Cell*, 29: 1007-1023.

Zhao S., Zhang Y., Gamini R., Zhang B., and von Schack D. (2018) Evaluation of two main RNA-seq approaches for gene quantification in clinical RNA sequencing: polyA+ selection versus rRNA depletion. *Scientific Reports*, 8: 4781.

Zhou M., Sng N. J., LeFrois C. E., Paul A.-L., and Ferl R. J. (2019) Epigenomics in an extraterrestrial environment: organ-specific alteration of DNA methylation and gene expression elicited by spaceflight in *Arabidopsis thaliana*. *BMC genomics*, 20: 205.

CHAPTER IV

THE UPR REGULATOR IRE1 PROMOTES BALANCED ORGAN DEVELOPMENT

BY RESTRICTING TOR-DEPENDENT CONTROL OF CELLULAR

DIFFERENTIATION IN ARABIDOPSIS

The work presented in this chapter has been submitted for publication.

ABSTRACT

Proteostasis of the endoplasmic reticulum (ER) is controlled by sophisticated signaling pathways that are collectively called the unfolded protein response (UPR) and are initiated by specialized ER membrane-associated sensors. The evidence that complete loss-of-function mutations of the most conserved of the UPR sensors, inositol requiring enzyme 1 (IRE1), dysregulates tissue growth and development in metazoans and plants raises the fundamental question as to how IRE1 is connected to organismal growth. To address this question, we interrogated the Arabidopsis primary root, an established model for organ development, using the tractable Arabidopsis IRE1 mutant, *ire1a ire1b*, which has marked root development defects in the absence of exogenous stress. We demonstrate that IRE1 is required to reach maximum rates of cell elongation and root growth. We also established that in the actively growing *ire1a ire1b* mutant root tips the Target of Rapamycin (TOR) kinase, a widely conserved pro-growth regulator, is hyperactive, and that, unlike cell proliferation, the rate of cell differentiation is enhanced in *ire1a ire1b* in a TOR-dependent manner. By functionally connecting two essential growth regulators, these results underpin a novel and critical role of IRE1 in organ development and indicate that, as cells exit an undifferentiated state, IRE1 is required to monitor TOR activity to balance cell expansion and maturation during organ biogenesis.

INTRODUCTION

The endoplasmic reticulum (ER) is responsible for the synthesis of one third of the cellular proteome. Therefore, its biosynthetic capacity is constantly monitored by a set of ER membrane-associated sensors that can upregulate the synthesis of ER protein chaperones and ER membrane while also limiting the rate of protein translation (Ron and Walter 2007, Han and Kaufman 2017). The UPR sensors conserved between metazoans and plants include the ER membrane protein kinase and ribonuclease IRE1 and ER membrane tethered transcription factors (TFs) (metazoan ATF6 and plant bZIP17 and bZIP28) (Angelos *et al.* 2017, Pastor-Cantizano *et al.* 2020). Through its ribonuclease domain, IRE1 catalyzes the unconventional cytosolic splicing of mRNA encoding of a transcription factor, XBP1 in mammalian cells, bZIP60 in Arabidopsis, and Hac1 in yeast (Kawahara *et al.* 1997, Calfon *et al.* 2002, Nagashima *et al.* 2011). In addition to the unconventional splicing of the mRNA of target TFs, IRE1 degrades cytosolic mRNAs through a process known as regulated IRE1-dependent decay (RIDD) to preserve cell proteostasis (Hollien *et al.* 2009, Mishiba *et al.* 2013).

Exogenous stress factors, such as hypoxia and metabolic stress in metazoans (Hetz and Papa 2018) as well as heat stress (Gao *et al.* 2008), pathogen attack (Guillemette *et al.* 2014, Zhang *et al.* 2015), and singlet oxygen generation (Beaugelin *et al.* 2020) in plants, are known to activate the UPR sensors. Interestingly, these sensors are also activated by endogenous cellular cues during physiological development (Mitra and Ryoo 2019). For example, the mammalian IRE1 has critical functions in placental and liver development during embryogenesis and during the differentiation of antibody-secreting B-lymphocytes (Reimold *et al.* 2000, Reimold *et al.* 2001). In *Drosophila*, IRE1 activity is required for the development of the digestive tract (Huang *et al.* 2017). In *Xenopus*

and medaka fish, IRE1 is required for proper notochord formation and hatching gland development, respectively (Tanegashima *et al.* 2009, Ishikawa *et al.* 2017). In these metazoan models, complete IRE1 loss-of-function mutations are embryo or larval lethal (Mitra and Ryoo 2019).

In Arabidopsis there are three homologs of the IRE1 gene, IRE1a, IRE1b, and IRE1c, which perform only partially overlapping functions (Mishiba *et al.* 2019, Pu *et al.* 2019). IRE1c is expressed primarily in reproductive tissues during gametogenesis, whereas IRE1a is primarily expressed in root tissues, and IRE1b is expressed at a similar level in nearly all tissue types (Pu *et al.* 2019). Single mutants of the Arabidopsis IRE1 homologs are phenotypically identical to wild type (WT) plants under physiological conditions of growth; however high-order mutations cause severe developmental defects. For example, the *ire1b ire1c* double mutant has a gamete lethal phenotype (Pu *et al.* 2019), and the *ire1a ire1b* double mutant, a functional IRE1 knock-down, reproduces normally but has a short root phenotype (Deng *et al.* 2011, Chen and Brandizzi 2012, Chen *et al.* 2014, Bao *et al.* 2019). Similar to *ire1b ire1c*, the *ire1a ire1b ire1c* triple mutant is also gamete lethal (Mishiba *et al.* 2019), and plants that are heterozygous for *ire1c* and homozygous for *ire1a* and *ire1b* have severe developmental defects in all tissue types (Mishiba *et al.* 2019). On the whole, these phenotypes support that IRE1 performs critical functions to promote the growth and development of several Arabidopsis tissue types with some degree of specificity likely linked to the expression of the IRE1 isoforms in their respective tissues.

How the Arabidopsis IRE1 controls tissue growth and development is completely unknown. In most metazoan model species, IRE1 primarily contributes to development through activation of XBP1 (Reimold *et al.* 2000, Reimold *et al.* 2001, Ishikawa *et al.* 2017). Indeed, XBP1 null mutations are also embryo lethal and affect the development of the same tissue types as IRE1

mutations (Mitra and Ryoo 2019). Surprisingly, loss-of-function mutations in the Arabidopsis bZIP60 do not have any growth or reproductive phenotypes (Nagashima *et al.* 2011, Chen and Brandizzi 2012, Moreno *et al.* 2012). Therefore, unlike the metazoan IRE1, the Arabidopsis IRE1 promotes organ growth through mechanisms that are independent from its canonical splicing target.

Similar to IRE1, the Target of Rapamycin (TOR) kinase is highly conserved across eukaryotes (Shi *et al.* 2018). TOR and its associated protein complexes act as cell regulatory hubs that integrate nutrient availability, energy status, hormone, and stress input signals to coordinate a wide variety of cellular activities ranging from cell proliferation and growth, to metabolism and autophagy (Shi *et al.* 2018, Burkart and Brandizzi 2020). While several of the key proteins in the TOR complex are conserved between plants and animals (such as LST8 and RAPTOR), the specific inputs and outputs have been evolutionarily adapted to meet organism-specific needs (Burkart and Brandizzi 2020). Indeed, plant TOR receives activating signals from light availability via photosynthetic production of carbohydrates (photosynthates) and light-dependent synthesis of the plant hormone auxin (Li *et al.* 2017, Chen *et al.* 2018). Photosynthate-dependent activation of TOR via glucose is necessary and sufficient to activate root tips and promote cell division in root meristematic zones via activation of E2F transcription factors (Xiong *et al.* 2013). TOR activity is also required for the polar growth of root hairs (Montané and Menand 2013), which necessitates substantial synthesis of new cytosolic, membrane, and cell wall components (Ovečka *et al.* 2005, Retzer and Weckwerth 2021). Nonetheless, how TOR activities are integrated into other aspects of development in actively growing roots is not well understood.

Despite the evidence that both IRE1 and TOR control growth, a functional connection between these essential regulators in the context of development has yet to be made. Earlier studies

of chemically induced ER stress and other stress situations in metazoan cells have demonstrated that TOR activity can lead to an induction of the IRE1-JNK pro-apoptotic kinase signal cascade, (Kato *et al.* 2012, Kato *et al.* 2013, Shanware *et al.* 2014), as well as IRE1 inactivation (Sanchez-Alvarez *et al.* 2017). Nonetheless to date, it is yet unknown whether IRE1 controls TOR activity under induced ER stress conditions or physiological conditions of growth in any model organism. To address these fundamental knowledge gaps, we used the tractable *Arabidopsis ire1a ire1b* model because it avoids the gamete lethality and extreme pleotropic phenotypes of other high-order UPR mutants (Kim *et al.* 2018, Mishiba *et al.* 2019). Furthermore in physiological conditions of growth, the plant phenotype of this mutant is restricted to the root (Chen and Brandizzi 2012, Ruberti *et al.* 2018). Due to their invariant cell ontogeny and cell organization the *Arabidopsis* root is an exquisite development model system (Scheres and Wolkenfelt 1998), and is therefore suitable to investigate the role of IRE1 in tissue development. Through an in-depth characterization of *ire1a ire1b* root development in normal conditions of growth, we demonstrate that IRE1 is required to reach maximum rates of root growth afforded by prolonged photoperiods and high carbohydrate availability during the transition from early seedling stage to adult vegetative stage. A detailed analysis of this developmental transition carried out in this work indicates that in the root meristem IRE1 is required for the correct timing of cell elongation in a manner that is dependent upon a strict regulation of TOR activity, and TOR-dependent cell differentiation. Hence this work brings to light a physiological role of IRE1 in tissue growth by connecting two essential and highly conserved growth-regulating pathways.

MATERIALS AND METHODS

Plant Material and High-Quality Seed Production

Seeds of the *Arabidopsis thaliana ire1a* (WISCDSLOX420D09) and *ire1b* (SAIL_238_F07) were obtained from the Arabidopsis Biological Resource Center (Columbus, OH, USA), and the *ire1a ire1b* double mutant was published previously (Chen and Brandizzi 2012). Special care was taken to produce high quality seeds to enable vigorous and reproducible growth of seedlings on sterile culture plates without any exogenously supplied carbohydrates. WT and *ire1a ire1b* seeds used for the same experiments were always produced simultaneously. Plate grown seedlings were transplanted to potting soil and grown in standard Arabidopsis growth chamber conditions (16 hr 150 μ E light/ 8 hr dark; 50% humidity, 23°C). Plants were watered exclusively with Hoagland's nutrient solution every ~7 days prior to bolting and then as needed after bolting (usually every 4 days). Prior to any silique senescence, inflorescences were staked and tied after they could not support their own weight to prevent seed loss. Two to four weeks after bolting, prior to any significant rosette senescence, ¼ to ½ of all formed siliques will had senesced. Seeds were harvested by tapping or gentle gripping of the tied inflorescence, and seeds that fell off with minimal physical disturbance were harvested and the remaining plant was discarded. Large number of plants were grown simultaneously to compensate for smaller seed yield per plant. Plants were not dried prior to seed harvest. In our experience seeds produced under these conditions had initial germination rates near 100% on 0% sucrose containing plates and had germination rates >98% on 0% sucrose after a year of storage in ideal conditions (seed envelope in humidity controlled, dark environment).

Plant Phenotyping

Unless otherwise stated, all sterile culture plates were made with half-strength Linsmaier and Skoog ($\frac{1}{2}$ LS) basal salts containing buffer (LSP03, Caisson Labs) with 1.0% w/v agar (NCM0236A, Neogen) added and without exogenous sucrose (or other carbohydrates). Media was adjusted to pH 5.7 and autoclaved for 20 min under standard conditions. Media was cooled on a stir plate until the external temperature of the bottle was 40°C, then dispensed into plates and allowed to cool in a single layer (as opposed to stacked plates) to allow for even cooling rates. Plates were always made the on the same day the seeds were sterilized and plated. Seeds were sterilized with 1x wash of 100% ethanol for 30 sec, 1x wash of 50% bleach with 0.1% Tween20 for 1 min, and 6x washes with sterile double distilled water (ddH₂O). Seeds were sterilized and wet plated using a 1 ml pipette immediately after plates had cooled. We suspect that extended incubation in ddH₂O in the microcentrifuge tube after sterilization may affect germination and initial growth rates on 0% sucrose media. After seed plating, plates were left open in the sterile hood for 3-5 min or until water from plating method evaporated. Plates were wrapped with 1-inch surgical tape (70200534694, 3M, MN, USA) with overlapping sections on the bottom of the plate and then wrapped in aluminum foil. Seeds were stratified at 4°C for 48 hr. Plates were incubated vertically in Percival growth chambers in continuous 150 μ E light (verified with an external PAR light meter) for the indicated growth periods. A minimum of 5 plate replicates per experimental group were used for each phenotyping experiment.

TORIN2 (MedChemExpress), AZD-8055(MedChemExpress), oryzalin (Sigma-Aldrich) latrunculin b (Sigma-Aldrich) 1-naphthaleneacetic acid (NAA, Sigma-Aldrich), and oligomycin B were dissolved in DMSO and antimycin A in 100% ethanol to 10 mM and stored at -80°C. These chemicals were removed from the -80°C after the external temperature of the media bottle reached

40°C and added simultaneously to all bottles in that experiment at the required concentrations. This was done to increase reproducibility, as the AZD-8055 was found to lose ~50% of its effect on WT root growth inhibition (at 150 nM) when left at room temperature for 10 min in DMSO.

After the indicated incubation period plates were removed from the Percival as needed, imaged, used for downstream analysis and then discarded. No repeated measures were performed on individual plates (i.e. different timepoints within the same experiment were recorded from two separate populations of seedlings). This was done to prevent possible confounding effects of altered gravity vectors from plate movement on the *ire1a ire1b* root phenotype during critical growth stages. Average shoot fresh weight was determined by excising shoots from all plants on one plate (usually 8-10 shoots) weighing the total and dividing by number of seedlings. Root length was measured using Image J. Root tip angles were also measured using ImageJ by placing an approximately 3 mm line over the root tip (beginning at the apex) and using the Feret's diameter measurement function which was then converted into a 360° scale.

mPS-PI Staining and Meristem Cellular Organization Analysis

Modified pseudo-Schiff propidium iodide (mPS-PI) staining protocol was adapted from Truernit *et al.* (2008). After the indicated growth period, whole seedlings (for 5- or 7-day old seedling) or 2 cm excised roots sections (for 10 day old seedlings) were fixed in a 5:4:1 methanol: ddH₂O:acetic acid solution and stored at 4°C for a minimum of 12 hr and for as long as two weeks in capped 2 dram vials. For the staining procedure seedlings/roots were treated in six well plates to avoid mechanical damage. After removal of fixative, tissue was washed with 10 ml of ddH₂O and then treated with 5 ml of a 1% periodic acid (PA) solution for 40 min. After removing the PA solution, tissue was washed with 10 ml of ddH₂O and then treated with 5 ml of freshly made mPS-PI working reagent (100 mM sodium metabisuphite, 0.15 M HCl, 100 µg/ml propidium iodide)

for 40 min in the dark. After removing the mPS-PI solution samples were washed with another 10 ml of ddH₂O then submerged in 3 ml of the chloral hydrate alternative Visikol to clear the tissue. Samples were sealed with parafilm and incubated for 2-3 days prior to confocal microscopy analysis.

Samples were imaged using a Nikon A1 confocal microscope with 488 nm laser excitation, and 520-720 nm emission collected. Transmitted light detection images were also collected in parallel to assist in root tip zone identification. For each root one 20x image was collected for accurate identification and quantification of meristem and transition zone metrics, and a 10x image was collected for identification of transition zone and elongation zone metrics. The beginning of the transition zone was defined as the first cell in the cortical cell layer which was >2 times as long as the previous one (Casamitjana-Martinez *et al.* 2003, Di Mambro *et al.* 2017). The first cortical cell which was twice as long as it was wide was identified as the beginning of the elongation zone. The end of the elongation zone was defined as the last cortical cell before the first visible root hair initiation, which was identified using the transmitted light image if no root hair initiations were visible in the same focal plane as the cortex cells. In some instances, (particularly for WT D10 samples) two images were required to fully measure the length of the elongation zone.

TOR Activity Assays

Tissue for TOR activity assays was collected from 7 day old seedlings. One biological replicate consisted of 60 seedlings grown on two plates. The plates were removed from the Percival and approximately 3 mm of the root tip from all 60 seedlings were quickly but carefully cut in situ using surgical scissors. A 3 mm reference object was used to ensure accuracy. After cutting, forceps were used to gently collect root tips into a prepared microcentrifuge tube with two glass beads and placed in liquid nitrogen. Then a second cut was used to excise the mature root tissues

which were collected into a second microcentrifuge tube with two glass beads. The excisions and collection of both tissue types took less than 5 min total for each biological replicate. This process was repeated, alternating experimental groups until all biological replicates were collected. Continuous light was used to eliminate potential sample variation caused by circadian dependent processes over the multiple hr required to harvest these samples by an individual researcher. Biological replicates in Figure 4.5 were collected over 4 separate experiments.

Frozen samples were ground to a powder using a Retch Mixer Mill (Retch; Haan, Germany) in 2x 10 sec bursts then 4x 20 sec bursts with refreezing in liquid nitrogen between bursts and after the final grinding. To the frozen root tip tissue, 100 μ ls of extraction buffer (EB) containing phosphate buffered saline (PBS) pH 7.4, plant protease inhibitor cocktail (P9599, Sigma-Aldrich), and PhosSTOP phosphatase inhibitor (4906845001, Roche) was added to the root tip samples and 200 μ ls of EB to the mature root samples. Tubes were shaken and vortexed until the sample/buffer was melted and homogenized then kept on ice (30 sec). The entire sample/supernatant was transferred into a new tube without the beads and sequentially spun down at 21,000x g for 5, 10, 15 min in a 4°C cooled centrifuge transferring the supernatant to a new tube between each spin. Protein content of the root tip extracts were sufficient to load 2.5 μ g of total protein on two 12% SDS-PAGE gels. Gels were transferred to PVDF membranes (1620177, Bio-Rad) and then blocked with 3% bovine serum albumin (BSA) in tris buffered saline plus Tween20 (TBST) for 1 hour at room temperature then, incubated with primary antibodies in TBST to detect total S6K (α S6K1/2, AS12 1855; Agrisera) or phosphorylated-S6K (ab207399, Abcam) overnight at 4°C. Blots were washed three times with TBST for 20 min each then incubated with secondary HRP conjugated goat anti-rabbit antibody (A0545, Sigma-Aldrich,) for 1 hour at room

temperature. Blots were developed using SuperSignal West Femto Kit (34096, ThermoFisher Scientific).

EdU Pulse-Chase Experiments

The 5-ethynyl-2'-deoxyuridine (EdU) pulse-chase was performed on 7-day old seedlings grown on plates containing DMSO or 150 nM AZD-8055 using the Click-iT EdU Alexa Fluor 488 Imaging Kit (C10337, ThermoFisher Scientific). Seedlings were transferred from Petri dishes to 6 well plates containing 10 μ M EdU in $\frac{1}{2}$ LS media (no sucrose) and then placed back in the Percival for 20 min. At the end of the incubation period, the $\frac{1}{2}$ LS media with EdU was removed and the seedlings were gently washed 3x with 5 ml of $\frac{1}{2}$ LS media (without EdU). Half of the seedlings were then transferred to fixation buffer (4% paraformaldehyde, 0.1% Triton X-100, 1x PBS pH 7.4) while the other half were returned to their growth plates. Plates were re-wrapped in surgical tape and placed back in the Percival for 6 hr. Chase samples were transferred to fixation buffer after the 6-hr chase period. Samples were then stored for between 12 hr and 1 week at 4°C. Samples were stained and imaged in small batches (with some samples from each experimental group) on each day over that week and no degradation of sample was found.

Click-iT reaction procedure was performed according to the manufacturer protocol with some modifications. Seedlings were removed from the fixation buffer and washed 3 times with 3% BSA in PBS. Click-iT reaction cocktail was prepared without modification and samples were incubated with the cocktail for 1 hr in the dark. Shorter incubation periods lead to incomplete tissue penetration of the reaction cocktail into the meristematic zone. After incubation, samples were washed 1x with 3% BSA in PBS, then washed 3x with PBS. Samples were then incubated with Hoechst 33342 provided with Click-iT kit (working solution created by diluting 1 μ l Hoechst 33342/ 1 ml of PBS) for 40 min in the dark. Samples were then washed with 2x washes of PBS.

Shoot tissue was removed and roots were mounted in PBS on slides using polypropylene packing tape to create a watertight imaging chamber of uniform depth (~70 μm). Z-series images were collected over the entire depth of the root tips using a Nikon A1 confocal microscope equipped with a 10x objective. Sum EdU intensity and EdU signal area were quantified in each root tip using the Nikon NIS-Elements Advanced Research software after transformation of Z-series images into max intensity projects and background subtraction (which was equally applied to all images). Length to the first root hair initial (RHI) and the number of EdU+ nuclei found after the first RHI were manually quantified using the Z-series images.

Data Reporting and Statistical Analysis

Sample sizes were determined by maximum number of replicates which could be grown simultaneously in a uniform incubation environment (i.e. on the same shelf of a Percival) or by maximum number of samples that could be collected by a single researcher in a reasonable time frame.

All statistical analysis was performed using R. Two-way or three-way, between-subjects analysis of variance (ANOVA) was conducted as needed on each data set to determine the effect of experimental variables on test outcomes. Type III ANOVAs were used for unbalanced data sets. For each dataset, residual analysis was performed in order to test for the assumptions of the ANOVAs. The Shapiro-Wilk test was used to check normality assumption and homogeneity of variance was assessed via studentized Breusch-Pagan test and Levene's test. In most of the data sets the homogeneity of variances assumption was violated due to the increased variance in the *ire1a ire1b* short root phenotype (see changes in standard deviation of the *ire1a ire1b* root length over time in Figure 4.1C and Figure 4.S3D, E). If the assumption tests were violated (p-value <0.05), Box-Cox or log transformations were applied to the dataset and the ANOVA re-run using

transformed data. If the assumption checks were still violated after Box-Cox or log transformations then weighted least squares regression was applied to the ANOVA model (referred to in the text as: wANOVA). All datasets which were subjected to weighted least squares regression passed the residual analysis. From the appropriate ANOVA model for each data set (standard, transformed, or weighted least squares) pairwise comparisons (CRAN R package: *emmeans*) were then run with Bonferroni adjustment applied. Significance markers in figure graphs were based on the results of these pairwise comparison tests. Code and list of used R packages for the analysis pipeline is found in Supplemental Data File 2.12.

To determine if there were significant differences in the coefficient of variation between root tip angles of two different experimental groups, we utilized the asymptotic Feltz and Miller test (Feltz and Miller 1996) as applied by Rodriguez *et al.* (2020) using the CRAN R package: *cvequality*.

RESULTS

IRE1 Promotes Root Growth in an Age-Dependent Manner

The reduced length of the *ire1a ire1b* root has been documented earlier (Chen and Brandizzi 2012, Deng *et al.* 2013, Chen *et al.* 2014, Bao *et al.* 2019), but has not been studied in detail during the transition from early seedling development to an adult vegetative state, which corresponds to a highly active growth period. To fill this gap and establish a robust platform for defining the role of IRE1 in organ growth, we set up a time-course analysis of *ire1a ire1b* growth with measurements of phenotypic traits at 5, 7, 10, and 12 days after germination (D5, D7, D10, D12; Figure 4.1A).

We first analyzed shoot development by quantifying the shoot fresh weight (SFW) in WT and *ire1a ire1b* seedlings at these time points (Figure 4.1B). To test the effect of our experimental variables, i.e. seedling age and genotype, on the SFW, we carried out a two-way between-subjects analysis of variance (hereafter referred to as a ANOVA; see materials and methods for the statistical analysis pipeline). The analysis indicated that there was not a significant interaction between the effects of seedling age and genotype on SFW ($F(3,76)= 0.344, p= 0.793$). We also found that there was not a significant effect of the individual variable (hereafter referred to as a simple main effect) of genotype alone on SFW ($F(1,76)= 0.684, p= 0.0411$). However, in both WT and *ire1a ire1b* genotypes, rapid and similar increases in SFW were found from D0 to D12 (Figure 4.S1A); accordingly, there was a highly significant effect of seedling age on SFW ($F(3,76)= 130, p= <2 \times 10^{-16}$). Together these results demonstrate that the level of IRE1 functional impairment in the *ire1a ire1b* mutant does not have an effect on shoot development.

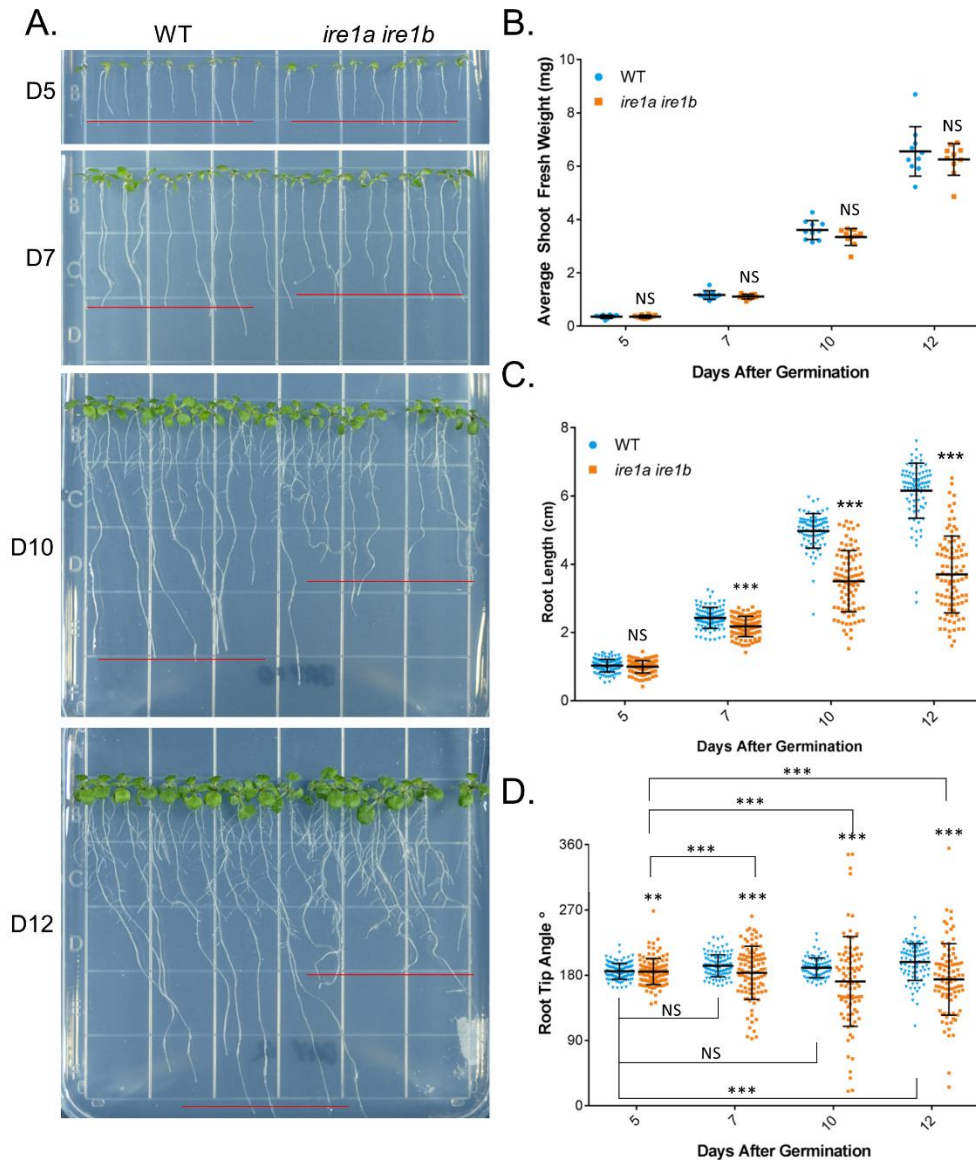


Figure 4.1. The *ire1a ire1b* double mutant shows age dependent primary root growth defects.

A) Representative images of WT and *ire1a ire1b* mutants grown for 5, 7, 10 or 12 days. **B)** Shoot fresh weight was determined by averaging WT or *ire1a ire1b* shoots grown in an individual plate for each plate replicate (n=10; error bars show SD). **C)** Root length of individual roots was measured using ImageJ. For Figure 4.1B and 4.1C: error bars show SD; p-values significance markers displayed above an *ire1a ire1b* experimental group are pairwise comparisons to the corresponding WT group for that specific treatment. Brackets denote other specific pairwise comparisons. Significance markers: NS = adj. $p > 0.01$; * = adj. $p < 0.01$ and > 0.001 ; ** = adj. $p < 0.001$ and > 0.0001 ; *** = adj. $p < 0.0001$ **D)** Angle of the root tip away from vertical (0°) was measured using ImageJ. Significant differences between coefficient of variation was tested using the asymptotic Feltz and Miller test as described in materials and methods. Error bars show SD; p-values: NS = > 0.0001 , ** = p -value < 0.0001 and $> 1.0e^{-10}$, *** = p -value $< 1.0 \times 10^{-10}$

We next analyzed primary root development by recording the root length of WT and *ire1a ire1b* at each time point (Figure 4.1C). We attempted to utilize an ANOVA to test the effect of, and interaction between, seedling age and genotype on root length. However, when we tested the normality and homogeneity of variance assumptions of the ANOVA by Shapiro-Wilk test and Levene's test, respectively, we found that these assumptions were violated. Box-Cox and log transformation of the data set were also attempted; however, the assumptions were still violated. We therefore carried out a two-way between-subjects ANOVA utilizing weighted least squares regression (hereafter referred to as a wANOVA; see materials and methods and Supplemental Data File 2.12) to analyze primary root length. The wANOVA showed a highly significant interaction between seedling age and genotype on root length ($F(3,753)= 133, p= <2 \times 10^{-16}$), although the simple main effect of genotype alone was not significant ($F(1,753)= 2.08, p= 0.149$). To determine the nature of these interactions, we performed pairwise comparisons between different experimental groups, the results of which are displayed as significance markers in the referenced figures. At D5, we found no significant differences in average root length between WT and *ire1a ire1b* (Figure 4.1C), indicating that the *ire1a ire1b* mutation does not affect root growth during early seedling development. Past D5, we found dramatic increases in the rate of root growth in WT from approximately 0.2 cm/day between D0-D5, to approximately 0.9 cm/day between D5-D10 (Figure 4.S1B); accordingly, there was also a highly significant simple main effect of seedling age on root length ($F(3,753)= 3001, p= <2 \times 10^{-16}$). Noticeably, during the D5-D10 phase of growth, the root growth phenotype of *ire1a ire1b* became increasingly more severe compared to the earlier phase of growth (i.e., D0-D5). Specifically, the average *ire1a ire1b* root length was significantly shorter than WT at D7, D10, and D12 (Figure 4.1C). Furthermore, while the rate of root growth in the *ire1a ire1b* mutant accelerated from approximately 0.2 cm/day to approximately

0.7 cm/day between D5-D7, it then declined to approximately 0.5 cm/day between D7-D10 (Figure 4.S1B). These results are consistent with the findings that IRE1 is required for root growth (Deng *et al.* 2011, Chen and Brandizzi 2012, Chen *et al.* 2014, Bao *et al.* 2019), but also expand on these results by demonstrating that IRE1 is required to maintain accelerated rates of primary root growth as seedlings mature.

Concurrent with altered growth rates in maturing *ire1a ire1b* primary roots, we observed that directional root growth was increasingly impaired as the seedlings matured. To analyze this, we determined the growth vector of the primary root tip by measuring the root tip angle away from a vertical axis (0°) in a counterclockwise orientation, such that roots growing directly downward would have a recorded angle of 180° (Figure 4.1D). We next tested the effect of genotype and seedling age on the average root growth vector and found that there was no significant effect of either variable (Data File 2.1). However, we observed increasingly large differences in standard deviation between WT and *ire1a ire1b* as seedlings matured (Figure 4.1D). In order to compare the relative distribution of the collected data points, we performed asymptotic Feltz and Miller tests to determine if there were significant differences between coefficients of variation (CoV) of the different experimental groups (Feltz and Miller 1996). We found that the CoV was not significantly different between WT root tip angles at D5, D7, and D10, but found a significant difference in WT CoV between D5 and D12 (Figure 4.1D). At all the tested time points, the CoV of *ire1a ire1b* root tip angles were significantly different from the corresponding WT CoV (Figure 4.1D). Furthermore, the *ire1a ire1b* root tip angles CoV significantly increased with seedling age at every time point compared to the baseline measurements at D5 (Figure 4.1D). Several different types of cell division and organization defects in the root tip can cause a short root phenotype (Lucas *et al.* 2011, Petricka *et al.* 2012). However, defective control of the primary root growth

vector is more likely due to aberrant cell elongation because tropic growth responses regulate asymmetric cell elongation on one side of the root to direct organ growth in a specific direction (Ishikawa and Evans 1993, Mullen *et al.* 1998, Sato *et al.* 2015). Therefore, the increasingly random root growth vectors displayed by maturing *ire1a ire1b* support the hypothesis that IRE1 may be required for proper cell elongation.

IRE1 is Required for Proper Cell Elongation in the Root Meristem

Next, we aimed to test the hypothesis that IRE1 is required to control cell elongation and map the role of IRE1 in the different root zones. To do so we performed modified pseudo-Schiff propidium iodide (mPS-PI) staining (Truernit *et al.* 2008) of fixed WT and *ire1a ire1b* roots at D5, D7, and D10 followed by confocal microscope imaging and quantitative image analysis (Figure 4.2; Figure 4.S2, 4.S3). For each root, we identified the meristematic zone (MZ), transition zone (TZ) and elongation zone (EZ) of the root tips according to previously published criteria (Casamitjana-Martinez *et al.* 2003, Di Mambro *et al.* 2017). Canonically, cells divide in the MZ, then undergo a transitional stage consisting of genomic endoreduplication and cytoarchitectural changes in the TZ followed by cell elongation in the EZ (Scheres and Wolkenfelt 1998, Hayashi *et al.* 2013). For each root tip zone, we recorded the length, the number of cells, and the average cell length. We then performed a series of two-way wANOVAs (or ANOVAs as indicated) to test the effects of seedling age and genotype on each these zone metrics in the MZ, TZ, and EZ. This was done to test if there were potential interactions between genotype and seedling age other than cell elongation in the EZ. We found significant interactions between seedling age and genotype on the zone length, cell number and average cell length of the EZ (wANOVA; $F(2,119)=37.0$, $p=3.24 \times 10^{-13}$, $F(2,119)=15.8$, $p=8.48 \times 10^{-7}$, $F(2,119)=13.2$, $p=6.54 \times 10^{-6}$, respectively).

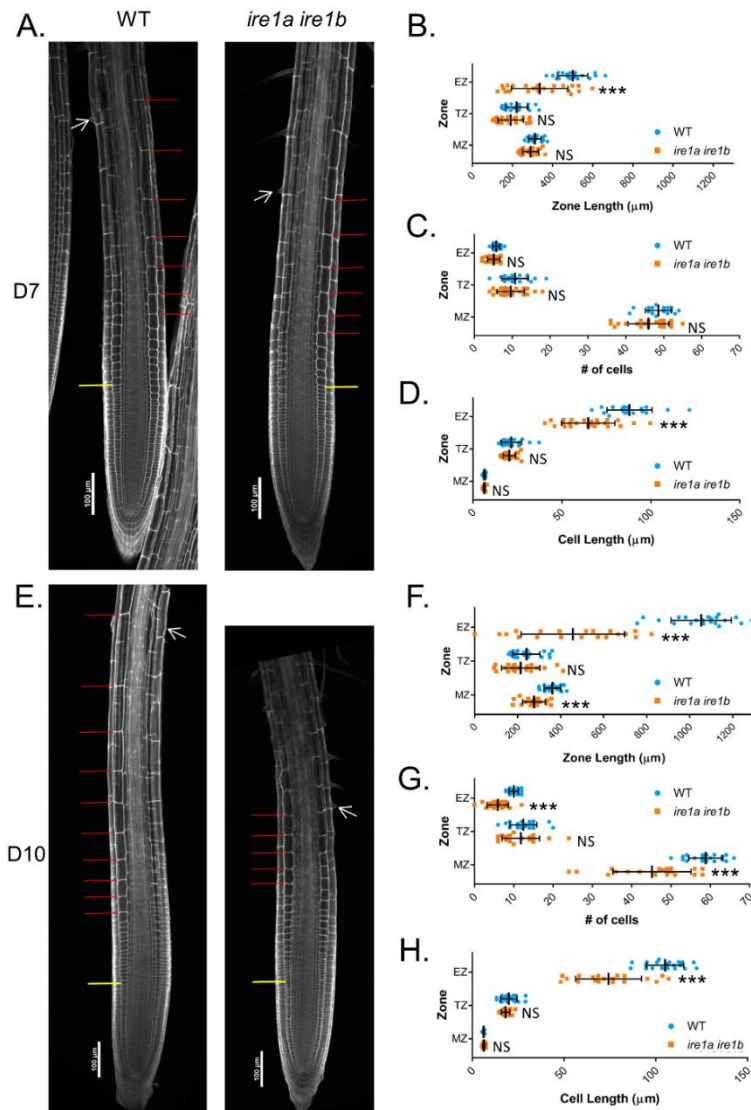


Figure 4.2. Meristem organization defects in *ire1a ire1b* are first manifested in cell elongation in the elongation zone.

At D7 and D10, root tips were subjected to mPS-PI staining and confocal microscopy to analyze root tip cellular organization. **A)** Representative 10x images of mPS-PI stained WT and *ire1a ire1b* roots at D7. The yellow line demarks the end of the meristem zone (MZ) and the beginning of the transition zone (TZ), the red lines marks all of the cells in the elongation zone (EZ), and the white arrow marks the first root hair initiation. For all measurements of the MZ secondary 20x images were used to collect data. **B-D)** Zone length, # of cells, and cell length at D7. **E)** Representative 10x images of mPS-PI stained WT and *ire1a ire1b* roots at D10 **F-G)** Zone length, # of cells, and cell length at D10. For all graphs error bars show SD; p-values significance markers displayed above an *ire1a ire1b* experimental group are pairwise comparisons to the corresponding WT group for that specific treatment. Brackets denote other specific pairwise comparisons. Significance markers: NS = adj. $p > 0.01$; * = adj. $p < 0.01$ and > 0.001 ; ** = adj. $p < 0.001$ and > 0.0001 ; *** = adj. $p < 0.0001$.

In addition, we also found significant interactions between the effects of seedling age and genotype on the zone length and cell number of the MZ (wANOVA; $F(2,119)=9.71$, $p= 1.23 \times 10^{-04}$, $F(2,119)=11.4$, $p= 2.83 \times 10^{-05}$, respectively) but not MZ cell size (wANOVA; $F(2,119)=1.08$, $p= 0.342$). We did not find any significant interactions between seedling age and genotype on any of the zone metrics in the TZ (zone length: wANOVA $F(2,119)=1.87$, $p= 0.157$; cell number: ANOVA $F(2,119)=0.674$, $p= 0.512$; cell length wANOVA $F(2,119)=1.03$, $p= 0.361$). We found that the simple main effect of genotype alone did not have a significant effect on any zone metrics measured in the MZ, EZ or TZ (Data File 2.2). Together, these results support that the differences in root tip cell organization between WT and *ire1a ire1b* map to the MZ and the EZ in a manner that is dependent upon the age of the seedlings. This is further supported by the evidence that at D5, where no significant differences in primary root length were found between WT and *ire1a ire1b* roots (Figure 4.1C), there were no significant differences between WT and *ire1a ire1b* for any of the root tip organization metrics recorded (i.e., zone length, number of cells, cell length; Supplemental Figure 4.2A-D). Therefore, the *ire1a ire1b* mutation does not affect root growth during early seedling development (Figure 4.1).

We then focused on defining the variables underpinning the dramatic increase in WT primary root growth rates from ~0.2 cm/ day at D5 to ~0.9 cm/day at D10; (Figure 4.S1B). We found that the length of both the MZ and EZ roughly doubled in WT root tips during this period, while the length of the TZ remained unchanged (Figure 4.S3A). Interestingly, we observed a significant 1.7-fold increase in the number of cells in the MZ, while the length of MZ cells remained unchanged, indicating that the increased size of the MZ was due to an increase in the cell number in this zone (Figure 4.S3B, C). We also found a 1.25-fold increase in cell size and a 2-fold increase in the number of cells in the EZ at D10 compared to D5, supporting that the

observed increased size of the EZ was due to an increase of both cell length and number in the EZ (Figure 4.S3B). Next, we compared the root tip organization of WT and *ire1a ire1b* when the mutant root phenotype is visible (i.e., D7 and D10; Figure 4.2A-H). At D7, we found that the *ire1a ire1b* MZ was not significantly different from WT MZ in terms of zone length, number of cells, and cell length (Figure 4.2B-D). However, when we examined the EZ, we found that the *ire1a ire1b* EZ was significantly shorter than WT EZ, due to significantly shorter cell length (Figure 4.2B, D). Therefore, at D7, the short root phenotype of *ire1a ire1b* coincides with the development of a defective EZ. At D10, we found that the *ire1a ire1b* MZ was significantly shorter than WT and contained a smaller number of cells (Figure 4.2F, H). Contrary to the WT MZ, we did not detect increase in *ire1a ire1b* MZ size at D10 compared to D7 (Figure 4.S2B, E), supporting that the expected increases in MZ size do not take place in the *ire1a ire1b* mutant. At D10, we also observed EZ length reduction in *ire1a ire1b* compared to WT (Figure 4.2F) with a significantly reduced cell size and number (Figure 4.2G, H). In summary, while the EZ length more than doubled between D5-D10 in WT, it did not significantly change in *ire1a ire1b* over this growth period (Figure 4.S2A, D). Together these data indicate that the *ire1a ire1b* roots fail to obtain the rapid rates of root growth achieved by WT plants as they mature, primarily due to defective cell elongation in the EZ. Furthermore, we have successfully established a solid working platform to study the mechanisms underpinning IRE1-dependent control of root growth.

The Emergence of the ire1a ire1b Root Growth Phenotype Depends on High Rates of Root Growth

We then sought to test whether the *ire1a ire1b* root growth phenotype exclusively depends upon seedling age or whether it could be responsive to increased rates of root growth. To do this, we grew seedlings under increasing photoperiod lengths and in the presence of exogenous sucrose

supply in the media. Extending the photoperiod results in an accumulation of photosynthates (i.e., sucrose) (Sulpice *et al.* 2014) and an increase in the overall rate of rate of root growth (Yazdanbakhsh *et al.* 2011). Adding sucrose to the growth medium also increases rates of root growth (Yazdanbakhsh *et al.* 2011). Therefore, we grew WT and *ire1a ire1b* seedlings for 10 days in three different light conditions with increasing photoperiods: 8 hr 150 μ E light/ 16 hr dark, 16 hr 150 μ E light/ 8 hr dark, and continuous 150 μ E light (hereafter abbreviated 8/16, 16/8, and CL respectively). In each photoperiod condition, we grew seedlings on plates containing no sucrose or 1% sucrose (Figure 4.3).

We first measured SFW and found no significant interaction between the effects of exogenous sucrose supply, photoperiod, and genotype via a three-way ANOVA (Figure 4.3B; $F(2,88)=0.626$, $p= 0.537$). However, we did find that there was a significant interaction between exogenous sucrose supply and photoperiod (Figure 4.3B; $F(2,88)=10.5$, $p= 7.81 \times 10^{-5}$; complete statistics results in Data File 2.3). We found that increased photoperiod had a dramatic effect on the development of WT shoots, with a ~2 fold SFW increase in 16/8 light compared to 8/16, and a further ~2 fold SFW increase in CL compared to 16/8 (Figure 4.3B). Exogenous sucrose had an additional significant growth-promoting effect in both 8/16 and 16/8 light conditions. In both light conditions, WT SFW was ~1.4 fold larger when grown on sucrose containing media compared to no sucrose controls (Figure 4.3B). In CL, there was no significant effect of sucrose on SFW accumulation (Figure 4.3B). In all conditions tested, the *ire1a ire1b* SFW was not significantly different from the respective WT controls (Figure 4.3B). Therefore, IRE1 is not required for shoot biomass accumulation regardless of the tested growth conditions.

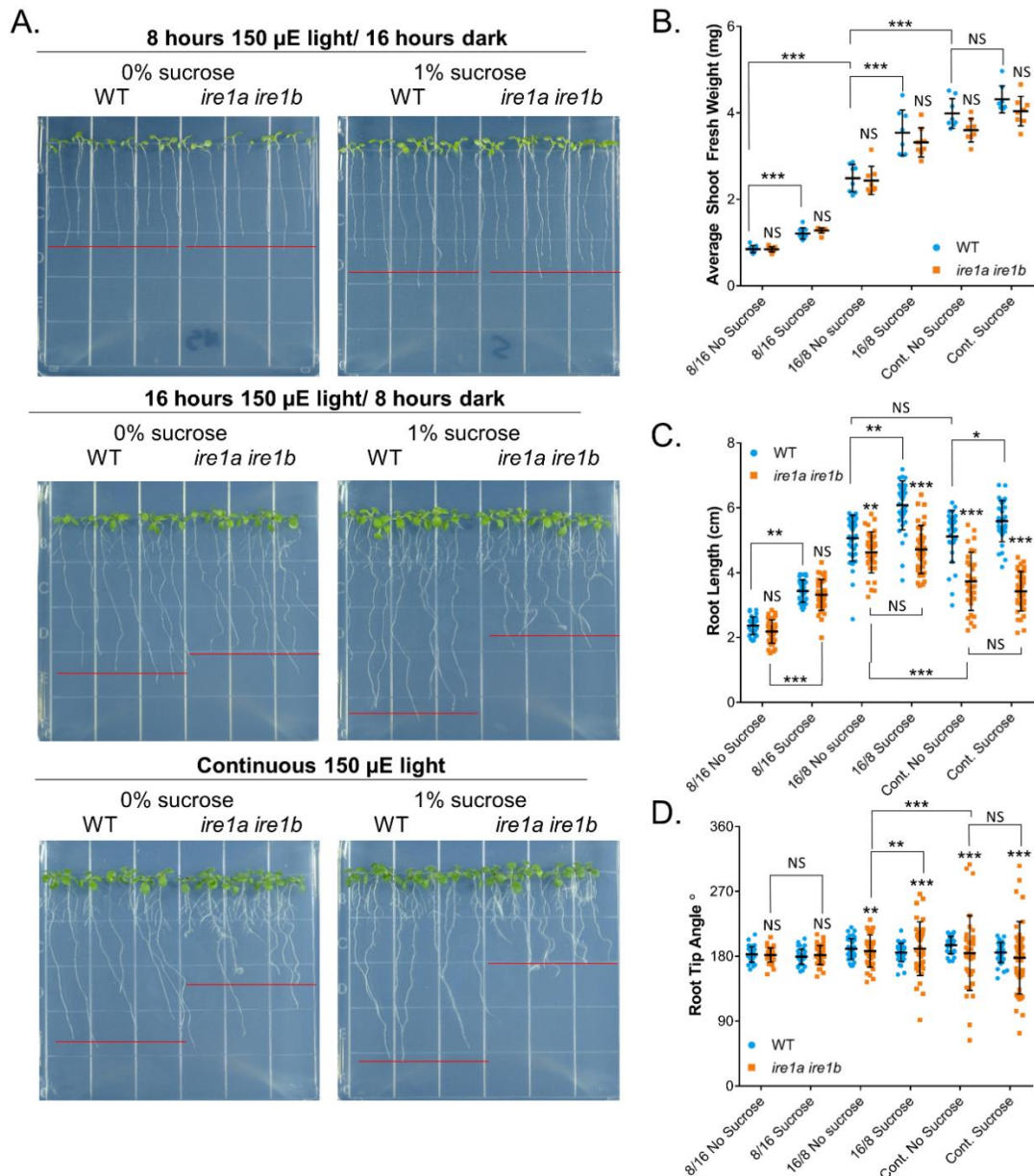


Figure 4.3. The emergence of the *ire1a ire1b* root phenotype depends on a high rate of root growth.

A) Representative images of WT and *ire1a ire1b* mutants grown in the indicated conditions. **B)** Shoot fresh weight was determined by averaging WT or *ire1a ire1b* shoots grown in an individual plate for each plate replicate (n=10; error bars show SD). **C)** Root length of individual roots was measured using ImageJ. For Figure 4.3B and 4.3C: error bars show SD; p-values significance markers displayed above an *ire1a ire1b* experimental group are pairwise comparisons to the corresponding WT group for that specific treatment. Brackets denote other specific pairwise comparisons. Significance markers: NS = adj. $p > 0.01$; * = adj. $p < 0.01$ and > 0.001 ; ** = adj. $p < 0.001$ and > 0.0001 ; *** = adj. p -value < 0.0001 . **D)** Angle of the root tip away from vertical (0°) was measured using ImageJ. Significant differences between coefficient of variation was tested using the asymptotic Feltz and Miller test as described in materials and methods. p -values: NS = > 0.05 , ** = p -value < 0.01 and > 0.001 , *** = p -value < 0.001

We then measured root length and found a significant interaction between the effects of exogenous sucrose supply, photoperiod, and genotype on primary root length (Figure 4.3C; three-way wANOVA: $F(2,397)=9.13$, $p= 1.32 \times 10^{-4}$; Data File 2.3). In WT seedlings, the root length increased significantly in 16/8 light conditions compared to 8/16 light conditions, but no significant differences were noted between 16/8 and CL (Figure 4.3C). We also found that exogenously supplied sucrose significantly increased root length of WT plants grown in 8/16 or 16/8 light photoperiod conditions but not CL, similar to the effect of exogenous sucrose on SFW (Figure 4.3B). In an analysis of root growth vector distribution under these conditions, we also found that the WT CoV was not significantly different from any WT samples across all tested conditions (Figure 4.3D). We then analyzed the *ire1a ire1b* mutant. In 8/16 light conditions, with and without sucrose in the media, the *ire1a ire1b* root length and growth vector distribution were identical to WT (Figure 4.3C, D). These results indicate that the *ire1a ire1b* root growth phenotype is not strictly dependent upon age alone. In 16/8 light, the *ire1a ire1b* roots were slightly but significantly smaller than WT on plates without sucrose (Figure 4.3C). Differently from WT root length, there were no significant differences in overall length between sucrose and no sucrose-treated *ire1a ire1b* roots in 16/8 light (Figure 4.3C). We also observed that 16/8 light led to significant differences in CoV in root growth vector between WT and *ire1a ire1b* (Figure 4.3D). Importantly, we also found that the addition of sucrose to the media significantly increased the root growth vector CoV compared to the *ire1a ire1b* no sucrose control, indicating that exogenous sucrose supply causes aberrant directional root growth in the *ire1a ire1b* mutant (Figure 4.3D). In CL conditions, we found that *ire1a ire1b* roots were significantly shorter than both WT roots grown in CL and *ire1a ire1b* roots grown in 16/8 light conditions. Furthermore, similar to the 16/8 light conditions, the roots of *ire1a ire1b* grown either on sucrose-containing plates or no sucrose

controls in CL were similar in length (Figure 4.3C). The *ire1a ire1b* root growth vector CoV was significantly increased by exposure to CL compared to the 16/8 conditions, confirming that prolonged photoperiod leads to aberrant directional root growth in the *ire1a ire1b* mutant. On the whole, these data indicate that, while prolonged photoperiod and sucrose availability equally promote shoot growth of WT and the *ire1a ire1b* mutant, IRE1 is absolutely required to reach the maximum rates of root growth afforded by extended photoperiod and increased carbohydrate availability.

TOR Inhibition Rescues the ire1a ire1b Primary Root Growth Phenotype

It has been documented that plant TOR integrates light and carbohydrate availability signals to control growth (Li *et al.* 2017), and that hyper-activation of TOR can lead to a short root phenotype (Cao *et al.* 2019). Based on the negative effect of pro-growth signals (i.e., prolonged photoperiod and exogenous sucrose supply) on *ire1a ire1b* root growth, we hypothesized that TOR could be hyperactive in *ire1a ire1b* and, therefore, that the IRE1 root growth phenotype might be alleviated by TOR inhibition. As a first step to test this hypothesis, we performed our growth phenotyping assays (Figures 4.1, 4.2), but also supplemented growth media with the TOR inhibitor AZD-8055 (hereafter referred to as AZD; Cao *et al.* 2019) or DMSO control vehicle. We first conducted a test using concentrations of AZD ranging from 50 to 200 nM in the culture media (Figure 4.S3). At a 150 nM concentration, AZD had a slight inhibitory effect on WT root length in line with previous results (Montané and Menand 2013, Cao *et al.* 2019), and significantly altered *ire1a ire1b* root length phenotype compared to DMSO control. (Figure 4.S3). Therefore, for our analyses we proceeded to use 150 nM AZD in the growth medium to induce a low-level inhibition

of TOR compared to the more commonly applied applications of 1 μ M or more AZD (Montané and Menand 2013, Schepetilnikov *et al.* 2017, Barrada *et al.* 2019, Zhuo *et al.* 2020).

We then performed a time-course analysis of *ire1a ire1b* root growth from D7-D12 on growth media containing either DMSO vehicle or 150 nM AZD (Figure 4.4A). We found a small effect of AZD on WT root growth. We then conducted ANOVAs to test for an interaction between seedling age, AZD effect, and genotype on seedling growth phenotypes (i.e. SFW and root length). While we found no significant interactions between these variables on average SFW (three-way ANOVA: $F(2,84)=0.150$, $p=0.861$; Figure 4.4B), we did find a highly significant interaction between seedling age, AZD treatment, and genotype on primary root length (three-way wANOVA: $F(2,887)=67.253$, $p= <2.2 \times 10^{-16}$; Figure 4.4C). Similar to our earlier results (Figure 4.1), we observed strong, age-dependent, root growth defects in the *ire1a ire1b* mutant in the DMSO conditions (Figure 4.4C, D). However, when *ire1a ire1b* was grown in the presence of AZD, at D7 and at D10 we found that the average primary root length was not significantly different from WT (Figure 4.4A, C). At D12, the average primary root length of AZD-treated *ire1a ire1b* was slightly but significantly smaller compared to WT; however, the AZD-treated *ire1a ire1b* roots were nearly 1.5 cm longer than their respective DMSO controls at this time point (Figure 4.4C). In an analysis of directional root growth, we found that, when *ire1a ire1b* was grown in the presence of AZD, there were no significant differences in the *ire1a ire1b* root CoV compared to AZD-treated WT at D7 and D10 (Figure 4.4D). At D12, while the CoV of AZD-treated *ire1a ire1b* root tip angles were significantly different from AZD-treated WT, we found that the AZD-treated *ire1a ire1b* root tip angles were significantly less variable than DMSO-treated *ire1a ire1b* root tip angles at D12 (Figure 4.4D). These results support the hypothesis that inhibition of TOR activity in *ire1a ire1b* rescues the short root and directional growth phenotypes of this mutant. To confirm

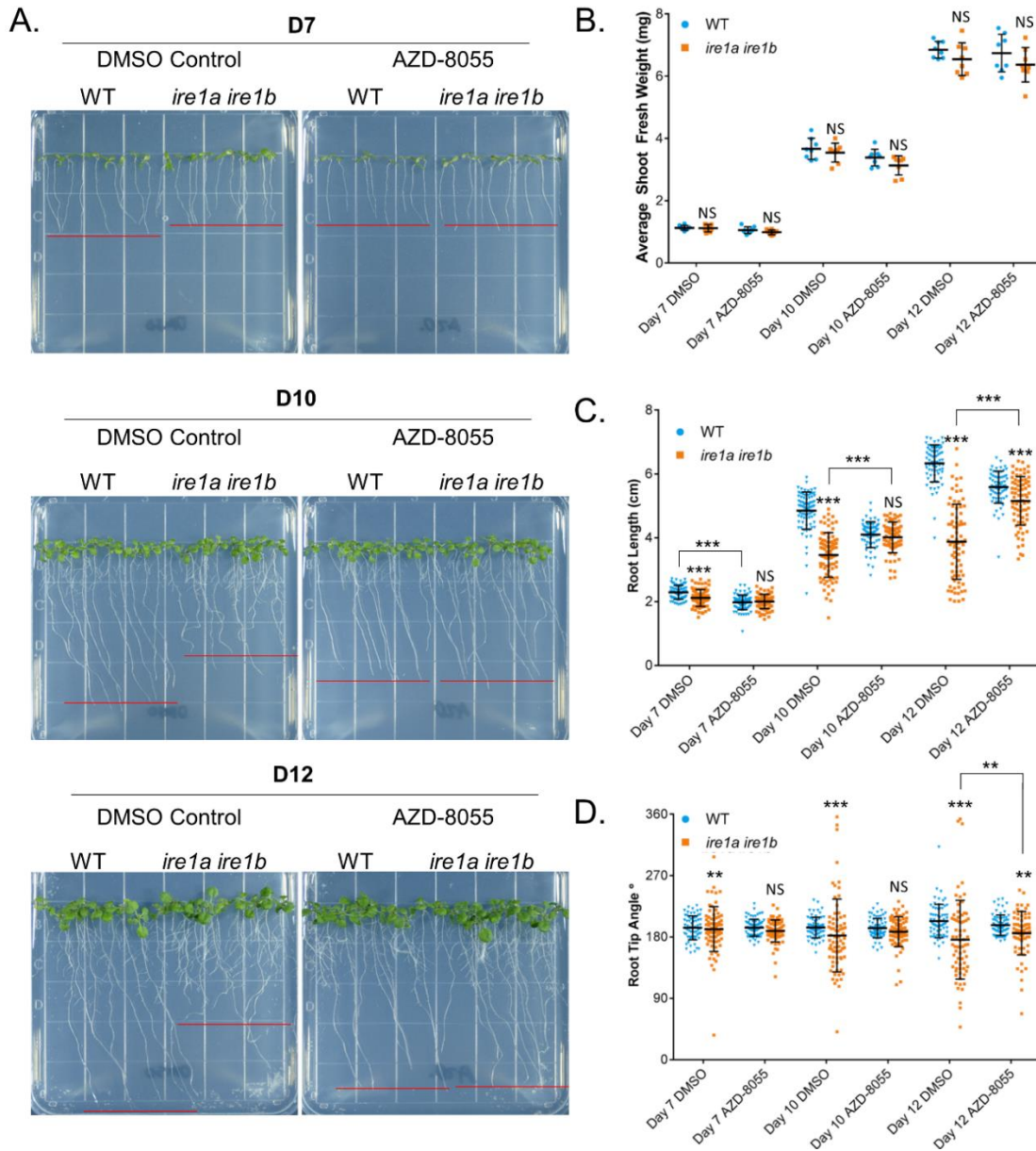


Figure 4.4. TOR inhibition rescues *ire1a ire1b* root growth phenotype.

A) Representative images of WT and *ire1a ire1b* mutants grown for 7, 10 or 12 days on plates containing 150 nM AZD-8055 or DMSO control. **B)** Shoot fresh weight was determined by averaging WT or *ire1a ire1b* shoots grown in an individual plate for each plate replicate (n=10; error bars show SD). **C)** Root length of individual roots was measured using ImageJ. For Figure 4.4B and 4.4C: error bars show SD; p-values significance markers displayed above an *ire1a ire1b* experimental group are pairwise comparisons to the corresponding WT group for that specific treatment. Brackets denote other specific pairwise comparisons. Significance markers: NS = adj. $p > 0.01$; * = adj. $p < 0.01$ and > 0.001 ; ** = adj. $p < 0.001$ and > 0.0001 ; *** = adj. p -value < 0.0001 . **D)** Angle of the root tip away from vertical (0°) was measured using ImageJ. Significance differences between coefficient of variation was tested using the asymptotic Feltz and Miller test as described in materials and methods. p-values: NS = > 0.0001 , ** = p -value < 0.0001 and $> 1.0e^{-10}$, *** = p -value $< 1.0 \times 10^{-10}$.

these results, we tested an additional chemical inhibitor of TOR activity, TORIN2 (Montané and Menand 2013, Cao *et al.* 2019), on WT and *ire1a ire1b*. Similar to AZD treatment, 200 nM TORIN2 rescued both the short root and root tip angle phenotypes of the *ire1a ire1b* mutant (Figure 4.S5).

We then tested whether the rescue of the *ire1a ire1b* root phenotype was specific to TOR inhibition or a general effect of slower root growth rates, which could be brought about by other chemical inhibitors or hormones. To do so, we first grew WT and *ire1a ire1b* on media containing low concentrations mitochondrial respiration inhibitors and cytoskeletal inhibitors, which are known to affect negatively the growth of WT roots (Van Aken *et al.* 2016, Renna *et al.* 2018, Cao *et al.* 2019). In all cases, we found that the treatments led to significant root growth inhibition in the *ire1a ire1b* mutant and not a rescue effect, indicating that general inhibitors of root growth are uninfluential to the rescue of the *ire1a ire1b* phenotype (Figure 4.S6, 4.S7). Next, because of the similarities between the *ire1a ire1b* root phenotype and root morphology phenotype induced by treatment with exogenous auxin (Evans *et al.* 1994, Fendrych *et al.* 2018), the connection between induced ER stress and auxin signaling (Chen *et al.* 2014), and the previous findings that auxin activates TOR (Schepetilnikov *et al.* 2017, Retzer and Weckwerth 2021), we tested whether the *ire1a ire1b* phenotype may be related to a possible auxin-dependent TOR hyper-activation. In the absence of a commercially available auxin synthesis or signaling inhibitor, we sought to test whether the auxin-dependent root growth inhibition of WT could be rescued by TOR inhibition. We found that TOR inhibition did not rescue growth inhibition induced by the synthetic auxin 1-naphthaleneacetic acid (NAA), but rather that the effects of AZD and NAA were additive (Figure 4.S8). We also found that *ire1a ire1b* seedlings treated with AZD responded to NAA identically to WT plants, supporting that, in the context of root growth inhibition, TOR and auxin most likely

act independently (Figure 4.S8). Together, these results that TOR inhibition rescues the short root and misdirected primary root growth vector phenotypes of the *ire1a ire1b* mutant indicate that TOR activity strongly and specifically contributes to the root growth phenotypes of the *ire1a ire1b* mutant.

TOR is Hyperactive at the Growing Primary Root Tips of the ire1a ire1b Mutant

Next, we sought to map the endogenous alterations to TOR activity in actively growing *ire1a ire1b* roots. To do this we utilized a common immunoblot based assay of phosphorylated Serine-Kinase 6 (phospho-S6K), a conserved target of TOR kinase activity (Xiong *et al.* 2013). We excised approximately 3 mm from 60 root tips and pooled these tips to create an individual biological replicate, and we executed 11 independent biological replicates. The remaining mature root tissue from each root was also excised and pooled. We performed this analysis using 7-day-old seedlings to avoid the possibly confounding effects of the more severe morphological differences between WT and *ire1a ire1b* observed at D10. We compared the relative phospho-S6K signal ratio, which was derived from detection of phospho-S6K over total S6K signal (α S6K1/2), and subsequent normalization to the average WT-DMSO ratio for each individual blot (Figures 4.5, 4.S8). We used WT and *ire1a ire1b* seedlings grown in DMSO or AZD-containing media. We then tested the effects of genotype and AZD treatment on the phospho-S6K signal ratio in root tips using a two-way wANOVA. While we found that there was no significant interaction between these variables on phospho-S6K signal ratio ($F(1,40)= 1.65, p= 0.206$), the simple main effects of genotype and AZD treatment on the phospho-S6K signal ratio were individually significant ($F(1,40)=9.58, p= 3.59 \times 10^{-3}$; $F(1,40)= 16.7, p= 2.02 \times 10^{-4}$ respectively). We found that the *ire1a ire1b* root tips had a ~2-fold higher S6K-ratio compared to WT in DMSO

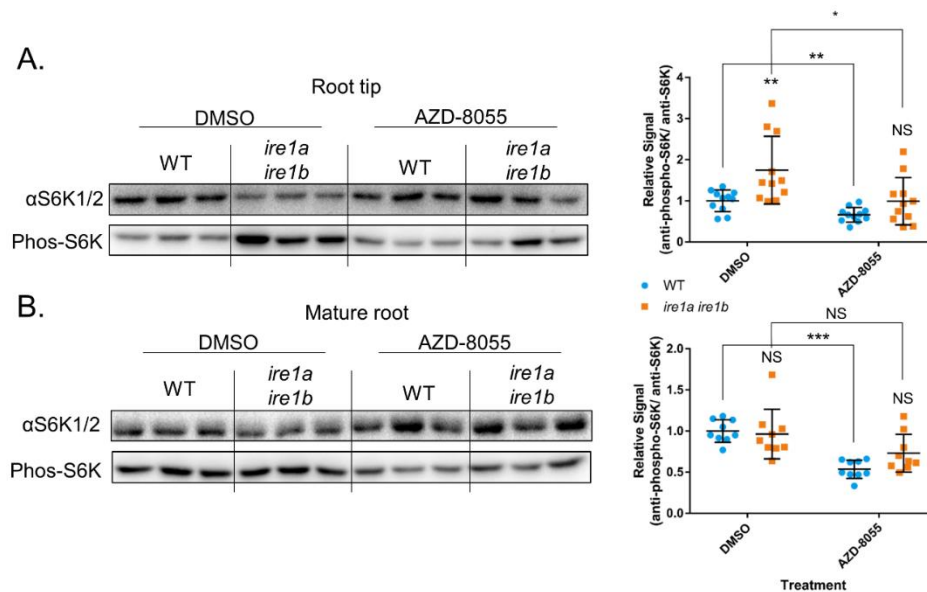


Figure 4.5. TOR is hyperactive in the *ire1a ire1b* mutant root tips but not in the mature root.

A) Representative immunoblot assay to determine relative S6K phosphorylation levels. Antibodies against total S6K (α S6K1/2) or Phosphorylated-S6K (Phos-S6K) were used against total soluble protein extracted from excised WT or *ire1a ire1b* root tips grown for 7 days on media containing AZD-8055 or DMSO control (see materials and methods). Relative signals (Phos-S6K/ α S6K1/2) in each experimental group was normalized to WT DMSO control (n=11). **B)** Same immunoblot method used in A) but used against total soluble protein extracted from excised mature WT or *ire1a ire1b* root tissues grown for 7 days on media containing AZD-8055 or DMSO control (n=9). For all graphs error bars show SD; p-values significance markers displayed above an *ire1a ire1b* experimental group are pairwise comparisons to the corresponding WT group for that specific treatment. Brackets denote other specific pairwise comparisons. Significance markers: NS = adj. $p > 0.05$; * = adj. $p < 0.05$ and > 0.005 ; ** = adj. $p < 0.005$ and > 0.0005 ; *** = adj. $p < 0.0005$ See Figure 4.S8 for full blot images and Ponceau's stain loading controls.

conditions (Figure 4.5A). As expected, AZD treatment led to significantly lower S6K-ratio in WT root tips (0.7-fold change) compared to DMSO. The AZD treatment also significantly reduced the S6K-ratio of *ire1a ire1b* root tips compared to DMSO control (Figure 4.5A). The S6K-ratio of AZD-treated *ire1a ire1b* root tips was not significantly different from AZD-treated WT (Figure 4.5A). When we analyzed the mature root tissues (Figure 4.5B), we found a significant effect of AZD treatment on the relative phospho-S6K signal ratio (two-way ANOVA: $F(1,32) = 24.9$, $p =$

2.03×10^{-5}). However, the genotype did not have a significant effect on the relative phospho-S6K signal ratio in mature root tissues ($F(1,32)= 1.26$, $p= 0.269$), and there were no significant differences between WT and *ire1a ire1b* S6K-ratios in mature root tissues in either DMSO or AZD treatments (Figure 4.5B). Together these results indicate that the loss of IRE1 leads to increased TOR activity in the root tips but not in mature tissues. Therefore, IRE1 is necessary to maintain proper TOR activity levels specifically in rapidly developing root tips.

TOR Inhibition Rescues the ire1a ire1b Cell Elongation Phenotype at the Root Meristem

The spatial specificity of TOR hyper-activation verified in growing root tips but not in mature tissues of the *ire1a ire1b* roots (Figure 4.5) prompted us to establish the cellular consequences of the TOR hyper-activity in the *ire1a ire1b* mutant. To do so, we performed mPS-PI analysis of root tips from WT and *ire1a ire1b* plants grown on DMSO or AZD-containing media (Figure 4.6A). We performed our analysis at D10 in order to test the effects of TOR inhibition on the strong defects in cell elongation in the EZ as well as the moderate defects in the MZ, which only were found at D10 (Figures 4.2E-H). In WT plants grown on AZD-containing media, we observed a small but significant decrease in the number of cells in the MZ, and a small but significant increase in the number of cells in the TZ (Figure 4.6C), consistent with previously published results of TOR inhibition on root tip meristem organization (Montané and Menand 2013). We then performed a series of two-way wANOVAs (or ANOVAs as indicated) to test the effects of AZD treatment and genotype on each these zone metrics in the MZ, TZ and EZ. We found significant interactions between AZD treatment and genotype on zone length, cell number and average cell length of the EZ (wANOVA; $F(1,76)= 62.8$, $p= 1.51 \times 10^{-11}$, $F(1,76)= 21.4$, $p= 1.51 \times 10^{-5}$, $F(1,76)= 34.1$, $p= 1.21 \times 10^{-7}$, respectively). We also found significant interactions

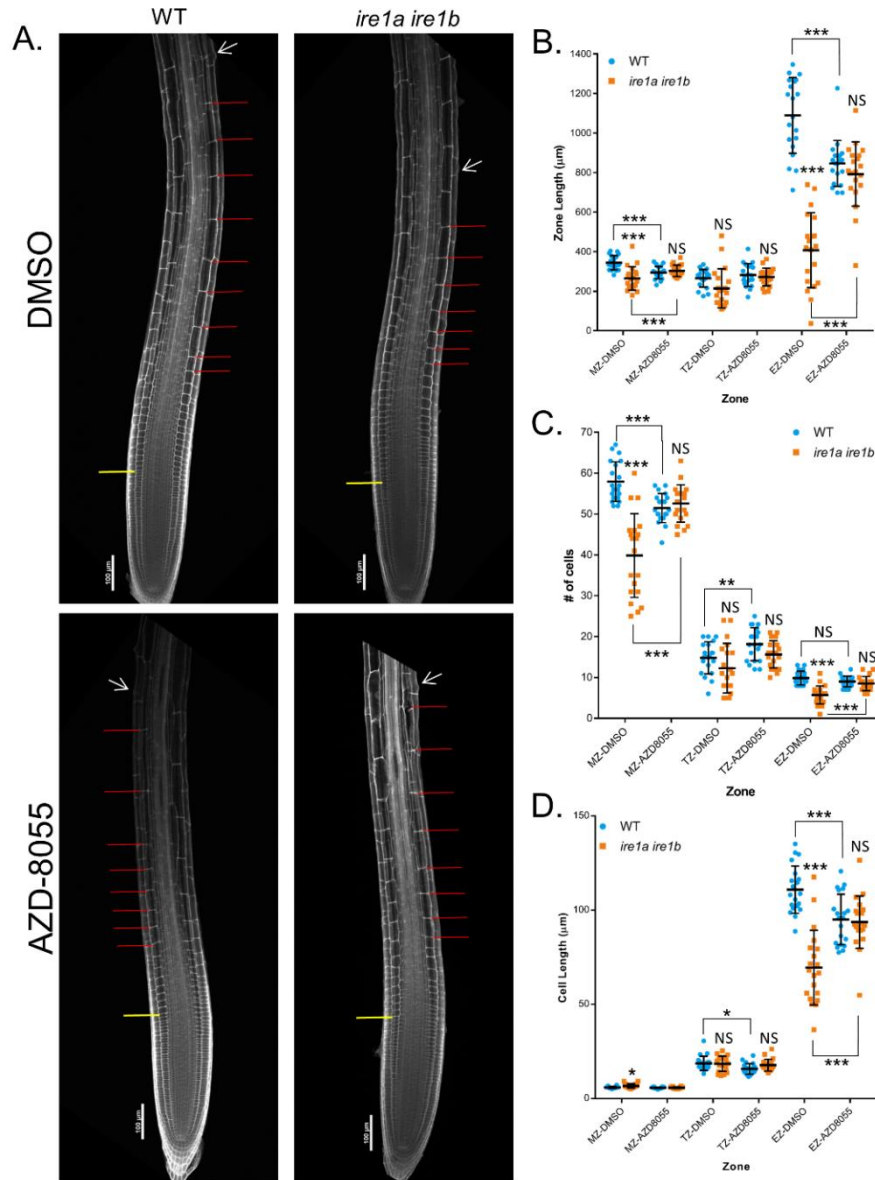


Figure 4.6. Meristem organization defects in *ire1a ire1b* are rescued by TOR inhibition.

At D10, root tips grown on DMSO or AZD media were subjected to mPS-PI staining and confocal microscopy to analyze root tip cellular organization. **A)** Representative 10x images of mPS-PI stained WT and *ire1a ire1b* roots. The yellow line demarks the end of the meristem zone (MZ) and the beginning of the transition zone (TZ), the red lines mark all of the cells in the elongation zone (EZ), and the white arrow marks the first root hair initiation. For all measurements of the MZ secondary 20x images were used to collect data. **B-D)** Zone length, # of cells, and cell length at D10 in roots grown on DMSO or AZD containing media. For all graphs error bars show SD; p-values significance markers displayed above an *ire1a ire1b* experimental group are pairwise comparisons to the corresponding WT group for that specific treatment. Brackets denote other specific pairwise comparisons. Significance markers: NS = adj. $p > 0.01$; * = adj. $p < 0.01$ and > 0.001 ; ** = adj. $p < 0.001$ and > 0.0001 ; *** = adj. p -value < 0.0001

between the effects of AZD treatment and genotype on the zone length and cell number of the MZ (wANOVA; $F(1,76)= 24.2$, $p= 4.80 \times 10^{-6}$, $F(1,76)= 43.9$, $p= 4.39 \times 10^{-9}$, respectively), and a marginally significant interaction on MZ cell length ($F(1,76)= 6.44$, $p= 0.0131$). We did not find any significant interactions between seedling age and genotype on any of the zone metrics in the TZ (wANOVA; zone length: $F(1,76)=1.87$, $p= 0.157$; cell number: $F(1,76)=0.674$, $p= 0.512$; cell length $F(1,76)=1.03$, $p= 0.361$). On the whole, these results demonstrate that the zone metrics exhibiting significant interactions between seedling age and genotype (Figure 4.2) also showed significant interactions between AZD treatment and genotype.

We then narrowed our analysis to determine the nature of the interaction between AZD treatment and genotype in the MZ and EZ by performing pairwise comparisons. In addition to the small but significant decrease in MZ cell number and increase in TZ cell number of the WT root tips treated with AZD, we also found that the EZ length was significantly shorter in AZD-treated WT, compared to DMSO controls (Figure 4.6B). Interestingly, we observed that while the number of EZ cells remained unchanged, the average cell length in the EZ of the AZD-treated WT root tips was significantly smaller than DMSO controls, indicating that the decreased size of the EZ was specifically due to a decrease in cell length in this zone (Figures 4.6C, D). This suggests that TOR activity is required to increase rates of cell elongation, consistent with previous reports (Yuan *et al.* 2020). However, in net contrast, we found that AZD inhibition of TOR in the *ire1a ire1b* mutant led to an increase in the zone length and number of cells in the both the MZ and EZ compared to DMSO-treated *ire1a ire1b* controls (Figures 4.6B, C). Additionally, we also verified an increase in cell size in the EZ of AZD-treated *ire1a ire1b* (Figure 4.6D). In every measured zone metric of the root tip organization, we found no significant differences between AZD-treated WT and AZD-treated *ire1a ire1b* root tips (Figure 4.6), consistent with an AZD-mediated rescue

of the *ire1a ire1b* root growth phenotype verified at D10 (Figure 4.4). These results support that, while basal TOR activity is needed to increase rates of cell elongation, TOR hyper-activity in the *ire1a ire1b* mutant is detrimental to elongation processes.

TOR Hyper-activity in the ire1a ire1b Mutant Promotes Cell Differentiation Rather than Cell Proliferation.

Based on the results that TOR hyper-activity in the *ire1a ire1b* mutant has a detrimental effect on cellular elongation (Figure 4.6), and on previous published reports that after cell elongation TOR activity is necessary to actuate root hair growth in the differentiation zone (also referred to as the maturation zone; Retzer and Weckwerth 2021), we hypothesized that a hyperactive TOR may lead to increased rates of differentiation, which would halt cell elongation. Therefore, we sought to test whether TOR hyper-activity in the *ire1a ire1b* mutant affected rates of cell proliferation, which have already been associated with TOR activity (Xiong *et al.* 2013), or led to increased rates of cell differentiation. We utilized 5-ethynyl-2'-deoxyuridine (EdU; a thymidine analog that marks cell cycle entry into S-phase; Hayashi *et al.* 2013) to perform a pulse-chase experiment of labelled nuclei in intact roots. This would allow us to determine the rate of DNA synthesis at the root tip as a measure of cell proliferation and would also allow us to track labeled meristematic cells over time to determine relative rates of cell differentiation, which is marked by root hair initiation (Dolan and Davies 2004). At D7, whole seedlings grown on DMSO or AZD-containing media were treated in liquid ½ LS media containing EdU for 20 min. Subsets of seedlings were then immediately fixed (0 hr; Figure 4.7) while the rest of the seedlings were returned to their original ½ LS plates for an additional 6 hr allowing for further root growth before fixation (6 hr; Figure 4.7). Z-series of consecutive images for each root tip were then collected by

confocal microscopy, and assembled into max intensity projections (Figure 4.7A). For each root dataset, the sum EdU intensity (Figure 4.7B) and area covered by EdU signal (hereafter EdU signal area; Figure 4.7C) were quantified after background subtraction, which was identical for each image. With this experimental set up, we then sought to determine if there were differences in cell proliferation between WT and *ire1a ire1b* under conditions of TOR inhibition. We therefore tested the effect of EdU-chase time, genotype, and AZD treatment individually on sum EdU intensity, and EdU signal area via three-way wANOVAs. We did not establish a significant interaction between chase time, genotype and AZD treatment on the sum of EdU intensity (three-way wANOVA: $F(1,196)= 0.160$, $p= 0.690$), and found only a marginally significant simple main effect of genotype or AZD treatment alone on sum EdU intensity ($F(1,196)= 5.93$, $p= 0.0157$, $F(1,40)= 2.83$, $p= 0.0937$, respectively). In contrast, we did find a highly significant effect of chase time on sum EdU intensity ($F(1,196)= 122$, $p= <2.2 \times 10^{-16}$). Pairwise comparisons of these values did not indicate any significant differences between WT and *ire1a ire1* in DMSO or AZD treatment, indicating that the IRE1 mutation and low-level TOR inhibition do not have a significant effect on the rates of EdU incorporation and, therefore, cell proliferation (Figure 4.7B). However, the AZD treatment altered the size of the root region marked by the EdU signal. This region appeared more confined in both WT and *ire1a ire1b* mutants in AZD conditions compared to DMSO (Figure 4.7A). While there was only a marginally significant interaction between chase time and AZD treatment on EdU signal area ($F(1,196)= 5.33$, $p= 0.0219$), pairwise comparisons demonstrated that EdU signal area was significantly lower in AZD-treated WT and *ire1a ire1b* at 6 hr chase compared to their respective DMSO controls (Figure 4.7C). Together these results indicate that the loss of IRE1 does not significantly compromise the rate of cell proliferation; however, AZD treatment may have a marginal negative effect

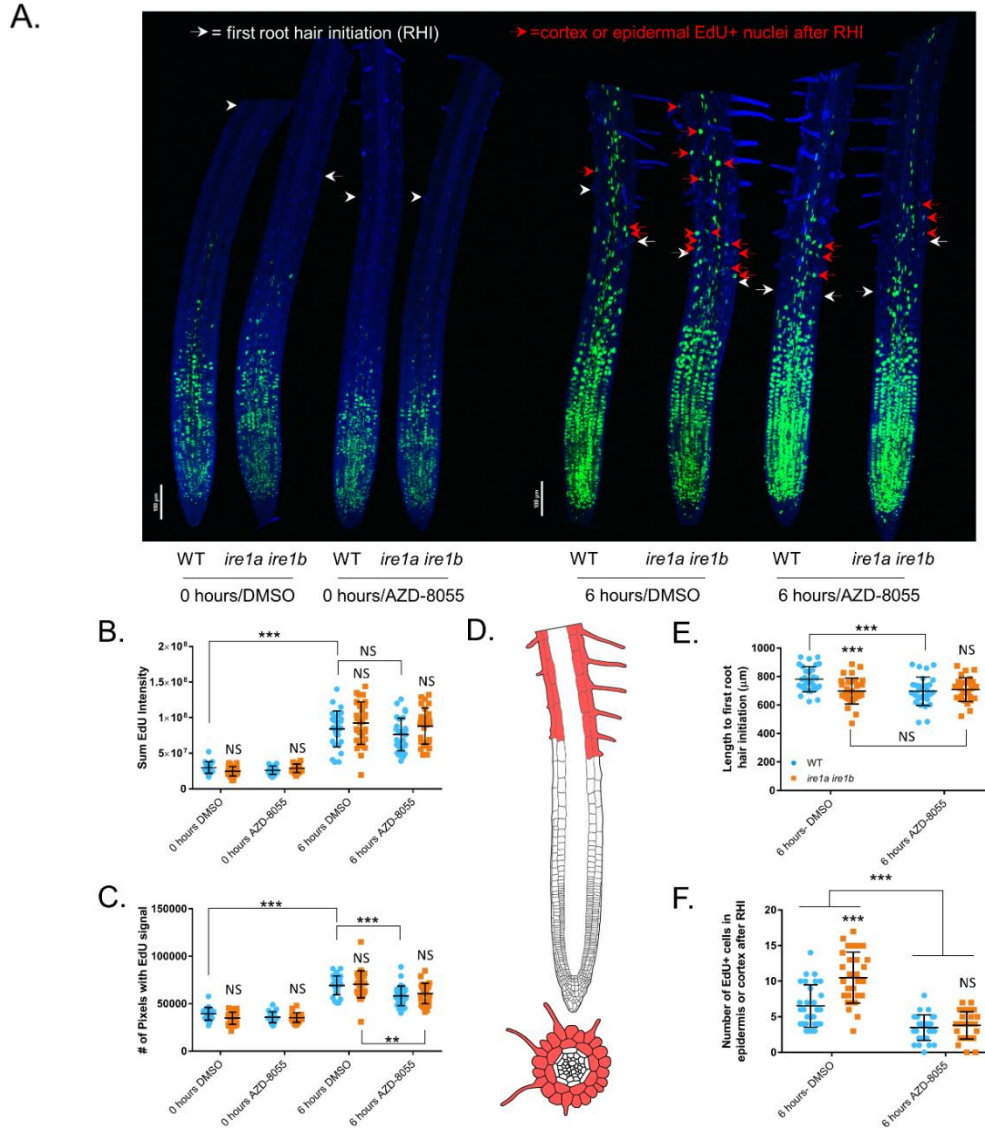


Figure 4.7. TOR hyper-activity in the *ire1a ire1b* mutant promotes differentiation rather than cellular proliferation.

Seedlings grown for 7 days on media containing DMSO or AZD-8055 were treated briefly with EdU and immediately fixed (0 hours) or returned to plates and allowed to grow for a further 6 hr (6 hours). See materials and methods for full analysis methods. **A)** Composite image compiled from representative 10x max projection images of root tips from all treatments. **B)** Sum EdU intensity and **C)** EdU signal area determined from max projection images of individual roots. **D)** Diagrams of vertical and horizontal cross sections of an Arabidopsis root tip highlighting the epidermal and cortex cell layers above the first RHI where EdU positive nuclei were counted. **E)** Length to the first RHI and **F)** number of differentiated EdU+ nuclei were determined for each root by manual assessment of z-series images. For all graphs error bars show SD; p-values significance markers displayed above an *ire1a ire1b* experimental group are pairwise comparisons to the corresponding WT group for that specific treatment. Brackets denote other specific pairwise comparisons. Significance markers: NS = adj. $p > 0.01$; * = adj. $p < 0.01$ and > 0.001 ; ** = adj. $p < 0.001$ and > 0.0001 ; *** = adj. p -value < 0.0001 .

on differentiation of newly generated cells away from the MZ over time.

We next aimed to test the effect of IRE1 on the rates of cell differentiation. To do this, we manually analyzed the Z-series images for each root in the 6-hr chase sample pool to identify along the root tip axis the first cells bearing root hairs (i.e., first root hair initials ; RHI), as markers for tissue differentiation (Figures 4.7D, E; Dolan and Davies 2004). We then counted the number of EdU positive (+) nuclei in the cortex or epidermal cells past the first RHI (hereafter referred to as differentiated EdU+ cells; Figures 4.7D, F). Nuclei that were uniformly labeled (corresponding to labeling during early S-phase) and nuclei that displayed a speckled pattern (corresponding to labeling during late S-phase) were both counted as EdU+ (Hayashi *et al.* 2013). We specifically counted EdU+ nuclei in the cortex and epidermal cell layers because they are unambiguously identifiable based on their size and because they only undergo cell division in the MZ (Dolan and Costa 2001). We found that there was a significant interaction between AZD treatment and genotype on the length to the first RHI (two-way ANOVA: $F(1,113)= 7.92, p= 5.76 \times 10^{-3}$; Figure 4.7E) as well as significant simple main effects of AZD treatment and genotype alone ($F(1,113)= 12.3, p= 6.38 \times 10^{-4}$; $F(1,113)= 12.6, p= 5.48 \times 10^{-4}$, respectively). We also established that the root tip length to first RHI was significantly shorter in *ire1a ire1b* than WT in DMSO conditions. AZD treatment significantly shortened the length to first RHI in WT but not in *ire1a ire1b*, which remained unchanged (Figures 4.7A, F). This pattern matches the D7 root growth phenotype where AZD-treated WT and *ire1a ire1b* roots have primary root lengths that are identical to the *ire1a ire1b* roots grown in DMSO (Figures 4.4A, C).

While we found that the outward morphological characteristics and rates of cell proliferation were similar between DMSO and AZD-treated *ire1a ire1b* roots, the number of differentiated EdU+ cells were markedly different (Figure 4.7E). Specifically, we found a

significant interaction between AZD treatment and genotype on the number of differentiated EdU+ cells (two-way wANOVA: $F(1,113)= 13.4$, $p= 3.81 \times 10^{-4}$), as well as significant simple main effects of AZD treatment and genotype alone ($F(1,113)= 22.0$, $p= 7.84 \times 10^{-6}$; $F(1,113)= 20.5$, $p= 1.51 \times 10^{-5}$, respectively). In the *ire1a ire1b* root tips, which had higher levels of TOR activity in DMSO conditions (Figure 4.5), we found that the number of differentiated EdU+ cells was nearly 2-fold higher than WT. We also established that AZD treatment led to a significant reduction in the number of differentiated EdU+ cells in both WT (~2 fold) and *ire1a ire1b* (~4 fold), such that there was not a significant difference between WT and *ire1a ire1b* in AZD conditions. Together these results support that an IRE1-dependent limitation of TOR activity is required to prevent uncontrolled increases in the rate of cell differentiation from the meristem in the shootward direction.

DISCUSSION

Loss-of-function mutations of *IRE1*, the most conserved master regulator of the UPR across eukaryotes, cause a wide variety of defects in growth and development in plants and metazoans (Chen *et al.* 2014, Kim *et al.* 2018, Bao *et al.* 2019, Mishiba *et al.* 2019, Mitra and Ryoo 2019). In metazoans, some of the causative relationships between the loss of IRE1 activity and developmental defects have been defined (Mitra and Ryoo 2019). In marked contrast in plants, prior to this work, a functional connection between the loss of *IRE1* and developmental defects had yet to be made. To address this significant gap, we performed a detailed analysis of the tractable *ire1a ire1b* model, which exhibits a distinctive defect in primary root growth. We found that the development of *ire1a ire1b* root growth defects are specifically brought on by age-related increases in rates of organ growth, which are most likely tied to increased availability of carbohydrates as the plants mature. We established that such defects primarily manifest through ineffective actuation of cellular elongation at the root tip, leading to shorter roots that do not maintain gravity-driven growth vectors. We found that in actively growing root tips of the *ire1a ire1b* mutant, TOR activity is significantly elevated compared to WT, and that low-level inhibition of TOR restores the *ire1a ire1b* root growth phenotype to WT levels. We further demonstrated that such TOR hyper-activation drives increased rates of cell differentiation at the root tips. Therefore, our work demonstrates that IRE1 controls TOR activity in specific developmental stages in physiological conditions of growth. In addition to supporting the canonical role for TOR as a driver of cell proliferation in the root tip, our results also reveal a new role of TOR in cell differentiation whose functional homeostasis depends on IRE1 availability.

IRE1 Regulates TOR Activity in a Multicellular Eukaryote

In mammalian models, some connections between mammalian TOR (mTOR) activity and IRE1 regulation have been found previously (Pfaffenbach *et al.* 2010, Kato *et al.* 2012, Kato *et al.* 2013, Young *et al.* 2013, Li *et al.* 2014, Shanware *et al.* 2014, Sanchez-Alvarez *et al.* 2017). In cases of light-induced retinal injury, hepatic lipotoxicity, chemically induced ER stress, cadmium toxicity, and lipid-starved solid tumor microenvironments, mTOR activity induces cell apoptosis either through aggravation of general ER stress (Pfaffenbach *et al.* 2010, Li *et al.* 2014), or through specific activation of the IRE1-induced apoptosis via the IRE1-JNK kinase signal cascade (Kato *et al.* 2012, Kato *et al.* 2013, Young *et al.* 2013). Significantly, in all of these studies modulation of IRE1 activity is a downstream effect of mTOR activation. In this work, we show that in actively growing root tips of the *ire1a ire1b* mutant TOR is hyperactive (Figure 4.5). These results, in conjunction with the observations that low-level TOR inhibition completely rescues all aspects of the *ire1a ire1b* root growth phenotype (Figures 4.4, 4.6, 4.7), lead us to conclude that not only does IRE1 control TOR activity, but this is the primary pathway by which IRE1 promotes proper organ biogenesis. To our knowledge, the results presented in this work are the first to demonstrate that IRE1 regulates TOR activity in any model organism, and that such activity occurs in the absence of induced ER stress.

IRE1 is Necessary to Control TOR Activity at Tissue- and Development-Specific Levels

Previous reports indicated that IRE1 contributes to Arabidopsis growth and development on a broad level and have repeatedly demonstrated that the *ire1a ire1b* mutant has a short root phenotype (Chen and Brandizzi 2012, Deng *et al.* 2013, Mishiba *et al.* 2019, Pu *et al.* 2019).

However, a detailed dissection of events leading to this phenotype at the cell- and tissue-level and an accounting of how variation in standard growth conditions could alter it were lacking. In our work, we have demonstrated that the increased rates of root growth maintained in WT plants as they mature cannot be actuated in the *ire1a ire1b* mutant (Figure 4.1). We established that this primary defect is restricted to the EZ and secondarily to the MZ as a function of seedling age (Figure 4.2), and is concurrent with hyper-activation of TOR in the *ire1a ire1b* mutant specifically at the root tips (Figure 4.5). At the initial phase of rapid root growth (day 7), we found that the *ire1a ire1b* EZ exhibits less and smaller cells compared to WT (Figure 4.2), but we did not observe any significant differences in cell size and proliferation rate in the *ire1a ire1b* MZ compared to WT (Figures 4.2, 4.7). Therefore, our results argue that, in early developmental stages in WT, IRE1 is necessary to maintain homeostatic levels of TOR activity in the EZ but not in the MZ. At the later stages of the *ire1a ire1b* phenotype development (i.e. day 10), we found that the *ire1a ire1b* MZ is shorter, and has not increased in size like the WT MZ (Figure 4.2). Fascinatingly, we also found that the reduction in the number of cells in the *ire1a ire1b* MZ is reverted to WT levels by chemical inhibition of TOR (Figure 4.6). Based on these results, we conclude that TOR activity levels may have opposite effects in the MZ during the rapid growth of the root tip: basal TOR activity promotes cell proliferation in MZ, as reported earlier (Xiong *et al.* 2013, Li *et al.* 2017), but TOR hyper-activity may also dampen it, as demonstrated in this work. In connection with our *ire1a ire1b* root phenotypic results, we infer that IRE1 activity is required to control TOR activity especially at stages of development requiring increased cell proliferation and elongation. Although the underlying mechanisms on the MZ size control exerted by IRE1 through TOR are yet unknown, our data support that IRE1 is absolutely required to antagonizes TOR hyper-activation to maintain proper organ development.

IRE1-Dependent Repression of TOR is Independent from the Unconventional Splicing of bZIP60

In conditions of induced ER stress, IRE1 splices the mRNA of its effector TF, bZIP60 (Nagashima *et al.* 2011). It is well established that in physiological conditions of growth, a *bzip60* complete loss-of function mutant does not exhibit a short root phenotype (Nagashima *et al.* 2011, Chen and Brandizzi 2012, Moreno *et al.* 2012). Based on our results that *ire1a ire1b* has a marked root length phenotype (Figure 4.1) and the notion that an *ire1a ire1b bzip60* triple mutant is phenotypically indistinguishable from *ire1a ire1b* under normal growth conditions (Ruberti *et al.* 2018), we deduce that the molecular mechanisms by which IRE1 controls root development and TOR activity are independent from a functional interaction with bZIP60. The loss of the mammalian homolog of *bZIP60*, *XBP1*, compromises tissue development in a similar way to *IRE1* loss-of-function mutations; for example, both mutations lead to defective embryonic liver development (Mitra and Ryoo 2019). Hence, the results that in physiological conditions of growth a *bzip60* mutant does not exhibit visible phenotype highlight a functional divergence between the IRE1-dependent TFs XBP1 and bZIP60 in organ development across kingdoms.

Metazoan and plant IRE1 proteins are known to cleave transcripts other than XBP1 or bZIP60 through RIDD (Hollien *et al.* 2009, Mishiba *et al.* 2013). Therefore, we hypothesize that under high growth pressure due to prolonged photoperiod and abundant carbohydrate supply, conditions that we selectively applied in our work (Figure 4.3), IRE1-mediated RIDD of a single or multiple RNA targets could lead to a strong limitation or cap on TOR activity in certain tissue types. Due to the fact that known Arabidopsis IRE1-RIDD targets have thus far been identified exclusively in ER stress conditions using RNA derived from whole seedlings (Mishiba *et al.* 2013), the identification of the intermediate targets between IRE1 and TOR under physiological conditions in actively growing root tissues remains an exciting topic for future study.

In *Arabidopsis*, TOR activity depends on a variety of cues (e.g., mitochondrial respiration, auxin, amino acids (Li *et al.* 2017, Schepetilnikov *et al.* 2017, Shi *et al.* 2018, Burkart and Brandizzi 2020). Hence potential RIDD targets may affect one or several of these pathways. Nonetheless, based on our observations that link the *ire1a ire1b* phenotype to photoperiod and carbohydrate-related increases in rates of root growth (Figure 4.3), we speculate that the most probable target may be associated with IRE1 and regulation of mitochondrial respiration. This is predicated by the evidence that the assembly of the mammalian TOR complex 1 (mTORC1) depends on the TTT-RUVBL1/2 complex, which leads to activation of TOR through formation of TOR obligate dimers (Kim *et al.* 2013). The activity of the TTT-RUVBL1/2 complex is in turn strongly dependent on mitochondrial ATP generation through respiration. ER functions and mitochondrial metabolism are closely linked in metazoan models primarily through calcium delivery to mitochondria via the ER (Szabadkai *et al.* 2006, Kaufman and Malhotra 2014, Hirabayashi *et al.* 2017, Rieusset 2018, Gutiérrez *et al.* 2020). In *Arabidopsis*, IRE1 activity has been tied to a regulation of mitochondrial stress responses, albeit under induced ER stress situations (Ng *et al.* 2013). Therefore, it is possible that in *Arabidopsis*, IRE1 may regulate mitochondrial respiration in rapidly growing tissues under physiological conditions.

TOR Activity Regulates Cellular Differentiation and Elongation in Actively Growing Arabidopsis Root Tips

Previous work supports that TOR activity can promote cell elongation. Specifically, TOR was shown to promote accumulation of the auxin efflux transporter PIN2 at the root meristem through a direct protein-protein interaction, leading to increased size of cells in the EZ without affecting cell proliferation (Yuan *et al.* 2020). In our work, we have demonstrated that low-level

TOR inhibition of rapidly growing WT roots leads to a small reduction root length (Figure 4.4, Day 7) and was sufficient to significantly impact TOR activity at the root tip (Figure 4.5). However, this minimal TOR inhibition does not strongly affect overall rates of cell proliferation and instead leads to smaller cells in the EZ and a reduced rate of cell differentiation (Figures 4.6, 4.7). In the *ire1a ire1b* root tips, we found that TOR hyper-activity coincided with increased rates of cell differentiation compared to WT, which were reduced to WT levels with low-level TOR inhibition (Figure 4.7).

A plausible model to illustrate the effect of *ire1a ire1b* mutation and TOR inhibition on cell differentiation is presented in Figure 4.S9. In this model, TOR activity is needed in the later stages of cell maturation to actuate cell differentiation programs in addition to the known roles of TOR in promoting cell proliferation. In contrast with the effect on cell differentiation, which responds in a linear manner to TOR activity, it seems that cell elongation has a biphasic response to TOR activation (Figure 4.S9). Similar to cell differentiation, our data support that a basal level of TOR activity is also required to promote cell elongation. However, at high levels of TOR activity cell elongation is negatively impacted and is rescued by TOR inhibition. We speculate that under TOR hyper-activity the increased rate of cellular differentiation negatively impacts the time that cells have to undergo cell elongation processes prior to root hair initiation, leading to a smaller maximum cell size in the EZ cells. Together these results provide further evidence that TOR has significant effects in determining cell fate outside of cell proliferation in the MZ and demonstrate that IRE1 is an upstream regulatory factor of TOR in these contexts. Therefore, this study provides an important foundation for future work by uncovering a novel link between two ancient eukaryotic signaling pathways. With this tractable *ire1a ire1b* model further investigation could

yield important information related to UPR and TOR dependent control over multicellular organism development.

ACKNOWLEDGEMENTS

We acknowledge support by the Chemical Sciences, Geosciences and Biosciences Division, Office of Basic Energy Sciences, Office of Science, U.S. Department of Energy (award number DE-FG02-91ER20021) for infrastructure, NASA (award 80NSSC19K0707), NIH GM136637, and a fellowship from Michigan State University under the Training Program in Plant Biotechnology for Health and Sustainability (T32-GM110523). We would also like to thank the Center for Statistical Training and Consulting at Michigan State University for their kind assistance and for providing the necessary code to perform the ANOVA tests utilizing weighted least squares regression.

APPENDIX

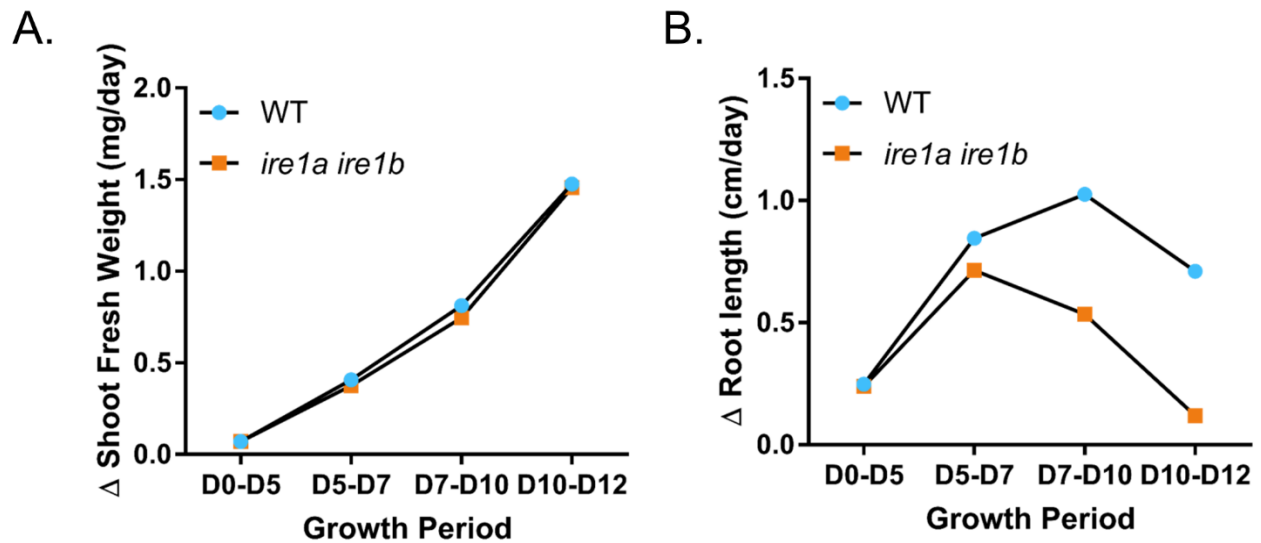


Figure 4.S1. Rate of shoot fresh weight accumulation, and rate of primary root growth for data displayed in Figure 4.1.

A) Average shoot fresh weight values from Figure 4.1B were reprocessed to show the rate of shoot fresh weight accumulation for a specific growth period (value= average shoot fresh weight accumulated during a growth period/ days in that growth period). **B)** Average root length values from Figure 4.1C were reprocessed to show the rate of primary root length increases for a specific growth period (value= average root length increases accumulated during a growth period/ days in that growth period).

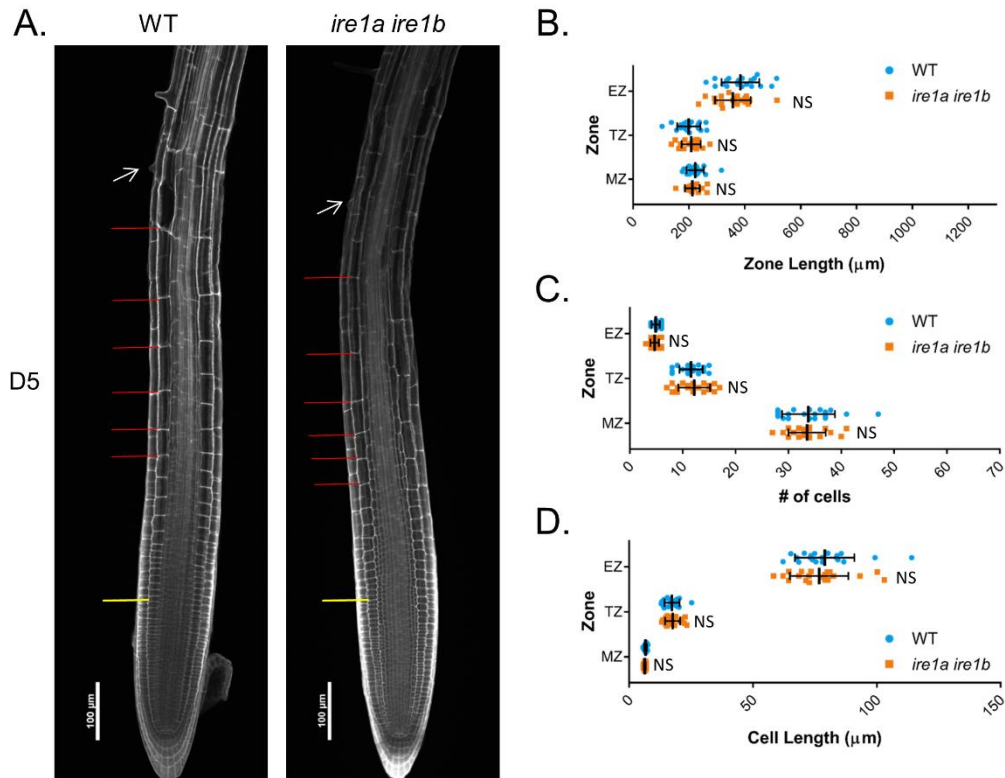


Figure 4.S2. At D5 there are no significant defects in *ire1a ire1b* meristem organization.

At D5, root tips were subjected to mPS-PI staining and confocal microscopy to analyze root tip cellular organization. **A)** Representative 10x images of mPS-PI stained WT and *ire1a ire1b* roots. The yellow line demarks the end of the meristem zone (MZ) and the beginning of the transition zone (TZ), the red lines marks all of the cells in the elongation zone (EZ), and the white arrow marks the first root hair initiation. For all measurements of the MZ secondary 20x images were used to collect data. **B)** The average length of each zone. **C)** The # of cells in each zone. **D)** Average cell length in each zone. For all graphs error bars show SD; p-values significance markers displayed above an *ire1a ire1b* experimental group are pairwise comparisons to the corresponding WT group for that specific treatment. Brackets denote other specific pairwise comparisons. Significance markers: NS = adj. $p > 0.01$; * = adj. $p < 0.01$ and > 0.001 ; ** = adj. $p < 0.001$ and > 0.0001 ; *** = adj. $p\text{-value} < 0.0001$

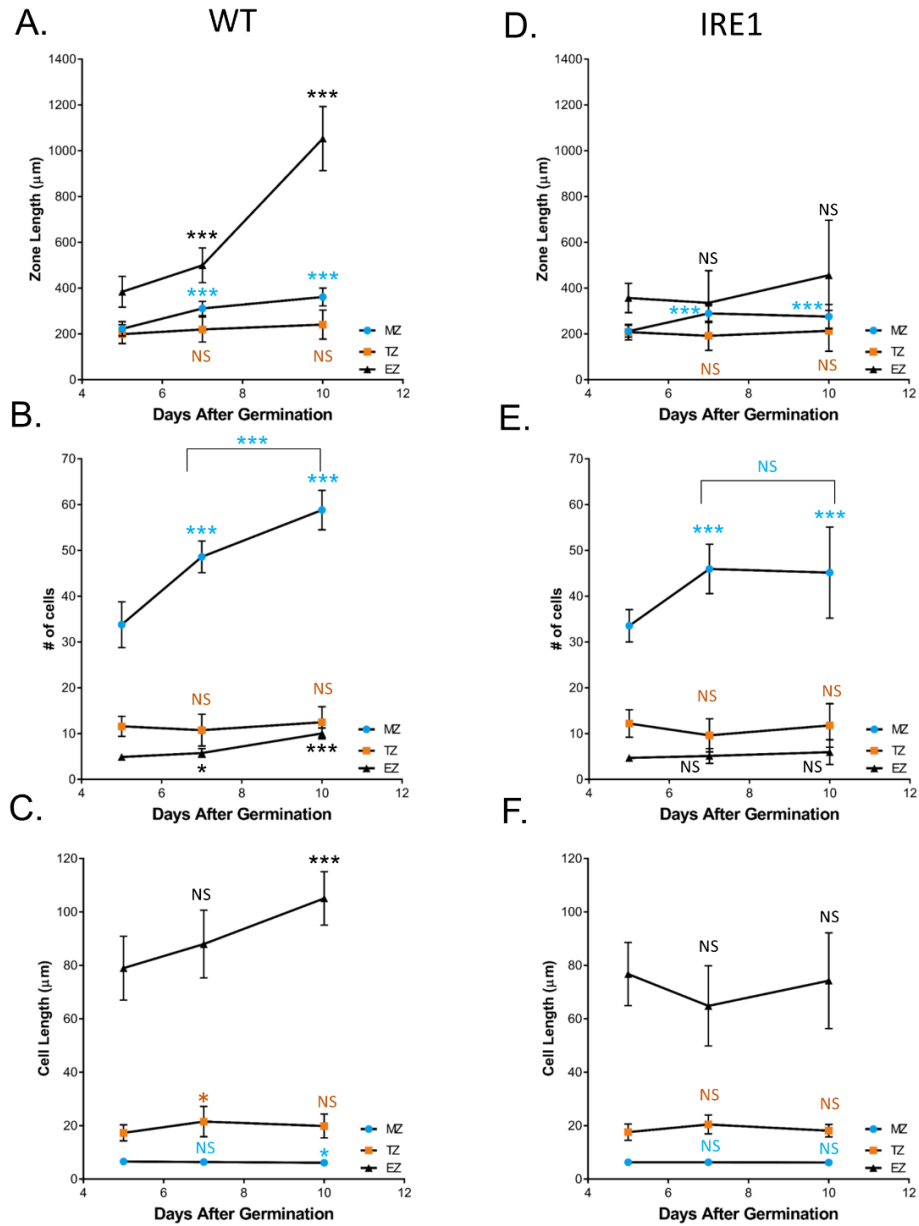


Figure 4.S3. Average root tip cellular organization metrics displayed over time in WT and *ire1a ire1b*.

Average values from the data presented in Figure 4.S2, and Figure 4.2 are plotted over time to compare differences over time in each genotype separately. **A-C)** Zone length, # of cells, and cell length in the WT root tips. **D-F)** Zone length, # of cells, and cell length in the *ire1a ire1b* root tips. For all graphs: Error bars are SD, p-values significance markers displayed over an experimental group at D7 or D10 are comparisons to the corresponding D5 value for that group. Brackets denote other specific pairwise comparisons. Significance markers: NS = adj. $p > 0.01$; * = adj. $p < 0.01$ and > 0.001 ; ** = adj. $p < 0.001$ and > 0.0001 ; *** = adj. p -value < 0.0001 . p-value indicator color matches the color of the corresponding root tip zone.

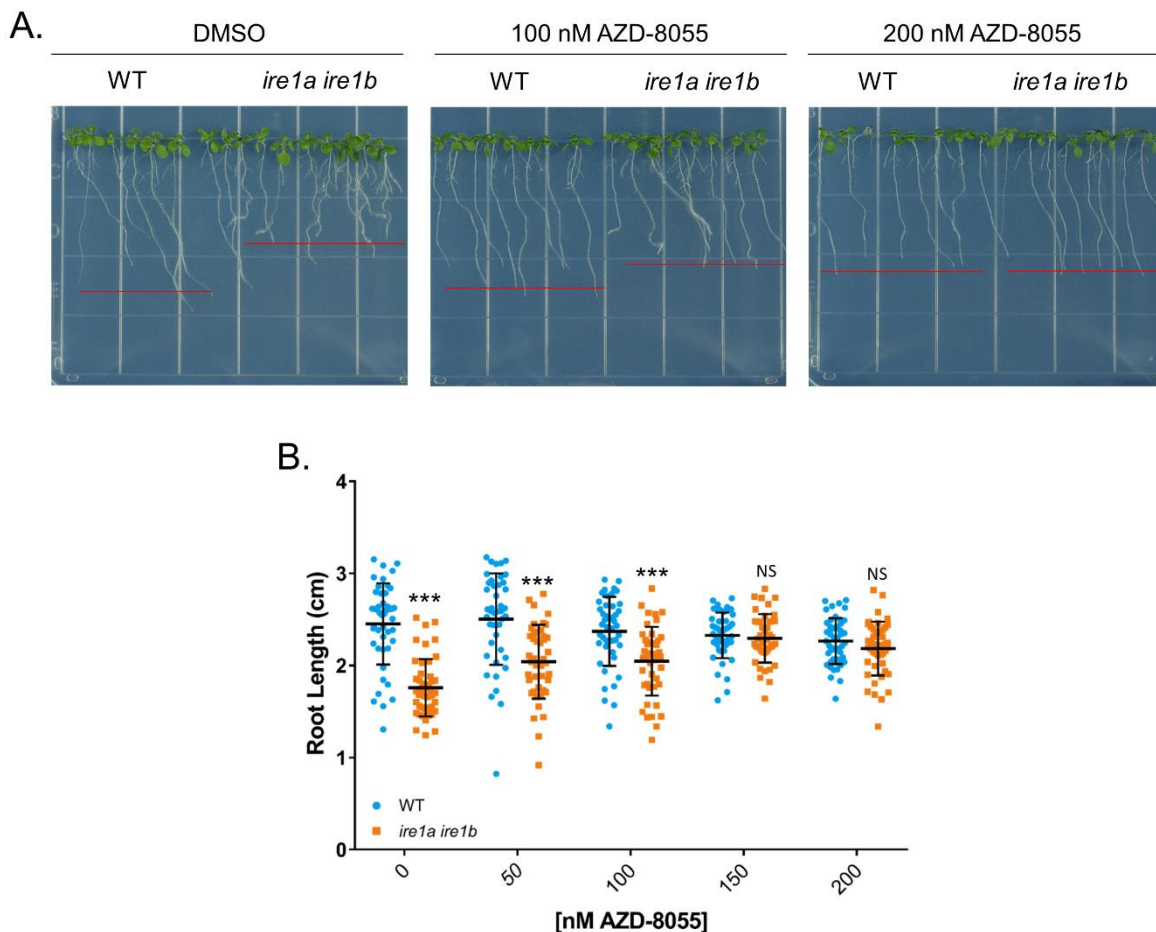


Figure 4.S4. TOR inhibitor AZD-8055 concentration response analysis.

A) Representative images from DMSO, 100 nm and 200 nm AZD-8055 conditions. **B)** Root length of individual roots was measured using ImageJ. For all graphs error bars show SD; p-values significance markers displayed above an *ire1a ire1b* experimental group are pairwise comparisons to the corresponding WT group for that specific treatment. Brackets denote other specific pairwise comparisons. Significance markers: NS = adj. $p > 0.01$; * = adj. $p < 0.01$ and > 0.001 ; ** = adj. $p < 0.001$ and > 0.0001 ; *** = adj. p -value < 0.0001 . For this experiment the growth chamber used had 200 μ E continuous light which caused proportionally shorter roots in both WT and *ire1a ire1b* compared to 150 μ E light, however the general conclusions from the DMSO vs AZD treatments are the same in both conditions.

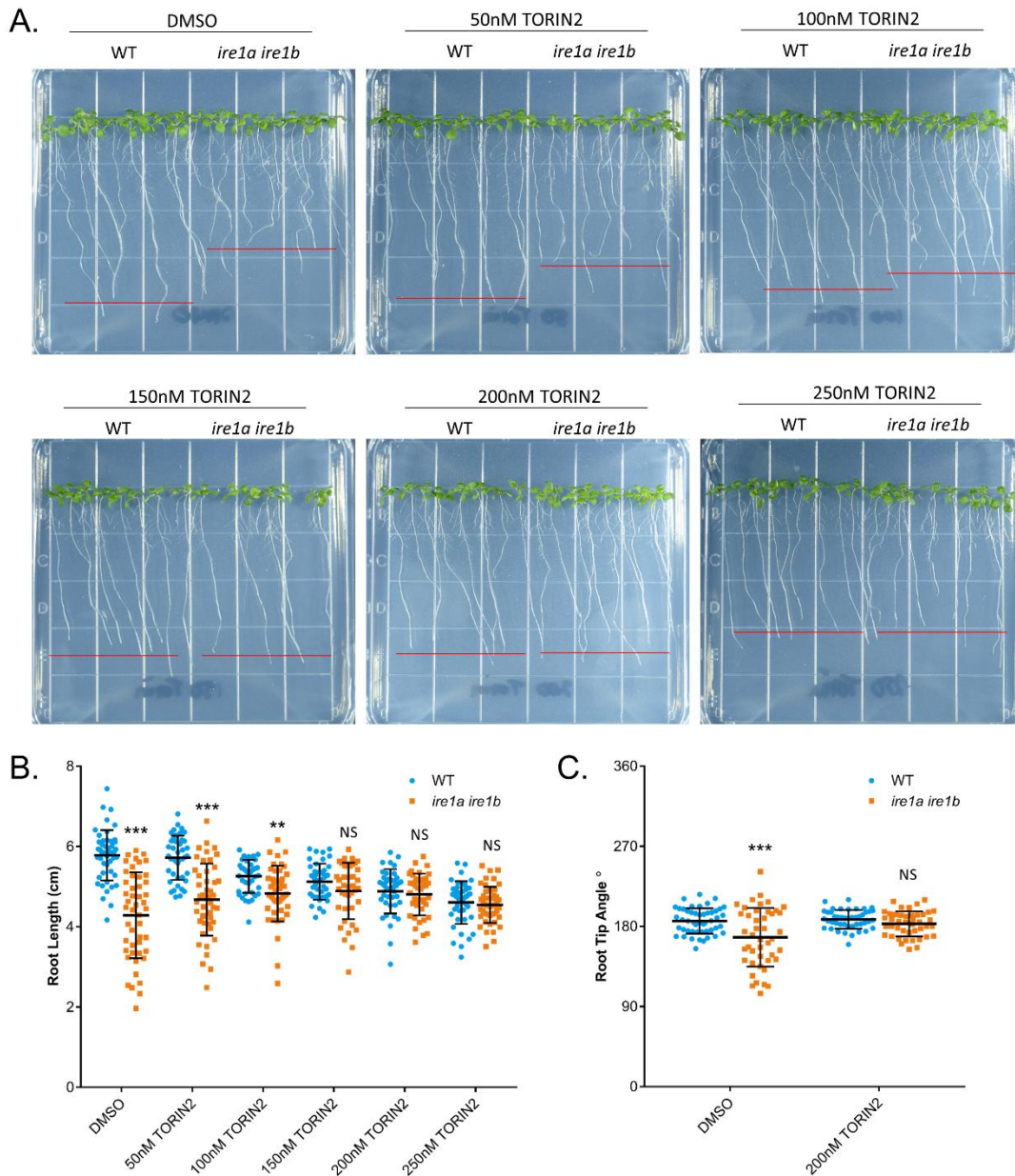


Figure 4.S5. TOR inhibitor TORIN2 rescues the *ire1a ire1b* root growth phenotypes.

A) Representative images from DMSO, and TORIN2 conditions. B) Root length of individual roots was measured using ImageJ. Error bars show SD; p-values significance markers displayed above an *ire1a ire1b* experimental group are pairwise comparisons to the corresponding WT group for that specific treatment. Brackets denote other specific pairwise comparisons. Significance markers: NS = adj. $p > 0.01$; * = adj. $p < 0.01$ and > 0.001 ; ** = adj. $p < 0.001$ and > 0.0001 ; *** = adj. p -value < 0.0001 C) Angle of the root tip away from vertical (0°) was measured using ImageJ. Significant differences between coefficient of variation was tested using the asymptotic Feltz and Miller test as described in materials and methods. p-values: NS = > 0.05 , ** = p -value < 0.01 and > 0.001 , *** = p -value < 0.001

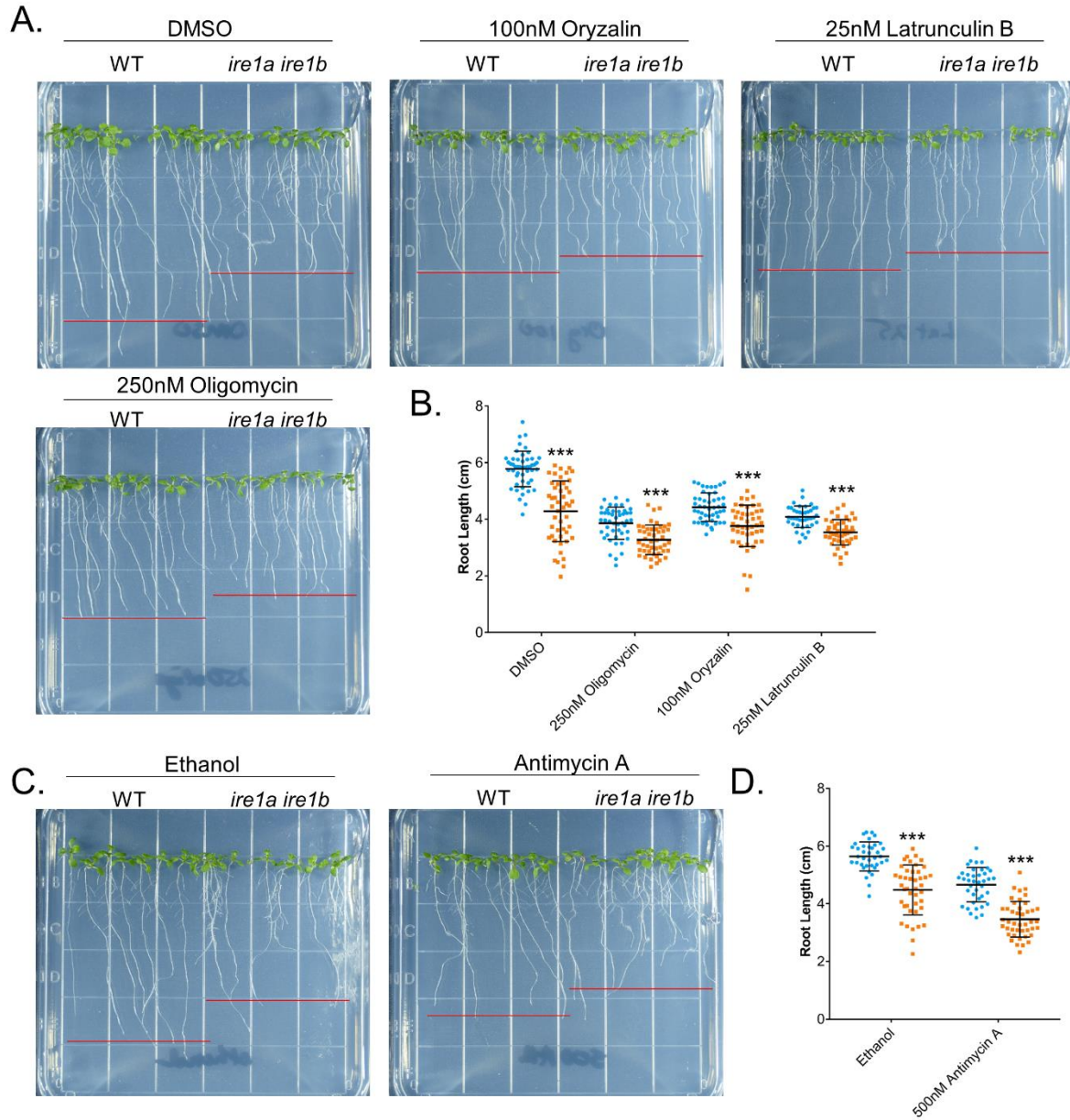


Figure 4.S6. Other chemical inhibitors of root growth do not rescue the *ire1a ire1b* root length phenotype.

A) Representative images from DMSO, Oryzalin, Latrunculin B and Oligomycin growth conditions. This experiment and TORIN2 experiments (Figure 4.S5.) were performed simultaneously and share the DMSO control data. B) Root length of individual roots was measured using ImageJ. C) Representative images from Antimycin A and ethanol control growth conditions. C) Root lengths of individual roots for ethanol and Antimycin A growth conditions. For all graphs error bars show SD; p-values significance markers displayed above an *ire1a ire1b* experimental group are pairwise comparisons to the corresponding WT group for that specific treatment. Brackets denote other specific pairwise comparisons. Significance markers: NS = adj. $p > 0.01$; * = adj. $p < 0.01$ and > 0.001 ; ** = adj. $p < 0.001$ and > 0.0001 ; *** = adj. p -value < 0.0001

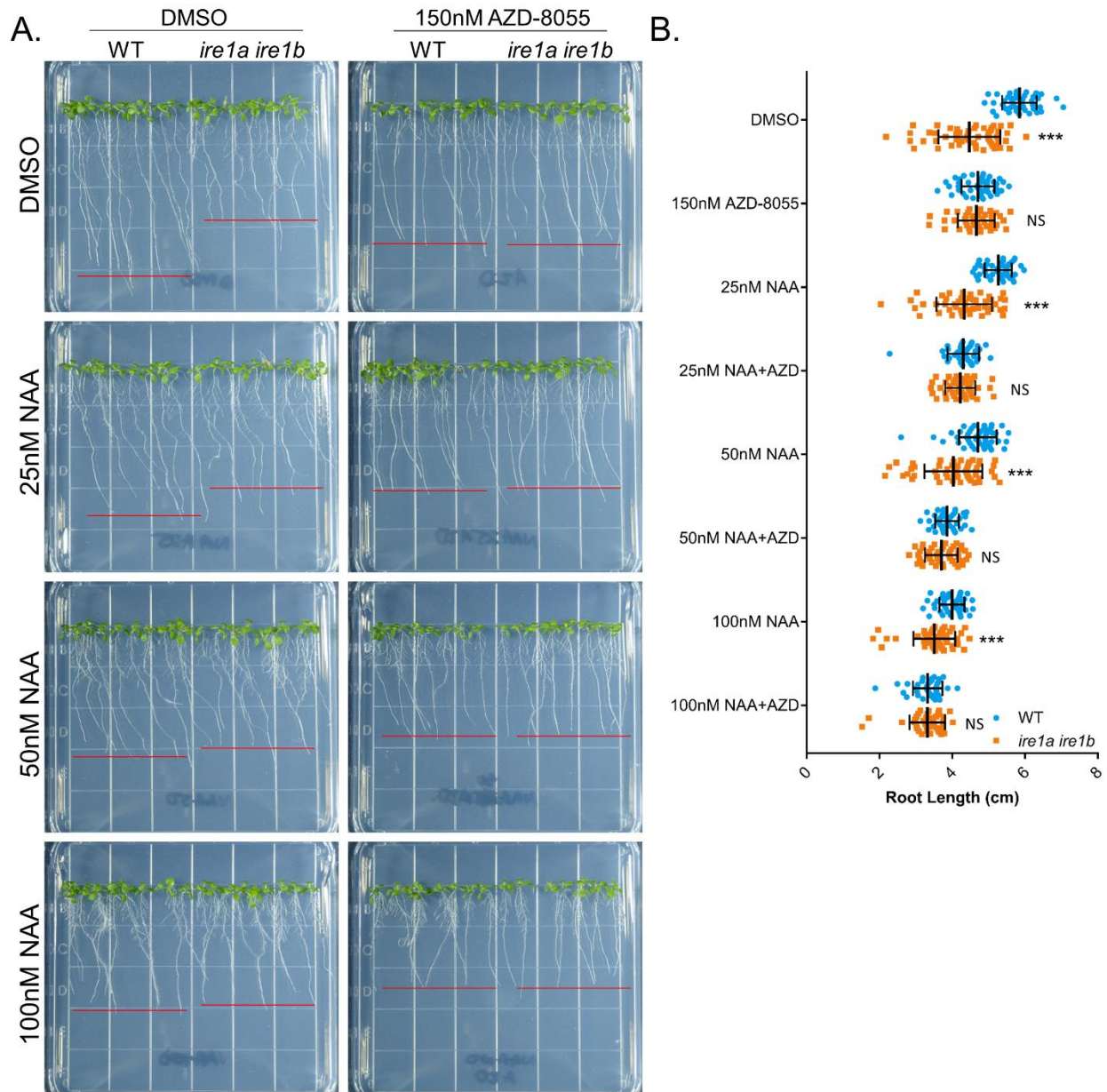


Figure 4.S7. Auxin inhibition of root growth and TOR inhibition of root growth are additive effects in WT plants.

A) Representative images of seedlings grown on plates containing various concentrations of NAA, with or without addition of AZD-8055. **B)** Primary root length after 10 days of growth. For graphs error bars show SD; p-values significance markers displayed above an *ire1a ire1b* experimental group are pairwise comparisons to the corresponding WT group for that specific treatment. Brackets denote other specific pairwise comparisons. Significance markers: NS = adj. $p > 0.01$; * = adj. $p < 0.01$ and > 0.001 ; ** = adj. $p < 0.001$ and > 0.0001 ; *** = adj. $p < 0.0001$

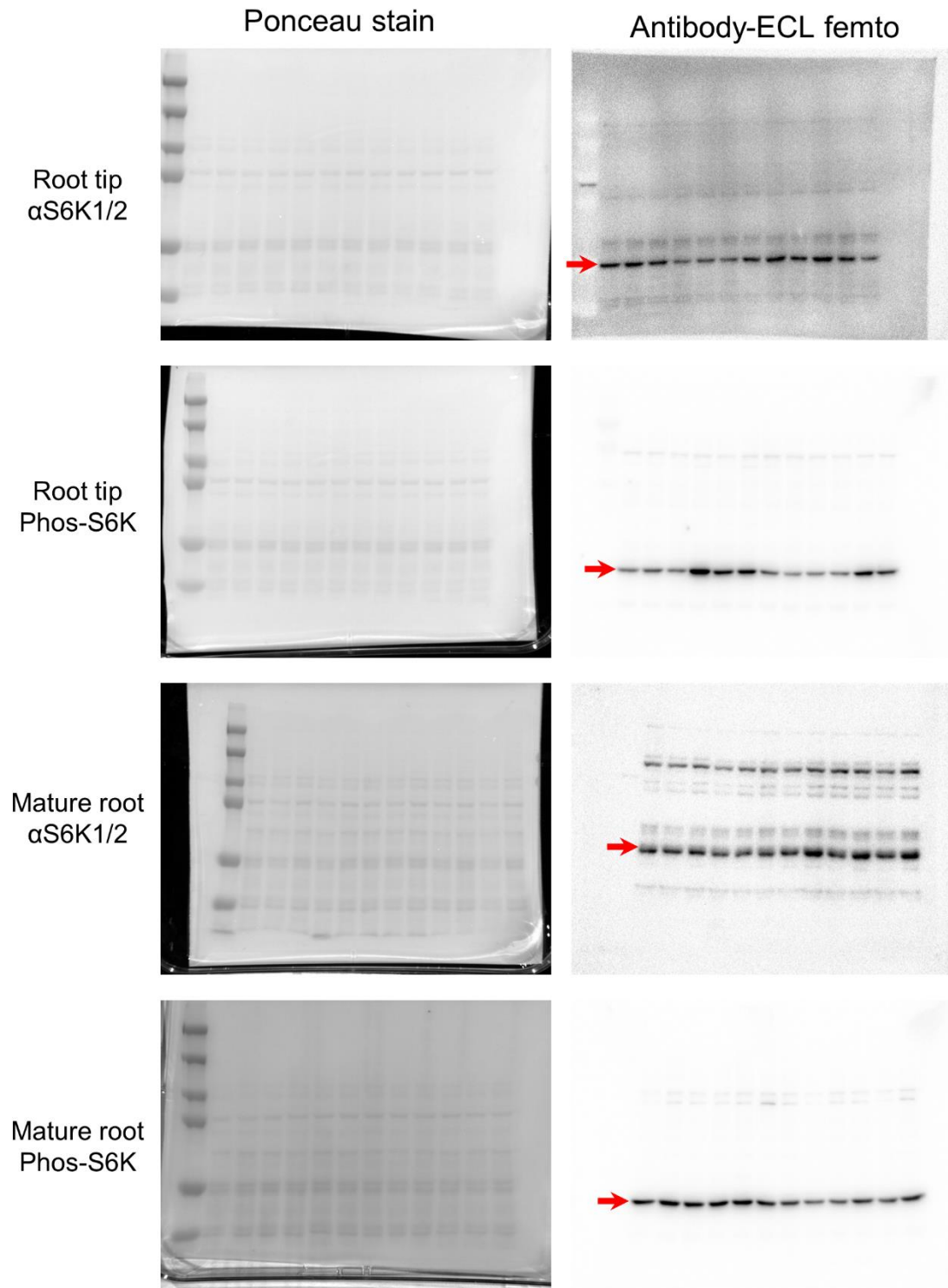


Figure 4.S8. Full blot images (from Fig 4.5) and the Ponceau's stain images to demonstrate equal protein loading.

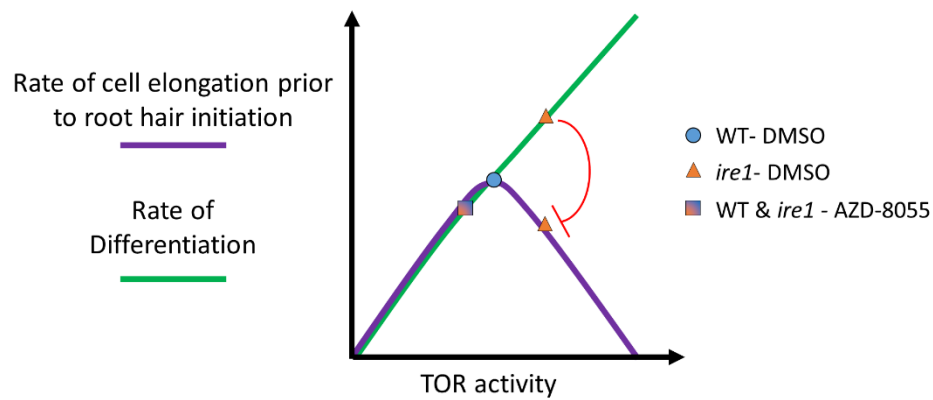


Figure 4.S9. Simplified model of the effect of TOR activity on cell elongation in the *ire1a ire1b* mutant.

Simplified model based on our results showing that TOR activity must be balanced by IRE1 to maintain optimal cell elongation. Basal TOR activity is needed for cell elongation, illustrated by the difference between WT-DMSO and WT- AZD-8055. However, TOR hyper-activity promotes faster and unbalanced rates of differentiation, which favors premature root hair initiation and cessation of cell elongation. This in turn leads to shorter length of mature cells and an overall shorter root length in the *ire1a ire1b* mutant.

REFERENCES

REFERENCES

- Angelos, E., Ruberti, C., Kim, S.-J. and Brandizzi, F. (2017). Maintaining the factory: the roles of the unfolded protein response in cellular homeostasis in plants. *The Plant Journal* 90(4): 671-682.
- Bao, Y., Bassham, D. C. and Howell, S. H. (2019). A Functional Unfolded Protein Response Is Required for Normal Vegetative Development. *Plant Physiology* 179(4): 1834-1843.
- Barrada, A., Djendli, M., Desnos, T., Mercier, R., Robaglia, C., Montané, M.-H. and Menand, B. (2019). A TOR-YAK1 signaling axis controls cell cycle, meristem activity and plant growth in *Arabidopsis*. *Development* 146(3).
- Beaugelin, I., Chevalier, A., d'Alessandro, S., Ksas, B. and Havaux, M. (2020). Endoplasmic reticulum-mediated unfolded protein response is an integral part of singlet oxygen signalling in plants. *The Plant Journal*.
- Burkart, G. M. and Brandizzi, F. (2020). A Tour of TOR Complex Signaling in Plants. *Trends in biochemical sciences*.
- Calfon, M., Zeng, H., Urano, F., Till, J. H., Hubbard, S. R., Harding, H. P., Clark, S. G. and Ron, D. (2002). IRE1 couples endoplasmic reticulum load to secretory capacity by processing the XBP-1 mRNA. *Nature* 415(6867): 92-96.
- Cao, P., Kim, S.-J., Xing, A., Schenck, C. A., Liu, L., Jiang, N., Wang, J., Last, R. L. and Brandizzi, F. (2019). Homeostasis of branched-chain amino acids is critical for the activity of TOR signaling in *Arabidopsis*. *eLife* 8: e50747.
- Casamitjana-Martinez, E., Hofhuis, H. F., Xu, J., Liu, C. M., Heidstra, R. and Scheres, B. (2003). Root-specific CLE19 overexpression and the *sol1/2* suppressors implicate a CLV-like pathway in the control of *Arabidopsis* root meristem maintenance. *Curr Biol* 13(16): 1435-1441.
- Chen, G.-H., Liu, M.-J., Xiong, Y., Sheen, J. and Wu, S.-H. (2018). TOR and RPS6 transmit light signals to enhance protein translation in deetirolating *Arabidopsis* seedlings. *Proceedings of the National Academy of Sciences* 115(50): 12823-12828.
- Chen, Y., Aung, K., Rolčík, J., Walicki, K., Friml, J. and Brandizzi, F. (2014). Inter-regulation of the unfolded protein response and auxin signaling. *The Plant Journal* 77(1): 97-107.
- Chen, Y. and Brandizzi, F. (2012). AtIRE1A/AtIRE1B and AGB1 independently control two essential unfolded protein response pathways in *Arabidopsis*. *The Plant Journal* 69(2): 266-277.
- Deng, Y., Humbert, S., Liu, J.-X., Srivastava, R., Rothstein, S. J. and Howell, S. H. (2011). Heat induces the splicing by IRE1 of a mRNA encoding a transcription factor involved in the unfolded protein response in *Arabidopsis*. *Proceedings of the National Academy of Sciences* 108(17): 7247-7252.

- Deng, Y., Srivastava, R. and Howell, S. H. (2013). Protein kinase and ribonuclease domains of IRE1 confer stress tolerance, vegetative growth, and reproductive development in Arabidopsis. *Proceedings of the National Academy of Sciences* 110(48): 19633-19638.
- Di Mambro, R., De Ruvo, M., Pacifici, E., Salvi, E., Sozzani, R., Benfey, P. N., Busch, W., Novak, O., Ljung, K., Di Paola, L., Marée, A. F. M., Costantino, P., Grieneisen, V. A. and Sabatini, S. (2017). Auxin minimum triggers the developmental switch from cell division to cell differentiation in the Arabidopsis root. *Proceedings of the National Academy of Sciences* 114(36): E7641.
- Dolan, L. and Costa, S. (2001). Evolution and genetics of root hair stripes in the root epidermis. *Journal of experimental botany* 52(suppl_1): 413-417.
- Dolan, L. and Davies, J. (2004). Cell expansion in roots. *Current opinion in plant biology* 7(1): 33-39.
- Evans, M. L., Ishikawa, H. and Estelle, M. A. (1994). Responses of Arabidopsis roots to auxin studied with high temporal resolution: comparison of wild type and auxin-response mutants. *Planta* 194(2): 215-222.
- Feltz, C. J. and Miller, G. E. (1996). An asymptotic test for the equality of coefficients of variation from k populations. *Stat Med* 15(6): 646-658.
- Fendrych, M., Akhmanova, M., Merrin, J., Glanc, M., Hagihara, S., Takahashi, K., Uchida, N., Torii, K. U. and Friml, J. (2018). Rapid and reversible root growth inhibition by TIR1 auxin signalling. *Nature Plants* 4(7): 453-459.
- Gao, H., Brandizzi, F., Benning, C. and Larkin, R. M. (2008). A membrane-tethered transcription factor defines a branch of the heat stress response in *Arabidopsis thaliana*. *Proceedings of the National Academy of Sciences* 105(42): 16398-16403.
- Guillemette, T., Calmes, B. and Simoneau, P. (2014). Impact of the UPR on the virulence of the plant fungal pathogen *A. brassicicola*. *Virulence* 5(2): 357-364.
- Gutiérrez, T., Qi, H., Yap, M. C., Tahbaz, N., Milburn, L. A., Lucchinetti, E., Lou, P.-H., Zaugg, M., LaPointe, P. G., Mercier, P., Overduin, M., Bischof, H., Burgstaller, S., Malli, R., Ballanyi, K., Shuai, J. and Simmen, T. (2020). The ER chaperone calnexin controls mitochondrial positioning and respiration. *Science Signaling* 13(638): eaax6660.
- Han, J. and Kaufman, R. J. (2017). Physiological/pathological ramifications of transcription factors in the unfolded protein response. *Genes & Development* 31(14): 1417-1438.
- Hayashi, K., Hasegawa, J. and Matsunaga, S. (2013). The boundary of the meristematic and elongation zones in roots: endoreduplication precedes rapid cell expansion. *Scientific reports* 3(1): 2723.
- Hetz, C. and Papa, F. R. (2018). The Unfolded Protein Response and Cell Fate Control. *Molecular cell* 69(2): 169-181.

- Hirabayashi, Y., Kwon, S.-K., Paek, H., Pernice, W. M., Paul, M. A., Lee, J., Erfani, P., Raczkowski, A., Petrey, D. S. and Pon, L. A. (2017). ER-mitochondria tethering by PDZD8 regulates Ca²⁺ dynamics in mammalian neurons. *Science* 358(6363): 623-630.
- Hollien, J., Lin, J. H., Li, H., Stevens, N., Walter, P. and Weissman, J. S. (2009). Regulated Ire1-dependent decay of messenger RNAs in mammalian cells. *Journal of Cell Biology* 186(3): 323-331.
- Huang, H.-W., Zeng, X., Rhim, T., Ron, D. and Ryo, H. D. (2017). The requirement of IRE1 and XBP1 in resolving physiological stress during *Drosophila* development. *Journal of Cell Science* 130(18): 3040-3049.
- Ishikawa, H. and Evans, M. L. (1993). The Role of the Distal Elongation Zone in the Response of Maize Roots to Auxin and Gravity. *Plant Physiology* 102(4): 1203-1210.
- Ishikawa, T., Kashima, M., Nagano, A. J., Ishikawa-Fujiwara, T., Kamei, Y., Todo, T. and Mori, K. (2017). Unfolded protein response transducer IRE1-mediated signaling independent of XBP1 mRNA splicing is not required for growth and development of medaka fish. *eLife* 6: e26845.
- Kato, H., Katoh, R. and Kitamura, M. (2013). Dual regulation of cadmium-induced apoptosis by mTORC1 through selective induction of IRE1 branches in unfolded protein response. *PLoS One* 8(5): e64344.
- Kato, H., Nakajima, S., Saito, Y., Takahashi, S., Katoh, R. and Kitamura, M. (2012). mTORC1 serves ER stress-triggered apoptosis via selective activation of the IRE1–JNK pathway. *Cell Death & Differentiation* 19(2): 310-320.
- Kaufman, R. J. and Malhotra, J. D. (2014). Calcium trafficking integrates endoplasmic reticulum function with mitochondrial bioenergetics. *Biochimica et Biophysica Acta (BBA)-Molecular Cell Research* 1843(10): 2233-2239.
- Kawahara, T., Yanagi, H., Yura, T. and Mori, K. (1997). Endoplasmic reticulum stress-induced mRNA splicing permits synthesis of transcription factor Hac1p/Ern4p that activates the unfolded protein response. *Molecular biology of the cell* 8(10): 1845-1862.
- Kim, J.-S., Yamaguchi-Shinozaki, K. and Shinozaki, K. (2018). ER-anchored transcription factors bZIP17 and bZIP28 regulate root elongation. *Plant Physiology* 176(3): 2221-2230.
- Kim, S. G., Hoffman, G. R., Poulgiannis, G., Buel, G. R., Jang, Y. J., Lee, K. W., Kim, B. Y., Erikson, R. L., Cantley, L. C., Choo, A. Y. and Blenis, J. (2013). Metabolic stress controls mTORC1 lysosomal localization and dimerization by regulating the TTT-RUVBL1/2 complex. *Mol Cell* 49(1): 172-185.
- Li, G. Y., Fan, B. and Jiao, Y. Y. (2014). Rapamycin attenuates visible light-induced injury in retinal photoreceptor cells via inhibiting endoplasmic reticulum stress. *Brain Res* 1563: 1-12.
- Li, X., Cai, W., Liu, Y., Li, H., Fu, L., Liu, Z., Xu, L., Liu, H., Xu, T. and Xiong, Y. (2017). Differential TOR activation and cell proliferation in *Arabidopsis* root and shoot apices. *Proceedings of the National Academy of Sciences* 114(10): 2765-2770.

- Lucas, M., Swarup, R., Paponov, I. A., Swarup, K., Casimiro, I., Lake, D., Peret, B., Zappala, S., Mairhofer, S., Whitworth, M., Wang, J., Ljung, K., Marchant, A., Sandberg, G., Holdsworth, M. J., Palme, K., Pridmore, T., Mooney, S. and Bennett, M. J. (2011). SHORT-ROOT Regulates Primary, Lateral, and Adventitious Root Development in Arabidopsis. *Plant Physiology* 155(1): 384-398.
- Mishiba, K.-i., Iwata, Y., Mochizuki, T., Matsumura, A., Nishioka, N., Hirata, R. and Koizumi, N. (2019). Unfolded protein-independent IRE1 activation contributes to multifaceted developmental processes in Arabidopsis. *Life science alliance* 2(5).
- Mishiba, K.-i., Nagashima, Y., Suzuki, E., Hayashi, N., Ogata, Y., Shimada, Y. and Koizumi, N. (2013). Defects in IRE1 enhance cell death and fail to degrade mRNAs encoding secretory pathway proteins in the Arabidopsis unfolded protein response. *Proceedings of the National Academy of Sciences* 110(14): 5713-5718.
- Mitra, S. and Ryoo, H. D. (2019). The unfolded protein response in metazoan development. *Journal of Cell Science* 132(5): jcs217216.
- Montané, M.-H. and Menand, B. (2013). ATP-competitive mTOR kinase inhibitors delay plant growth by triggering early differentiation of meristematic cells but no developmental patterning change. *Journal of experimental botany* 64(14): 4361-4374.
- Moreno, A. A., Mukhtar, M. S., Blanco, F., Boatwright, J. L., Moreno, I., Jordan, M. R., Chen, Y., Brandizzi, F., Dong, X. and Orellana, A. (2012). IRE1/bZIP60-mediated unfolded protein response plays distinct roles in plant immunity and abiotic stress responses. *PLoS One* 7(2).
- Mullen, J. L., Ishikawa, H. and Evans, M. L. (1998). Analysis of changes in relative elemental growth rate patterns in the elongation zone of Arabidopsis roots upon gravistimulation. *Planta* 206(4): 598-603.
- Nagashima, Y., Mishiba, K.-i., Suzuki, E., Shimada, Y., Iwata, Y. and Koizumi, N. (2011). Arabidopsis IRE1 catalyses unconventional splicing of bZIP60 mRNA to produce the active transcription factor. *Scientific reports* 1: 29.
- Ng, S., Ivanova, A., Duncan, O., Law, S. R., Van Aken, O., De Clercq, I., Wang, Y., Carrie, C., Xu, L., Kmiec, B., Walker, H., Van Breusegem, F., Whelan, J. and Giraud, E. (2013). A Membrane-Bound NAC Transcription Factor, ANAC017, Mediates Mitochondrial Retrograde Signaling in Arabidopsis. *The Plant Cell* 25(9): 3450-3471.
- Ovečka, M., Lang, I., Baluška, F., Ismail, A., Illeš, P. and Lichtscheidl, I. (2005). Endocytosis and vesicle trafficking during tip growth of root hairs. *Protoplasma* 226(1-2): 39-54.
- Pastor-Cantizano, N., Ko, D. K., Angelos, E., Pu, Y. and Brandizzi, F. (2020). Functional Diversification of ER Stress Responses in Arabidopsis. *Trends in biochemical sciences* 45(2): 123-136.
- Petricka, J. J., Winter, C. M. and Benfey, P. N. (2012). Control of Arabidopsis Root Development. *Annual Review of Plant Biology* 63(1): 563-590.

- Pfaffenbach, K. T., Nivala, A. M., Reese, L., Ellis, F., Wang, D., Wei, Y. and Pagliassotti, M. J. (2010). Rapamycin Inhibits Postprandial-Mediated X-Box-Binding Protein-1 Splicing in Rat Liver. *The Journal of Nutrition* 140(5): 879-884.
- Pu, Y., Ruberti, C., Angelos, E. R. and Brandizzi, F. (2019). AtIRE1C, an unconventional isoform of the UPR master regulator AtIRE1, is functionally associated with AtIRE1B in Arabidopsis gametogenesis. *Plant Direct* 3(11): e00187.
- Reimold, A. M., Etkin, A., Clauss, I., Perkins, A., Friend, D. S., Zhang, J., Horton, H. F., Scott, A., Orkin, S. H. and Byrne, M. C. (2000). An essential role in liver development for transcription factor XBP-1. *Genes & Development* 14(2): 152-157.
- Reimold, A. M., Iwakoshi, N. N., Manis, J., Vallabhajosyula, P., Szomolanyi-Tsuda, E., Gravalles, E. M., Friend, D., Grusby, M. J., Alt, F. and Glimcher, L. H. (2001). Plasma cell differentiation requires the transcription factor XBP-1. *Nature* 412(6844): 300-307.
- Renna, L., Stefano, G., Slabaugh, E., Wormsbaecher, C., Sulpizio, A., Zienkiewicz, K. and Brandizzi, F. (2018). TGNap1 is required for microtubule-dependent homeostasis of a subpopulation of the plant trans-Golgi network. *Nature Communications* 9(1): 5313.
- Retzer, K. and Weckwerth, W. (2021). The TOR–Auxin Connection Upstream of Root Hair Growth. *Plants* 10(1): 150.
- Rieusset, J. (2018). The role of endoplasmic reticulum-mitochondria contact sites in the control of glucose homeostasis: an update. *Cell death & disease* 9(3): 1-12.
- Ron, D. and Walter, P. (2007). Signal integration in the endoplasmic reticulum unfolded protein response. *Nature reviews Molecular cell biology* 8(7): 519-529.
- Ruberti, C., Lai, Y. and Brandizzi, F. (2018). Recovery from temporary endoplasmic reticulum stress in plants relies on the tissue-specific and largely independent roles of bZIP 28 and bZIP 60, as well as an antagonizing function of BAX-Inhibitor 1 upon the pro-adaptive signaling mediated by bZIP 28. *The Plant Journal* 93(1): 155-165.
- Sanchez-Alvarez, M., del Pozo, M. A. and Bakal, C. (2017). AKT-mTOR signaling modulates the dynamics of IRE1 RNase activity by regulating ER-mitochondria contacts. *Scientific reports* 7(1): 16497.
- Sato, E. M., Hijazi, H., Bennett, M. J., Vissenberg, K. and Swarup, R. (2015). New insights into root gravitropic signalling. *Journal of experimental botany* 66(8): 2155-2165.
- Schepetilnikov, M., Makarian, J., Srour, O., Geldreich, A., Yang, Z., Chicher, J., Hammann, P. and Ryabova, L. A. (2017). GTPase ROP2 binds and promotes activation of target of rapamycin, TOR, in response to auxin. *The EMBO journal* 36(7): 886-903.
- Scheres, B. and Wolkenfelt, H. (1998). The Arabidopsis root as a model to study plant development. *Plant Physiology and Biochemistry* 36(1): 21-32.

- Shanware, N. P., Bray, K., Eng, C. H., Wang, F., Follettie, M., Myers, J., Fantin, V. R. and Abraham, R. T. (2014). Glutamine deprivation stimulates mTOR-JNK-dependent chemokine secretion. *Nat Commun* 5: 4900.
- Shi, L., Wu, Y. and Sheen, J. (2018). TOR signaling in plants: conservation and innovation. *Development* 145(13): dev160887.
- Sulpice, R., Flis, A., Ivakov, A. A., Apelt, F., Krohn, N., Encke, B., Abel, C., Feil, R., Lunn, J. E. and Stitt, M. (2014). Arabidopsis Coordinates the Diurnal Regulation of Carbon Allocation and Growth across a Wide Range of Photoperiods. *Molecular Plant* 7(1): 137-155.
- Szabadkai, G., Bianchi, K., Várnai, P., De Stefani, D., Wieckowski, M. R., Cavagna, D., Nagy, A. I., Balla, T. and Rizzuto, R. (2006). Chaperone-mediated coupling of endoplasmic reticulum and mitochondrial Ca²⁺ channels. *The Journal of cell biology* 175(6): 901-911.
- Tanegashima, K., Zhao, H., Rebbert, M. L. and Dawid, I. B. (2009). Coordinated activation of the secretory pathway during notochord formation in the *Xenopus* embryo. *Development* 136(21): 3543-3548.
- Truernit, E., Bauby, H., Dubreucq, B., Grandjean, O., Runions, J., Barthélémy, J. and Palauqui, J.-C. (2008). High-resolution whole-mount imaging of three-dimensional tissue organization and gene expression enables the study of Phloem development and structure in Arabidopsis. *The Plant Cell* 20(6): 1494-1503.
- Van Aken, O., De Clercq, I., Ivanova, A., Law, S. R., Van Breusegem, F., Millar, A. H. and Whelan, J. (2016). Mitochondrial and chloroplast stress responses are modulated in distinct touch and chemical inhibition phases. *Plant Physiology* 171(3): 2150-2165.
- Xiong, Y., McCormack, M., Li, L., Hall, Q., Xiang, C. and Sheen, J. (2013). Glucose-TOR signalling reprograms the transcriptome and activates meristems. *Nature* 496(7444): 181-186.
- Yazdanbakhsh, N., Sulpice, R., Graf, A., Stitt, M. and Fisahn, J. (2011). Circadian control of root elongation and C partitioning in *Arabidopsis thaliana*. *Plant, Cell & Environment* 34(6): 877-894.
- Young, R. M., Ackerman, D., Quinn, Z. L., Mancuso, A., Gruber, M., Liu, L., Giannoukos, D. N., Bobrovnikova-Marjon, E., Diehl, J. A., Keith, B. and Simon, M. C. (2013). Dysregulated mTORC1 renders cells critically dependent on desaturated lipids for survival under tumor-like stress. *Genes Dev* 27(10): 1115-1131.
- Yuan, X., Xu, P., Yu, Y. and Xiong, Y. (2020). Glucose-TOR signaling regulates PIN2 stability to orchestrate auxin gradient and cell expansion in Arabidopsis root. *Proc Natl Acad Sci U S A* 117(51): 32223-32225.
- Zhang, L., Chen, H., Brandizzi, F., Verchot, J. and Wang, A. (2015). The UPR branch IRE1-bZIP60 in plants plays an essential role in viral infection and is complementary to the only UPR pathway in yeast. *PLoS genetics* 11(4).
- Zhuo, F., Xiong, F., Deng, K., Li, Z. and Ren, M. (2020). Target of Rapamycin (TOR) Negatively Regulates Ethylene Signals in Arabidopsis. *International journal of molecular sciences* 21(8): 2680.

CHAPTER V

Future Perspectives

In my dissertation research I examined how conserved elements of the UPR interact with plant-specific physiological mechanisms in the context of development and stress response. By exploring how the canonical UPR responds in non-canonical and tissue-specific ways my research has helped to broaden our knowledge of the plant UPR and better integrate our understanding of the UPR functionality in plant life. In the Chapter 1 literature review, I examine how broadly conserved elements of the UPR, such as IRE1, have evolved novel biochemical mechanisms in different eukaryotic organisms (Figure 5.1). I further outline our current understanding of how the functional diversification of the UPR in plants affects a variety of stress responses and developmental processes. In Chapter 2, I add to this knowledge by studying the functional interaction between the Arabidopsis UPR regulators and the conserved NADPH Oxidase proteins (also known as RBOH enzymes) in the contexts of the ER stress response. In Chapter 3, I explore

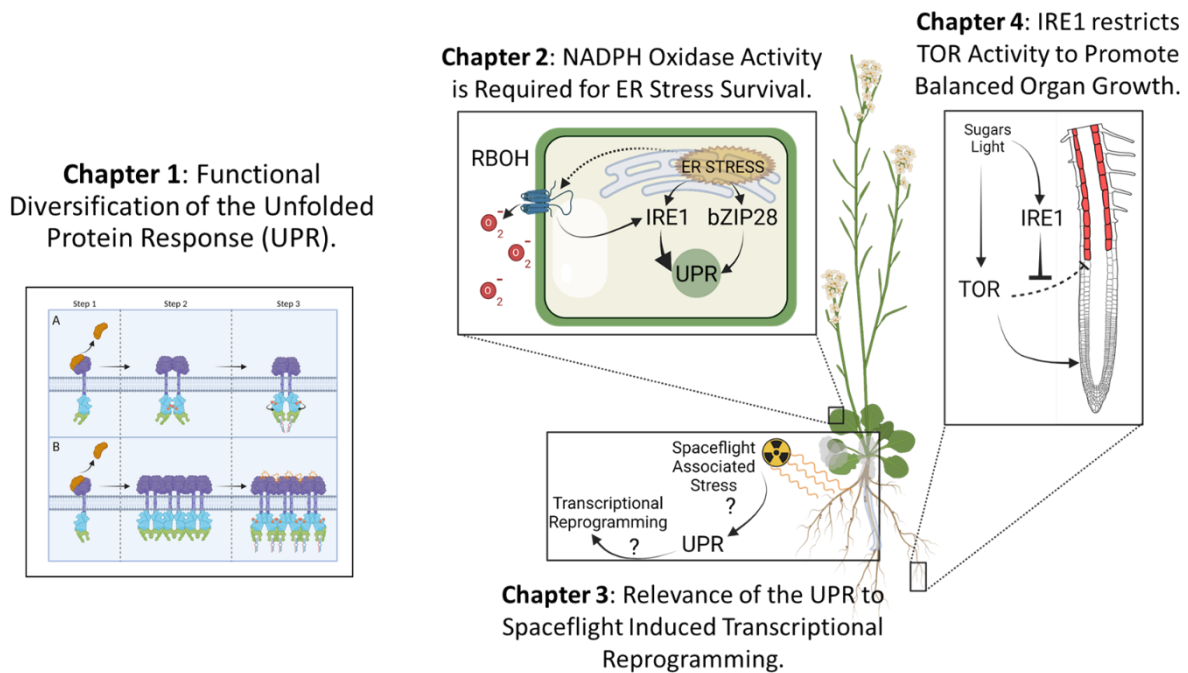


Figure 5.1. Summary Graphic of Dissertation Investigations.

how the UPR may be connected with other plant signaling mechanisms through an analysis of UPR-dependent transcriptional reprogramming in spaceflight conditions. In Chapter 4, I sought to better understand how the UPR functions specifically contribute to plant development, by looking at the relationship between IRE1 and the TOR kinase in the context of root growth. In this chapter, I further expand upon the context of these findings and discuss how they might be explored in the future.

Chapter 2: Integrating ER Stress Response with NADPH Oxidase Signaling

In Arabidopsis, NADPH oxidase-dependent ROS signaling is already known to mediate a wide variety of stress responses including abiotic stress (i.e. light, mechanical, heat), and biotic stress (i.e. bacterial, fungal, and viral infection) (Miller *et al.* 2009). In particular, the RBOH proteins expressed in plant vasculature mediate systemic signaling to prime unstressed portions of the plant with pre-emptive stress signals (Suzuki *et al.* 2011). Interlinked signal transduction mediated by RBOH-dependent H₂O₂ and Ca²⁺ propagate from cell to cell over long distances in plants (Mittler 2017). This signal transduction, which is analogous to nerve impulses in metazoans, has been called ROS wave signaling.

In chapter 2, I built on previous work that demonstrated ROS accumulation during ER stress in Arabidopsis, and examined the specific role of RBOHD and RBOHF in the UPR response at the organism level. I was able to demonstrate that H₂O₂ accumulation which occurs with prolonged ER stress is almost entirely dependent on the functional activities of RBOHD and RBOHF. Furthermore, I demonstrate that the functions of these proteins are a strongly pro-survival influence under these conditions. This may be explained by my observations which demonstrate RBOHD and RBOHF dependent functions promote IRE1 activation under prolonged

stress treatments. With this established, it will now be important to understand whether these observations are due to localized RBOH activity at the primary sites of stress, or whether RBOHs participate in long distance signaling to prime the plant UPR in unstressed tissues.

Recent work from our lab has demonstrated that ER stress does transmit a systemic signal in the root to shoot direction (Lai *et al.* 2018). Roots that are stressed by tunicamycin application promote a local UPR response as expected, however shoot tissues in these plants also show a significant UPR response dependent upon UPR activation in root tissues (Lai *et al.* 2018). It was demonstrated that the tunicamycin itself is not taken up in the vascular streams and transported to the shoot, instead a secondary signal leads to UPR activation in connected tissues. One explanation supplied by the authors is the potential for cell-to-cell transport of the bZIP60 mRNA or protein, which was shown to be transported from a specific cell type at the root tip to the surrounding tissues (Lai *et al.* 2018). This transport was ablated in plasmodesmata deficient mutants suggesting that short-distance transportation of bZIP60 is likely (Lai *et al.* 2018). However, given the prominent role of RBOH activity in long-distance systemic signaling, it may be possible that RBOH dependent ROS waves may be involved in transmitting the ER stress signal from root to shoot. In my study I demonstrate that superoxide production initially begins at the root tip after 24 hr, but is transferred to the mature root tissues, including the vascular column, after 48 hr of ER stress. This superoxide production in mature tissues was dependent on RBOHD and RBOHF. Therefore, it may be possible that RBOH activity in these mature tissues leads to systemic signaling. Future work in this area could explore whether ER stress in the root tissues requires RBOHD or RBOHF to transmit the systemic UPR signals observed by Lai *et al.* (2018), and could utilize selective tissue applications of ER stress agents and ROS scavengers to explore this possibility.

The connection between ER stress signaling and RBOH-dependent ROS signaling may also play an important role in other types of abiotic and biotic stresses. As discussed in Chapter I, the UPR and IRE1 play an important role in establishing systemic acquired resistance (SAR) to different types of pathogens through an unknown mechanism (Verchot and Pajerowska-Mukhtar 2021). ROS wave signaling also has a demonstrated role in promoting SAR and plant survival in these contexts as well (Torres *et al.* 2005). Given the results discussed in Chapter II, it may be possible that ER stress at the site of the infection may lead to ROS wave propagation, promoting ER stress and pathogen resistance in systemic tissues. A similar ER-stress dependent activation of ROS wave signaling may exist in the response to high light as well, given the verified roles that RBOHD and the UPR have in regulating high-light stress resistance (Miller *et al.* 2009, Beaugelin *et al.* 2020). Taken together, my work has demonstrated an important link between ER stress response and the RBOH-dependent ROS signaling network. In doing so, this work has helped to connect the conserved component of the plant UPR with the wider network of plant signaling pathways and provide possible contexts for UPR functions in a variety of biotic and abiotic stress responses.

Chapter 3: UPR Transcriptome in Spaceflight Experiment Reveals Possible Novel Roles for UPR TFs

Spaceflight conditions impose a novel set of environmental stressors on plants, including microgravity, radiation, vibration, and limited exchange of gases, which can affect plant development and yield (Paul *et al.* 2012, Paul *et al.* 2013). Given the broad versatility of the UPR in responding to a number of environmental stressors, I explored the possibility that the UPR contributes to transcriptional regulation during spaceflight associated stress conditions. I did this by sterile culturing *Arabidopsis* etiolated hypocotyls in orbit at the International Space Station

(ISS), utilizing the available BRIC-PDFU hardware. This hardware has been used previously in the study of Arabidopsis transcriptomes in spaceflight conditions, and a number of the transcriptional responses observed in previous studies were also found in our WT transcriptome. However, a study published after the execution of my spaceflight experiment demonstrated that seedlings grown in this hardware experience extensive stresses which are independent of spaceflight associated stress (Basu *et al.* 2017). In these contexts, I observed a surprising downregulation of multiple stress responsive processes at the transcript level in spaceflight compared to ground controls, including water deprivation and starvation responses. Although the limitations of this experiment and the inability to perform additional experimental replicates prevented further investigation, observations of plant growth patterns in culture plates led me to hypothesize that in spaceflight conditions the lack of directional growth in microgravity improved seedling access to water and nutrients by increased contact with the media. The improved access to these nutrients may have suppressed the BRIC-PDFU induced stress responses. While there were very few differences between WT and UPR mutant transcriptomes in the spaceflight samples, in the ground controls samples I found a large requirement for intact bZIP60 and bZIP28 signaling in the regulation of a number of stress responses, including water deprivation and abscisic acid signaling. These results demonstrate for the first time, the possible connection between UPR TFs and abscisic acid/ water deprivation stress. However, further investigation is needed to dissect the causative nature of the stress experienced by seedlings cultured inside BRIC-PDFUs and determine whether the outcomes of this stress are applicable to other biological contexts. In the future, spaceflight associated research of plants would be better performed in hardware which can better replicate normal growth conditions of plants on Earth. In that respect, the open-air growth of plants in the VEGGIE growth chamber on the ISS may be better suited to future research of

plant spaceflight stress responses, and may help to re-evaluate the role of the UPR in these conditions.

Chapter 4: Old Friends with a New Relationship, IRE1 and TOR

Given the near universal occurrence of IRE1 and TOR in the genomes of most eukaryotic organisms, including animals, fungi and plants (Ruberti and Brandizzi 2014, Shi *et al.* 2018), it is plausible to assume that these two cell status regulators have coexisted on a broad evolutionary timescale. However, few interactions between their regulatory networks have been elucidated. This is peculiar given the strong influence that both regulators have on protein synthesis at the cell level (Walter and Ron 2011, Xiong *et al.* 2013, Shi *et al.* 2018, Bashir *et al.* 2021). Although a small number of studies have demonstrated that TOR activity can affect UPR or IRE1 signaling in stressed mammalian cells (Pfaffenbach *et al.* 2010, Kato *et al.* 2012, Kato *et al.* 2013, Young *et al.* 2013, Li *et al.* 2014, Shanware *et al.* 2014, Sanchez-Alvarez *et al.* 2017), to my best knowledge, no previous studies have demonstrated that IRE1 can affect TOR activity under cell stress or developmental contexts.

In the work presented in Chapter IV, I demonstrate the requirement of IRE1 specifically in the rapid development of *Arabidopsis* primary root tips. I show that IRE1 is required to reach maximum rates of growth afforded by prolonged photoperiod and increased carbohydrate availability. I further show that the *ire1a ire1b* root growth phenotype is dependent upon hyperactivation of TOR, which leads to increased rates of cell differentiation. Prior to this work, the signaling and physiological pathways by which IRE1 activities controls development in plants were completely unknown. These findings help to establish that IRE1 controls growth via a negative regulation of TOR activity.

The molecular mechanism which connects IRE1 to TOR activity is yet unknown, but of considerable interest. Although it is highly unlikely that TOR is regulated via bZIP60 splicing, it will take considerable work to elucidate whether IRE1 affects these outcomes via its kinase activity, alternative RNase activity, or another novel signaling pathway. Furthermore, the tissue specific contexts of this interaction will complicate future studies. Tissue-specific or single cell RNA-sequencing of WT and IRE1 mutant root tips may be required to elucidate potential RNA-targets of IRE1 in these transient developmental contexts. These putative targets could then be examined by standard reverse genetics approaches. Elucidation of this mechanism may allow for broader control over plant growth, development, and metabolism via the IRE1 pathway and help to establish new routes for biotechnological utilization of UPR mechanisms in crop species to improve productivity.

REFERENCES

REFERENCES

- Bashir S., Bandy M., Qadri O., Bashir A., Hilal N., Nida i F., Rader S. and Fazili K.M. (2021). "The molecular mechanism and functional diversity of UPR signaling sensor IRE1." *Life Sciences* 265: 118740.
- Basu P., Kruse C.P.S., Luesse D.R. and Wyatt S.E. (2017). "Growth in spaceflight hardware results in alterations to the transcriptome and proteome." *Life Sciences in Space Research* 15: 88-96.
- Beaugelin I., Chevalier A., d'Alessandro S., Ksas B. and Havaux M. (2020). "Endoplasmic reticulum-mediated unfolded protein response is an integral part of singlet oxygen signalling in plants." *The Plant Journal*.
- Kato H., Katoh R. and Kitamura M. (2013). "Dual regulation of cadmium-induced apoptosis by mTORC1 through selective induction of IRE1 branches in unfolded protein response." *PLoS One* 8(5): e64344.
- Kato H., Nakajima S., Saito Y., Takahashi S., Katoh R. and Kitamura M. (2012). "mTORC1 serves ER stress-triggered apoptosis via selective activation of the IRE1–JNK pathway." *Cell Death & Differentiation* 19(2): 310-320.
- Lai Y.-S., Stefano G., Zemelis-Durfee S., Ruberti C., Gibbons L. and Brandizzi F. (2018). "Systemic signaling contributes to the unfolded protein response of the plant endoplasmic reticulum." *Nature Communications* 9(1): 3918.
- Li G.Y., Fan B. and Jiao Y.Y. (2014). "Rapamycin attenuates visible light-induced injury in retinal photoreceptor cells via inhibiting endoplasmic reticulum stress." *Brain Res* 1563: 1-12.
- Miller G., Schlauch K., Tam R., Cortes D., Torres M.A., Shulaev V., Dangl J.L. and Mittler R. (2009). "The Plant NADPH Oxidase RBOHD Mediates Rapid Systemic Signaling in Response to Diverse Stimuli." *Science Signaling* 2(84): ra45-ra45.
- Mittler R. (2017). "ROS Are Good." *Trends Plant Sci* 22(1): 11-19.
- Paul A.-L., Wheeler R.M., Levine H.G. and Ferl R.J. (2013). "Fundamental Plant Biology Enabled by The Space Shuttle." *American Journal of Botany* 100(1): 226-234.
- Paul A.-L., Zupanska A.K., Ostrow D.T., Zhang Y., Sun Y., Li J.-L., Shanker S., Farmerie W.G., Amalfitano C.E. and Ferl R.J. (2012). "Spaceflight Transcriptomes: Unique Responses to a Novel Environment." *Astrobiology* 12(1): 40-56.
- Pfaffenbach K.T., Nivala A.M., Reese L., Ellis F., Wang D., Wei Y. and Pagliassotti M.J. (2010). "Rapamycin Inhibits Postprandial-Mediated X-Box-Binding Protein-1 Splicing in Rat Liver." *The Journal of Nutrition* 140(5): 879-884.
- Ruberti C. and Brandizzi F. (2014). "Conserved and plant-unique strategies for overcoming endoplasmic reticulum stress." *Front Plant Sci* 5: 69.

- Sanchez-Alvarez M., del Pozo M.A. and Bakal C. (2017). "AKT-mTOR signaling modulates the dynamics of IRE1 RNase activity by regulating ER-mitochondria contacts." *Scientific reports* 7(1): 16497.
- Shanware N.P., Bray K., Eng C.H., Wang F., Follettie M., Myers J., Fantin V.R. and Abraham R.T. (2014). "Glutamine deprivation stimulates mTOR-JNK-dependent chemokine secretion." *Nat Commun* 5: 4900.
- Shi L., Wu Y. and Sheen J. (2018). "TOR signaling in plants: conservation and innovation." *Development* 145(13): dev160887.
- Suzuki N., Miller G., Morales J., Shulaev V., Torres M.A. and Mittler R. (2011). "Respiratory burst oxidases: the engines of ROS signaling." *Current opinion in plant biology* 14(6): 691-699.
- Torres M.A., Jones J.D. and Dangl J.L. (2005). "Pathogen-induced, NADPH oxidase-derived reactive oxygen intermediates suppress spread of cell death in *Arabidopsis thaliana*." *Nat Genet* 37(10): 1130-1134.
- Verchot J. and Pajerowska-Mukhtar K.M. (2021). "UPR signaling at the nexus of plant viral, bacterial, and fungal defenses." *Current Opinion in Virology* 47: 9-17.
- Walter P. and Ron D. (2011). "The Unfolded Protein Response: From Stress Pathway to Homeostatic Regulation." *Science* 334(6059): 1081-1086.
- Xiong Y., McCormack M., Li L., Hall Q., Xiang C. and Sheen J. (2013). "Glucose-TOR signalling reprograms the transcriptome and activates meristems." *Nature* 496(7444): 181-186.
- Young R.M., Ackerman D., Quinn Z.L., Mancuso A., Gruber M., Liu L., Giannoukos D.N., Bobrovnikova-Marjon E., Diehl J.A., Keith B. and Simon M.C. (2013). "Dysregulated mTORC1 renders cells critically dependent on desaturated lipids for survival under tumor-like stress." *Genes Dev* 27(10): 1115-1131.